DEVELOPMENT OF A PORTLAND CEMENT BASED SYSTEM FOR VERTEBROPLASTY

By

Gareth David Wynn-Jones

A thesis submitted to the
Faculty of Medicine and Dentistry
of the
University of Birmingham
for the degree of
DOCTOR OF PHILOSOPHY

Biomaterials Unit
School of Dentistry
St. Chad's Queensway
Birmingham
B4 6NN
March 2013

SYNOPSIS

Portland cement (PC) is generally known for its various applications in the construction industry. However, since mineral trioxide aggregate (MTA), a PC based root filling material, obtained food and drug administration (FDA) approval in the late 1990's there has been an increased interest in the use of the cement for other *in vivo* applications. PCs are durable, possess high compressive strengths, set in aqueous environments such as those found *in vivo* and have demonstrated desirable tissue responses as an endodontic sealant.

The injectability of PC with various additives was investigated for use in clinical applications such as vertebroplasty (the stabilisation of a fractured vertebra with bone cement) using a syringe with a 2 mm aperture. Additives significantly improved cement injectability, decreased setting times from over 2 h to below 20 minutes while maintaining the compressive strength of the material. Cement characterisation methods including X-ray diffraction (XRD), helium pycnometry and zeta potential measurements were employed to elucidate the effect of the additives on the cement setting reaction. The biocompatibility of PC was investigated with fibroblast and bone marrow cells. The freshly mixed cement appeared cytotoxic while set cement upregulated genes associated with the osteogenic phenotype.

ACKNOWLEDGEMENTS

Firstly and foremost I would like to sincerely thank both my supervisors, Dr M.P Hofmann and Dr R.M Shelton for their supervision, advice and support throughout the PhD. I would like to extend my warmest thanks to Dr Hofmann for his encouragement, advice and guidance throughout the entire process. I would also like to extend my gratitude to Dr Shelton for teaching me to always question my data and to carefully assess my experimental planning.

I am very grateful to the EPSRC and the projects industrial collaborators Orthos Ltd for funding this PhD and giving me the opportunity to research at the forefront of material science. I would also like to thank Professor T. Miles for hosting me at the University of Bath.

I would also like to express my gratitude to Mrs S. Fisher, Dr J. Deans, Dr J. Wilson, Dr J. Liu Mrs G. Smith, Dr W. Palin and Dr O. Addison for their assistance and advice.

Finally, I would like to thank my family and fellow postgraduate students for their support, patience and encouragement throughout this PhD, without whom this would truly be impossible.

Dedicated to my wife and our beautiful daughter

TABLE OF CONTENTS

PUBLICATIONS:

Wynn-Jones G, Shelton RM, Hofmann MP. 2012. Development of Portland cement for orthopedic applications, establishing injectability and decreasing setting times. J Biomed Mater Res Part B 2012:100B:2213–2221 (attached to appendices).

SUBMITTED FOR PUBLICATION:

Wynn-Jones G.D, Shelton R.M, Hofmann M.P. Modification of Portland cement with the citrate anion: elucidating the underlying mechanisms. Submitted to the Journal of Materials Chemistry.

PATENT:

Patent application: P113642PCT

LIST OF ABBREVIATIONS

ALPase: Alkaline phosphatase

Bis-EMA: Bisphenol-a-ethoxy dimethacrylate

Bis-GMA: Bisphenol-a-glycidyl dimethacrylate

BMP: Bone morphogenic protein

BSP: Bone Sialoprotein

C_2S: Belite

C_3S: Alite

CMS: Colimethate sodium

col1: Collagen type 1

CPCs: Calcium phosphate cements

CS: Compressive Strengths

C-S-H: Calcium-silicate-hydrate

DMP 1: Dentin matrix protein

DSC: Differential scanning calorimetry

DSPP: Dentin sialophosphoprotein

EDX: Energy dispersive X-ray spectroscopy

FDA: Food and drug administration agency

FE: Numerical finite element

FTIR: Fourier transform infrared

Gypsum: Calcium sulphate di-hydrate

HA: Hydroxyapatite

hDPCs: Human dental pulp cells

HPMC: Hydroxyproplymethylcellulose

HRWR: High range water reducer

KP: Kyphoplasty

LCCPCs: Light cured calcium phosphate cement

MAPK: Mitogen-activated protein kinases

MG-63: Human osteosarcoma cells

MMA: methylmethacrylate monomer

MRI: Magnetic resonance imaging

MTA: Mineral trioxide aggregate

Na-HP: Sodium hexaphosphate

OC: Osteocalcin

ODI: Oswestry Disability Index

OFMSCs: Orofacial bone mesenchymal stem cells

ON: Osteonectin

OPN: Osteopontin

OSAD: Osteoadherin

PC: Portland cement

PMMA: Polymethymethacrylate

PVP: Percutaneous vertebroplasty

QCT: Quantitative computer tomography

RT-PCR: Real-time polymerase chain reaction

Saos-2: Osteoblast like cells

SEM: Scanning electron Microscopy

TEGDMA: Triethylene glycol dimethacrylate acid

VAS: Visual analogue scale

VCFs: Vertebral compression fractures

XRD: X-ray diffraction

LIST OF FIGURES

LIST OF TABLES

CHAPTER 1: INTRODUCTION

1 INTRODUCTION

1.1 Project background

Portland cement (PC) is generally known for its various applications in the construction industry (1). However, since mineral trioxide aggregate (MTA), a PC based root filling material, obtained food and drug administration (FDA) approval in the late 1990's there has been an increased interest in the use of the cement for other *in vivo* applications (2-4). PCs are durable, possess high compressive strengths, set in aqueous environments such as those found *in vivo* and have demonstrated desirable tissue responses as an endodontic sealant (5-8).

Vertebral compression fractures (VCFs) are caused by the collapse of a vertebra due to diseases such as osteoporosis or vertebral myelomas (5, 9-12). Vertebroplasty is the minimally invasive surgical procedure which stabilises a fractured vertebral body by the injection of bone cement into the fracture (13). At present the cement used in the majority of these procedures is polymethylmethacrylate (PMMA) (14). PMMA has a compressive strength in the region of 80 MPa and a setting time of approximately 6.5 to 15 minutes, which permits complete immobilisation of vertebrae while the patient is in the operating theatre and allows the patient to be discharged on the same day (15, 16). However, the use of PMMA is associated with several procedural complications including the highly exothermic polymerisation of the methyl methacrylate monomer which may lead to localised tissue necrosis (17). In contrast, PCs setting reaction is only weakly exothermic and has been shown not to increase localised tissue temperature during setting (18). The toxic PMMA monomer has also been shown to diffuse from the site of application and has been linked to increased morbidity for patients through pulmonary embolism (19).

There are two key challenges which need to be addressed before PC can be considered as suitable bone cement for applications such as vertebroplasty. Firstly, it would be desirable if the cement was injectable through the aperture of a needle using a force applicable for manual injection. Secondly, the extended setting times of PC of 3-4 hour at the manufacturers standard powder-to-liquid ratio (PLR) of 3 g ml^{-1} needs to be reduced (20). There are several commercially available liquefying and accelerating additives available for PC from the building industry (21-24). However, these additives were not developed for *in vivo* use and can contain biologically harmful chemicals such as formaldehyde (25). Hence a range of non-biologically harmful chemicals will be selected from the cement chemistry literature.

1.2 Vertebral column anatomy and mechanics

The vertebral column, (spine), normally consists of twenty four separate vertebrae, together with five fused vertebrae that form the sacrum and four fused vertebrae that form the coccyx (figure 1.2.1). The separate vertebrae can be further subdivided according to their location on the spine, into (starting from the skull), 7 cervical, 12 thoracic and 5 lumbar vertebra regions (26). Vertebral sizes increase down the spinal column, with the cervical vertebrae being the smallest and the lumbar vertebrae being the largest. The lumbar region supports the majority of the bodies load during movement (27).

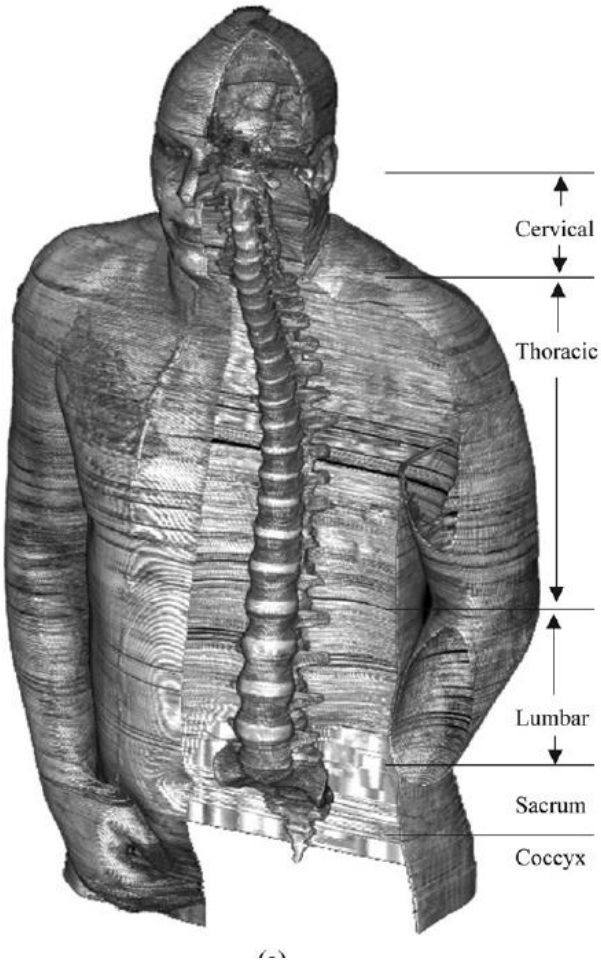

Figure 1.2.1 MRI of the vertebral column highlighting the different regions of the spine [27].

The vertebral column has many functions these include:

1. Protecting the spinal cord and spinal nerves.
2. Supporting the majority of the body weight.
3. Providing a partly rigid and flexible axis for the body and a pivot for the head.
4. Playing an essential role in locomotion (28) (26).

A typical vertebra consists of, a vertebral body, a vertebral (neural) arch and seven processes (figure 1.2.2). The vertebral body is the anterior part of the vertebra that gives strength to the vertebral column and provides support for body weight (26). The inner cores of the vertebral bodies are composed of spongy trabecular or cancellous bone and are surrounded by dense, hard cortical bone (27). This design is lighter than purely solid bone and is better suited for coping with dynamic loads as it is more flexible (29). Between the vertebral bodies are inter-vertebral discs that are largely responsible for transferring load between vertebral bodies (26).

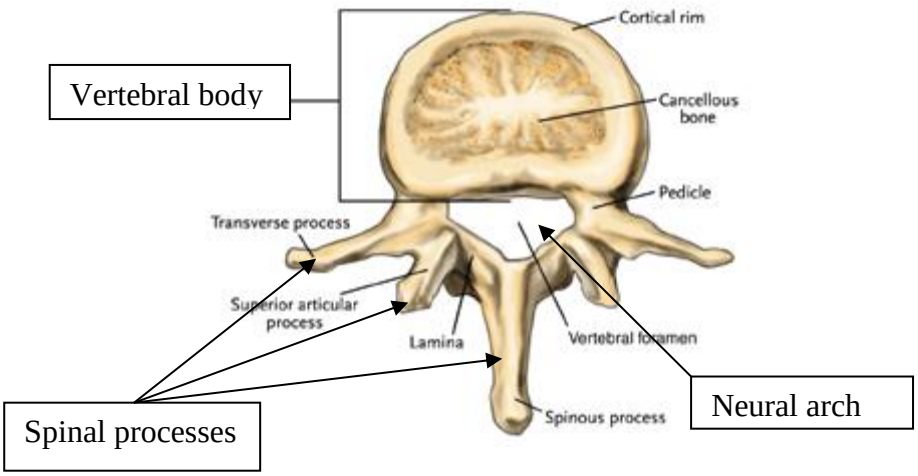

Figure 1.2.2 A typical vertebrae of the spine illustrating the vertebral body, consisting of cancellous bone the neural arch, where the spinal cord threads and the spinal processes. Adapted from (30).

The spine possesses two degrees of movement with flexion extension (forward and back) and lateral bending (side to side). Experimental compressive strength for lumbar vertebrae ranges from approximately 1.4-9 MPa (31-33). The flexural strength of vertebrae is only 1.58 ±

0.61 MPa the strength being limited by the brittle nature of the major mineral phase hydroxyapatite (31).

1.3 Predominant causes of vertebral compression fractures

Osteoporosis is defined as 'A systemic skeletal disease characterised by low bone mass and micro-architectural deterioration of bone tissue causing (trabecular thinning), with a consequent increase in bone fragility and susceptibility to fracture risk' (34).

In developed countries, osteoporosis is the leading cause of vertebral compression fractures (VCFs) (35) (36), with more than 1.4 million spinal fractures occurring worldwide each year (37). Medical annual costs in Europe and the USA alone total in excess of $1.1 billion dollars (38). Osteoporosis is predominantly an age related disease (figure 1.3.1), it particularly affects post-menopausal women. This population bias has been attributed to increased remodelling and resorption of bone, by osteoclasts, in women after the menopause (27) (39). (26% of women over 50 years old and 40 % of women over 80 years old are reported to have sustained a VCF (40) (41).)

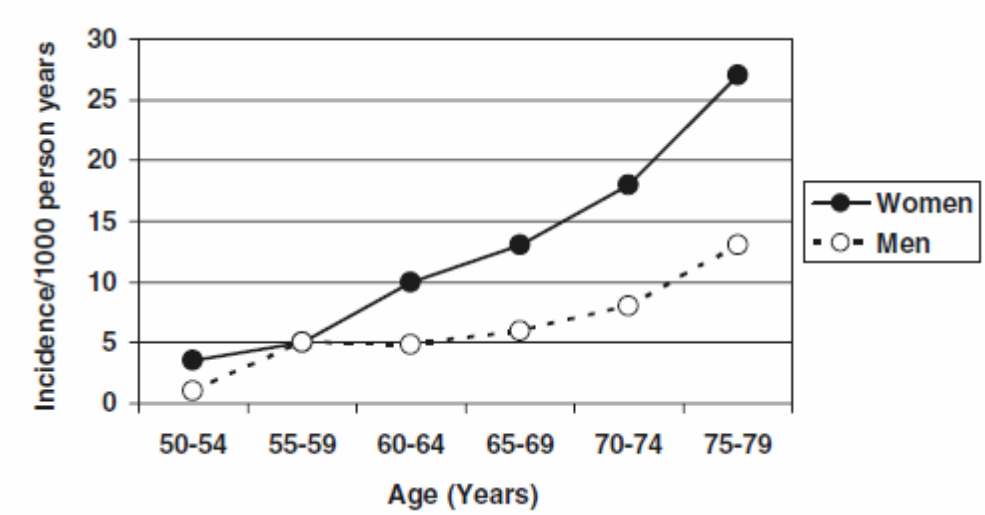

Figure 1.3.1 Graph illustrating the age related incidence of osteoporosis with increasing prevalence particularly in post-menopausal women (42).

With the rapidly aging population in developed countries, the number of osteoporosis cases are expected to increase greatly, escalating the financial burden of treatment for developed economies (43). Vertebral fractures can also be caused by vertebral myelomas and spinal sporting injuries therefore, research into an effective, safe and efficacious treatment for VCF is essential (44). The most widely used treatment for VCFs is percutaneous vertebroplasty (PVP); the procedure has changed little in over 20 years and still uses polymethylmethacrylate (PMMA) cement as the main vertebral body filler. This cement satisfactorily performs its PVP function; however, it also has many inadequacies and for improved treatments should ideally be revised or replaced.

1.4 Overview of vertebroplasty, kyphoplasty and skyphoplasty

Percutaneous vertebroplasty (PVP) and kyphoplasty (KP) are the main procedures for treatment of VCFs including those caused by osteoporotic vertebral compression fractures, spinal metastases and vertebral myelomas (45) (46). Both PVP and KP are minimally invasive surgical procedures which stabilise the fractured vertebral body by injection of a bone cement material into the vertebral fracture (47). KP varies from normal PVP at the injection stage, prior to injection of the cement a balloon is inflated in the vertebra in order to restore the vertebral body height and kyphotic angle of 8.5° (48) (49). Evidence suggests that this modified technique also reduces cement leakage which can lead to reduced cases of pulmonary embolism (50).

Lordoplasty (51) (49) and Skyphoplasty (13) are subcategories of KP in the former technique the vertebra adjacent to the fracture are also cemented and the needles are left in the vertebral body during the cement curing process. The needles can then be subsequently used as levers to try and restore the vertebral body height. Skyphoplasty uses an expanding polymer in place

of a balloon. The disadvantage with this technique is that the introduced polymer could also have toxic side effects (52).

1.4.1 Description of the vertebroplasty procedure

The patient is placed in the prone position, before being locally anaesthetised in the paraspinal muscles and periosteum (51). Under fluoroscopic guidance[1] K-wires[2] are then inserted through the paraspinal muscle and pedicles into the vertebral body holding the vertebra in place (53-55). Bore needles are subsequently inserted over the K-wires into the vertebral body, at which point the supporting wires can be removed (figure 1.4.1). The bone cement is then mixed before being injected into the fracture cavity (56).

[1] Fluoroscopy is a 4-D imaging technique which allows surgeons to view the spine and surrounding tissue in real time during the operation. It requires an x-ray source and a fluorescent screen behind the patient.
[2] A Kirschner wire (also called a K-wire) is a thin, rigid wire that can be used to stabilize bone fragments. These wires can be drilled through the bone to hold the fragments in place.

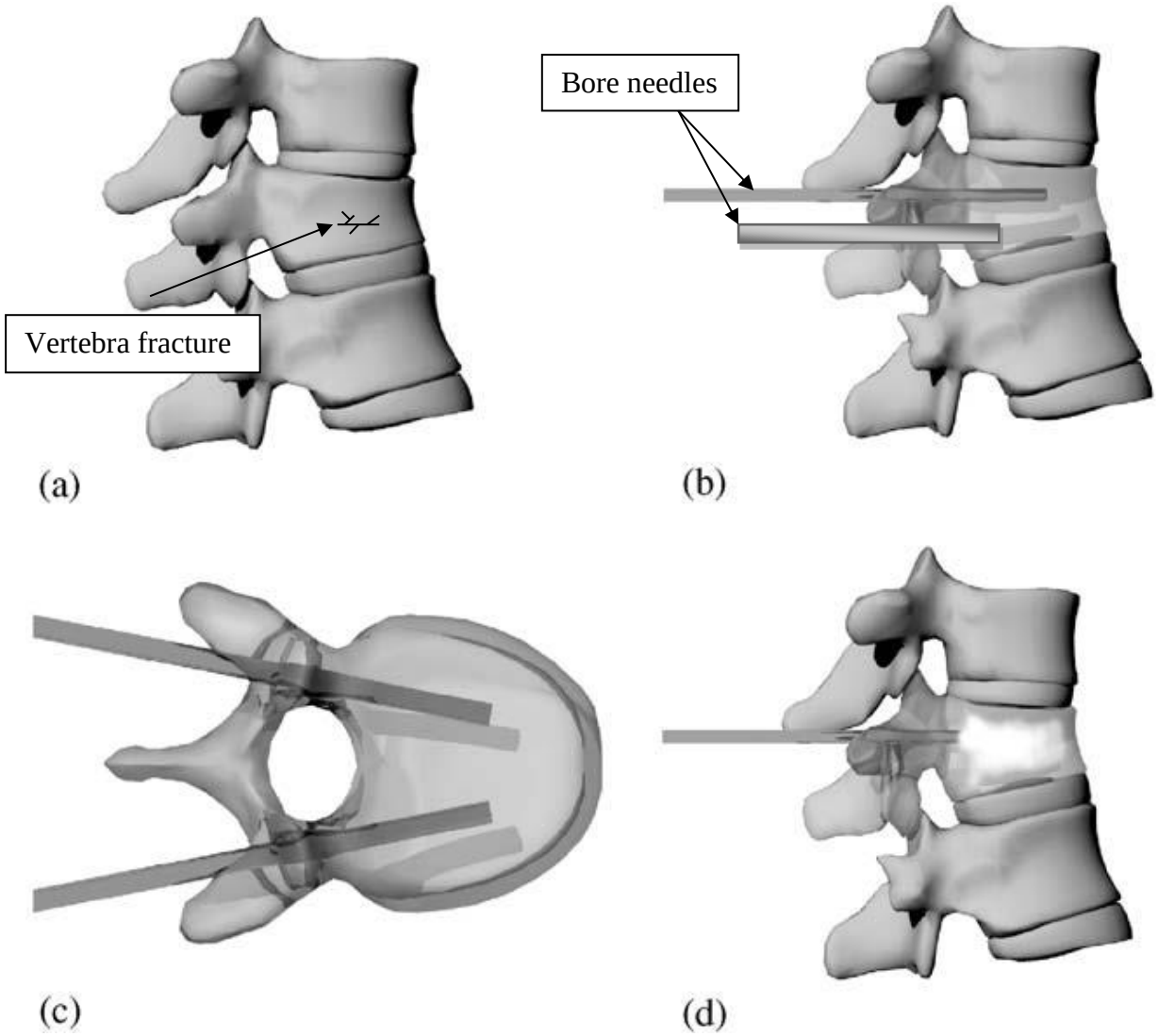

Figure 1.4.1 Adapted from [50] Diagrammatic representation of the vertebroplasty procedure depicting: (a) lateral view of the lumbar spinal segment with a compression fracture; (b) two large bore needles that are introduced in the vertebral body; (K-wires have been omitted). (c) Vertical view of the correct transpedicular needle placement (d) stabilization of the compressed vertebral body with bone cement into the fracture.

After the procedure is complete the surgeon usually prescribes bed rest for patients in a supine position for another 6 h prior to discharge.

1.5 Review of model systems used to assess efficacy of the vertebroplasty procedure

Computational, human cadaver and animal studies are presently being researched in order to discover new methods for improving the vertebroplasty procedure.

1.5.1 Vertebroplasty computational models

Kozic *et al* (57) modelled patients vertebrae based on computerised tomography (CT) scans and subsequently during the vertebroplasty procedure utilised a developed algorithm to predict real-time cement volumes in various parts of the vertebrae based on the flow rate of the surgeons syringe. The aim of the study was to devise a warning system for cement leakage which could prevent instances of localised tissue necrosis and pulmonary embolism. Widmer *et al* (58) developed a similar computational model that described the flow of acrylic bone cements in porous bone structures by considering the materials porosity and the cements rheology. The predicted final filling volume of the computational model was compared with actual volumes used during the vertebroplasty procedure and demonstrated a 17 % relative error. In the future a refined model may be used to predict 3D filling shape of the bone cement prior to surgery assisting the surgeon in assessing if any complications may arise such as cement leakage.

Rohlmann *et al* (59) composed a numerical finite element (FE) model of augmented lumbar vertebrae from CT scans in order to investigate the synergistic effect of the multiple stresses produced by bone cements. The study measured cement filling shape, cement volume and effect of elastic moduli of the bone cement on the mechanical properties of the augmented bone. The study concluded that maximum stresses in the augmented vertebral body mainly depended on the original fracture shape. Kinzl *et al* (60) also composed an FE model based on CT images of lumbar vertebrae before and after the PVP augmentation procedure. Subsequently, cylindrical PMMA/bone specimens were extracted from the augmented

vertebrae and tested in compression and axial strain measured with an extensometer. The elastic modulus was defined as the maximum slope of the stress-strain curve and yield stress calculated using the offset-method. The elastic modulus and yield stresses were then correlated with the bone volume fraction and porosities calculated from the model. There was an R^2 correlation of 0.98 between the elastic modulus of the experimental biopsies and the materials porosity leading the author to conclude that porosity was a determining factor in mechanical properties of augmented vertebrae.

Unikrishnan *et al* (61) developed a new mapping procedure to build a more accurate and precise quantitative computer tomography model (QCT). In addition to producing a mesh of the vertebrae based on CT scans the mechanical properties (e.g. material stiffness) of the vertebrae were also predicted based on bone mineral density. Since the model differentiates between materials densities it may find particular use the refinement between vertebral myelomas and hard bone tissue.

1.5.2 Vertebroplasty models based on the human cadaver

Vertebroplasty models based on the human cadaver have provided useful insights into the dissipation of heat through vertebrae and cement leakage.

Cadaver models were used to assess the temperature in various parts of lumbar vertebrae during the exothermic setting reaction of PMMA. Rodrigues *et al* (62) inserted thermocouples in the midbody of the vertebrae and after equilibration at 37 °C, 5 ml of commercial PMMA (KyphX, Medtronic, USA) was injected into the vertebrae reaching temperature's of over 75 °C. At temperatures above 70°C it was determined tissue necrosis could have occurred. Golz *et al* (63) used a cadaver model to assess localised tissue temperatures during a simulated cranioplasty procedure. As the heat dissipated from the

PMMA after injection localised tissues experienced a temperature of 50 °C, 25 °C lower than the injection site but still high enough to cause tissue necrosis.

Another cadaver model simulated cement leakage into the local arterial blood supply of vertebrae. The arterial blood supply was simulated by means of saline irrigation via 2 needles into the ventral section of the vertebral body. The authors found that PMMA injection actually resulted in trabecular fractures and the subsequent movement of the bone fragments into the spinal canal (64).

1.5.3 Vertebroplasty models based on animal studies

There are a limited number of human vertebrae for evaluating PVP augmentation procedures. Animal testing provides critical insights into PVP and forms an essential part of the clinical trials process (65).

A major problem with animal studies is that the test species are often quadrupeds with different forces being exerted on the spine than human subjects. As a consequence animal vertebrae possess altered mechanical properties to humans and may not represent an accurate PVP model. However, animals can be bred and selected for a particular disease phenotype of interest. Galovich *et al* (66) bred osteoporotic sheep and performed PVP on several vertebrae of each sheep with novel calcium phosphate cement. In over 20 % of the vertebrae the fracture site was found to be devoid of cement after sacrificing the animals which may have been caused in part by excessive cement leakage as cement escaped from the wide cancellous pores.

Animal studies also provide the possibility to obtain histological information at precise time points which in many cases cannot occur for ethical reasons in human studies. Krebs *et al*

(67) investigated the reported effect of inter-vertebral disc degeneration following the PVP augmentation procedure. The vertebroplasty procedure was performed on mature sheep which were sacrificed 6 or 12 months after the augmentation procedure. The histomorphological data indicated that there was no significant difference anatomically between the disks in contact with vertebrae containing PMMA and those which were not.

Patients are monitored for improvements in mobility after the PVP operation. However, performing the procedure on an animal with initial excellent mobility allows researchers to closely assess degradation in movements. Lu *et al* (68) monitored the effect of bone cement in a dog model. The status of the tissues adjacent to the injection site was monitored with MRI and demonstrated little inflammation. The range of movement of the dogs following the procedure was observed and found to be largely unaffected.

Animal studies also provide insights into rare human diseases such as vertebral cancers. Axelsen *et al* (69) designed an animal study to investigate tissue migration from the vertebrae to the lungs with patients suffering from spinal metastases. A labelled albumin marker was injected into the centre of each pigs L5 and L6 lumbar vertebrae prior to vertebroplasty to assess tissue migration. The study concluded that there was a significant risk of tissue migration to the lungs for vertebroplasty patients who suffer from vertebral myelomas and the procedure was not suitable for these patients.

1.6 The use of Polymethylmethacrylate (PMMA) as an orthopaedic bone cement

Polymethylmethacrylate (PMMA) is an acrylic polymer based on the methylmethacrylate monomer. It was first used clinically for cranioplasty in the Second World War and was developed into orthopaedic cement by the surgeon Sir John Charnley in the late 1950's (70).

1.6.1 Advantages and disadvantages of Polymethylmethacrylate (PMMA)

PMMA has many benefits as a vertebroplasty bone cement; it is injectable through a wide bore needle, allows the addition of radiopacifiers for fluoroscopic monitoring, has demonstrated a long-term stabilising effect on vertebrae and sets after mixing in 5-15 minutes which is considered a working time for the vertebroplasty operation (15, 71, 72).

However, there are many procedural complications associated with PVP and its related techniques. Some of these complications, such as haemorrhage, infection and increased risk of vertebral collapse (VC), are due to the surgical procedure and are independent of the type of bone cement used (19). The other main reason for complication is the use of the bone cement PMMA.

The polymerisation of methyl methacrylate is an exothermic process leading to possible necrosis of contacting tissues (44). Exothermic setting also lowers the activity of biologically active ingredients such as growth factors through their denaturation at high temperatures. The same monomer has also shown to lead to hypersensitivity, allergic dermatitis and mucosal irritation (73). The material also suffers from poor osseointegration (bonding between bone and biomaterial) (74).

The PMMA cement monomer, through radiopacity monitoring, has been shown to leak from its site of injection in the vertebra (75). The methyl methacrylate monomer is toxic and has been shown to damage osteocytes (76) and has also been linked to pulmonary embolism (19).

PMMA cement once set is a relatively inert material that does not resorb and thus will reside in the body for many years. This may pose little problem for elderly patients where the cement will probably have a clinical life span of approximately 20 years, but for younger sufferers of VCFs the high modulus cement could increase the possibility of fractures in adjacent vertebrae in later life (51).

1.7 Current developments in vertebroplasty bone cements

1.7.1 Current developments in acrylic bone cements

Given the extensive clinical history of PMMA and the probability of obtaining clinical equivalency for any future products based on the material, many researchers have used it as a starting material.

1.7.1.1 Reducing polymerisation temperature of PMMA

Reducing polymerisation temperatures to permit incorporation of biologically active drugs has been widely researched. Bone cements containing a mixture of linear PMMA with either cross-linked PMMA nanospheres (η-spheres) or microspheres (μ-spheres) were investigated as a solution for reducing polymerisation temperatures (62). The cements were injected into cadaveric lumbar vertebrae and temperatures measured by thermocouples in the midbody of each vertebrae (located halfway between the superior and inferior end plates along the intersection of the middsagittal axis). Mean curing temperatures for the η-sphere containing cement were 30 °C lower than the commercial control cement KyphX (HV-R; Medtronic, Sunnyvale, CA, USA). The 45 °C setting temperatures of the η-sphere containing cements were low enough for antibiotic encapsulation.

Xyloglucan is a highly substituted starch like polysaccharide which has been grafted onto the methylmethacrylate monomer (MMA). The grafted material has demonstrated a decreased exotherm during polymerisation compared with standard PMMA (77).

Chitosan, another polysaccharide, significantly lowered curing temperatures when used as PMMA filler. Tan *et al* (78) suggested that the large polysaccharide particles lowered the MMA concentration per ml of bone cement which may explain the lower curing temperature when the filler was present.

Carbon nanotube filling materials also lowered cure temperatures. It was proposed that the nanotubes decreased the propagation reaction speed of the PMMA free radical reaction (79, 80).

1.7.1.2 Induction of bone formation:

Osseointegration does not occur readily with PMMA. Following a vertebroplasty operation this can result in a fibrous layer of tissue surrounding the implant impairing effective load transfer with the bone (74).

Calcium phosphate cements bond well with bone and have been researched extensively as filler materials for PMMA to improve osseointegration (bone bonding). G2B1 is one of the composite cements containing β-tricalcium phosphate particles (81). Its osseointegration was evaluated by implanting the cement into the proximal tibia of a randomised group of rabbits and comparing fibrous layer around the implant build-up with a control group with ordinary PMMA implants. The histological findings indicated that the calcium phosphate containing cement contacted the bone directly with no fibrous layer of soft tissue unlike the commercial PMMA. Bone bonding strength was also significantly higher than the control after 4-8 weeks of implantation.

Arabmotlagh *et al* (82) recently investigated a similar composite material consisting of PMMA and nanocrystalline HA (70:30 v/v). The composite material and control PMMA were each implanted into opposing distal femurs of a group of 18 adult female sheep. After 3 and 6 months the femurs were histologically investigated and the composite implants exhibited “a tight junction to the surrounding bone tissue” in contrast, the control PMMA implants exhibited “fibrous connective tissue encapsulating the implant”. The group concluded that nanocrystalline HA enabled osseointegration of PMMA in bone tissue.

The structure of PMMA has also been modified to try and improve osseointegration. Surface phosphorylated poly (2-hydroxyethyl methacrylate-co-methyl meth-acrylate [poly HEMA-co-MMA]) a phosphorylated form of PMMA was investigated for biocompatibility (74). The bone cement was implanted into rabbits according to ISO 10993-6 (83) and demonstrated biomineralisation based on the mineral staining Von Kossa assay.

1.7.1.3 The addition of antibiotics to Polymethylmethacrylate (PMMA)

Biomaterial associated infections such as osteomyelitis are rare in orthopaedic procedures. However, infections do routinely occur at a rate of 1 % worldwide which creates an argument for the direct incorporation of antibiotics into bone cements in addition to the drugs being systematically administered (78, 84, 85).

Antibiotics are routinely mixed into PMMA prior to PVP in order to provide localised drug release. However, the simple incorporation of antibiotics during mixing often results in a sharp initial burst of the drug with over 90% of the antibiotic remaining trapped in the materials matrix (86). Specialised cement fillers are presently being investigated to extend the antibiotic release profile.

Lactose and hydroxypropylmethylcellulose (HPMC) are PMMA fillers that have been investigated as "antibiotic release modulators" and were found to increase quantities of gentamicin release up to four-fold compared to the commercial antibiotic containing cement (CMW1) (87).

Giavaresi *et al* (88) considered the filler material (β-tricalcium phosphate) to prolong the effect of gentamicin release and indicated the drug release profile was sufficient to prevent MRSA infection in animal studies 7 weeks after initial infection.

Wei *et al* (89) loaded clay nanotubes with antibiotic prior to the PMMA cement being doped with between 5-8 wt% of the nanotubes. The nanotubes isolated the drug from the cement monomers and served as nano-containers sustaining drug release for several weeks. The tensile strength of the composite material was also not significantly different compared with the standard cement and adhesion of the material to bone also noticeably improved. The only commercial cement with antibiotic preloaded is CMW1 (Depuy, Leeds, UK). The material contains 1 g of the antibiotic gentamicin per 40 g pack of cement. The cement has demonstrated significant reductions in localised infections in knee operations over a 2 week post-operative period to less than 2 % (90).

1.7.2 Calcium Phosphate Cements (CPCs)

Calcium phosphate cements (CPCs) have been developed to closely match the composition of bone. Examples of CPCs include; hydroxyapatite which is a naturally occurring form of calcium apatite ($Ca_5(PO_4)_3(OH)$) (91) the natural mineral component of bone and brushite ($CaHPO_4 \cdot 2H_2O$) an acidic calcium phosphate cement (92). The cements demonstrate excellent osseointegration with bone, release encapsulated drugs over weeks not hours like unmodified PMMA, do not cure exothermically and are all too some degree resorbable (51). The bone cements have been used in a variety of non-loading clinical applications such as cranioplasty, alveolar ridge augmentation and as a coating for metal prostheses.

However, in the cements native form, the mechanical properties are not suited to the transfer of physiological loads. They are inferior, in terms of both flexural and shear stress capabilities to PMMA, possess setting times in the region of 90 minutes (93) which is in excess of the 6-15 minutes permitted for acrylic bone cements and are friable (15, 94, 95).

β-tricalciumphosphate cements are also known for possessing high viscosities which lead to low cement injectabilities (96, 97).

Recent research into chemical additives has attempted to address the materials shortcomings as a PVP material. Di-sodium hydrogen phosphate accelerated cement setting times to13 ± 3 minutes and increased compressive strength strengths to 26 ± 2.4 MPa (98). Citric acid at a concentration of 800 mM increased the compressive strength of brushite cements to 51.6 ± 6.9 MPa and reduced setting times to 4.5 ± 0.5 minutes (99). Addition of the silicate mineral mullite to calcium phosphate cements created a composite which increased both the compressive and flexural strengths of CPCs to similar values to PMMA (100).

Phosphate and/or calcium ions have been added to CPCs to accelerate the setting reaction according to the common ion effect (101). Sulphates, with concentrations of 0.3M have been shown to increase the diametral tensile strength of CPCs (102). Sodium hyaluronate has shown to decrease cohesion, increasing injectability improving CPCs for PVP (103).

One very interesting new development is light cured calcium phosphate cement (LCCPCs). The cements were developed by mixing powdered tetracalcium phosphate and di-calcium phosphate with a photo-curable resin. At a powder-to-liquid (PLR) ratio of 2.8 g ml^{-1} the initial compressive strengths of the material was 80 MPa similar with PMMA. However, unlike PMMA initial cell studies indicated that the material could support proliferation of osteoblasts cultured on the surface of the material (104).

Commercial orthopaedic calcium phosphate bone cements are already available and were recently tested for both compressive and flexural strengths according to ISO 5833: 2002. Calcibon Biomet (Berlin, Germany) and Graftys HBS (Aix En Provence, France) had compressive strengths of 9.9 ± 2.5 MPa and 4.0 ± 0.4 MPa respectively and flexural strengths

of 4.3 ± 0.5 MPa and 2.1 ± 0.6 MPa respectively. These values were significantly lower than the control PMMA (Gentafix 3, Bettlach, Switzerland) with compressive strengths of 88.5 ± 0.8 MPa and flexural strengths of 54.8 ±7.4 MPa. However, the CPCs values are close to both the mean compressive strength of lumbar vertebrae 5 ± 2.3 MPa (32) and flexural strength of 1.58 ± 0.61 MPa. As discussed earlier, there is an argument that high modulus maybe negative for the long-term stability of adjacent vertebrae. However, it would appear that through the use of additives, calcium phosphate cements will play an important role in the PVP procedure.

One of the reasons for the popularity of PMMA is that it is viewed as "long-term" stabilising bone cement. To assess whether calcium phosphate produced similar long-term clinical outcomes to PMMA during vertebroplasty, 86 patients were followed up to 44 months after the initial operation (105). All patients reported decreased pain according to the visual analogue scale (VAS). Radiographs indicated complete bone union had occurred and no follow up surgery was required. In a supporting study, calcium phosphate cements were used in kyphoplasty operations, the material demonstrated the ability to significantly reduce the pain of the patient in addition to a decrease in the Oswestry Disability Index (ODI) (106). However, the study also discovered that nearly 50 % of patients suffered cement leakage into the spinal canal.

1.7.3 Filamentary composite cements

Presently the only medically approved resin based PVP materials are Cortoss and Comp06. Cortoss is composed of the matrix polymers; Bisphenol-a-glycidyl dimethacrylate (Bis-GMA) and Bisphenol-a-ethoxy dimethacrylate (Bis-EMA). Both are high molecular weight and cross-linked which provides the implants with strength and reduces leaching, Triethylene glycol dimethacrylate acid (TEGDMA) is added for improved viscosity, the accelerator Dihydroxyethyl-p-toluidine and the initiator Benzoyl peroxide (107-109).

There are also a number of reinforcing materials in Cortoss bone cement; Boro-alumino silicate glass acts as the radiopacifier, silica particles act as reinforcing particles improves mechanical strength coupled to the matrix by silica coupling agents, Combeite glass is included to improve biological compatibility (109).

There are many advantages of Cortoss as a bone cement; it has a high degree of monomer conversion decreasing the amount of leachable monomer (107), the curing process generates less heat than PMMA (108), more radiopaque than PMMA so easier to detect and minimise leaks (108), possesses higher initial compressive strengths than PMMA and tensile fatigue (109), sets in 5-8 minutes a time appropriate for PVP and is injectable (107).

However, there are several disadvantages with the bone cement. The compressive strength of the material decreases with maturation (179 MPa to 91 MPa) in 30 days. The hydroxyl groups of Bis-GMA cements contribute to water sorption leading to plasticisation of the cement matrix in time resulting in filler failure and filler matrix debonding and decreased strength (107). In comparison Portland cements strength matures over time. The exothermic reaction of Cortoss is lower than PMMA (63 °C compared with up to 90 °C respectively). Nevertheless, it is still higher than the threshold required to cause necrosis in healthy tissue (56 °C) (107).

1.8 Introduction to Portland cement (PC) and the materials use in mineral trioxide aggregate (MTA)

Portland cement, (PC), is manufactured from 60-70 wt% lime (CaO), 20-25 wt% silicon dioxide (SiO_2), 5-7 wt% aluminium oxide (Al_2O_3) and 3-5 wt% iron oxide (Fe_2O_3) (21). The components are crushed, finely ground then proportioned into the desired composition prior to heating at 1400-1600 °C to form the clinker phase (110). The hydraulic cement contains four major anhydrous phases after heating (111) including the calcium silicates, alite ($3CaO.SiO_2$) and belite ($2CaO.SiO_2$) constituting ~75 wt% of the cement clinker phase (21), tricalcium aluminate ($3CaO.Al_2O_3$) and ferrite (calcium aluminoferrite, ($4CaO.Al_2O_3.Fe_2O_3$)) contributing 5-10 wt% and 5-15 wt% respectively. The final phase gypsum (calcium sulphate di-hydrate ($CaSO_4.2H_2O$) is added at ~5 wt% to the cement after heating. PC is typically grey in colour; however, white PC is also available and is produced by increasing the cements Al_2O_3 and Fe_2O_3 content (110).

1.8.1 The hydration of Portland cement

1.8.1.1 Hydration of calcium silicates

The hydration of alite and belite forms calcium-silicate-hydrate (C-S-H) which possesses more than 30 polymeric forms, all of which have the general formula $CaO_x.\ SiO_2.H_2O_y$ (112-114). Formation of alite hydrated C-S-H occurs within a few hours after the start of cement hydration and is essential for the initial strengthening of the cement paste (Equation 1.8.1) (113). In contrast belite reacts slower and begins to form C-S-H after several days contributing to long-term cement strength (Equation 1.8.2) (110).

$$2(3CaO.SiO_2) + 11\ H_2O \longrightarrow 3CaO.2SiO_2.8H_2O + 3Ca(OH)_2$$

(Tricalcium silicate + water ⟶ calcium silicate hydrate (C-S-H) + calcium hydroxide)

(Equation 1.8.1)

$$2(2CaO.SiO_2) + 9\ H_2O \longrightarrow 3CaO.2SiO_2.8H_2O + Ca(OH)_2$$

(Dicalcium silicate + water ⟶ calcium silicate hydrate (C-S-H) + calcium hydroxide)

(Equation 1.8.2)

1.8.1.2 Hydration of aluminate phases: tricalcium aluminate

Tricalcium aluminate is a highly reactive cement phase and in the absence of calcium sulphate dihydrate (gypsum) hydrates leading to the formation of calcium aluminate hydrate (equation 1.8.3), causing premature stiffening of the cement paste without adding to the structural integrity (110).

$$3CaO.Al_2O_3 + Ca(OH)_2 + 12\ H_2O \longrightarrow 4CaO.Al_2O_3.13H_2O$$

(Tricalcium aluminate + calcium hydroxide + water = calcium aluminate hydrate)

(Equation 1.8.3)

However, in the presence of gypsum the tricalcium aluminate reacts to form ettringite, which has shown to be a set cement phase crucial in providing early cement strength (equation 1.8.4) (110, 111, 113, 115).

$$3CaO.Al_2O_3 + 3CaSO_4.2H_2O + 26\ H_2O \longrightarrow 6CaO.Al_2O_3.3SO_3.32H_2O$$

(Tricalcium aluminate + gypsum + water ⟶ ettringite)

(Equation 1.8.4)

The ettringite forms a coating across the cement matrix resulting in a reduction in the rate of cement hydration and increasing cement working time (116). Typically, in PC when all the gypsum has been consumed by the formation of ettringite, occurring after 1-2 days, the remaining aluminate will begin to react with the formed ettringite to create calcium monosulphate which possesses a lower sulphate content (equation 1.8.5) (117).

$$2(3CaO.Al_2O_3) + 6CaO.Al_2O_3.3SO_3.32H_2O + 4H_2O \longrightarrow 3(4CaO.Al_2O_3.SO_3.12H_2O)$$

(calcium aluminate + ettringite + water $\longrightarrow$ calcium monosulphate)

(Equation 1.8.5)

1.8.2 Mineral trioxide aggregate

Mineral trioxide aggregate (MTA) is a type of "hydraulic silicate cement" (118) initially developed by Torabinejad *et al* (119) as a root end filing material in the 1990's. It was the first PC based cement to obtain approval for medical use by the U.S food and drug administration agency (FDA). The materials *in vivo* effects have been extensively investigated the cement has demonstrated hard tissue induction (calcification) of connective tissue adjacent to the material (120), antimicrobial abilities (121) and the ability to stimulate genes associated with both the odontogenic (122) and osteogenic phenotypes (123). There are presently three commercially available varieties of MTA ProRoot MTA (grey and white), MTA Angelus (grey) and MTA Bio (tooth coloured). Commercial MTA differs chemically from PC with the incorporation of ~20 wt% bismuth oxide (124).

1.8.3 Properties of Portland cement in relation to its use as a PVP material

PC has many physical, chemical and biological properties that would be advantageous as a PVP cement.

- **Compressive strengths comparable with PMMA:** With a powder weight to liquid ratio (PLR) of 3 g/l for an ordinary PC, a compressive strength of 82 MPa ± 11 MPa can be achieved after 10-days of setting (125).
- **Hydraulic setting:** PC sets in an aqueous environment (hydraulic), this is crucial as blood will be present when the cement sets near the spinal tissues.
- **Durability:** PC has demonstrated long-term durability and stability which is important for non-resorbable bone cements clinical application (9).
- **Less exothermic setting:** PC has a less exothermic setting reaction, therefore avoiding problems associated with tissue necrosis. It also means inclusion of thermally labile biologically active compounds such as antibodies, hormones and growth factors are not denatured and rendered inactive (126).
- **Simple incorporation of radiopacifiers:** As outlined earlier radiopacity is important for PVP cement in order to monitor cement leakage using radiography. Barium sulphate ($BaSO_4$), lanthanum oxide (La_2O_3) and tantalum pentoxide (Ta_2O_5) can all be used as radiopacifiers for PC (124).
- **Clinical history:** PCs have been investigated for dental applications, so translation of existing knowledge is possible and is likely to improve feasibility of producing a product approved by regulatory bodies (127).
- **High alkalinity:** of PCs provides intrinsic antibacterial action but also increases cell death (128).

1.9 Overview of the cytocompatibility of Portland cement (PC) and mineral trioxide aggregate (MTA).

1.9.1 The effect of Portland cement (PC) and mineral trioxide aggregate on the proliferation and viability of cells in vitro

Scanning electron micrographs (SEM) of human marrow stromal cells (HMSC) seeded onto PC demonstrated adherence and an even spread of the cells on the material (129). Using light microscopy Human osteosarcoma cells (MG-63) were also found to adhere closely to MTA when incubated with the cement (130). Growth rates of fibroblasts and human dental pulp cells (hDPCs) in the presence of MTA have been reported to be significantly higher than indicated with controls (122, 131). However, flow cytometry indicated that the proportion of hDPCs in the DNA replication "S" phase was not significantly different between cells incubated with MTA and wells containing no cement (132). If the proportion of cells in replication phase was similar between the control and cement exposed to MTA then the growth rates should theoretically have also been similar. Primary osteoblast cells incubated with set MTA for a week have also demonstrated viability using the Trypan blue staining method (133). Calcium phosphate has also been observed on the surface of MTA confirmed independently by energy X-ray analysis (EDX) for both hDPCs and human osteoblast like cells (Saos-2) (129) (134). Mineralisation of calcium phosphate on the cements surface may indicate that the presence of the material was causing the cells to undergo osteogenesis. Osteoblastic differentiation has also been indicated by calcium deposits in wells that had contained MTA using the Von Kossa staining method (133).

The biocompatibility of PC containing cements has been attributed to several biochemical mechanisms. The cements pore solution contains a higher concentration of calcium and phosphorus ions than the culture medium and will diffuse down the gradient (3, 135). As these ions are the principal components of vertebral and dental hard tissues they have been

linked with the activation of intracellular pathways for osteogenesis and dentinogenesis (136, 137). The hydroxyapatite reported by EDX may also act as an interface between PC and cells adjacent to the material (137).

1.9.2 Osteogenic and dentinogenic properties of PC and mineral trioxide aggregate

PC demonstrated upregulation of the osteogenic gene markers vascular cell adhesion molecule-1, alkaline phosphatase (ALPase) and bone sialoprotein (BSP) when the cements were incubated for 10 days with orofacial bone mesenchymal stem cells (OFMSCs) (123). The interleukin cytokines (Il-1 and Il-6) associated with the osteoblast phenotype have also been shown to be upregulated by real-time polymerase chain reaction (RT-PCR) (130) which was confirmed using an ELISA assay (138). MTA has also demonstrated odontoblastic gene marker upregulation when hDPCs were seeded onto tricalcium-silicates in culture medium (122). There was increased expression of the odontoblastic marker genes dentine sialophosphoprotein (DSPP), dentine matrix protein 1 (DMP 1), osteocalcin (OC), alkaline phosphatase (ALP), and collagen type 1 (Col 1) (122). The expression of Mitogen-activated protein kinases (MAPK) important for odontoblastic differentiation in hDPCs has also been investigated using Western blotting which indicated the phosphorylated forms of MAPK proteins p42 and p44 were present after incubation of the DPSCs with MTA (139).

Microarray analysis indicated that there was over a two-fold up-regulation of over 100 genes when hDPCs cells were incubated with MTA (140). Some of the upregulated genes corresponded with cell adhesion such as the extracellular matrix proteins COL10A1 and FN1 which indicated that the cells may be producing proteins to bind to MTA.

1.9.3 In vivo studies

MTA was reported to induce little or no inflammation when implanted into guinea pig mandibles (8). MTA also generated only a moderate inflammatory response in subcutaneous connective tissues after 7 days in rats, by evaluating Von Kossa stained section and a scoring system to determine the level of inflammation (120). However, another study observed acute inflammation around the implant site after 2 weeks and white blood cell macrophages were present in the radicular pulp (141). After 4 weeks of an *in vivo* study in rats, MTA caused the formation of dentine bridges surrounding pulps that were capped with the material (142) and did not alter the pulp histology in rat molars containing MTA (141). A fibrous layer was detected surrounding MTA after 8 weeks of an in vivo study in rats with no evidence of inflammation, collagen or mineralised tissue deposition (143).

1.10 Challenges of using Portland cement as a percutaneous vertebroplasty material

There are several challenges that need to be addressed before PCs full potential can be realised as a PVP material. Firstly, aqueous cement systems, like PCs are prone to phase separation, leading to in-homogeneity and weakening of the cement structure (101). The possibility of phase separation is increased during the high 100 N pressure applied to the cement paste during injection.

Secondly, the setting time of the cement is 3-12 hours which is significantly longer than the 20 minutes typical for acrylic based cements used in vertebroplasty (126).

1.10.1 Improve injectability with a liquefier to prevent phase separation

Liquefiers reduce the amount of water required to mix a cement paste by 12-30% (144). Thus, aiding liquefaction of Portland cements at high PLRs. Table1.10.1 below outlines a list of PC liquefiers:

Table 1.10.1 Liquefiers and Viscosity Modifying Agents (VMA) of PC.

Admixture name/ formula	Proprietary name/ company purchase	Powder to liquid ratio (PLR) Range ($g\ ml^{-1}$)	Admixture Quantity (w/w) Range	Setting Temperature °C	Mechanism of action/ further comments
Sulfonated melamine-formaldehyde condensates (SMF)	Melement (21) (145) (increase the compressive strength). Ruredil Fluiment 33M (22) W.R Grace chem (23) Cementa 92 M (24) F,FS,G20 (146)	2.5:1 (147) 2.5:1 (23) 3:1 (24) 3:1 (146) 3:1 (145)	3% (148) 1.8-2% (149) 0.5% (21) 0.1-0.6% (147) 0-2% (23) 0.5% (24) 1-2% (146) 1% (145)	20 (148) 20 (21) 25 (24)	'Adsorption of the admixture molecules on the cement surface causes steric hindrances' (148) 'Admixture adsorbed by the cement particles act as a thin layer bringing about repulsion forces between cement particles due to negative electrical charge so that flocculation is prevented, cement particles are dispersed homogeneously in the fresh concrete.' (148)
Sulfonated naphthalene-formaldehyde condensates (SNF)	Lomar-D (21) Mighty 100 (146) NFS (145)	3.8:1 (150) 2.5:1 (147) 3:1 (146) 3:1 (145)	3% (148) 1.8-2% (149) 0.5% (21) 1-2% (146) (145)	20 (150) 20 (148)	'Retardation with naphthalene-based liquefiers at 2%' (149)
Modified lignosulfonates (MLS)	Concretan (22) Cementa P40 (24)	2.5:1 (147) 3:1 (24)	3% (148) 3% (22)	20 (148) 25 (22)	'most effective retarder 10-40 h' (147) 'Liquefiers strong polyelectrolytes

	Ligtek (146)	3:1 (146)	0.5% (24) 1-2% (146)	25 (24)	(anionic)' (23)
Polycarboxylate derivatives (151) (150)		2.5:1 (151) 2.5:1 (147)	3% (148)	20 (151) 20 (150)	'Induces cement grains dispersions as a result of both the electrostatic and especially steric repulsion generated by the long side chains.' (151) 'PC disperses cement particles with the help of steric hindrance effects that results from the extension of their graft chains away from the surface of cement particles.' (150) 'Polycarboxylate liquefier was much more intense in calcium aluminate cements.' (151)
Methylcellulose (126)	Sigma Aldrich (126)	3:1 (126)	1% (126)	20 (126)	'Used in conjunction with $CaCl_2$ ' (126)
High molecular wt hydroxylated polymer (152)	Viscosity Modifying Admixture (152)		0.05-0.15% (152)		
Citrate (102)	Haneseler, Switzerland (102)			23 (102)	A calcium phosphate cement liquefier.
sodium hexaphosphate (153)		2.5:1 (153)	1-2% (153)	23 (153)	A calcium phosphate cement liquefier

Many of these additives in table 1.10.1 are used in the building industry in, 'self-levelling cements', where the biological effects of the chemical constituents are not considered. However, the formaldehyde monomer in both SMF and SNF could prove to be acutely toxic if extravasation occurs during PVP (154). Therefore, these two liquefying agents will be discounted from the study.

A second problem with the liquefiers is the use of 'black box' formulations. It is difficult to deduce the exact chemical formulation of, 'Polycarboxylate derivatives' and many authors have had to utilise advanced analytical techniques in order to decipher complex proprietary formulations (150). Thus, one of the aims of the project will be to use only liquefiers where the full chemical formula of the compound is known.

Unfortunately, the liquefier additives often have a dual functionality, they can act as both liquefiers and 'retarders' increasing the setting times of the PC by as much as 40 h (e.g. MLS) (147). Liquefiers are highly charged anionic species which bind and adsorb onto the surface of the PC constituents. Binding results in both electrostatic, and due to the large size of the polymeric liquefiers, a steric repulsion. This disperses cement aggregates leading to the liquefying effect, although it also leads to a reduction in the reaction rate of the cement with water leading to slower reaction kinetics, thus causing cement setting retardation (148).

1.10.2 Decreasing setting times of Portland cement

There are many chemically simple, setting accelerators, available from the building industry, see table 1.10.2. Many of setting accelerators increase the formation of C-S-H bonds contributing to long term strength of the PC. This combination of accelerated setting and hardening is essential for supporting the vertebral column shortly after the PVP operation is completed.

Table 1.10.2 Various Portland cement accelerators and their properties

Accelerant name/ formula	Proprietary name/ company purchase	Powder to liquid ratio (PLR)	Accelerant Quantity (w/w)	Setting Temperature (°C) Portland cement + accelerant	Setting times (minutes)	Compression Strengths (MPa)	Accelerant Mechanism of action
$Al_2O_{3(s)}$=17% $SO_{3(s)}$=40% (155) $Al_2O_{3(l)}$ Refer table 1 (156) $NaAlO_2$ (157)	Mapequick AFK 777 by Mapei (155) Not Stated (156) Strem Chemicals (157)	3:1 (155) 3.5:1 (156) 1:1 (157)	7% (155) 3.8% (156)	32 (155) Not Stated (156) 20 (157)	10-150 (155) 120 (156)	Not Stated (155) 0.31 (20 minutes) (156)	Al^{3+} and SO_4^{2-} ions interact with C_3A and Ca^{2+} to form ettringite (158) $NaAlO_2$ accelerates the hydration of alite and belite which results in long C-S-H phases. (157)
Calcium Chloride ($CaCl_{2(s)}$) (126)	Sigma Aldrich (159)	3:1 (126)	2% (126) 2% (160) 5% (159)	37 (126)	83 (126) final 100 (160) final 32 (159) initial	35.6 (24h) (126) 62 (7 days) (160)	$CaCl_2$ increases heat evolution during early hydration (126)
Calcium Nitrite/ Nitrate $CaNO_3$ (25-50%) (159)	DCI corrosion inhibitor (159)	3:1 (159) 3:1 (161)	Not stated (159) 1% (161) 1% (162)	20 (161) 20 (162)	7 (159) 125 (161) 125(162) Initial and 195 final	Not stated (159) 27 (After 1 day) (161)	Calcium nitrate effects have been linked to the belite content of the Portland Cement (162).

Calcium Formate ($CHOO^-$) (159)	Target Set Accelerator (159)	3:1 (159)	20% (159)	20 (159)	10 (159)	Not Stated (159)	
Triethanolamine (TEA) $N(CH_2CH_2OH)_3$ (162)	Not stated (162)	Not stated (162)	0.05% (162)	20 (162)	150 (162) Initial and final 235	28 (162) (After 1 day)	
Trisopropanolamine (TIPA) $(CH_2CH_2\ CH_2\ OH)_3$ $[C_9H_{21}O_3N]$ (162)	Not Stated (162)	Not Stated (162)	0.05% (162)	20 (162)	140 (162) Initial and final 210	32 (162) (After 1 day)	
Oxalic Acid ($H_2C_2O_4$) (163)	Not Stated (163)	3:1 (163)	4% (163)	20 (163)	65 (163) Initial and final 100	37.13 (163) (After 1 day)	Anionic binding
Calcium Carbonate ($CaCO_3^{2-}$) (156)	Proprietary Powder (156)	Not Stated (156)	10% (156)	Not Stated	13.1 (156) Initial and final 72.5	0.38 (156) (After 20 minutes)	
Sodium phosphate monobasic (Na_2HPO_4) (164) Sodium phosphate dibasic ($Na_2H_2PO_4$)	JT baker (164)	3:1 (164)	10% and 15% (164)	37 (164)	26 (164) 33 (164) dibasic	-	
Calcium Acetate (165)			2% (165)				Acts as both an accelerator and liquefier

In the literature many of these hardening accelerators have been used in conjunction with each other and have shown a synergistic relationship (162). In addition, various accelerators e.g. $CaCl_2$ have been used in conjunction with liquefiers and the setting times recorded (160).

1.11 Project Aims:

The initial aim of the project will be to develop an injectable PC that can pass through a 2-4 mm needle without the occurrence of blockages at a force that is applicable for manual injection. A customised holder for the syringe and needle will be designed and produced. Injectability of PC without any liquefying agents will then be tested at a range of powder-to-liquid ratios (PLRs) to investigate whether by adding more water to the cement, it is possible to significantly increase cement extrusion from the syringe. Previous research has indicated that powder based cements such as calcium phosphates suffer from phase separation of the powder from the liquid phase during injection and a liquefiers may limit this separation (166). Injectability of PC at different rates of plunger depression will be assessed during the current study and compared with the manual speed of injection of spinal surgeons performing the vertebroplasty operation. If liquefiers are required for injection, the optimum method of delivery in either the liquid (water) or solid (cement) phase will also be determined. During the initial stages of the project, X-ray diffraction will be used to assess the effect of filtering cement (aggregate removal) and cement batch aging.

A range of liquefying additives and setting accelerants will then be studied for their effect on cement injectability and influence on cement setting time. The material properties of the additives on the compressive strength, porosity and density of the cement will be tested concurrently with the injectability and setting time experiments. The cements will be characterised with scanning electron microscopy (SEM) (surface morphology), energy dispersive X-ray spectroscopy (EDS) (elemental analysis), X-ray diffraction (XRD) (phase analysis), Zeta potential measurements (charge analysis) and differential scanning calorimetry (DSC) (heat evolution of the cement).

A bespoke porous vertebral model to test percolation of the cement within the vertebrae will be created in collaboration with Bath University. A universal testing machine will provide force on a piston connected to a chamber containing PC which will be injected into a synthetic bone substitute (sawbone). The pressure drop during injection will be recorded with a monitor and assessed against commercial acrylic cement. Subsequently, the synthetic bone model will be replaced by a section of sheep vertebral cancellous bone and the pressure drop during injectability retested. The rheology of the final cement will be investigated using a parallel plate rheometer and Micro-CT (μ-CT) will be investigated as a technique for assessing phase separation of PCs during injection.

Following the development of appropriate injectable cement, the biological responses of primary osteoblast and bone marrow cells will be assessed according to the cells ability to colonise the cements, along with the subsequent growth, proliferation and differentiation on these materials. Mineralisation of calcium species by osteoblasts exposed to PC will be assessed by incubating cells exposed to the cement for 14-days with Alizarin red stain. The expression levels of genes associated with the osteoblast phenotype including osteoadherin (OSAD), alkaline phosphatase (ALPase), bone morphogenic protein (BMP) and bone sialoprotein will be studied by reverse transcriptase PCR (RT-PCR).

CHAPTER 2: MATERIALS AND METHODS

2 MATERIALS AND METHODS

2.1 Materials and methods for chapters 3.1-3.5

2.1.1 Materials

Portland cement (Mastercrete, Lafarge, UK) was initially passed through a 500 µm steel mesh sieve (Endecotts Ltd, UK) to remove agglomerates present in the powder phase. In chapter 3.2 the additives sodium chloride, sodium aluminate, sodium hexaphosphate, calcium acetate, methyl cellulose, calcium sulphate dihydrate, calcium carbonate and oxalic acid (Sigma, UK) were added at between 2-10 wt% into the powder phase and mixed by vortexing (Miximatic, Jensons, UK). In chapter 3.3 the additives calcium chloride and calcium nitrate (Sigma, UK) were added at between 5 and 10 wt%. In chapter 3.4 sodium citrate, potassium citrate, calcium citrate and citric acid (Sigma, UK) were added at between 0.5 to 5 wt%. Finally in chapter 3.5 Bismuth oxide was added at 10 wt% to the cement (as indicated) (Sigma, UK). Filtered reverse osmosis water (5 µm filter, Aquarium Solutions, UK) was added at a powder-to-liquid (PLR) of 5.0 g ml^{-1} (unless otherwise stated) and samples were hand mixed for 1 minute to produce cement slurries.

In the chapter 3.1 the sieve mesh size was varied between 45-500 µm, the additives were mixed in the liquid phase (Vortexer, Jensons, UK) prior to adding to the powder phase and the powder to liquid ratios were varied between 3 and 5 g ml^{-1}.

2.1.2 Injectability testing

Five grams of PC slurry were transferred into a 5 ml disposable syringe (Starstedt, UK) and extruded through an outlet diameter of 2 mm (for each additive addition n=4). A mechanical testing machine (Instron 1185, High Wycombe Bucks, UK) was used to apply a cross-head

speed of 30 mm min^{-1} (3-30 mm min^{-1} in chapter 3.1) and the maximum force to the syringe plunger was restricted to 100 N. The force and crosshead speed were selected to mimic the maximum force and typical rate of extrusion used during manual injection (based on communications with surgeons) (167). The amount of cement remaining within the syringe was weighed and the injectability (I) was calculated according to Equation 2.1.1:

$$I\ (wt\%) = \frac{mass\ of\ cement\ paste\ injected\ through\ syringe}{original\ mass\ of\ cement\ in\ syringe} x\ 100$$

(Equation 2.1.1)

2.1.3 Setting time

The initial setting times of the cements were measured in a temperature controlled laboratory environment (20–23 °C and 50–60 % humidity) using the Gilmore needles test. After mixing (section 2.1.1) each individual cement slurry (n=3) was poured into a cell culture well (BD Falcon, UK) with a surface area of 3 cm^2 which provided an adequate surface area (and thickness of the cement paste) to observe needle indentation on the setting cement surface. At 3 minute intervals the Gilmore needle (0.21 mm, mass 113.4 g) was indented into the cement paste and assessed for setting in accordance with ASTM standard C266-99 (168).

2.1.4 Compressive strengths

After sample preparation, the cement pastes were cast into cylindrical Polytetrafluoroethylene (PTFE) moulds (6mm diameter, 12mm height) and left to set for 6h at 37°C in a drying oven (Laboratory thermal equipment, UK) before removal from the moulds and storage in distilled water at 37°C for a further 1 or 30-days. After storage the wet samples were weighed and the dimensions measured with a digital Vernier (Linear Tools, UK). The wet compressive strengths (CS) of the cement samples (n =30 per sample set) were then measured using a Universal testing machine (Instron 5544, Instron, UK) at a cross-head speed of 1mm min^{-1}. CS values were calculated using the following equation:

$$CS = \frac{L}{A} = \frac{L}{\pi.\left(\frac{d}{2}\right)^2}$$

(Equation 2.1.2)

CS= Compressive strength (MPa) A= Cross-sectional area (mm^2) of cylindrical sample,

L= Load (N), d= Diameter (mm)

2.1.5 Calculating the dry densities of the cement samples

Fragments obtained following the compressive strength testing were collected, weighed and then dried in a desiccator containing calcium chloride (Nalgene, UK) until the weight of the samples remained constant. Wet densities (ρ_{dry}) were determined by dividing the individual wet weight (W_w) by the respective sample volumes.

The dry densities of the cement samples were then calculated using the following equation:

$$\rho_{dry} = \frac{W_D}{W_W} x\ \rho_{wet}$$

Equation 2.1.3

ρ_{dry}= Apparent dry density (g cm^{-3}) W_D= Dry weight of fragments (g)

ρ_{wet}= Apparent wet density (g cm^{-3}) W_W= Wet weight of fragments (g)

2.1.6 Calculating cement relative porosities

After drying of the compressive strength fragments the materials' strut densities were measured in a helium pycnometer (Accupyc 1330, Micromeritics, USA). The relative porosities of the cement samples were then calculated using the following equation:

$$RP = 1 - \frac{\rho_{dry}}{\rho_{strut}}$$

(Equation 2.1.4)

ρ_{dry}= Apparent dry density (g cm^{-3})

ρ_{strut}= Strut density (g cm^{-3})

2.1.7 Biaxial-flexural strengths

The hand mixed slurries were poured into PTFE split moulds producing 30 nominally identical disc-shaped specimens (12 mm diameter by 2 mm thickness). The samples were set for 24 h at 37 °C, removed from the split moulds and subsequently immersed in water at 37 °C for 29 days.

The bi-axial flexure strength of the disc-shaped specimens was determined by generating a central load (using a 4 mm ball indenter) on a 10 mm knife-edge support at a cross-head speed of 1 mm min^{-1}. The samples were loaded using a universal testing machine (Instron 5544, Instron, England) and the fracture load for each disc recorded. The biaxial flexure strength was calculated according to Eq. 2.1.5 (169)

$$\sigma_{max} = \frac{P}{h^2}\left\{(1+v)\left[0.458 \times \ln\left(\frac{a}{h}\right) + 0.52\right] + 0.48\right\}$$

(Equation 2.1.5)

σ_{max} was the maximum tensile stress (MPa), P the measured load at fracture (N), a the radius of the knife-edge support (mm), h was the sample thickness (mm) and v, the Poisson's ratio for the material. The Poisson's ratio of a material is defined as the lateral contraction per unit breadth divided by the longitudinal extension per unit length (169) and a value of 0.160 was substituted for Portland cement (170). The sample thickness was measured at the point of fracture for each disc-shaped specimen using a micrometre screw gauge (Moore and Wright, Sheffield, England) accurate to 10 μm.

2.1.8 Scanning electron microscopy (SEM)

Dried cement fragments were attached onto an aluminium stub with a conducting electrodag 1415 paste (Agar Scientific, Stanstead UK) before being gold sputter coated (Emitech K550X, UK). A scanning electron microscope (SEM) (JEOL 7000F, Japan) was then used to image the samples at an accelerating voltage of 20kV capturing images at 2000-8000x magnification.

2.1.9 Energy dispersive X-ray spectrophotometer (EDX)

Backscattered X-rays emitted by the elements on the surface of the cement, after irradiation with a beam of electrons were collected and recorded by a detector (Inca, Oxford instruments, UK) before analysis of the elemental composition using Software CMax (Wycombe, Bucks). The software assigned both a weight % (wt%) and an atomic % for each element present. The wt% ratio of each element pair (e.g. Ca/O or Ca/Fe) was then calculated and compared with theoretical compounds known to be present during cement hydration using the following equation (see appendices):

$$Percentage\ difference\ of\ observed\ vs\ theoretical\ compounds$$

$$= 1 - \left(\frac{observed\ ratio}{theortical\ ratio}\right) \times 100$$

(Equation 2.1.6)

2.1.10 X-ray diffraction (XRD)

X-ray diffraction patterns of the set cements were recorded using a D8 Advance diffractometer (Bruker, Germany). Data sets were collected from 2θ = 5-20 ° with a step size of 0.02 and the count time was normalised to 1 s step^{-1}. The phase compositions of the

cements were determined according to the inorganic crystal structure database, calcium hydroxide (PDF Ref. 04-010-3117), calcium silicate (PDF Ref. 04-011-1393) and ettringite (PDF 00-041-1451). The calcium silicate hydrate (CSH) standard was supplied by Supleco analytical (UK).

2.1.11 Zeta-potential measurements

The effective surface charge of PC with various additives was measured using a Zeta-Sizer Delsa-Nano Z (Beckman-Coulter, UK). Suspensions of 0.1 g l^{-1} Portland cement were produced just prior to the zeta-potential measurements. Sodium and potassium citrate were added at 0.2 g l^{-1} to the PC solutions resulting in an excess of anions to bind with the PC particles. The Zeta-Sizer calculated the zeta-potential by determining electrophoretic mobility using Henry's equation (171). For each suspension, the average zeta-potential value was obtained from 5 measurements.

2.1.12 Fourier transform Infrared (FTIR)

One gram of newly mixed PC was placed on the diamond window of an attenuated total reflectance (ATR) FTIR (Nicolet 6700, Thermo scientific) set to either 23 °C or 37 °C and covered with a glass slide with spectra recorded at 0 and 60 minutes. At each time point the samples were scanned 32 times with a resolution of 2.0 cm^{-1}.

2.1.13 Differential Scanning Calorimetry (DSC)

Eighty to one 120 milligrams of cement paste was transferred to an aluminium crucible before being inserted into the sample compartment of a differential scanning calorimeter

(DSC 7, Perkin-Elmer, UK). The enthalpy change of the cement was then recorded for the proceeding 2 h and calculated by integrating the DSC-curves from the heat capacity base line using the Pyris^{TM} DSC software (n=3 for each variation).

2.1.14 Statistical analysis

Data sets derived from the injectability, setting time, compressive strength, cement specific densities, zeta potential measurements, calorimetry, biaxial flexure testing and biological growth curves were tested for normality prior to further analysis (Kologorov-Smirnov). For normally distributed data sets, comparisons of group means were achieved utilising statistical tests appropriate to the experimental design and included, one-way analysis of variance (1-way ANOVA) two-way analyses of variance (2-way ANOVA) and three-way analyses of variance (3-way ANOVA) tested at a 95 % significance level. A statistical software package SPSS for Windows 19.0 supplied by IBM, UK was utilised in the current investigation.

In addition, as ceramic materials contain flaws which can vary significantly in size, orientation and severity, strength is often expressed in terms of failure probability. Weibull (172) developed a statistical theory to analyse failure probabilities that enabled the prediction of survival rates at different stress levels, allowing comparison of the relative performance of different materials. The Weibull approach assumes a weakest link principle whereby the strength of a body is determined by the products of the survival probabilities of the individual elements and the most critical flaw in a specimen is responsible for its failure. The Weibull distribution for a body failing under tensile stress and can be expressed as:

$$P_f = 1 - \exp\left[-V\left(\frac{\sigma - \sigma_{min}}{\sigma_0}\right)^m\right]$$

(Equation 2.1.7)

Where σ is the applied stress failure (MPa) and σ_{min}, σ_0 and *m* are the Weibull m are the Weibull parameters. The Weibull modulus (*m*) characterises the brittleness of a material (173) and reflects the shape parameter of the Weibull probability density function describing flaw size and distribution and therefore the resultant scatter and associated reliability of the flexure strength data. σ_{min} is the threshold stress occurring when the failure probability approaches zero and σ_0 is the characteristic stress and is the scale parameter of the Weibull distribution.

In the current investigation bi-axial flexure strength data was ranked in ascending order and a Weibull analysis performed on the resultant data by plotting ln ln $(1/P_s)$ against lnσ. The gradient *m* was calculated by superimposing a regression line along the data points to provide the Weibull modulus for each group of specimens tested. To determine statistical differences between the Weibull moduli of the flexure strength data the 95 % confidence intervals for the specimen groups under investigation were calculated by least squares regression analysis (using excel). The differences in Weibull modulus of the flexure strength data was considered to be significantly different when the 95 % confidence interval failed to overlap. Confidence in the linearisation of Weibull data was reflected by R^2 values and the range of the 95 % confidence intervals. The Weibull distribution is employed to provide improved validation of the fracture strength data rather than depending on the average fracture strength.

2.2 Materials and methods for chapter 3.6 (Investigating the rheology and injectability of Portland cement)

2.2.1 Materials

Portland cement (Mastercrete, Lafarge, UK) was prepared according to section 2.1.1. Sodium citrate (Sigma, UK) was added at 2 or 5 wt% into the powder phase of the cement and mixed by vortexing (Miximatic, Jensons, UK). The liquid phase was added to the cement at a powder-to-liquid (PLR) of 5.0 g ml^{-1} and samples were hand mixed for 1 minute to produce cement slurries. Bismuth oxide 10 wt% was added to the samples for µ-CT scanning.

2.2.2 Dynamic viscosity measurements using a plate rheometer

Viscosity measurements were performed at room temperature (23°C +/- 1°C) using a rotational parallel plate rheometer (Malvern Instruments Ltd, UK) using 30 mm plates separated by a 2 mm gap. Gap size was chosen based on previous investigations of large-particle size suspensions which indicated that the "gap-to-particle size ratio" should be at least 10:1 (174). The largest particle size of PC was approximately 200 µm (175). The complex viscosity (Pa.s) was measured at constant strain amplitude of 0.06 with a rotational frequency of 0.3 Hz.

Cements were initially mixed at 0 minutes and then tested for viscosity at 0, 10, 20 and 30 minutes (n=3). The PC standard was stored in the mixing vessel. In contrast, the 0 and 10 minute replicates of citrate were added to 5 ml syringes and tested using the rheometer at the appropriate time points. The 20 and 30 minute samples were added directly to the rheometer at time 0 as it was not possible to extrude the cement containing 2 wt% citrate from the syringe after 20 minutes.

2.2.3 Injectability of Portland cement through a 5cm needle

The injectability experiments were performed in accordance with section 2.1.2. For injectability testing requiring a needle the Luer ™ lock fitting system on each of the disposable syringes was used to attach a 5 cm long 11 G needle.

2.2.4 Micro-CT

2.2.4.1 Standard preparation

The slurries were cast into PTFE moulds producing cylindrical samples with 3mm height and 6mm diameter. The samples were stacked vertically starting with PLR 5.0 g ml^{-1} and decreasing to PLR 2.5 g ml^{-1} in 0.5 g ml^{-1} intervals (n=3 stacks)

2.2.4.2 Testing pressure drop during injection

Sawbone (Pacific research laboratories, USA) was drilled into 3 cm by 6 cm shapes using a pillar drill (Sealey SDM 30, UK).

PC slurry (100 ml) was loaded into a 120 ml piston chamber connected to a universal testing machine (Instron 5544, Bucks, UK) used to control flow rate. The cement was injected from the chamber into a sealed injection compartment containing the sawbone model. A pressure monitor (FPM 100, Maretron, USA) was used to assess the pressure drop during injection

2.2.4.3 Creation of artificial fractures in sheep and porcine vertebrae

A universal testing machine (Instron 5544, UK) was used to artificially create a fracture in the posterior lumbar vertebra of both a sheep and pig. Five grams of cement paste was manually injected into the fracture using an 11 G needle.

2.2.4.4 Micro-CT imaging

A high resolution micro-CT (Skyscan 1172, Belgium) was used to image the standard cements and vertebral models. The samples were secured on the rotating central stage and imaged by the scanners 11 MP camera. The fine detail resolution of the images was 13.59 µm the source voltage was set at 80 kV and the source current at 100 uA. The images were recorded on the Skyscan control software (Skyscan, Belgium) in TIFF format at 8 bit depth. Reconstruction of the 3D image was performed with N-Reconn (Skyscan, Belgium) and Fiji (Open source, international free license). Each individual pixel in the standard cement images was assigned a grey scale value from 1 to 250. These values were then plotted as a percentage of total pixel number.

2.3 Materials and methods for chapter 3.7: Investigating the cytocompatibility of Portland cement

2.3.1 Cement sterilisation

Portland cement (Mastercrete, Lafarge, UK) was prepared according to section 2.1.1 before being heat sterilised in an oven (BRF 16/5, Elite, UK) at 180 °C for 2 h. Sodium citrate, calcium chloride and calcium nitrate (Sigma, UK) were added at 2 or 5 wt% into double distilled water which was then autoclaved. The liquid phase was added to the cement at a powder-to-liquid ratio (PLR) of 5.0 g ml^{-1} and samples were hand mixed for 1 minute to produce cement slurries. The slurries were cast into PTFE moulds, under aseptic conditions in a laminar flow hood, producing cylindrical samples with 3mm height and 6mm diameter. The samples were incubated at 37 °C in a universal test tube then removed at the following time points 0.3, 1, 3, 6, 12 and 24 hours. The cements set for 6 h after removal were incubated in water for a further 18 h.

2.3.2 Media preparation

Minimum essential medium (alpha modification) (all reagents in this section were from Sigma, UK) was used as the basis of both the growth and transport medium. Growth medium was supplemented with 1% penicillin/ streptomycin (100 unit's ml^{-1} of penicillin with 100 µg ml^{-1} streptomycin), 2.5% HEPES buffer and 10% (v/v) foetal calf serum (FCS). Transport medium contained 10 % penicillin/ streptomycin with 1 % amphotericin.

2.3.3 3T3 fibroblast cell line

The 3T3 cells were defrosted from liquid nitrogen (BOC chemicals, UK). Based on the fibroblast cell line initially established in 1962 (176) and seeded in 25 ml of media (alpha modification). The cell line was selected due to its comparatively short doubling time (1.5 days per cell cycle) compared with stromal cells. The cell lines are also more resistant to changes in extracellular conditions (176) making them ideal as an initial cell line to investigate pH change.

2.3.4 Bone marrow stromal cell extraction

The femora of young adult albino Wistar (250 g) male rats were extracted for bone marrow stromal cells (BMSC) using an established method (177). A surgical scalpel (Swann Morton, Sheffield, UK) was used to cut through the rats epidermis to gain access to the underlying connective tissues from which the femora were removed. Femora were stored in a petri dish containing transport medium and the remaining soft tissues cleaned away using a scalpel and forceps. Sterile wire cutters were used to remove the epiphyses of the femora. An 18 gauge needle (Tyco healthcare, Northern Ireland) was used to flush the marrow cavity using growth medium. The BMSCs cells were then pelleted using a centrifuge (Thermo, Durafuge 100) at 1200 rpm for 3 minutes and transferred to a T-75 tissue culture flask and incubated at 37°C, in an atmosphere of 5% CO_2 (IG150, Jouan, UK) until the flask was approximately 80-90% confluent.

2.3.5 Incubation of cells with the setting cement

0.1 M phosphate buffered saline, PBS (Sigma Aldrich, UK) was used to remove any non-adherent or dead cells from the surface of the T-75 before 5 ml of Trypsin/EDTA 0.25% (w/v) (Sigma, UK) was used to detach the confluent cell monolayer. Once detached, an equal volume of supplemented α-MEM containing 10% FCS was added to neutralise the enzyme. After centrifugation the supernatant was removed from the pellet, discarded and replaced with growth medium. At the time points outlined in section 2.3.1 the cements were removed from the moulds and aligned in the centre of a 35 mm petri dish. Three millilitres of growth medium was then added to each well before 3×10^4 cells (bone marrow cells) or 5×10^3 cells (3T3 fibroblasts) were seeded directly on top of the cements. At 2-day intervals the culture dishes were viewed using a phase contrast microscope (Flovert, UK) and imaged using a digital camera (Coolpix, Nikon, Tokyo, Japan). For each type of cement in the experiment three petri dishes (n=3) were harvested at 0, 1, 3, 5, 7, 9 and 11 days or at 0, 2, 6, 8 and 10 days using 2 ml of trypsin (including the cement in the well). After centrifugation the trypsinised cells were resuspended in 1 ml of growth medium. Cell suspensions were mixed with an equal volume of 0.2 % trypan blue before counting using an improved Neubauer haemocytometer (Agar Scientific, UK) viewed with a phase contrast microscope (Zeiss, Germany) to determine cell numbers and viabilities.

2.3.6 Investigating gene expression with RT-PCR

2.3.6.1 Experimental set-up

Two sets of disc cement samples (n=24) of 3 mm height and 6 mm diameter containing 2 wt% of the accelerant sodium citrate were set for 1 and 12 hours respectively. The samples were aligned in the centre of a 35 mm petri dish (Sarstedt, USA) to which 3 ml of growth medium was added before seeding with 1 x 10^5 mesenchymal bone marrow stem cells (passage 1) on top of the cement and incubated at 37 °C for 5 days, whilst controls contained no cement.

2.3.6.2 Isolation of RNA

After the incubation period each 35 mm petri dish (Sarstedt, USA) was washed with 1 ml of PBS before being treated with 350 µl of lysate solution (Buffer RLT, Qiagen, Rneasy Kit, UK), containing 10 µl of beta-mercaptoethanol (Promega, UK). Each lysate was homogenised for 30 s using a 21 gauge needle (Terumo, UK). An equal volume of 70 % ethanol (Sigma-Aldrich, UK) was then added to each homogenised lysate and mixed on a vortexer (Vortex genie 2, Scientific Industries, USA) for 10 s. Each sample was transferred to an RNA binding spin column (Rneasy, Qiagen, UK) with a 2 ml collection tube and centrifuged for 30 s at 10,000 rpm (eppendorf centrifuge 5415D, UK). The flow-through was discarded before 350 µl of wash buffer (RW1, Qiagen, UK) was added to the column before a second round of centrifugation at 10,000 rpm for 30 s. A Dnase I digest mix produced by adding 10 µl of Dnase I (Qiagen, UK) to 70 µl of Buffer RDD (Qiagen, UK) was added directly to the columns membrane followed by a 15 minute incubation period. A 350 µl aliquot of another wash buffer (RW1, Qiagen, UK) was then spun through the column at 10,000 rpm for 30 s followed by two times 500 µl of a third wash buffer (RPE, Qiagen, UK)

at 10,000 rpm for 1 minute. The column was then placed in a new collection tube and spun at 14,000 rpm for 1 minute to extract the remaining buffer. The column was finally placed in a 1.5 ml collection tube to which 30 µl of RNase free water was added and spun for 10,000 rpm for 1 minute to elute the RNA.

2.3.6.3 RNA quantification

The RNA was diluted 1:35 before single stranded RNA concentration was measured using a UV/ visible spectrophotometer (Eppendorf Biophotometer, Germany) at 260/280 nm.

2.3.6.4 RNA visualisation

TAE buffer (Fermentas, Lithuania) was diluted 1:50 with RNase free water (Qiagen, UK). A 1 % agarose gel was made by adding 0.7 g of agarose (Web Scientific, UK) to 70 ml of TAE buffer stock. The gel was then heated for 2 minutes in a microwave (Samsung 850W, Germany) to melt the agarose, 3 µl of SYBR gold stain (Invitrogen, UK) was added before the agarose was set in a Perspex mould. The set gel was then transferred to an electrophoresis tank (Consort 132) filled with TAE buffer stock. Five microlitres of RNA was loaded into each well and a DNA ladder (PCR Ranger, Norgen) added adjacent to the samples. The gels were then run for 20 minutes at 120 V before being viewed using a lightbox (Gbox, geneflow, UK) and imaged with Genesnap software (Version 7, Syngene, UK).

2.3.6.5 Reverse transcription of RNA

A reverse transcription kit was used to convert the RNA samples into cDNA (Omniscript, Qiagen, UK). Twelve microlitres of each RNA sample was added to individual eppendorf tubes (Eppendorf, UK) with two microlitres of 10 µM stock oligo-dT (Qiagen, UK) and heated to 80 °C for 10 minutes in a water bath (Echotherm, UK) before being quenched in ice for 5 minutes. A reverse transcription mastermix comprising of 2 µl of both Buffer RT (Qiagen, UK) and dNTP (Qiagen, UK) with 1 µl of both RNase Inhibitor (Qiagen, UK) and Omniscript Reverse Transcriptase (Qiagen, UK) was prepared. To each RNA/oligodT sample 6 µl of the mastermix was added and the mixture vortexed and centrifuged before incubation for 60 minutes at 37 °C followed by 5 minutes at 95 °C before storage at -80 °C (Nuaire, UK)

2.3.6.6 Concentrating cDNA with micron filters

The samples were thawed and a micron filter (Amicon Ultra, UK) labelled for each sample. To each filter 18 µl of RNA/oligodT/Mastermix was added to 482 µl of RNA free water to achieve a total volume of 500 µl. The column was then repeatedly centrifuged for 1 minute at 8,000 rpm until the column had an approximate volume of 60- 70 µl. The column was then inverted in a new collection tube before again centrifuging at 8000 rpm for 1 minute. The cDNA samples were then stored at -20 °C (Zanussi, UK).

2.3.6.7 Normalising cDNA using GAPDH

Forward and reverse primers were prepared by diluting the primer master mixes (Invitrogen, UK) in a 1: 4 dilution with RNase free water. RED Taq master mix was then made in a PCR tube consisting of 12.5 µl REDTaq (Sigma-aldrich, UK), 2 µl of the reverse primer mastermix dilutions, 2 µl of cDNA and RNase free water to achieve a total volume of 25 µl.

A PCR thermal cycler (Eppendorf Mastercycler, Germany) was then used to run 18, 21 and 24 cycles of the GAPDH gene which were collected in a 96 well plates (Sarstedt, UK). A 1.5 % agarose gel made by adding 0.9 g of Agarose to 60 ml of TAE buffer with 5 µl of GelRed stain (Biotium, USA). The gel was then loaded with the cDNA samples and a DNA ladder and ran at 120 V for 30 minutes.

2.3.6.8 Semi-quantification of PCR using gel imaging and quantification software

The gels were placed in a light box (G-box, Geneflow, UK) and imaged using Genesnap software (Version 7, SynGene, UK) at an exposure time of 80 ms. Genetools software (version 4, SynGene, UK) was used to semi-quantitatively assess the intensity of the cDNA bands and the results exported to a spread sheet (Excel, Microsoft, U.S) Based on the GAPDH band intensities the cDNA content of each sample was increased or decreased until the intensity of each band was within a 10 % error margin.

2.3.7 Alizarin red assay to determine the presence of mineralisation in cell cultures

Cells were grown according to section 2.3.5. Media was aspirated from each 35 mm dish/well and cells washed gently with 1 ml of PBS (Sigma, UK). The cells were then fixed with 1 ml of 10 % formalin (Sigma, UK) for 15 minutes at room temperature. After the incubation period the formalin was removed before the cells were washed three times with 1 ml PBS for 5 minutes ensuring that any excess solution was removed after each washing. Alizarin red solution (BDH laboratory supplies, UK) (13.69 g l^{-1}) adjusted to pH 4.1-4.2 using 1.0 % ammonium hydroxide (Sigma, UK) was added to each well. The cells were then gently agitated for 20 minutes. Any unincorporated dye was aspirated off and each plate washed three times with 1 ml PBS. Each well was then filled with 1 ml of ddH2O to prevent

the cells from drying. Cells were viewed using a microscope (Flovert, UK) and imaged with a digital camera (Coolpix, Nikon, Japan).

2.3.8 Buffer addition to Portland cement (PC)

Sodium dihydrogen orthophosphate, potassium dihydrogen dibasic and TRIS EDTA (Sigma, UK) were added individually at either 2 or 10 wt% into the powder phase of PC. The cement slurries were then cast into moulds of 3 mm by 6 mm and left to set for 25 minutes. The cements were then removed and exposed to 3 ml of cell culture medium for 20 minutes. In the event the cements had not set in the allotted time frame they were removed from the split mould based on the initial setting times indicated by the Gilmores needles test. A pH meter (Mettler Toledo, UK) was used to assess the change in alkalinity after 20 minutes of incubation

CHAPTER 3: RESULTS

3 RESULTS

3.1 CHAPTER: Investigating the parameters of an injectability model

3.1.1 Effect of varying the powder-to-liquid ratio

3.1.1.1 Injectability

A gradual increase in cement extrusion was observed as the powder-to-liquid ratio (PLR) was decreased from 4.2 to 2.4 g ml^{-1} (figure 3.1.1). Lafarge, the manufacturers of Mastercrete® (Lafarge, UK) recommend a PLR of 3 g ml^{-1} (178) which without a liquefying agent produced an extrusion of 77%.

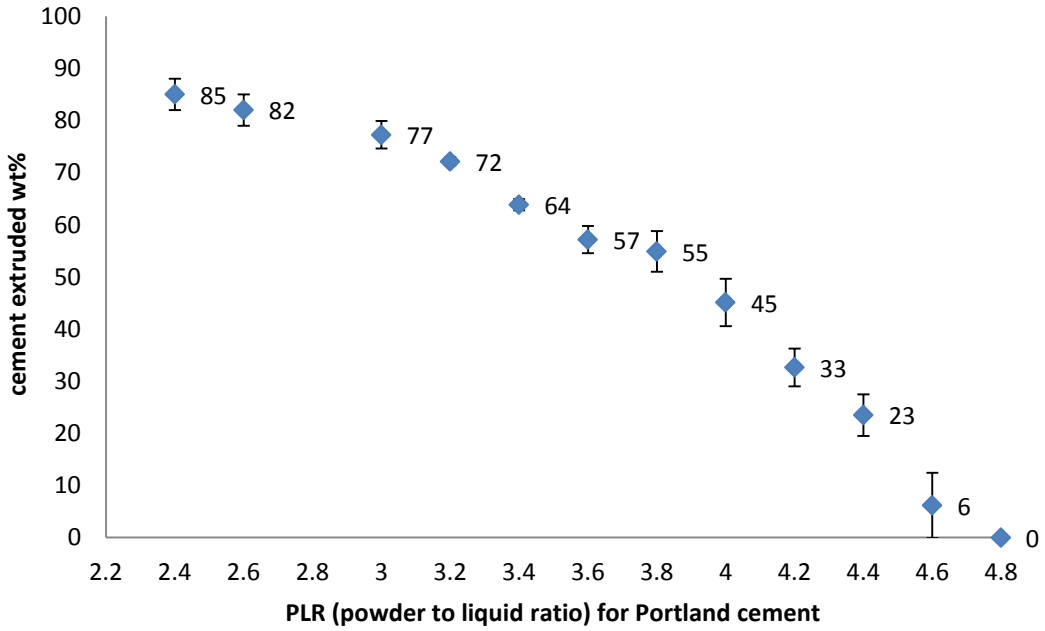

Figure 3.1.1 Graph illustrating the effect of the cements powder: liquid ratio (PLR) on cement extrusion (injectability) of standard Portland cement. Reducing the PLR from 4.8 to 2.4 g ml^{-1} significantly ($p<0.05$) increased cement extrusion to 85 wt% (sample number n=4).

Below a PLR of 2.6 g ml^{-1} a low initial force under 10 N was required to extrude the majority of the cement from the 2 mm syringe aperture. An increase in force was required only when the syringe was nearly empty (figure 3.1.2). In contrast, cements with a PLR above 2.8 g ml^{-1} demonstrated an initial increase in force followed by a shallow force plateau before a marked increase in force as the cement failed to extrude from the syringe.

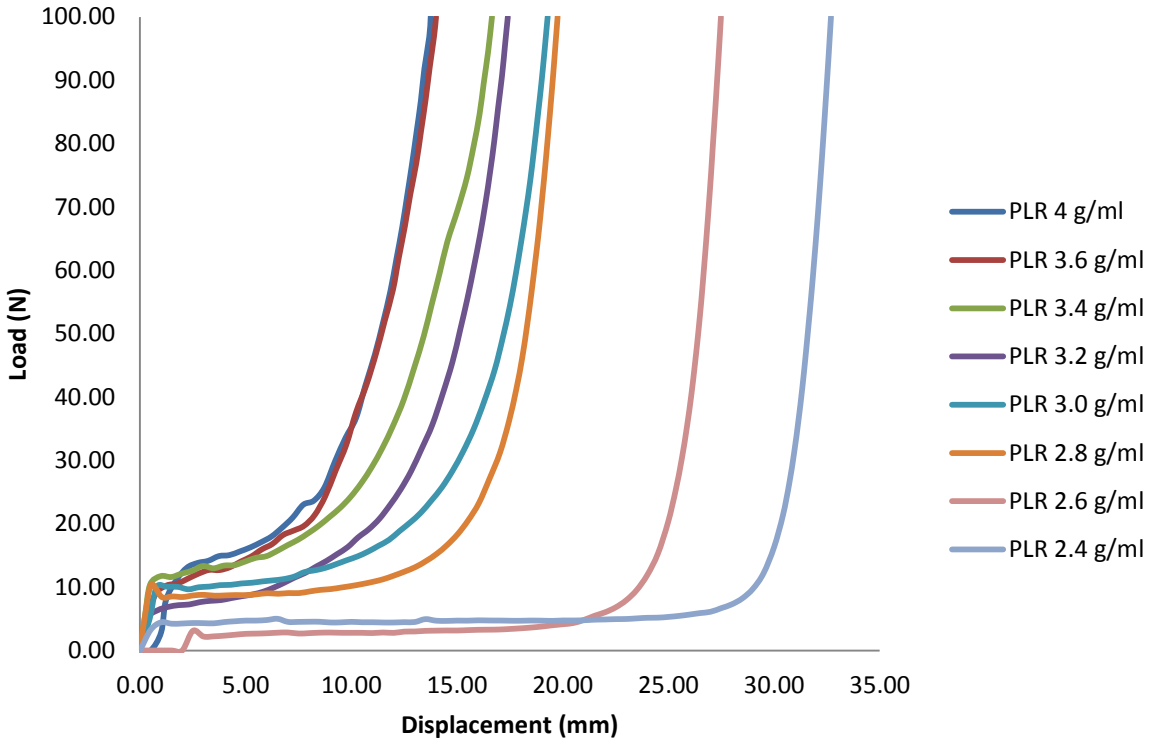

Figure 3.1.2 Force/displacement graph showing traces for different PLRs recorded during the injectability experiments. Reducing the PLR from 4 to 2.4 g ml^{-1} decreased the force required to displace the syringe plunger during cement injection. At 2.4 g ml^{-1} less than 5 N was required to extrude 85 wt% of the cement.

3.1.1.2 Setting times

Decreasing the PLR of the cement from 4.2-2.4 g ml^{-1} significantly ($p<0.05$) increased the setting time (figure 3.1.3). However, without a setting accelerant the setting times were in excess of the 6.5-15 minutes required for the vertebroplasty operation (15).

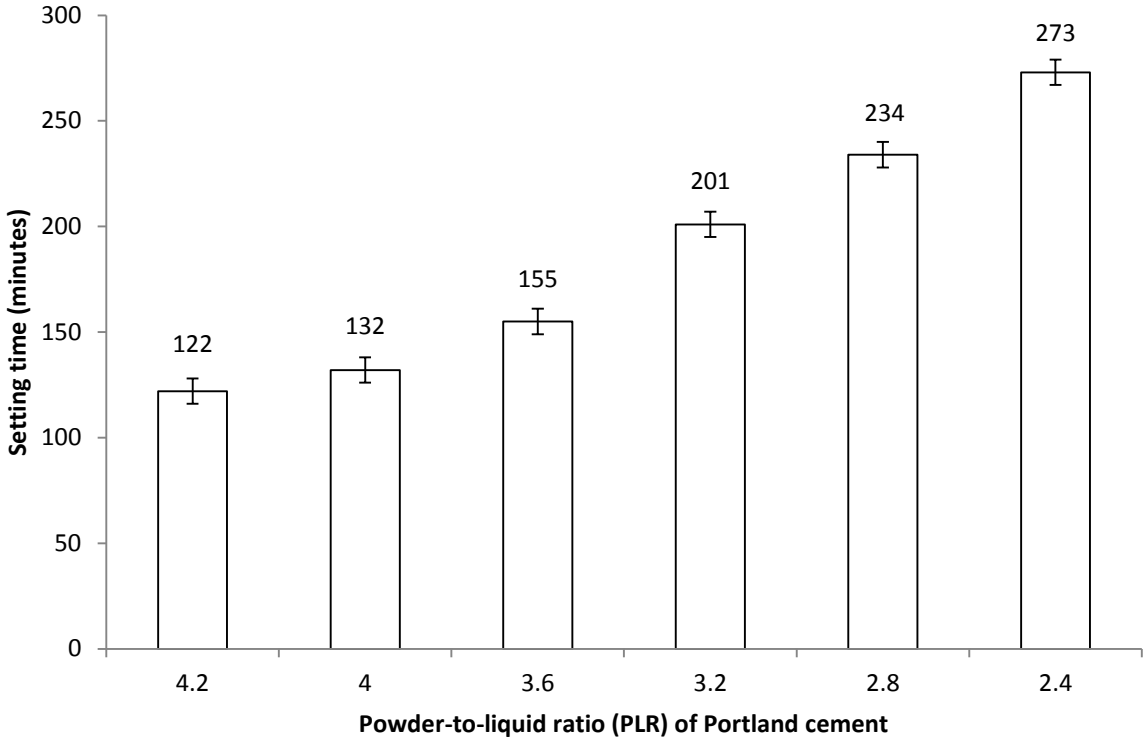

Figure 3.1.3 Graph demonstrating the effect of Powder-to-liquid ratio on the setting time of Portland cement. Decreasing the PLR of the Portland cement standard from 4.2 to 2.4 g ml^{-1} significantly ($p<0.05$) increased cement setting time from 2 to over 4 hours (sample number n=3).

3.1.2 Initial injectability set-up investigating the effect of different cross-head speeds

Increasing the cross-head speed of the universal testing machine from 3 to 10 mm minute^{-1} significantly ($p<0.05$) increased cement extrusion for both the standard cements and those containing a liquefying agent (figure 3.1.4). There was less of an effect on extrusion when increasing the cross-head speed from 10 to 30 mm minute^{-1}.

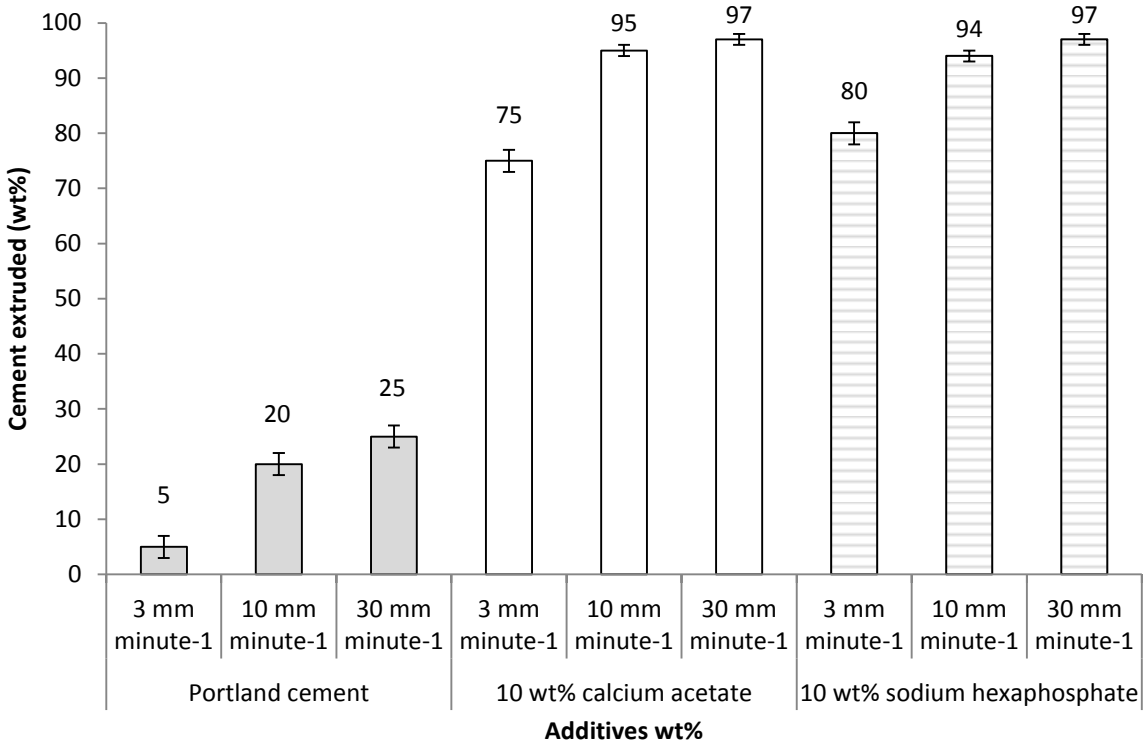

Figure 3.1.4 Graph demonstrating the increase in cement extrusion (injectability) when the cross-head speed of the universal testing machine supplying the injection force was increased from 3 to 30 mm minute^{-1} (sample number n=4).

3.1.3 Investigating additive addition to PC in the powder vs. liquid phase

3.1.3.1 Injectability

Both calcium acetate and sodium hexaphosphate acted as liquefying agents for PC. A 5 or 10 wt% addition of either additive significantly ($p<0.05$) increased cement extrusion compared with the PC standard (fig. 3.1.5). There was a further significant ($p<0.05$) increase in extrusion when the liquefiers were vortex mixed into the powder phase (striped lines) as opposed to being dissolved in the liquid phase (white bars) prior to hydration of the cement powder.

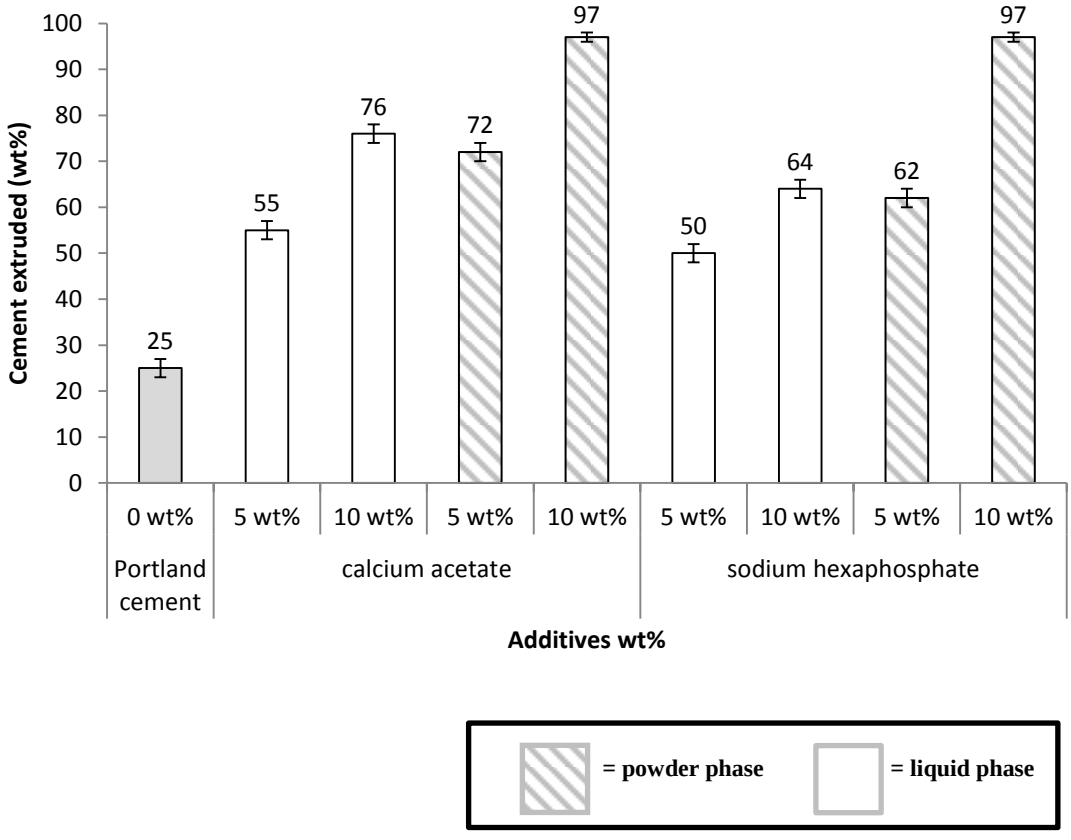

Figure 3.1.5 Graph demonstrating the effect of calcium acetate and sodium hexaphosphate liquefiers on cement extrusion (injectability). The liquefiers were either dissolved in the liquid phase (white bars) prior to adding to the powder phase or mixed directly with the powder phase (striped bars) prior to hydration. There was a significant ($p<0.05$) increase in cement extrusion values when the additives were mixed in the powder phase as opposed to being dissolved in the liquid phase (sample number n=4).

3.1.3.2 Setting times

Calcium acetate and sodium hexaphosphate both acted as setting accelerants, significantly ($p<0.05$) decreasing setting times from over 2 hours to below 30 minutes (figure 3.1.6). There was also a significant ($p<0.05$) decrease in setting times when the additives were mixed with the powder phase as opposed to being dissolved with the liquid phase prior to the setting reaction occurring.

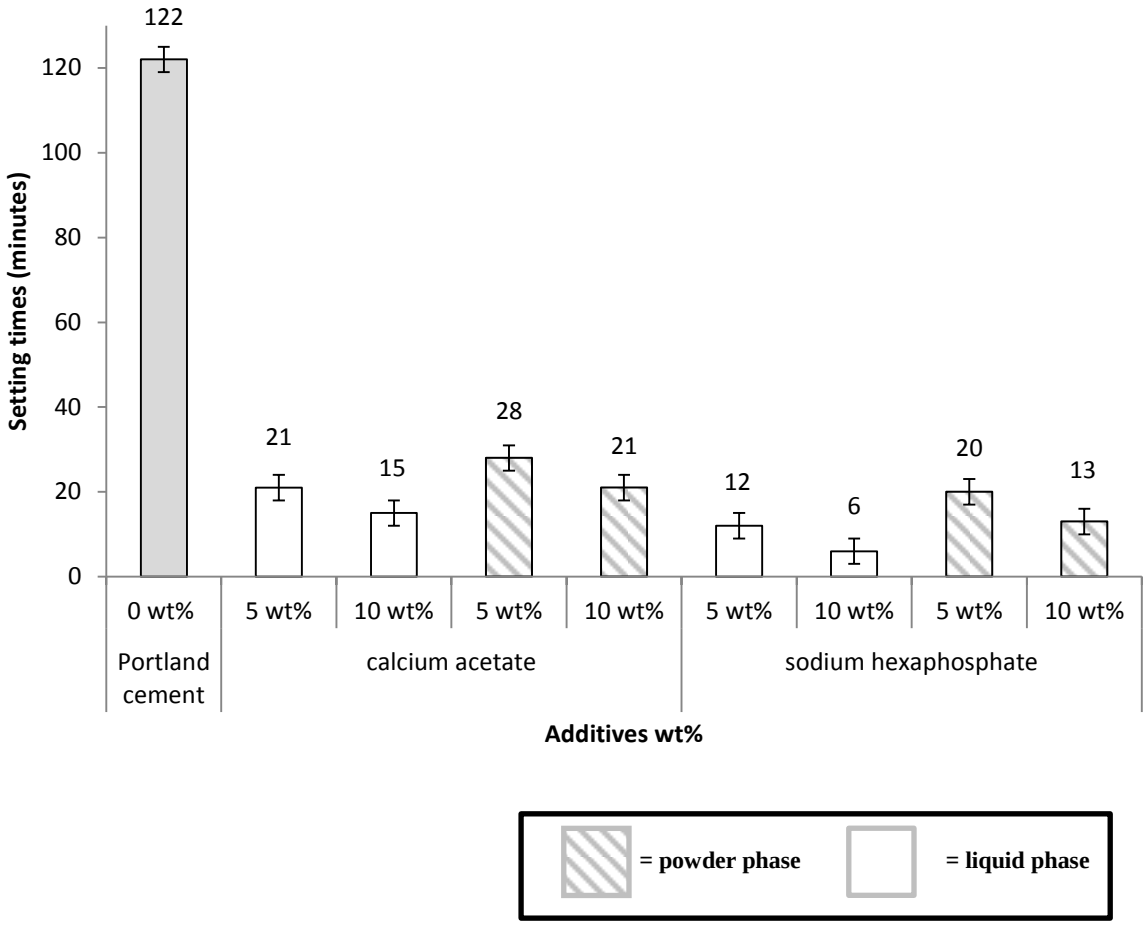

Figure 3.1.6 Graph showing the influence of adding setting accelerants into the powder vs. liquid phase of the cement. There was a significant ($p<0.05$) decrease in setting times when the additives were dissolved in the liquid phase prior to adding to the hydraulic cement powder (sample number n=3).

3.1.4 Phase analysis of a new versus aged batch of cement

The overall peak intensities for the 2005 batch of PC were less intense than for the 2010 batch (figure 3.1.7). The 'Full-width half peak maximum' values for the peak at 32.5° Theta were 0.140 and 0.114 for the old batch and new batch respectively. Both of these features indicate a general degradation of the old batch of cement (179). However, lack of formation of any of the hydration product calcium-silicate-hydrate at 29° theta indicated that neither of the cement powders was degraded by reaction with water.

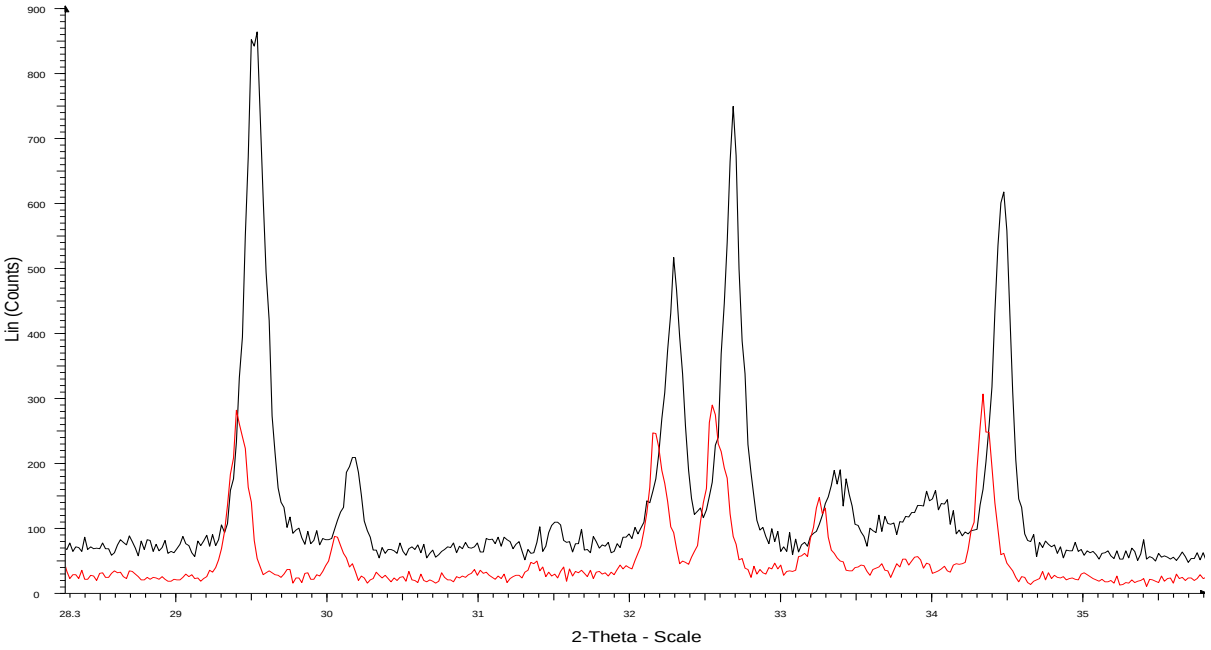

Figure 3.1.7 XRD patterns of a 2005 (red line) and 2010 (black line) batch of Portland cement. Peak intensities were greater in the new batch compared with the old batch.

3.1.5 Elemental analysis of a new versus aged batch of cement

The elemental composition of the cement powder was analysed using energy dispersive X-ray spectroscopy (EDX) there was approximately an 11% difference between the observed and theoretical optimum Ca/Si ratio for tricalcium silicate in the aged batch of cement. In comparison, there was a 22% difference in the Ca/Si ratio with the new batch (refer to appendices for full calculations).

Table 3.1.1 Elemental composition of Mastercrete® (Lafarge, UK) cement from both a 2005 and 2011 batch. There were no major differences in the cements composition between the batches which were produced 6 years apart.

	2005 batch of Mastercrete® PC		**2011 batch of Mastercrete® PC**	
Element	Weight %	Atomic %	Weight %	Atomic %
O	52.35	71.4	53.16	72.20
Na	0.50	0.47	0.47	0.44
Mg	0.73	0.65	0.69	0.62
Al	2.10	1.70	1.76	1.41
Si	6.83	5.31	6.31	4.88
S	2.07	1.41	2.05	1.39
K	1.15	0.64	0.87	0.49
Ca	32.66	17.78	33.14	17.97
Fe	1.61	0.63	1.55	0.60

3.1.6 Investigating the effect of sieving cement powder

3.1.6.1 XRD characterisation

The overall peak intensities for the cement sieved through a 63 µm mesh size were greater than the cement passed through a 500 µm mesh (figure 3.1.8). The 'Full-width half peak maximum' values for the peak at 32.5° Theta were 0.182 and 0.122 for the 500 µm and 63 µm sieved batches respectively. This may indicate the cement passed through the 63 µm filter possessed less cement aggregates which does not absorb strongly on the XRD trace.

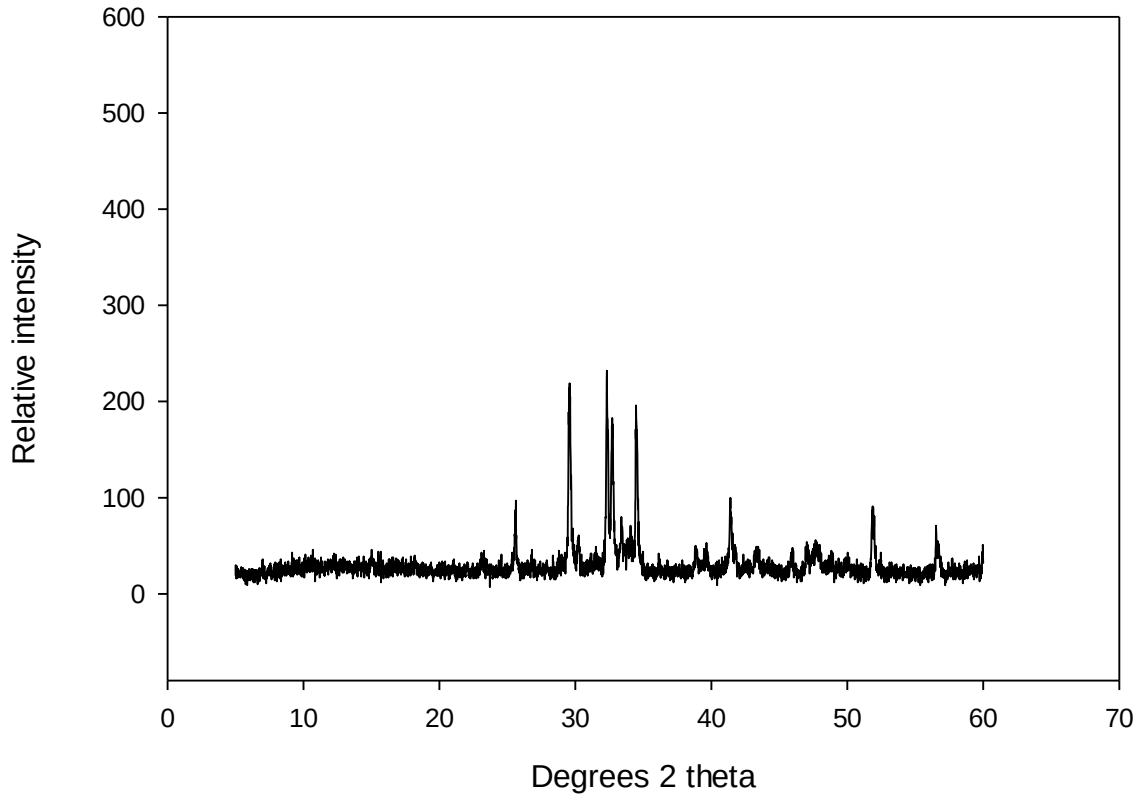

Figure 3.1.8 XRD patterns of a 63 µm mesh (red line) and 500 µm mesh (black line) sieved batches of Portland cement powder. Peak intensities were greater when a smaller sieve size had been used. Phase composition appeared identical.

3.1.6.2 Setting times

Preparing the PC with a 63 µm sieve significantly ($p<0.05$) reduced the setting time of the PC from over 3.5 hours to just over 1 hour (figure 3.1.9).

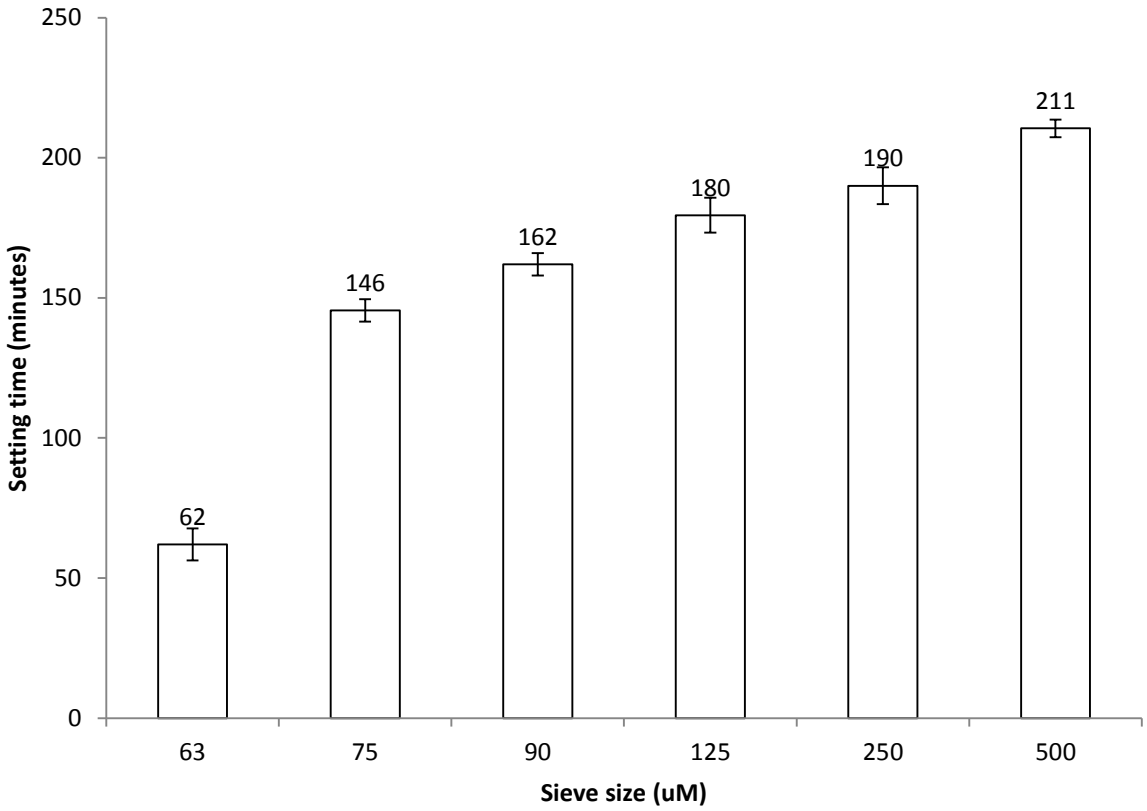

Figure 3.1.9 Graph demonstrating the effect of sieving Portland cement powder using different mesh sizes on the materials setting time. Decreasing the sieve diameter from 500 to 62 µm significantly decreased cement setting time (sample number n=3).

3.2 CHAPTER: Development of Portland cement for orthopaedic applications, establishing injectability and decreasing setting times using researched additives

Liquefiers and setting accelerants were identified from tables 1.10.1 and 1.10.2 which met two criteria.

1. The PC additives have previously not demonstrated to be hazardous according to HAZDAT data sheets.
2. The chemical structures of the additives were available and not patented.

3.2.1 Injectability studies (powder-to-liquid ratio 4 g ml^{-1})

Sodium chloride, sodium aluminate, sodium hexaphosphate and calcium acetate all acted as liquefiers significantly ($p<0.05$) increasing the injectability of PC with 2- 10wt% additions to the cement (figure 3.2.1a). The liquefiers exerted greatest influence at 10 wt% with sodium chloride, sodium aluminate and calcium acetate producing extrusion values of over 95 wt% with a plunger force of less than 100 N. In contrast, methyl cellulose, calcium sulphate dihydrate, calcium carbonate and oxalic acid significantly ($p<0.05$) reduced cement extrusion values compared with the standard PC (figure 3.2.1b).

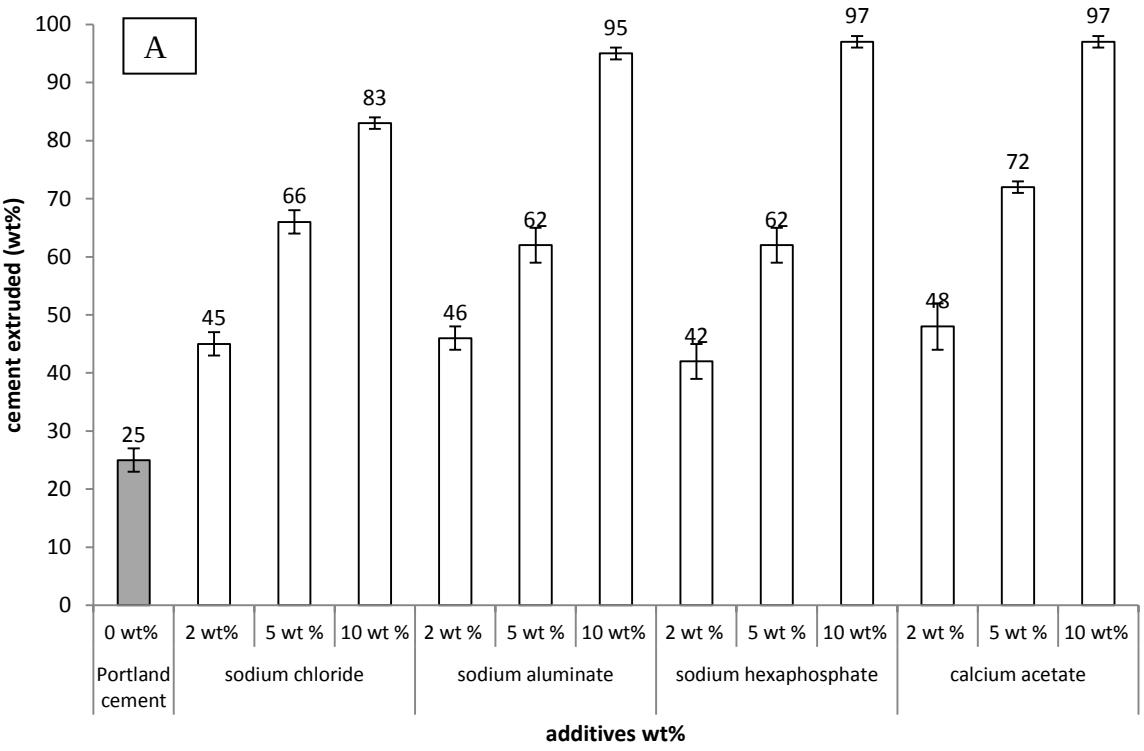

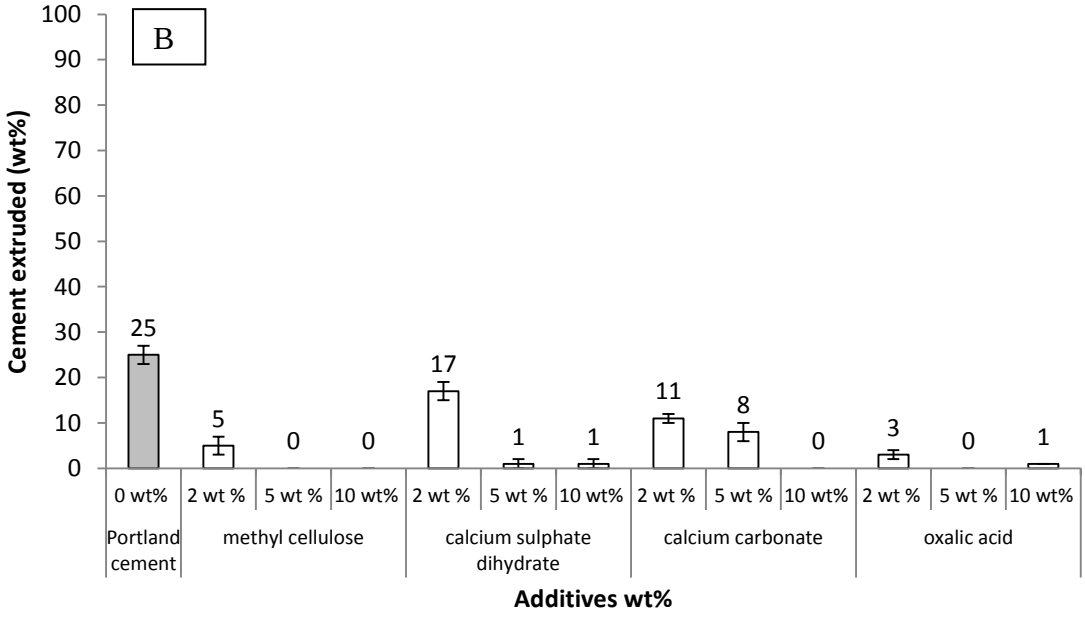

Figure 3.2.1(A) PC injectability significantly ($p<0.05$) increased with the additions of sodium chloride, sodium aluminate, sodium hexaphosphate and calcium acetate. Maximum injectability was achieved with 10 wt% additions of sodium aluminate, sodium hexaphosphate and calcium acetate all extruded over 95 wt% of cement from the syringe. (B) In contrast, Additions of methyl cellulose, calcium sulphate dihydrate, calcium carbonate and oxalic acid significantly ($p<0.05$) decreased cement injectability. (Error bars represent standard deviations) (sample number n=4).

The force required to extrude cement during injection decreased as the wt% of sodium chloride, sodium aluminate, sodium hexaphosphate and calcium acetate were increased from 2 to 10 wt% (figure 3.2.2). For cements with 5-10 wt% of these liquefiers a relatively low initial force i.e. 5 to 30 N was required to extrude the majority of the cement and an increase in force was observed only when the syringe was nearly empty. In contrast, PC without a liquefier and cements with the additives methyl cellulose, calcium sulphate dihydrate, calcium carbonate, and oxalic acid did not demonstrate a characteristic force plateau but exhibited a sharp increase in displacement as the cements failed to extrude from the syringe.

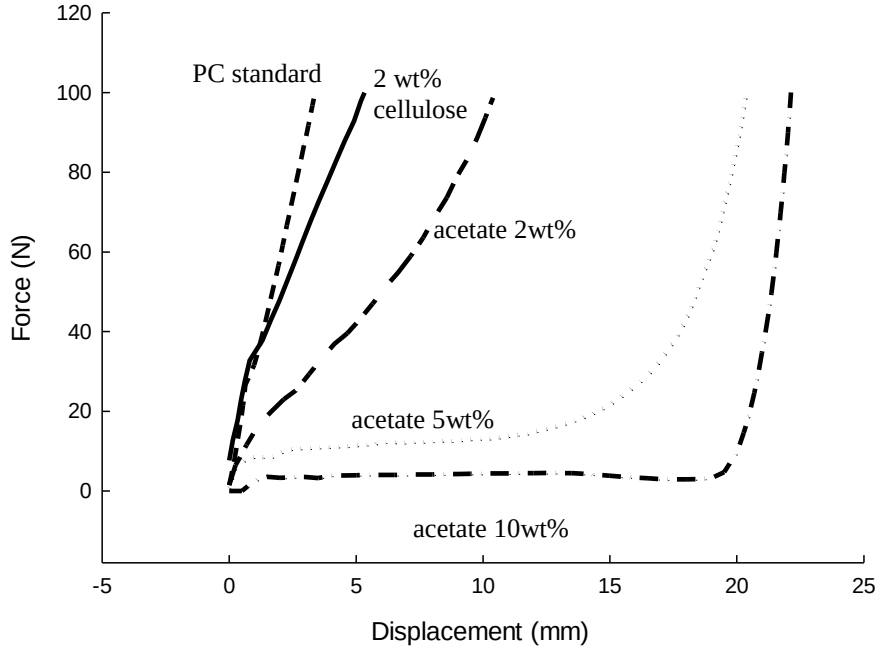

Figure 3.2.2 Graph depicting the force required to displace the cement plunger during the injectability experiments. A gradual decrease in extrusion force was observed when cement liquefiers were increased from 2-10 wt% (calcium acetate given as an example). In contrast, the PC standard and additives which reduced PC injectability did not noticeably displace the syringe plunger as the cement failed to extrude from the syringe (methyl cellulose given as an example.

3.2.2 Setting time measurements (powder-to-liquid ratio 4 g ml^{-1})

A 5 or 10 wt% addition of sodium chloride, sodium aluminate, sodium hexaphosphate, calcium acetate or calcium sulphate dihydrate significantly ($p<0.05$) reduced the setting times of PC from over 2 hours to below 55 minutes (figure 3.2.3). The shortest setting times were observed with a 10 wt% addition of the accelerants. Sodium hexaphosphate at 10 wt% was the most powerful accelerant used generating setting of under 10 minutes. Cements containing methyl cellulose, calcium carbonate and oxalic acid were too dry to assess setting using the Gilmore's needles test.

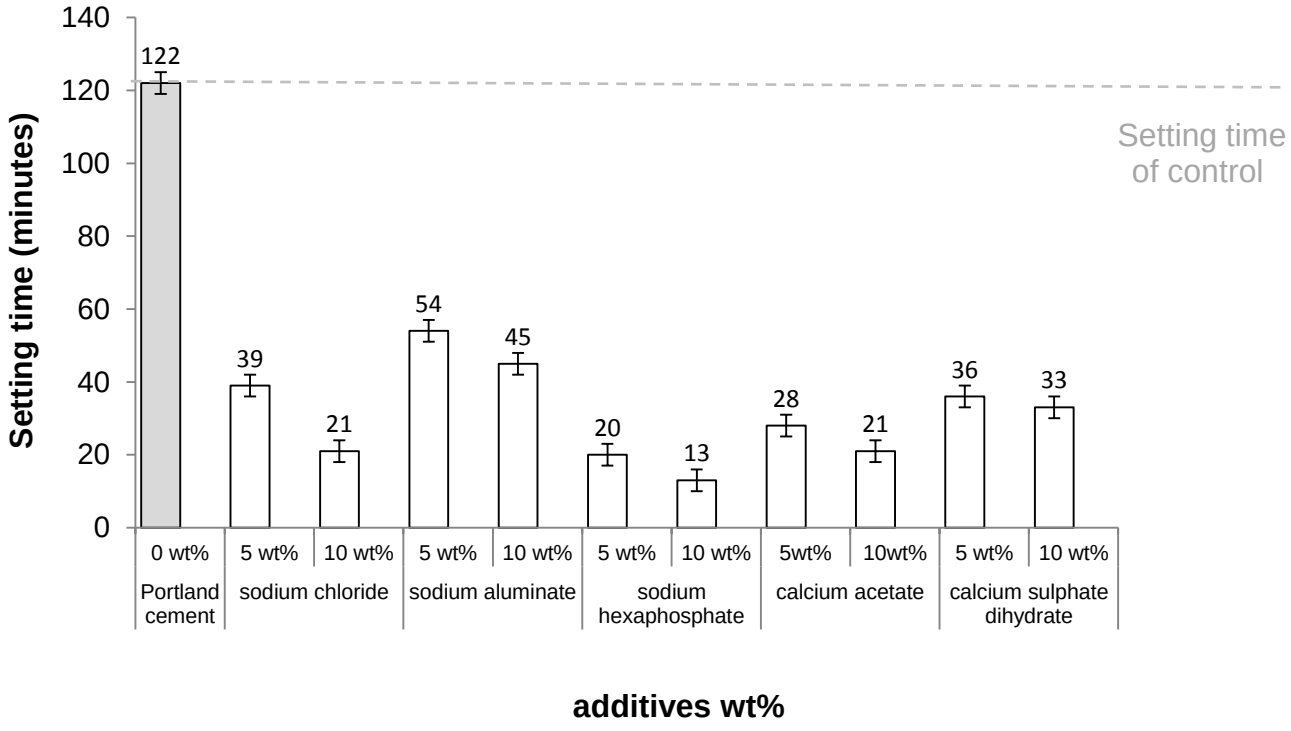

Figure 3.2.3 Sodium chloride, sodium aluminate, sodium hexaphosphate, calcium acetate and calcium sulphate dihydrate significantly ($p<0.05$) reduced cement setting times compared with PC standard (error bars equal minimum error of method) (sample number n=3).

3.2.3 Compressive strengths, porosity and density measurements

The highest compressive strengths were obtained by 5 wt% additions of sodium chloride (table 3.2.1). The three remaining liquefiers at 5 wt% sodium aluminate, sodium hexaphosphate and calcium acetate all had significantly ($p<0.05$) lower compressive strength values compared with the unmodified control but were still higher than the 1.4- 9 MPa compressive strength for lumbar vertebrae (31). An addition of 5 wt% sodium chloride and calcium acetate had lower relative porosities and specific densities than the standard. In contrast, sodium aluminate and sodium hexaphosphate generally possessed higher porosities and specific densities than the standard. It was not possible to obtain values for 10 wt% calcium acetate as after setting the cements appeared to possess very low cohesive properties and broke apart on handling.

Table 3.2.1 After both 1 and 30-days setting there was no significant ($p<0.05$) difference in the compressive strength values between the standard and cement containing 5 wt% sodium chloride, In comparison, the compressive strengths of cements containing the other three additives were all significantly ($p<0.05$) lower but still higher than cancellous bone. There was also little difference between the relative porosities of the standard and cements containing 5 wt% chloride. In contrast, the other additives, with the exception of calcium acetate after 30-days setting all possessed higher porosities. The specific densities of chloride and acetate cements were lower than the standard, whereas, aluminate and hexaphosphate cements after 1-day were approximately equal to the standard and after 30-days the 10 wt% additions were lower (compressive strength n=30).

Additive	Wt% additive	Compressive strength/MPa (1-day)	Compressive strength/MPa (30-day)	Relative porosities % (1-day)	Relative porosities % (30-day)	Specific densities g cm^{-3} (1-day)	Specific densities g cm^{-3} (30-day)
PC standard		53 ± 3	79 ± 7	21 ± 1	13 ± 1	2.61 ± 0.05	2.50 ± 0.05
Sodium chloride	5	*51 ± 4*	*80 ± 5*	*21 ± 1*	*12 ± 1*	*2.51 ± 0.05*	*2.35 ± 0.05*
	10	**28 ± 4**	**56 ± 5**	**26 ± 1**	**16 ± 1**	**2.49 ± 0.05**	**2.28 ± 0.05**
Sodium aluminate	5	*33 ± 4*[3]	*42 ± 3*	*23 ± 1*	*15 ± 1*	*2.65 ± 0.05*	*2.53 ± 0.05*
	10	**23 ± 4**[4]	**29 ± 5**	**28 ± 1**	**16 ± 1**	**2.72 ± 0.05**	**2.41 ± 0.05**
Sodium	5	*42 ± 4*	*52 ± 3*	*22 ± 1*	*16 ± 1*	*2.61 ± 0.05*	*2.53 ± 0.05*
hexaphosphate	10	**25 ± 4**	**42 ± 4**	**31 ± 1**	**20 ± 1**	**2.69 ± 0.05**	**2.53 ± 0.05**
Calcium acetate	5	*29 ± 4*	*59 ± 3*	*25 ± 1*	*11 ± 1*	*2.54 ± 0.05*	*2.20 ± 0.05*

[3] Numbers in italic indicate 5 wt% additions
[4] Numbers in bold indicate 10 wt% additions.

3.2.4 Sulphate analysis using FTIR

There was a sharp increase in the calcium sulphate dihydrate (gypsum) peak at 1100 cm^{-1} during the first 60 minutes of setting for cements containing 5 wt% sodium hexaphosphate and sodium aluminate (see figure 3.2.4a and 3.2.4b). The absorbance band of sulphate (SO_4^{2-}) has previously been indicated to be in this region and based on the profiles of standard calcium sulphates, the observed peak most closely relates to calcium sulphate di-hydrate (gypsum) (180-182). In contrast, the gypsum peak for the PC standard and cements containing 5 wt% sodium chloride and calcium acetate did not noticeably increase during the first 2 h of the setting reaction. When 5 wt% calcium sulphate dihydrate (gypsum) was added directly to the cement the peak corresponding with the additive understandably increased (figure 3.2.4c). However, when 5 wt% gypsum was added with 5 wt% sodium hexaphosphate, the peak was higher than when gypsum was added alone (see figures 3.2.4c and 3.2.4d). In addition, to the increase in peak heights for cements containing gypsum and hexaphosphate the cement setting time was increased from 9 minutes to 15 minutes.

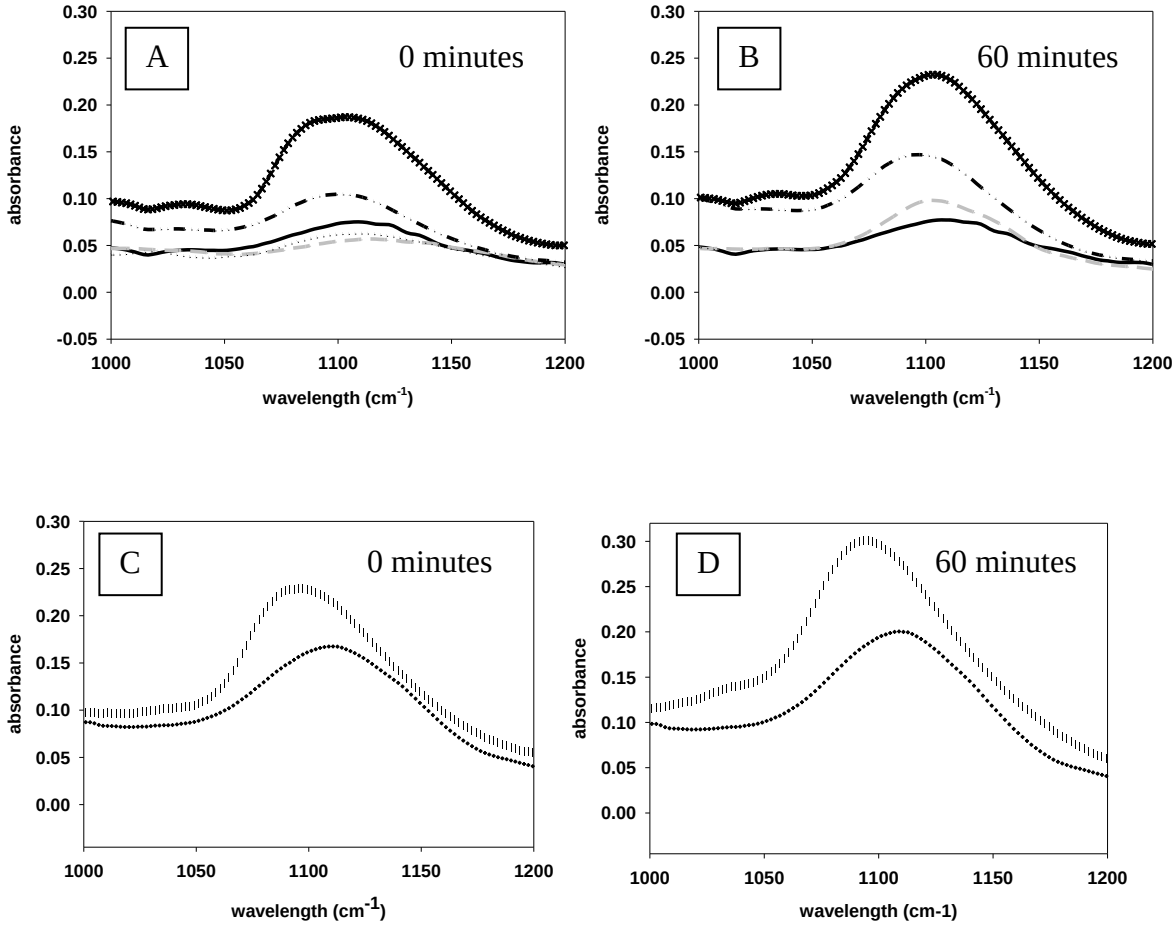

Figure 3.2.4 FTIR spectra illustrating the absorbance of the sulphate band of PC during the first 60 minutes of setting. (A) After initially mixing the cements there was an increase in peak heights in cements containing 5 wt% sodium hexaphosphate and sodium aluminate. (B) Peak height continued to increase during the first 60 minutes of setting. (C) When 5 wt% calcium sulphate dihydrate (gypsum) was added to the cement there was an increase in peak height. However, there was an even greater increase in peak height when 5 wt% sodium hexaphosphate was added in addition to the calcium sulphate. (D) Peak height of the calcium sulphate/hexaphosphate combined cement continued to increase over 60 minutes setting (sample number n=3).

Key

A-B

PC standard
5 wt% chloride
5 wt% aluminate
5 wt% hexaphosphate
5 wt% acetate

C-D

PC + 5 wt% calcium sulphate dihydrate
PC + 5wt% calcium sulphate dihydrate + hexaphophate

3.2.5 Phase analysis using X-ray diffraction (XRD)

After 1-days setting crystalline peaks representing calcium hydroxide (18° theta), ettringite (9° and 16° thetas) and C-S-H (29° theta) were present in the PC standard and cements containing sodium chloride and calcium acetate (figure 3.2.5). In contrast, PC containing sodium hexaphosphate and sodium aluminate demonstrated none of these peaks. After 30-days setting all the cements had developed crystalline peaks indicating the presence of calcium hydroxide and C-S-H.

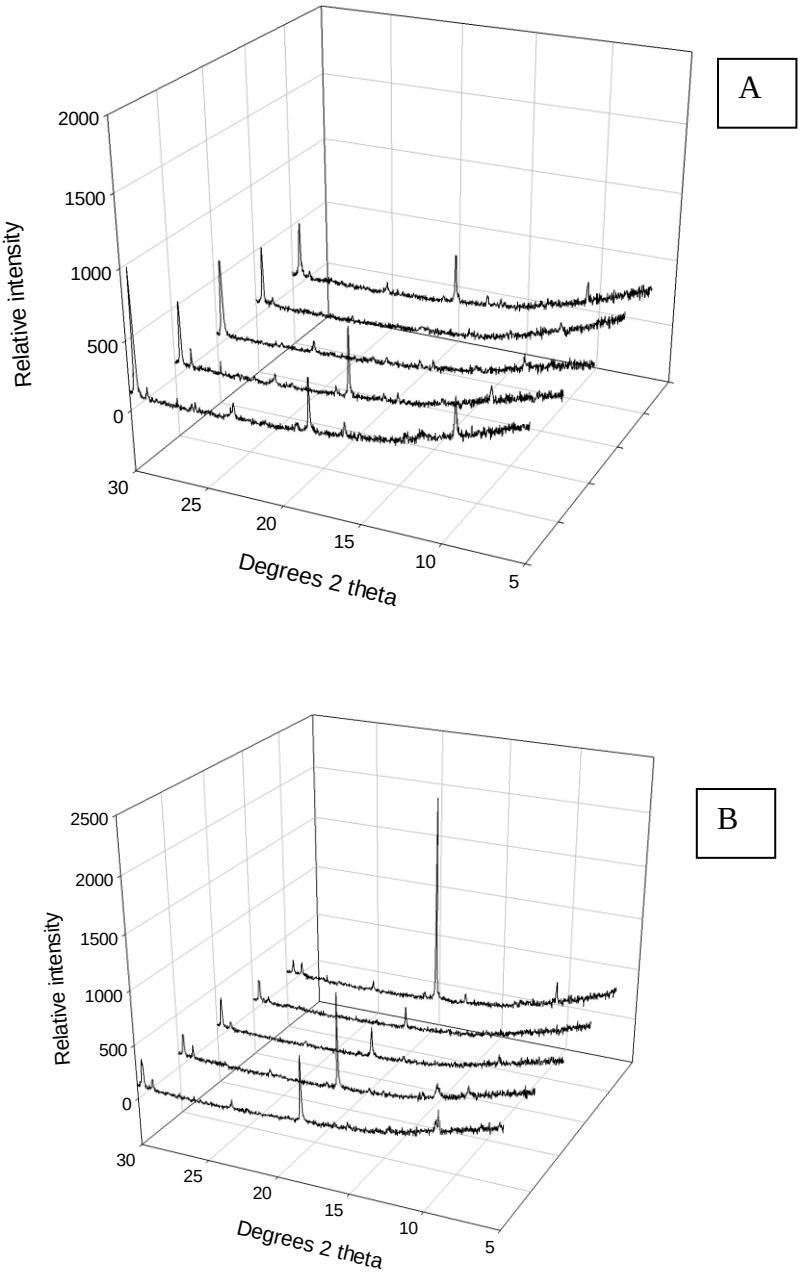

Figure 3.2.5 X-ray diffraction patterns of PC after (A) 24h and (B) 30-days. From front to back PC, 5 wt% sodium chloride, sodium aluminate, sodium hexaphosphate and calcium acetate. Both the standard and cements containing chloride and acetate developed ettringite (9 and 16° thetas) and C-S-H peaks (29° theta) after 24h. All the cements developed C-S-H peaks after 30-days.

3.2.6 Cement elemental analysis using energy dispersive X-ray spectroscopy

Elemental analysis of the surface crystals of cements modified with sodium hexaphosphate most closely resembled unhydrated tetracalcium aluminoferrite with only a 17% difference between the theoretical optimum and observed ratios for the Ca/O ratios. The O/Al ratio of the cements modified with calcium aluminate indicated that there was a 6% difference between the ideal structure for calcium monosulphate and the Ca/O ratio only a 13% different (for full calculations refer to appendices).

3.2.7 Cement surface morphology using scanning electron microscopy (SEM)

Standard PC (figure 3.2.6a) and PC containing 5 wt% sodium chloride (figure 3.2.6b) both possessed ordered surface crystals of approximately 10 - 20 µm in length (figure 3.2.6c). In contrast, PC containing 5 wt% sodium hexaphosphate was composed solely of ordered cubic crystals approximately 5-10 µm in width. The surface of PC containing 5 wt% calcium acetate possessed cuboid crystals (< 10 µm) (figure 3.2.6d), whilst 5 wt% sodium aluminate additions generated flat hexagonal crystals approximately 10 µm in diameter and needle shaped crystals over 20 µm in diameter (figure 3.2.6e).

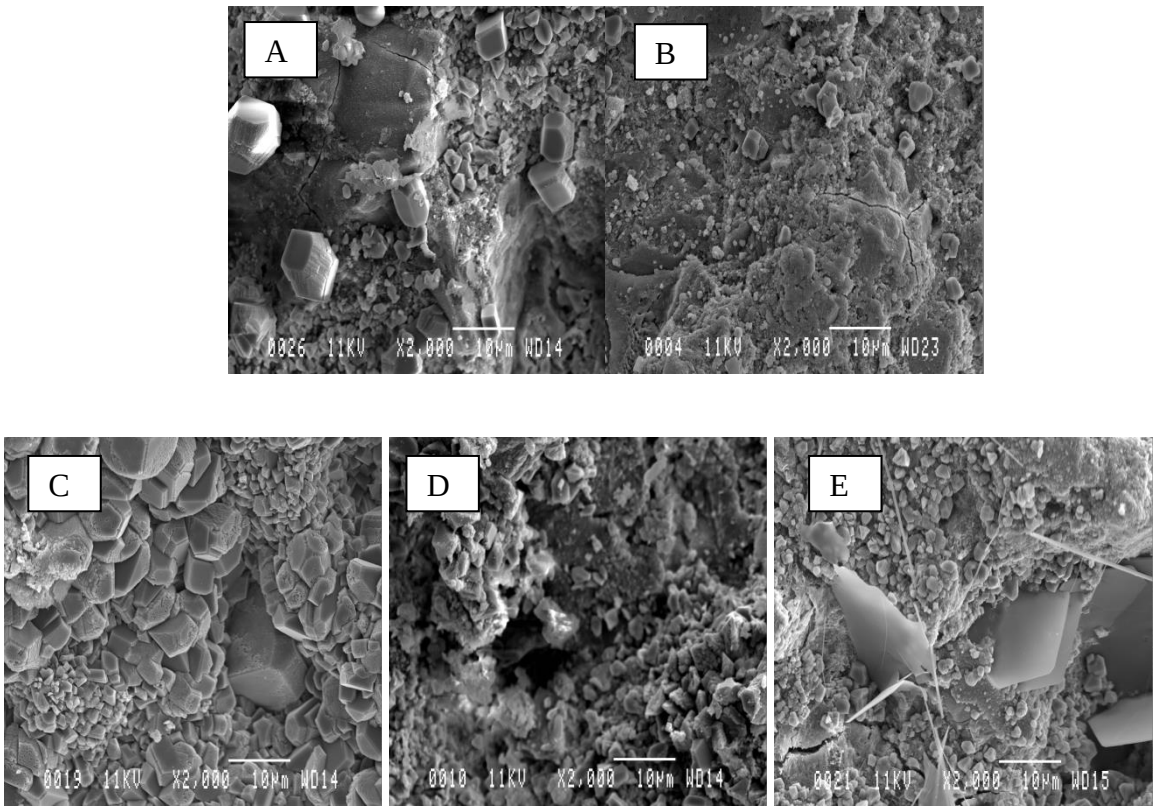

Figure 3.2.6 SEM micrographs demonstrating the surface morphology of (A) PC standard and cements containing 5 wt% (B) sodium chloride (C) sodium hexaphosphate (D) calcium acetate (E) sodium aluminate. Cements containing sodium hexaphosphate possessed a cubic shape, whereas sodium aluminate cements possessed hexagonal crystals and rod shaped crystals approximately 20 um long. The calcium acetate cements contained many small crystals less than 5 µm in diameter.

3.3 CHAPTER: Establishing injectability and decreasing setting times using the additives calcium chloride and calcium nitrate

3.3.1 Injectability studies

Both calcium chloride and calcium nitrate acted as liquefying agents for PC. A 5 wt% addition of either salt or an equal 2.5 wt% combination of the two significantly ($p<0.05$) increased cement extrusion compared with the PC standard (figure 3.3.1). There was a further significant ($p<0.05$) increase in extrusion when the total additive wt% was increased to 10 wt%. Mixing the additives also increased the injectability of the cement increasing extrusion by 10 wt%. The apparent limit on injectability was 98 wt% extrusion with 2 wt% of the cement remaining in the tip of the syringe.

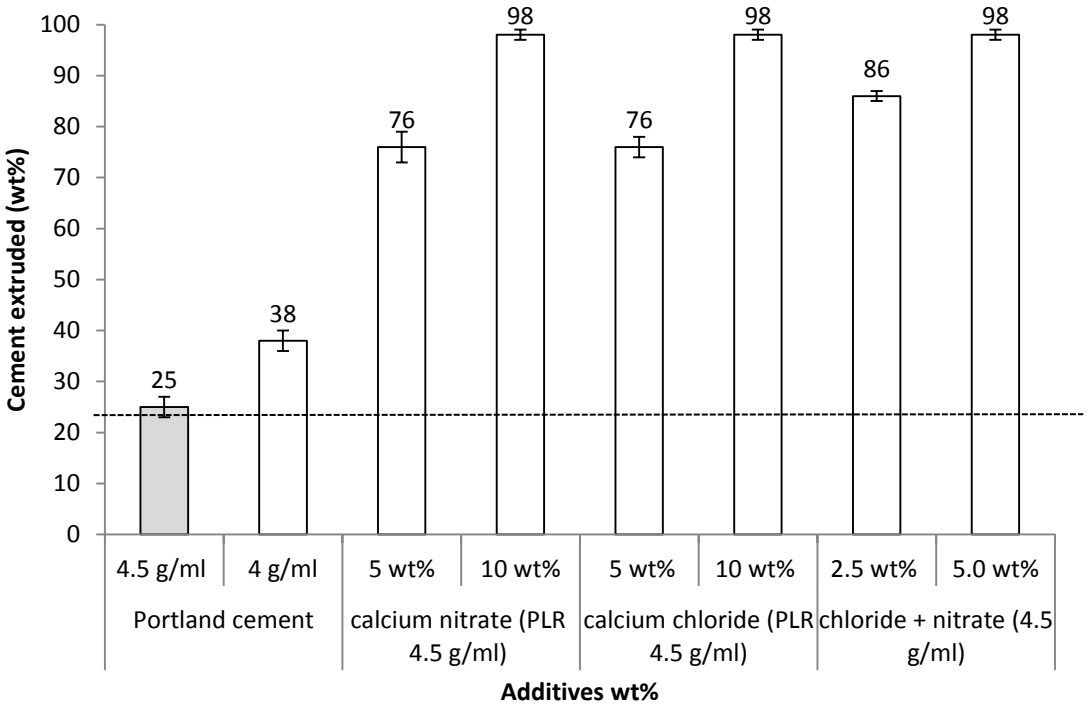

Figure 3.3.1 Graph demonstrating the significant ($p<0.05$) increase in cement extrusion (injectability) when calcium chloride, calcium nitrate or a combination of the two was added to PC (standard injectability indicated by dotted line. There was a significant ($p<0.05$) increase in extrusion with a 5 wt% addition of either additive to PC, there was a further significant ($p<0.05$) increase in injectability when the additions were increased to 10 wt% (sample number n=4).

3.3.2 Extension graphs

Cements containing calcium chloride and/or calcium nitrate liquefiers either individually or in combination required only a relatively low initial force of between 3 and 30 N to extrude the majority of the cement from the 2 mm syringe aperture, an increase in force was required only when the syringe was nearly empty (figure 3.3.2). In contrast, PC without a liquefier demonstrated no characteristic force plateau but exhibited a sharp increase in force necessary for displacement as the cement failed to be extruded from the syringe.

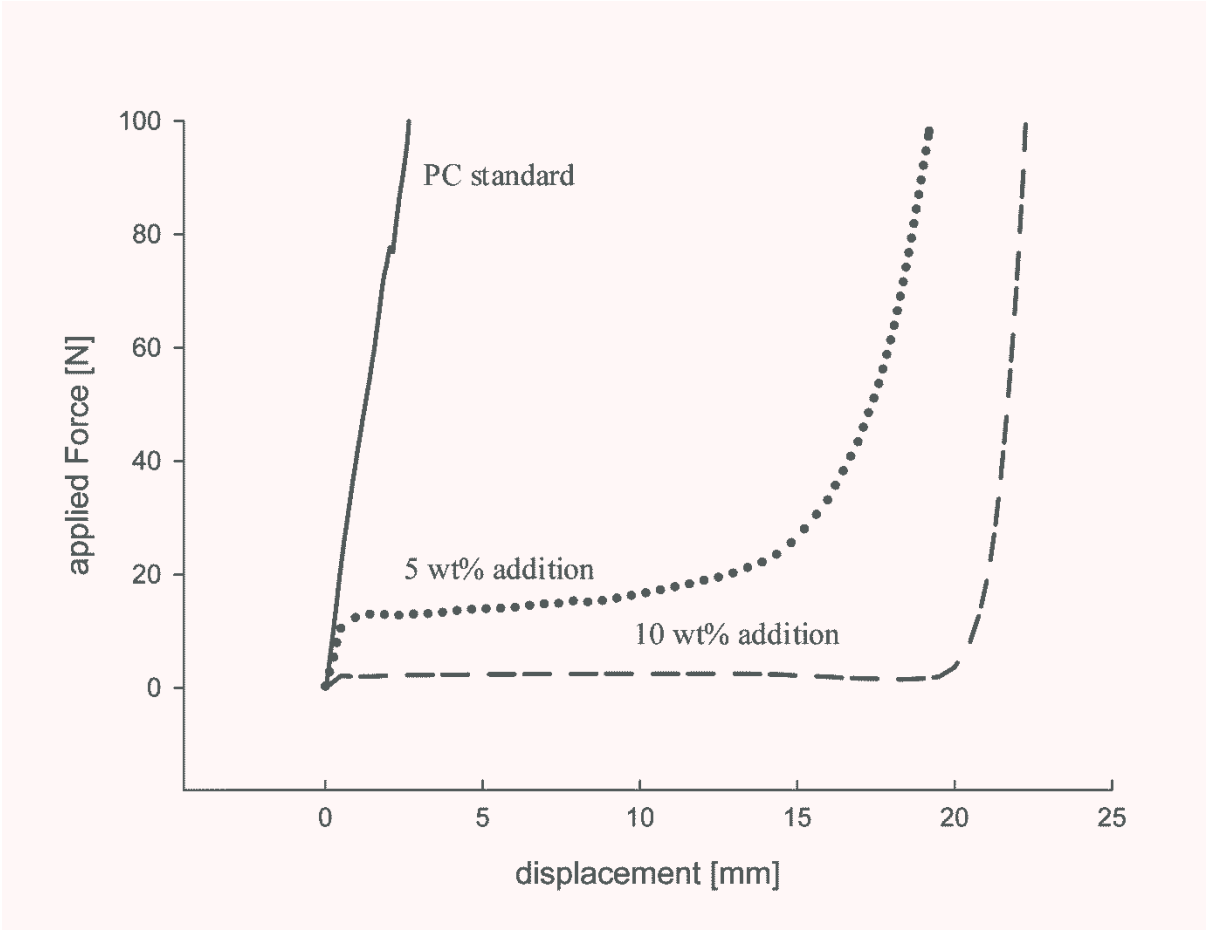

Figure 3.3.2 A typical force/displacement graph recorded during the injectability experiments. Adding 5 wt% of calcium chloride or calcium nitrate reduced the force required to displace the syringe plunger during cement injection. Increasing the additive content to 10 wt% further reduced the force to a point where less than 5 N was required to extrude over 90 wt% of the cement.

3.3.3 Initial cement setting time, compressive strength and density measurements

The two additives both acted as setting accelerants when added individually or in combination (figure 3.3.3). The addition of calcium chloride or calcium nitrate significantly ($p<0.05$) decreased setting times from over 2 h to below 60 minutes with 5 wt% additions and there was a further significant ($p<0.05$) decrease to below 22 minutes for the 10 wt% additions.

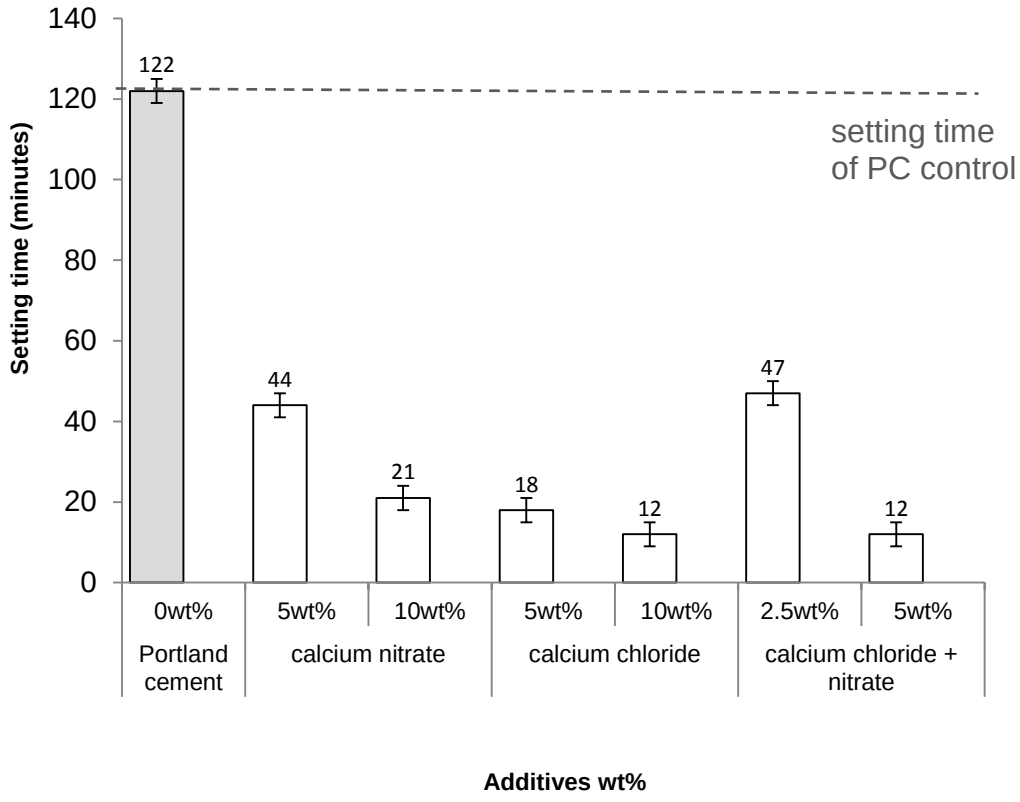

Figure 3.3.3 Graph showing the influence of different additives on the setting time compared with control cement (Dotted line indicates standard setting time). The addition of 5 wt% calcium chloride, calcium nitrate or a combination of the two significantly ($p<0.05$) decreased cement setting times compared with the PC standard. There was also a significant ($P<0.05$) decrease in setting times when increasing additives to 10 wt% (sample number n=3).

After 24 h setting cements containing 5 wt% additions of calcium chloride, calcium nitrate or 2.5 wt% combination of the two produced compressive strengths which were comparable or higher than the PC standard (Table 3.3.1). In contrast, cements containing 10 wt% additions had significantly ($p<0.05$) lower compressive strengths. After 30 days cements 5 wt% additions all possessed significantly ($p<0.05$) higher compressive strengths than the standard cements. The compressive strengths of the 10 wt% additions of calcium chloride and nitrate were still significantly ($p<0.05$) lower than the standard cements but the 5 wt% combination of the two were not significantly different ($p<0.05$) with the standard.

After both 1 and 30-days the relative porosities of the cements containing 5 wt% calcium chloride or nitrate or a 2.5 wt% combination of the two all possessed lower relative porosities than the PC standard. In contrast, after 24 h cements containing a total of 10 wt% additive all had lower porosities, but after 30-days the porosities were comparable with the standard cement. The specific density of the cement in the presence of chloride and nitrate was consistently lower than the standard regardless of the wt% used. As the specific density of cement decreases with adsorption of water this indicated that in the presence of chloride and nitrates the cements hydrated more quickly, i.e. the setting reaction was accelerated.

Table 3.3.1 Compressive strength, relative porosities and specific densities for cements containing additions of either calcium chloride, calcium nitrate or a combination of the two. After both 1 and 30-days setting, cements containing 5 wt% calcium nitrate or 2.5 wt% combinations of calcium chloride and calcium nitrate possessed significantly ($p<0.05$) higher compressive strengths than the PC standard. In contrast, cements containing a total additive addition of 10 wt% possessed significantly ($p<0.05$) lower compressive strengths than the PC standard. The relative porosities of the cements containing 5 wt% additions were lower than the PC standard, whereas the cements containing 10 wt% additions were consistently higher. Adding 5 or 10 wt% of any additive reduced the specific densities of the set cements. Standard deviation (compressive strength) and minimum error of method (specific density, porosity) are given as error (compressive strength n=30).

Additive	Wt% of admixture	Compressive strength/MPa (1-day)	Compressive strength/MPa (30-day)	Relative porosities\ % (1-day)	Relative porosities\ % (30-day)	Specific densities\ g/cm^3 (1-day)	Specific densities\ g/cm^3 (30-day)
PC standard		56 ± 4	73 ± 7	23 ± 1	20 ± 1	2.55 ± 0.05	2.44 ± 0.05
Calcium chloride	5	*57 ± 7*	*88 ± 8*	*19 ± 1*	*15 ± 1*	*2.45 ± 0.05*	*2.38 ± 0.05*
	10	**43 ± 6**	**63 ± 7**	**25 ± 1**	**19 ± 1**	**2.43 ± 0.05**	**2.32 ± 0.05**
Calcium nitrate	5	*66 ± 7*	*89 ± 8*	*18 ± 1*	*13 ± 1*	*2.47 ± 0.05*	*2.37 ± 0.05*
	10	**45 ± 6**	**62 ± 6**	**26 ± 1**	**22 ± 6**	**2.43 ± 0.05**	**2.33 ± 0.05**
Calcium chloride/nitrate combination	2.5	*67 ± 7*	*99 ± 6*	*17 ± 1*	*13 ± 1*	*2.47 ± 0.05*	*2.36 ± 0.05*
	5	**44 ± 7**	**73 ± 7**	**27 ± 1**	**19 ± 1**	**2.43 ± 0.05**	**2.32 ± 0.05**

3.3.4 Surface charge investigations using zeta-potential measurements

The surface charge of the standard cement particles was approximately -12 mV. Calcium nitrate and calcium chloride addition significantly ($p<0.05$) reduced the negative charge of the cement resulting in charge neutralisation of the cements (figure 3.3.4).

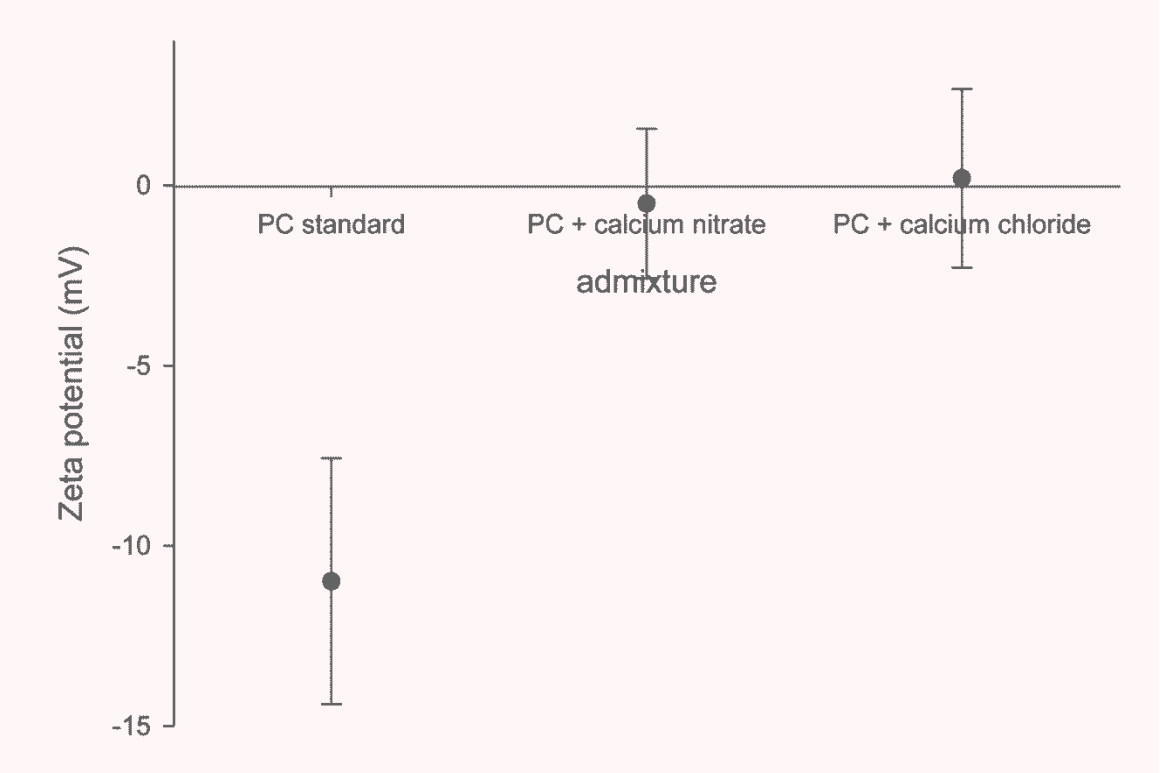

Figure 3.3.4 Zeta potential measurements of hydrating PC in the presence of calcium chloride and calcium nitrate. Inclusion of the additives to Portland cement caused an inflection in the surface charge of the hydrating cement (sample number n=3).

3.3.5 Cement enthalpy change investigations by differential scanning calorimetry (DSC)

An addition of 5 wt% calcium chloride to PC produced an overall exotherm which was not significantly ($p<0.05$) different from the standard cement, mean of 25 and 29 J g^{-1} cement respectively (figure 3.3.5). The profile of the chloride cements heat signature indicated that the exotherm was predominantly generated within the first 10 minutes of setting, which coincided with the setting time of the cement as determined via the Gilmore needles test. On closer inspection the peak appeared to be composed of three distinct shoulders. The PC standard and cements containing 5 wt% calcium nitrate both possessed similar heat signatures where the exotherm was released in a single asymmetric peak over 2 h. Addition of calcium nitrate did not produce a significantly higher exotherm compared with the PC standard but the exothermic peak at approximately 40 minutes appeared consistently earlier than the PC standard.

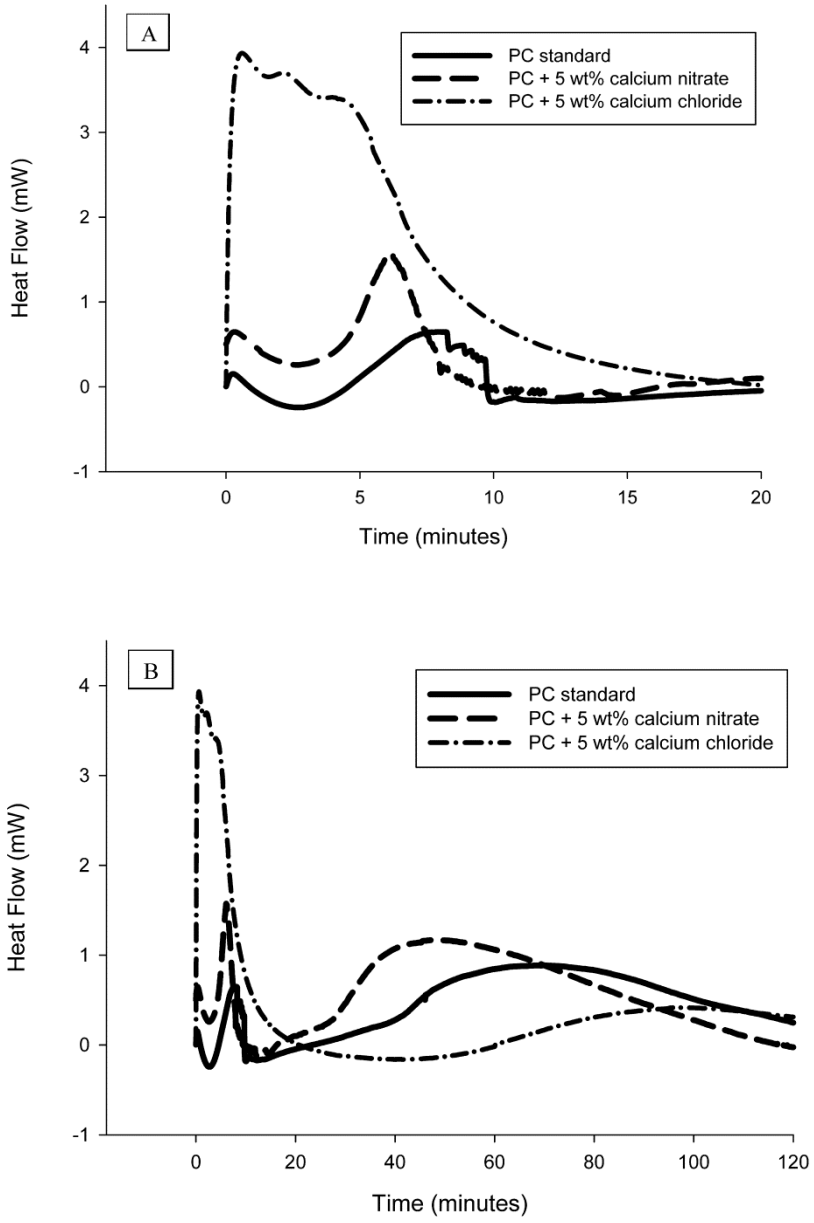

Figure 3.3.5 (a) Graphs illustrating the isothermal calorimetry traces of PC standard and cements containing either 5 wt% calcium nitrate or 5 wt% calcium chloride during the first 120 minutes of cement setting. The addition of calcium chloride produced a similar overall energy release with the standard cement except that the majority of energy with the chlorides was released early during the setting reaction. In contrast, cements containing nitrate had a similar trace profile with the standard cements. (b) When the chloride exotherm was investigated more closely the trace appeared to comprise 3 distinct exotherms which all occurred within the first 10 minutes of the start of the setting reaction (sample number n=3).

3.3.6 FTIR analysis

The absorbance peak at 3640 cm^{-1} appeared to correspond with calcium hydroxide the major by-product of the hydration phase C-S-H (figure 3.3.6). Therefore, this peak may have indicated the early presence of this setting phase in the cements containing calcium nitrate.

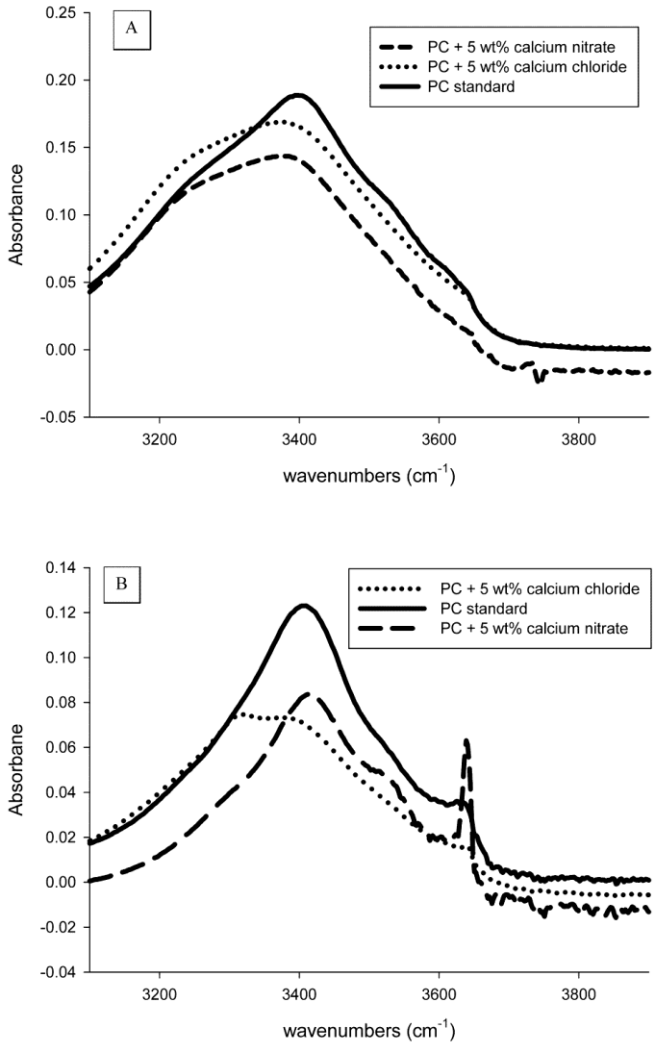

Figure 3.3.6 (A) FTIR spectra of PC standard and cements containing either 5 wt% calcium chloride or calcium nitrate 2 minutes after cement mixing. 6 (B) After 120 minutes the calcium nitrate cements had developed a peak at 3640 cm^{-1} indicating the presence of calcium hydroxide (sample number n=3).

3.3.7 Phase analysis using X-ray diffraction

After 2 h setting cements containing 5 wt% calcium chloride demonstrated peaks at 9° and 16° theta corresponding with the set cement phase ettringite (figure 3.3.7). Whereas cements containing 5 wt% calcium nitrate had a small peak at 18° theta corresponding with calcium hydroxide. The only noticeable PC standard peak was at 25° theta corresponding with anhydrous calcium sulphate. After 24 h all of the cements contained ettringite and calcium hydroxide peak in addition to a small peak at 29° theta corresponding with C-S-H formation. After 30-days of setting the calcium hydroxide peak in all the cements appeared significantly higher than the 1-day set cements.

A

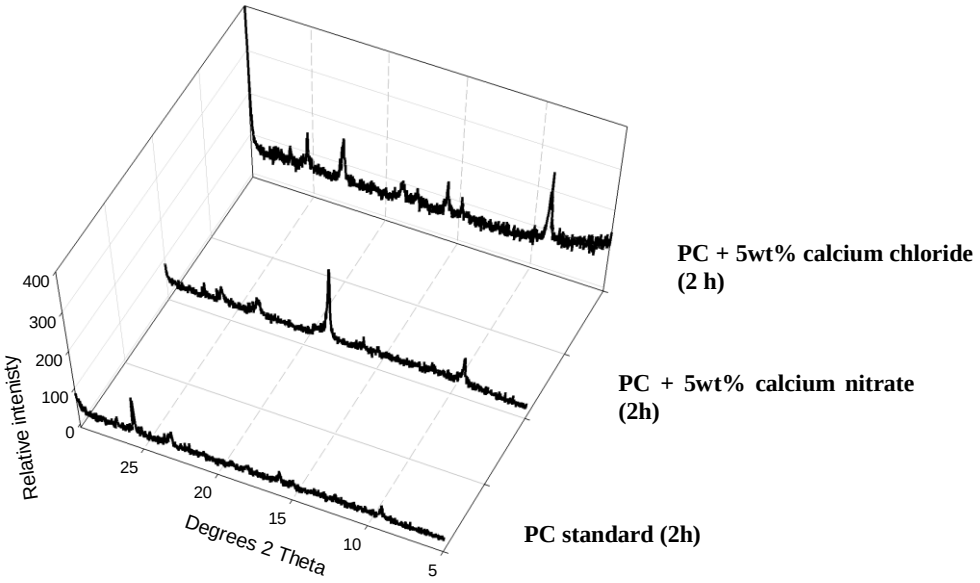

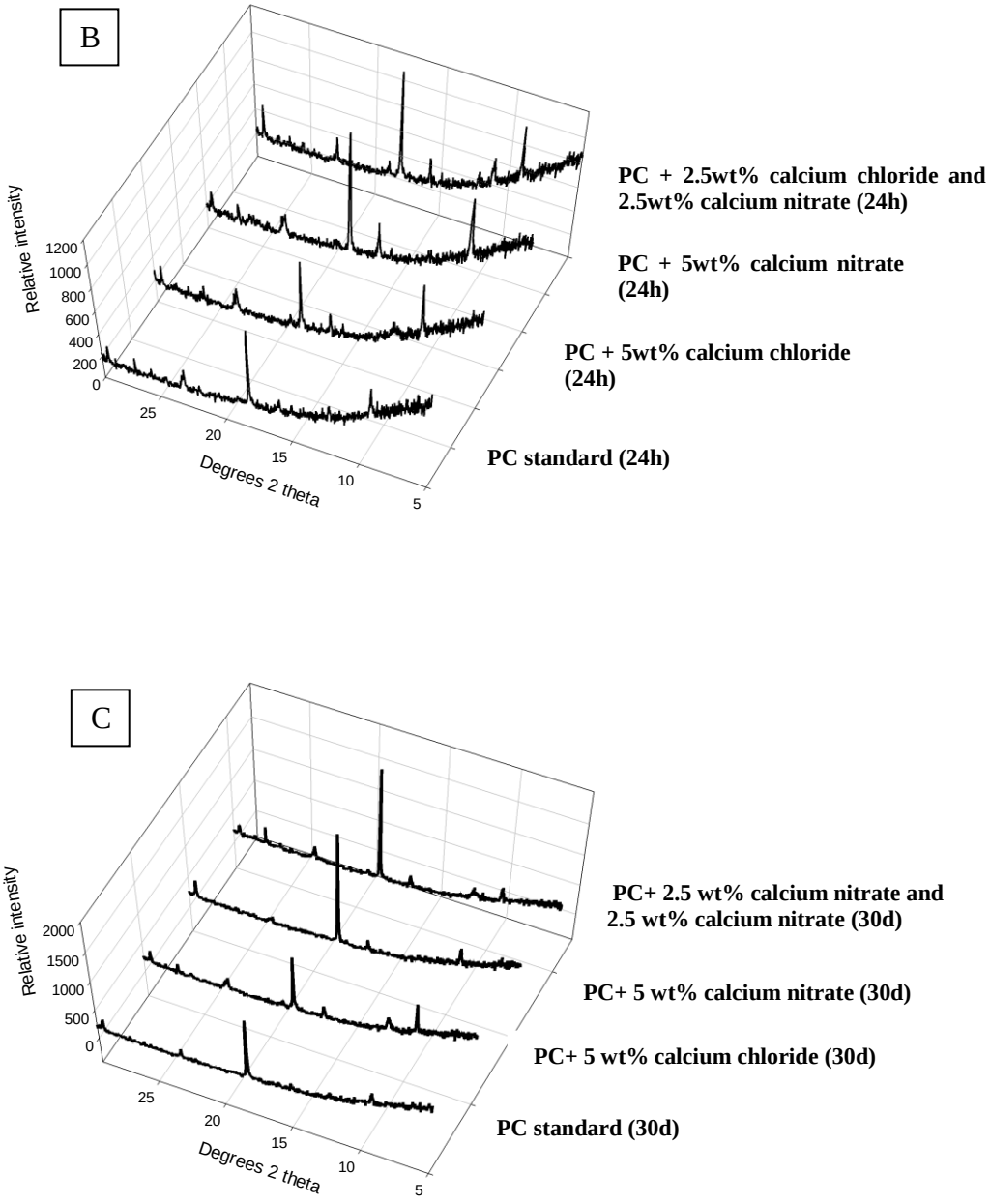

Figure 3.3.7 X-ray diffraction patterns of set cements after 2 h (7A), 24 h (7B) and 30-days (7C). After 2 h calcium chloride enhanced peaks at 9° and 16° thetas corresponding with the set cement phase ettringite. Cements containing calcium nitrate possessed a calcium hydroxide peak at 18° theta. In contrast, after 2 h the only discernible peak for the PC standard was calcium sulphate di-hydrate at 25° theta. After 24 h all of the cements had developed ettringite peaks in addition to those corresponding with C-S-H formation at 29° theta. After 30-days setting the peaks corresponding with calcium hydroxide were significantly higher.

3.4 CHAPTER: Modification of Portland cement with the citrate anion

3.4.1 Injectability studies

Cement injectability was highest for an addition of either 2 wt% sodium or potassium citrate with both additions enabling 90 wt% cement extrusion (figure 3.4.1). However, when increasing the additive content to 5 wt% the injectability significantly ($p<0.05$) decreased to a value lower than the PC standard. For cement containing calcium citrate the injectability was significantly ($p<0.05$) higher than the PC standard whereas cements containing citric acid showed significantly ($p<0.05$) lower injectabilities. The standard cement was also injected at a PLR of 4.75 g ml^{-1} (equivalent to the PLR of PC minus a 5 wt% citrate addition) indicating that by simply increasing the water content of the cement it was not possible to increase cement injectability to the level that could be achieved with an additive addition.

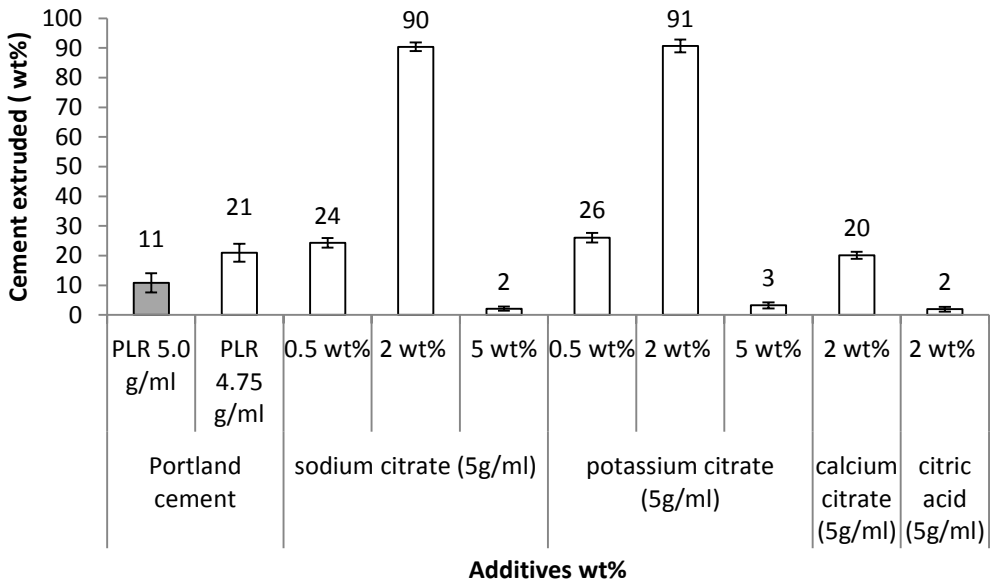

Figure 3.4.1 Graph showing cement extrusion in the presence of various citrate additives. Injectability significantly ($p<0.05$) increased with the additions of sodium and potassium citrate up to a limit of 2 wt%. Further increasing the additions of either of these citrates to 5 wt% significantly reduced cement injectability. Calcium citrate significantly ($p<0.05$) increased cement injectability compared with the PC standard, whereas citric acid significantly ($p<0.05$) reduced injectability (sample number n=4).

3.4.2 Extension graphs

For cements containing a 2 wt% addition of sodium or potassium citrate only a relatively low initial force of between 3 to 5 N was required to extrude the majority of the cement. An increase in force was required only when the syringe was nearly empty (figure 3.4.2). In contrast, with 5 wt% sodium or potassium citrate no characteristic force plateau was evident but a sharp increase in force with little displacement became apparent as the cement failed to extrude from the syringe.

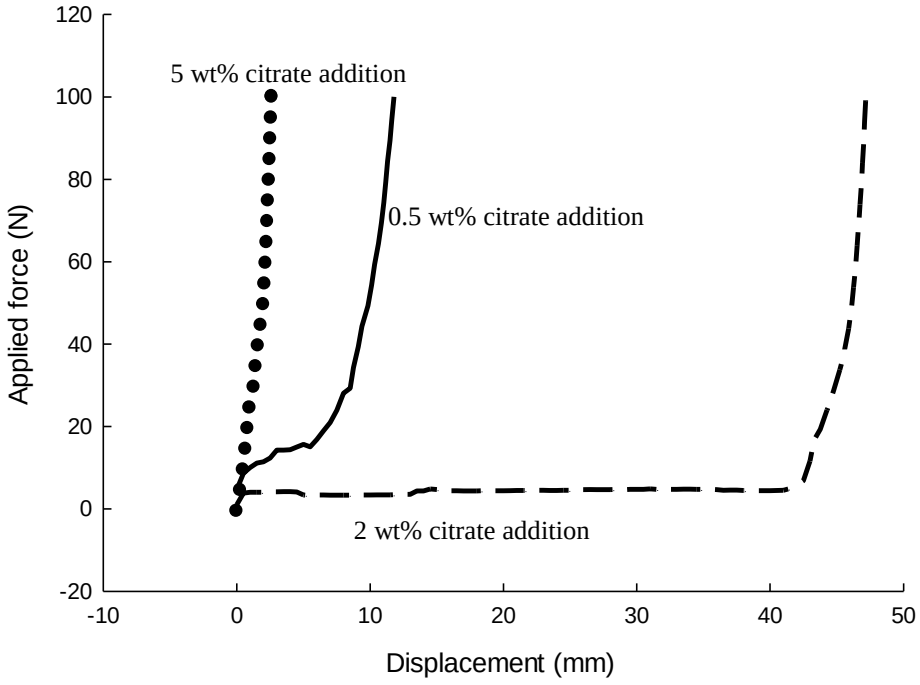

Figure 3.4.2 A typical force/displacement graph recorded during the injectability experiments. With a 2 wt% addition of sodium or potassium citrate a force of less than 10 N was required to extrude the cement. Altering the wt% produced reduced injectabilities.

3.4.3 Setting time measurements

Increasing the addition of sodium or potassium citrate from 0.5-5 wt% significantly ($p<0.05$) reduced PC setting times (from 123 minutes for the PC standard to 3 minutes with a 5 wt% addition of citrate) (figure 3.4.3). The setting time for cements containing either calcium citrate or citric acid could not be measured as the paste was too dry to assess the imprint of the Gilmore needle.

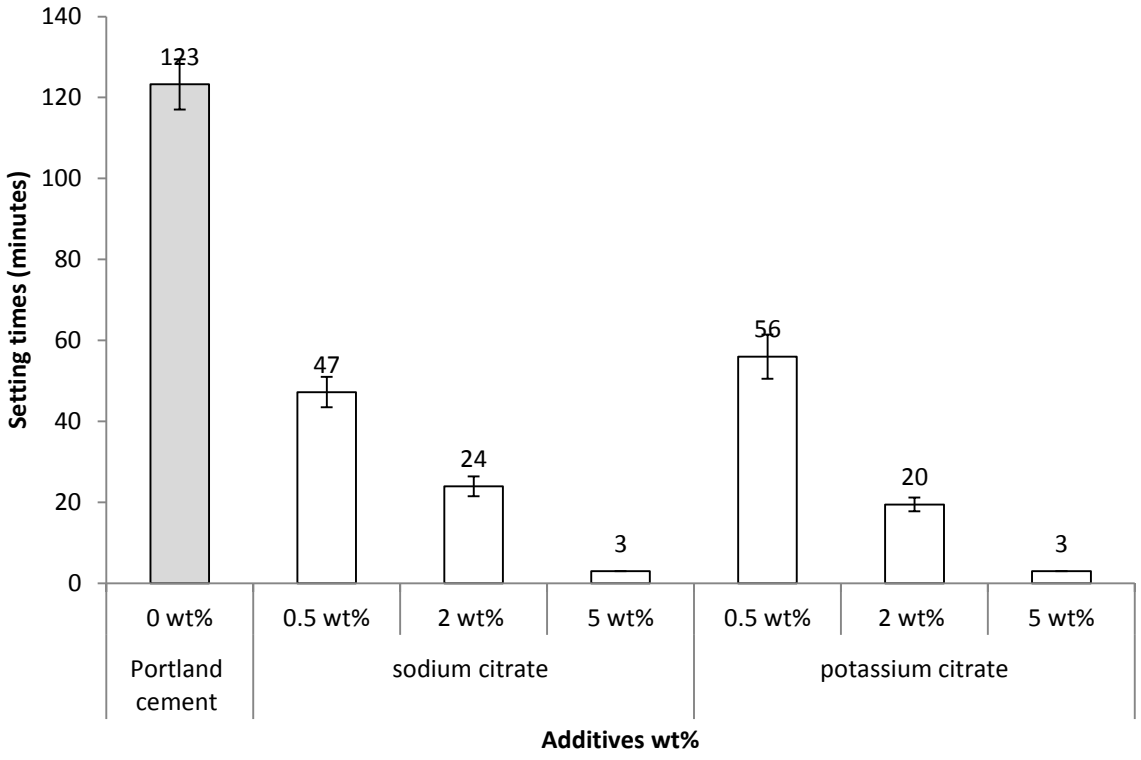

Figure 3.4.3 Graph showing the initial setting times of cements in the presence of 2-5 wt% sodium and potassium citrate indicating that both additives acted as accelerants (sample number n=3).

3.4.4 Compressive strengths

The highest compressive strengths were obtained by 2 wt% additions of either sodium or potassium citrate to the cement (98 and 125 MPa respectively after 30 days setting) (table 3.4.1). Observation indicated that calcium citrate and citric acid did not set within the moulds after 6 h so it was not possible to obtain compressive strength values for either of these additives.

The lowest porosities and strut densities were also observed with the 2 wt% additions of potassium and sodium citrate. For each individual additive addition the 30 day relative porosity and specific density values were lower than measured at 1 day.

Table 3.4.1 Compressive strength, relative porosities and specific densities for cements containing additions of 0.5- 5 wt% sodium and potassium citrate. Maximum compressive strengths were achieved by the additions of either 2 wt% sodium or potassium citrate. The 2 wt% cements also possessed lower porosities and strut densities than the 0.5 and 5 wt% additions and were also lower than the PC standard (compressive strength n=30).

Admixture	Wt %	Compressive strength/MPa (1-day)	Compressive strength/MPa (30-day)	Relative porosities % (1-day)	Relative porosities % (30-day)	Specific densities g/cm^3 (1-day)	Specific densities g/cm^3 (30-day)
PC standard		66 ± 8	83 ± 7	19 ± 1	13 ± 1	2.62 ± 0.01	2.51 ± 0.01
Sodium citrate	0.5	57 ± 9	71 ± 7	18 ± 1	15 ± 1	2.57 ± 0.01	2.44 ± 0.01
	2	75 ± 8	98 ± 11	14 ± 1	10 ± 1	2.55 ± 0.01	2.40 ± 0.01
	5	44 ± 6	75 ± 8	19 ± 1	14 ± 1	2.54 ± 0.01	2.43 ± 0.01
Potassium citrate	2	72 ± 7	125 ± 14	13 ± 1	8 ± 1	2.54 ± 0.01	2.35 ± 0.01
	5	44 ± 7	79 ± 6	21 ± 1	13 ± 1	2.60 ± 0.01	2.39 ± 0.01

3.4.5 Investigating surface charge with zeta-potential measurements.

The addition of sodium or potassium citrate to PC significantly ($p<0.05$) increased the magnitude of the negative surface charge compared with the PC standard (figure 3.4.4). In contrast, the addition of both citric acid and calcium citrate did not significantly ($p<0.05$) effect the magnitude of the overall negative surface charge.

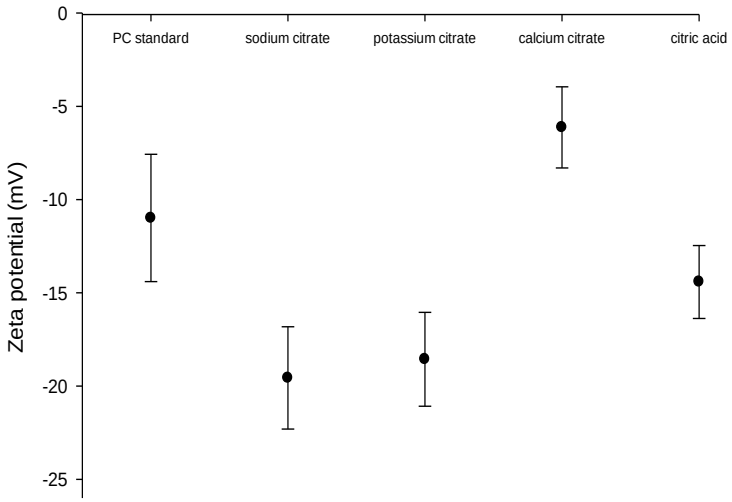

Figure 3.4.4 Graph depicting zeta potential measurements of PC in the presence of various citrates. Cements containing sodium or potassium citrate (-18 and -19 mV respectively) were both significantly ($p<0.05$) more negative than the PC standard (-11 mV). Citric acid (-14 mV) and calcium citrate (-6 mV) were not significantly ($p<0.05$) from the pc standard (sample number n=3).

3.4.6 Cement enthalpy changes measured using differential scanning calorimetry (DSC)

The mean enthalpy changes during the hydration of PC in the presence of either 2wt% sodium or potassium citrate were 83 and 96 J g^{-1} respectively (figure 3.4.5a). Both of these values were significantly ($p<0.05$) greater than those obtained from the PC standard with a value of 30 J g^{-1}. The heat trace profiles of potassium and sodium citrate additions to PC were also similar with an initial exotherm after approximately 20 minutes followed by a lower peak after approximately 40 minutes. For both sodium and potassium citrate additions the first peak corresponded with the initial setting of the cement which occurred at 24 and 20 minutes respectively. The addition of calcium citrate produced one exotherm with a single peak after 84 minutes with a mean enthalpy change of 40 J g^{-1}. PC with addition of 2 wt% citric acid did not to yield any heat from the setting reaction.

An addition of 2 wt% calcium citrate to PC appeared to generate a similar but extended trace profile as seen for the sodium and potassium citrate additives (figure 3.4.5a). When the kinetics of the setting reaction of the 2 wt% calcium citrate were accelerated by testing the enthalpy change at 37 °C a similar double peak profile was obtained (figure 3.4.5b). On addition of 5 wt% sodium citrate there was a significant acceleration of the hydration reaction which prevented measurement of the initial exotherm after sample preparation with this additive. However, based on the height and width of the initial peak the overall hydration enthalpy appeared greater than when only 2 wt% of the additive was used. The trace contained a second exotherm shoulder at 18 minutes which was also seen in the 2 wt% additions. The initial setting times of the 5 wt% sodium citrate cements also corresponded with the position of the first major exotherm occurring within the first 3 minutes of setting.

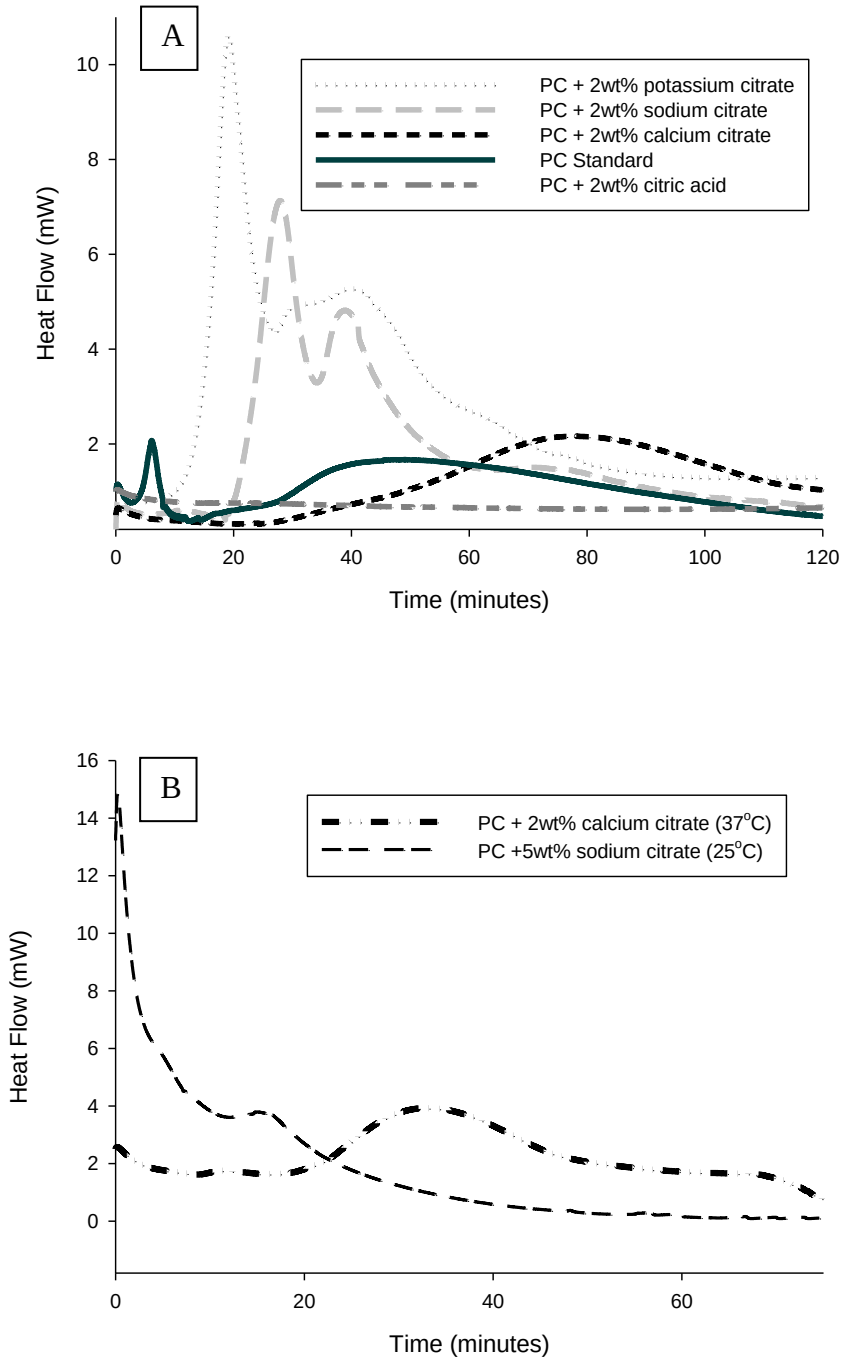

Figure 3.4.5 (a) 3 Graph showing the enthalpy change of PC with 2wt% of various citrate compounds during the first 2 h of cement hydration. The greatest enthalpy changes were observed with potassium and sodium citrate which also possessed similar profiles. (5b) Enthalpy change with PC containing 5 wt% sodium citrate (25°C) and calcium citrate set at 37°C. For the 5 wt% sodium citrate cement the kinetics of reaction were so fast that it was not possible to measure the initial exotherm (sample number n=3).

3.4.7 Cement phase analysis using X-ray diffraction (XRD).

There was no ettringite present in the PC standard or cements containing 2 wt% citric acid after 2h setting as indicated by the lack of peaks at 9 and 16° thetas (figure 3.4.6a). In contrast, cements containing 2 wt% sodium, potassium and calcium citrate possessed peaks corresponding with ettringite. After 24 h of setting the PC standard had developed an ettringite peak in addition to a calcium hydroxide peak at 18° theta (figure 3.4.6b). None of the citrate containing cements developed a calcium hydroxide peak before 24 h. Between 1 and 30-days both the cements containing 2 wt% sodium and potassium citrate developed peaks at 18° theta (figure 3.4.6c).

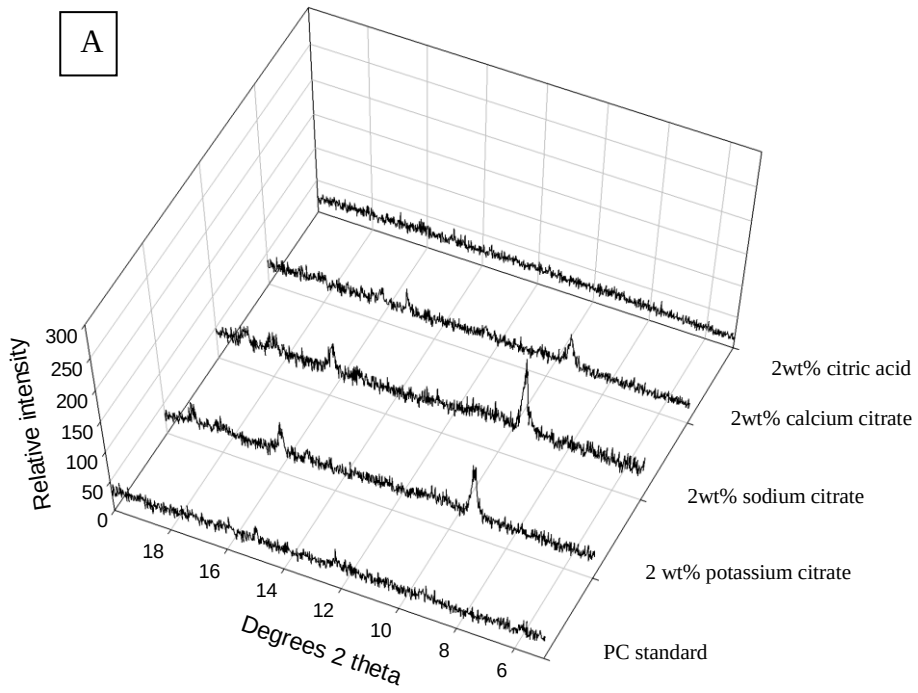

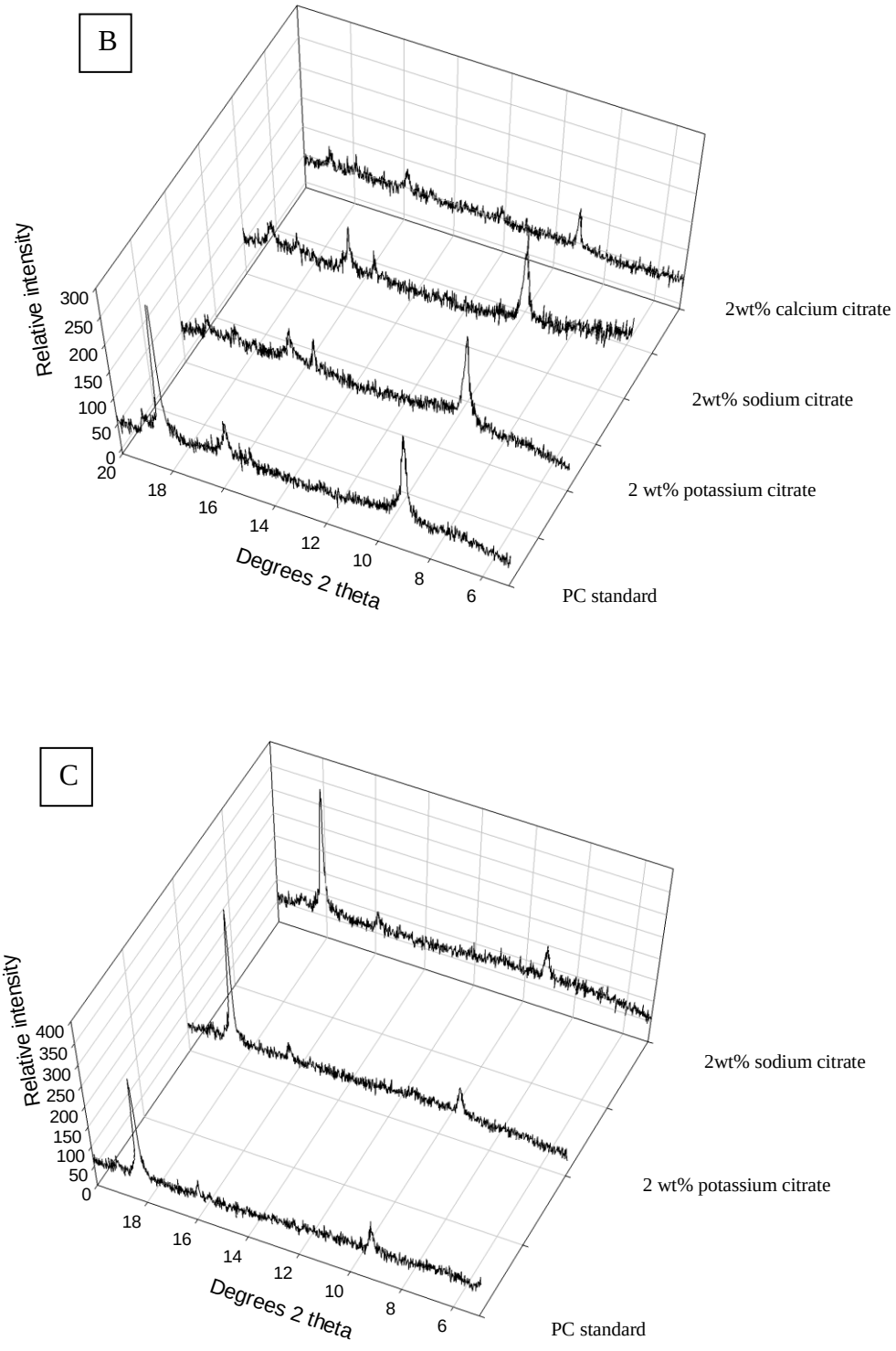

Figure 3.4.6 Spectra showing the X-ray diffraction patterns for PC containing 2 wt% of various citrate compounds. (A) after 2 h of setting only sodium and potassium citrates possessed ettringite peaks at 2 ° and 16 ° theta. (B) In contrast, after 24 h PC standard had also developed this peak in addition to another peak at 18 theta corresponding with $Ca(OH)_2$. (C) After 30-days both standard and citrate cements possessed ettringite and $Ca(OH)_2$.

3.4.8 FTIR analysis

There was a sharp increase in the calcium sulphate dihydrate (gypsum) peak at 1100 cm^{-1} during the first 60 minutes of setting for cements containing 2 wt% sodium and potassium citrate (figure 3.4.7a). The υ_3 absorption band of sulphate (SO_4^{2-}) is in this region and based on the profiles of standard calcium sulphates the peak related most closely to gypsum (180-182). In contrast, the gypsum peak for the PC standard and cements containing 2 wt% sodium citrate and citric acid did not increase during the first 2 h of reaction. When 5 wt% sodium citrate was added to the cement the gypsum peak was noticeably higher than with a 2 wt% addition (figure 3.4.7b). When 5 wt% gypsum was added in addition to the 5 wt% sodium citrate the gypsum peak was higher compared with when the citrate was used independently.

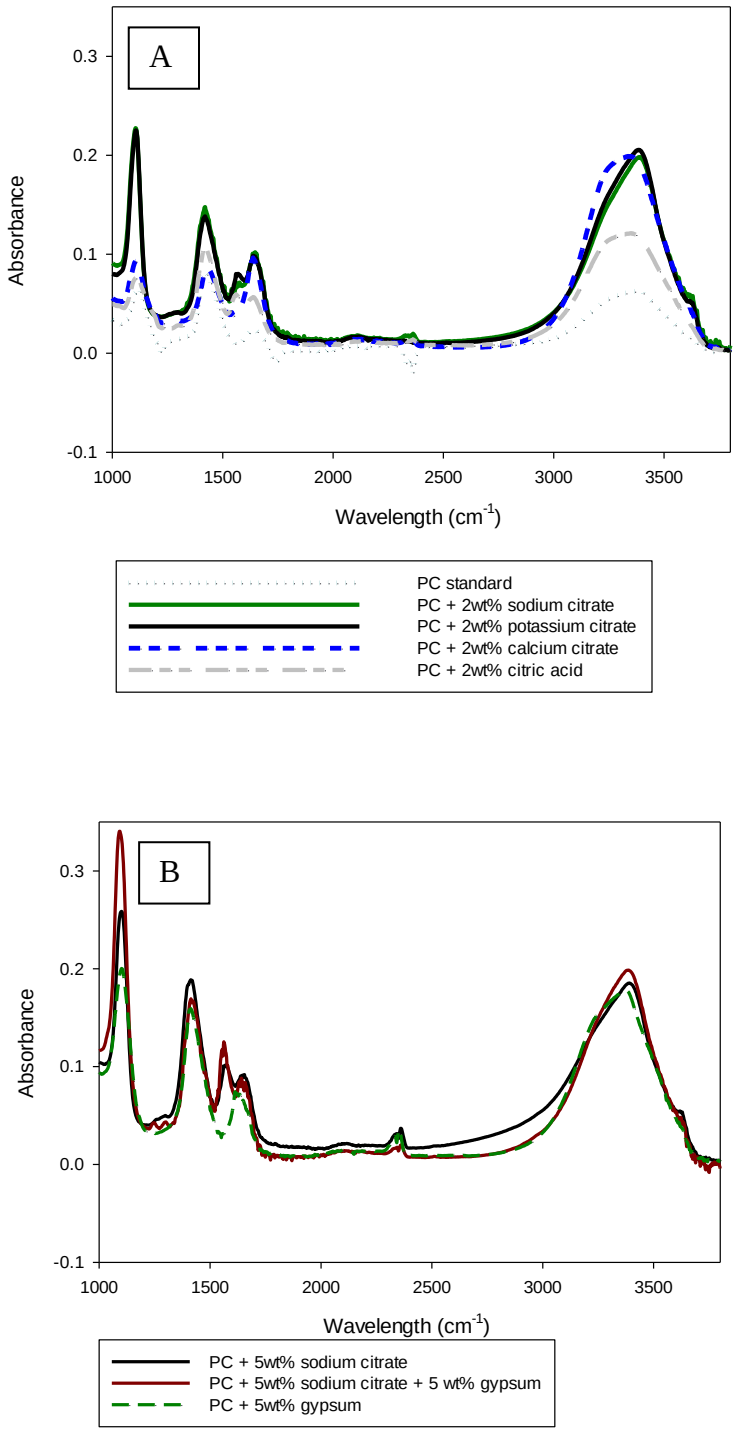

Figure 3.4.7 (a) FTIR spectra for PC and PC containing 2 wt% citrates after the first hour of setting. The absorbance of the sulphate band (1100 cm^{-1}) in the cements containing sodium and potassium citrate was noticeably higher than the PC standard. In contrast, the wide water peak at (3500 cm-1) of PC had decreased noticeably compared with the citrate containing cements. (B) When 5 wt% gypsum was added to the cement the sulphate band increased compared with the PC standard. The highest peak heights were achieved by adding gypsum in conjunction with citrate (sample number n=3).

3.4.9 Investigating surface morphology using scanning electron microscopy (SEM)

Crystals approximately 2-4 μm in diameter matching the morphology of ettringite were present after 24 h setting on the cement surface containing both 2 wt% sodium and potassium citrate (figures 3.4.8b and 3.4.8c respectively). PC standard and cement containing 2 wt% calcium citrate did not possess any crystals of similar morphology (figures 3.4.8a and 3.4.8d respectively). After 24 h the crystals on the surface of both the PC standard (figure 3.4.8e) and the cement containing 2 wt% sodium citrate (figure 3.4.8f) had extended to approximately 10μm, see figures 8e and f respectively.

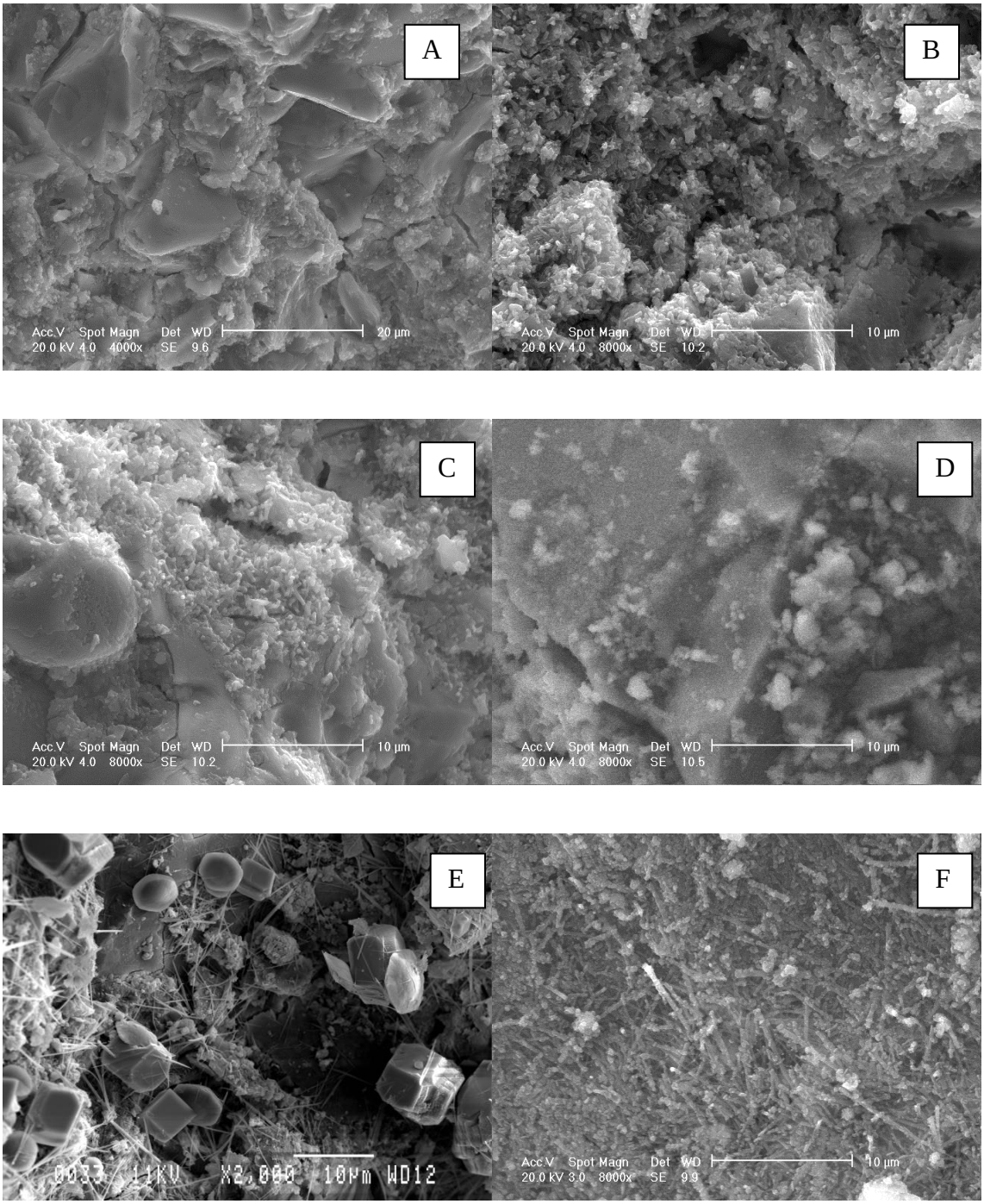

Figure 3.4.8 Scanning electron micrographs showing the surface morphology of (A) PC standard after 2h of cement setting (B) PC containing 5 wt% sodium citrate and (C) 2 wt% potassium citrate. The addition of both of these additives produced small needle shaped crystals 3 µm in length. (D) The addition of calcium citrate after 2 h did not produce any of these crystals. After 24 h of cement setting larger, 10 µm, needle shaped crystals were present in both the (E) PC standard and (F) 2 wt% sodium citrate.

3.4.10 Elemental analysis using energy dispersive X-ray spectroscopy (EDX).

When the elemental composition of the 10 µm crystals were analysed using energy dispersive X-ray spectroscopy (EDX) there was only a 3 % and 12 % difference to the theoretical values for ettringite in the O/Al and O/S ratios respectively (for full calculations refer to appendices).

3.5 Chapter: Effect of additives on the flexural strength of Portland cements.

Additions of 2 wt% sodium citrate to PC or 2.5 wt% combinations of calcium chloride and calcium nitrate were shown to increase cement injectability, reduce setting times and maintain compressive strength values (see chapters 3.3 and 3.4). A survival probability plot of the biaxial flexural strengths of the PC based materials indicated an asymmetrical distribution of the sample groups (figure 3.5.1).

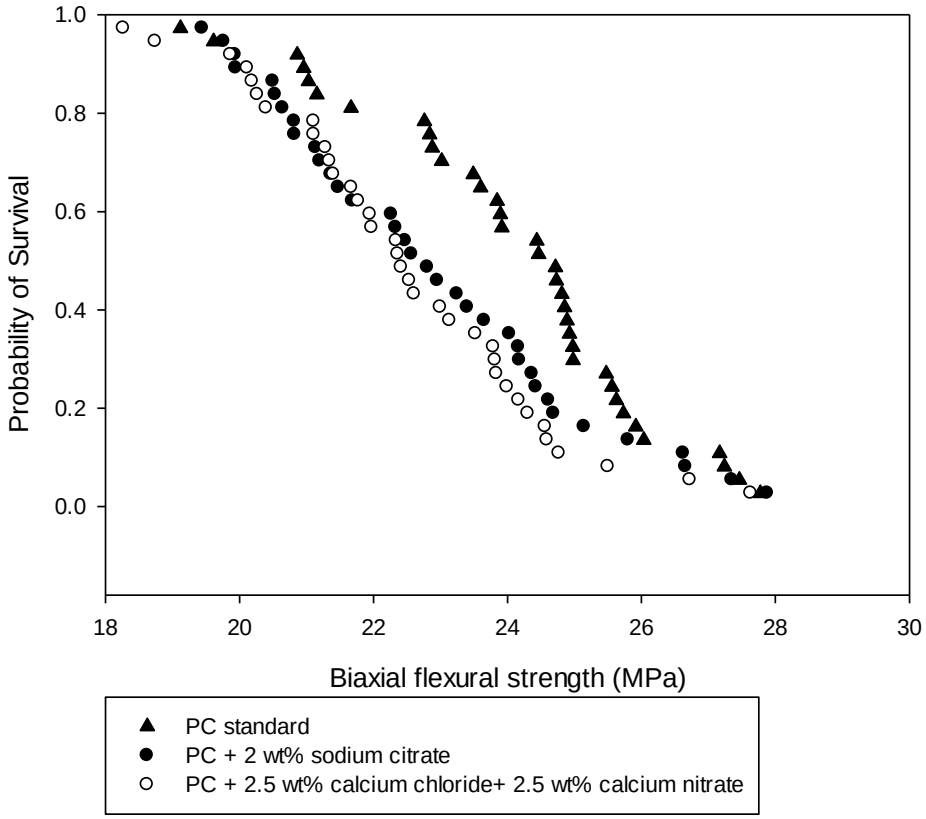

Figure 3.5.1 Probability of survival curves for different cements illustrating the flexural strengths at which samples of a group of cements (n=30) failed (Portland cement (PC) standard, PC with 2 wt% sodium citrate and PC with 2.5 wt% of both calcium chloride and calcium nitrate). There was an asymmetrical distribution of flexural strengths in cements containing both calcium chloride and nitrate (sample number n=30).

A 10 wt% addition of the radiopacifier bismuth oxide did not significantly ($p<0.05$) decrease the flexural strength of the material with mean strengths for all specimen groups above 20 MPa (figure 3.5.2).

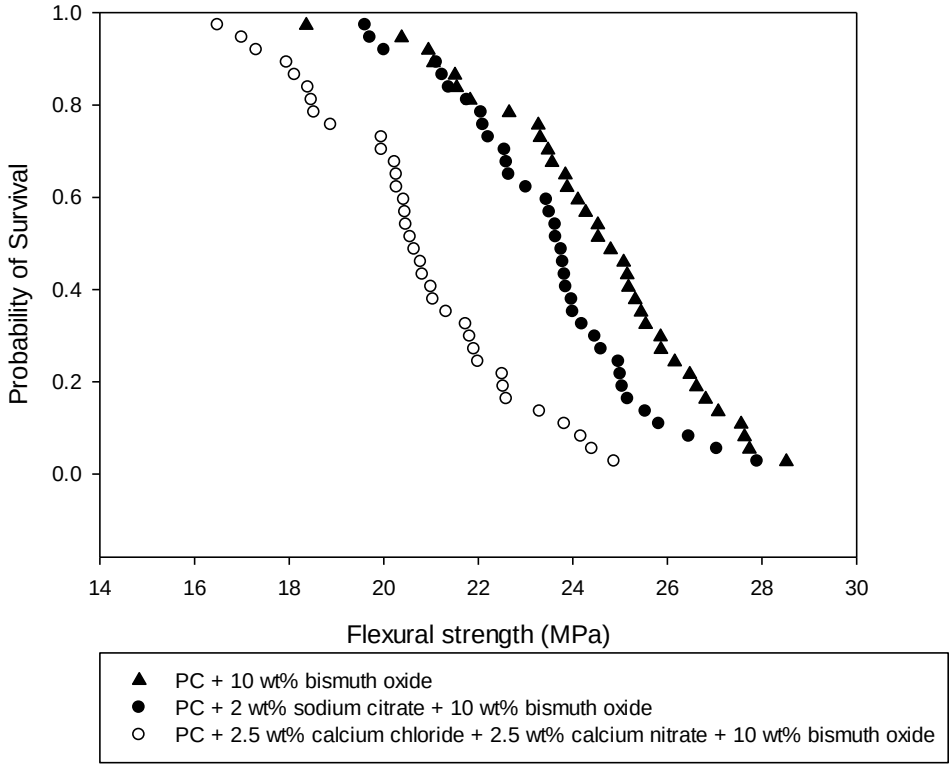

Figure.3.5.2 Graph demonstrating the flexural strengths of groups (n=30) of Portland cement (PC) containing 10 wt% bismuth oxide and PC containing bismuth oxide in addition to other setting accelerants (sample number n=30).

The confidence intervals of the Weibull modulus for all the PC variations overlapped indicating the additives did not significantly ($p<0.05$) affect the defect distribution within the brittle material. However, the linerisation of the Weibull data produced an R^2 value below 0.9 (figure 3.5.3).

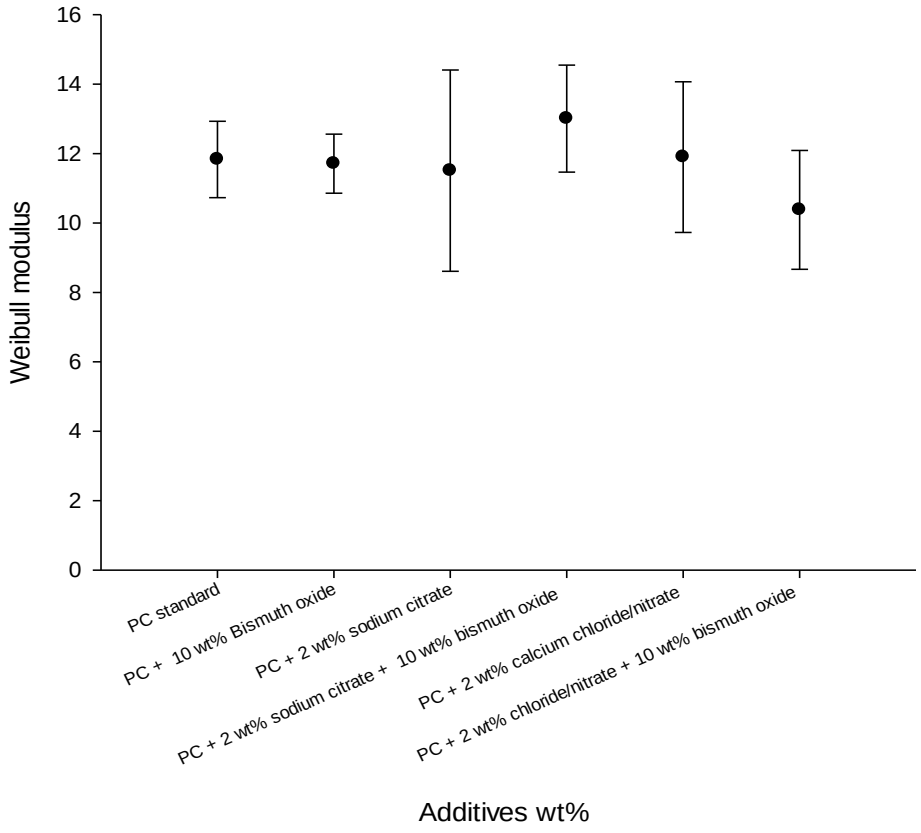

Figure 3.5.3 The Weibull modulus of all the Portland cement variations were plotted on a single graph including 95% confidence intervals. The confidence intervals for all the variations overlapped indicating the distribution of defects were similar in all samples.

Table 3.5.1 Confidence in the linearisation of Weibull data was reflected by R2 values. Only 2 wt% sodium citrate produced a value below 0.90.

Additives	R^2
PC standard	0.98
PC + 10 wt% bismuth oxide	0.99
PC + 2 wt% sodium citrate	0.89
PC + 2 wt% sodium citrate + 10 wt% bismuth oxide	0.97
PC + 2.5 wt% calcium chloride and calcium nitrate	0.94
PC + 2.5 wt% calcium chloride and calcium nitrate + 10 wt% bismuth oxide	0.95

3.6 CHAPTER: Investigating the rheology and injectability of Portland cement

3.6.1 Investigating the dynamic viscosity of Portland cement with sodium citrate additives using a parallel plate rheometer

The PC standard had an initial viscosity of approximately 1400 Pa.s which increased by 1000 Pa.s during the 30 minute experiment (figure 3.6.1b). In contrast, cements containing 2 wt% sodium citrate possessed a significantly ($p<0.05$) lower initial dynamic viscosity of 30 Pa.s which increased significantly ($p<0.05$) after 10 minutes as the cement was observed to set (figure 3.6.1a).

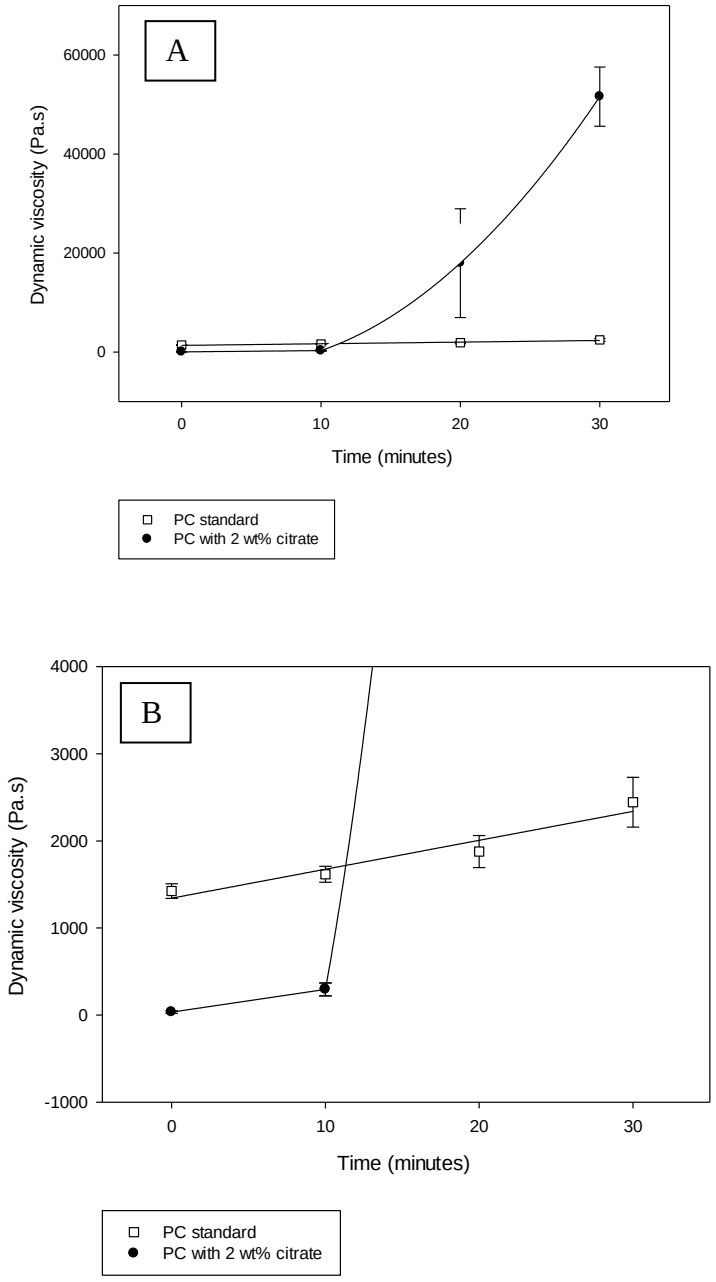

Figure 3.6.1 (a) Graphs depicting dynamic viscosity of Portland cement (PC) standard and PC containing a 2 wt% sodium citrate addition at 10 minute intervals for 30 minutes. The dynamic viscosity of the standard cement remained relatively constant during the setting period. In contrast, the viscosity of the cements containing 2 wt% sodium citrate significantly increased after 10 minutes. (b) The PC standard possessed an initial viscosity of approximately 1400 Pa.s. In contrast, the initial dynamic viscosity of cements containing 2 wt% sodium citrate was 40 Pa.s and increased to approximately 300 Pa s after 10 minutes (sample number n=3).

For the first 60 s of the viscosity testing the PC standard remained between ~1000-1400 Pa.s (figure 3.6.2). However, from 1-4 minutes the viscosity increased to 8000 Pa s and the cement was observed to begin to set on the wide aspect plate rheometer.

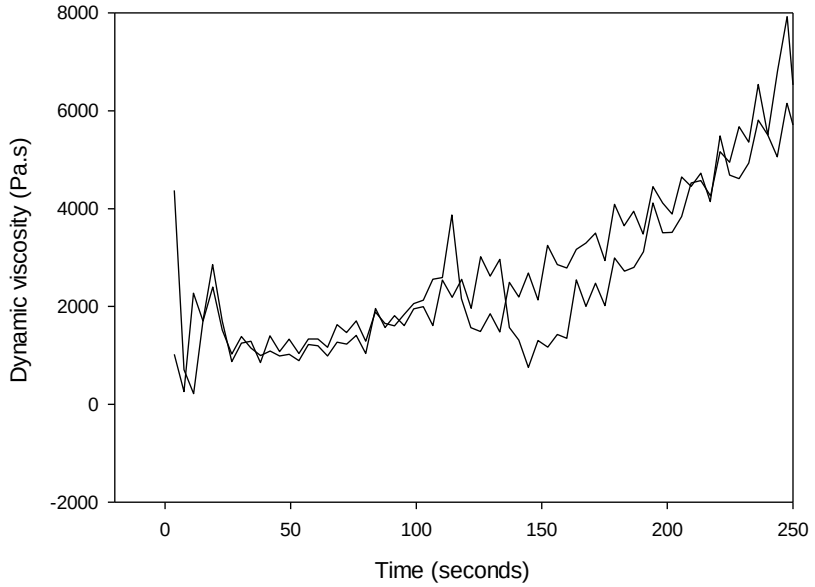

Figure 3.6.2 Graph of dynamic viscosity of PC standard during setting demonstrating the gradual increase in viscosity over 250 seconds.

Cements containing 5 wt% sodium citrate demonstrated a fluctuating viscosity during the first 10 minutes of setting (figure 3.6.3). The Gilmore needles test has previously indicated that the cement sets in under 3 minutes. The fluctuations may have occurred as a result of the cycle of cement bond formation proceeded by bond breakage as a consequence of the shear forces applied by the rheometer.

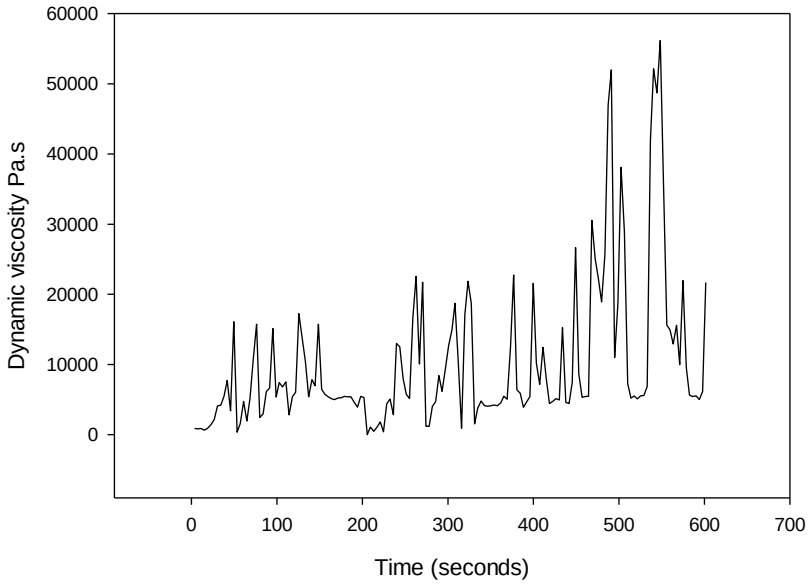

Figure 3.6.3 Graph showing the viscosity of PC containing 5 wt% sodium citrate over 10 minutes on the plate rheometer at a shear rate of 0.3 s^{-1}. The fluctuations in the dynamic viscosity indicated that the cement bonds were created and then instantly broken.

3.6.2 Injectability of Portland cement through a 5cm needle

Adding needles to the syringes containing PC standard significantly ($p<0.05$) reduced cement extrusion (figure 3.6.4). In contrast, needle addition had little effect on the extrusion of cements containing liquefying additives.

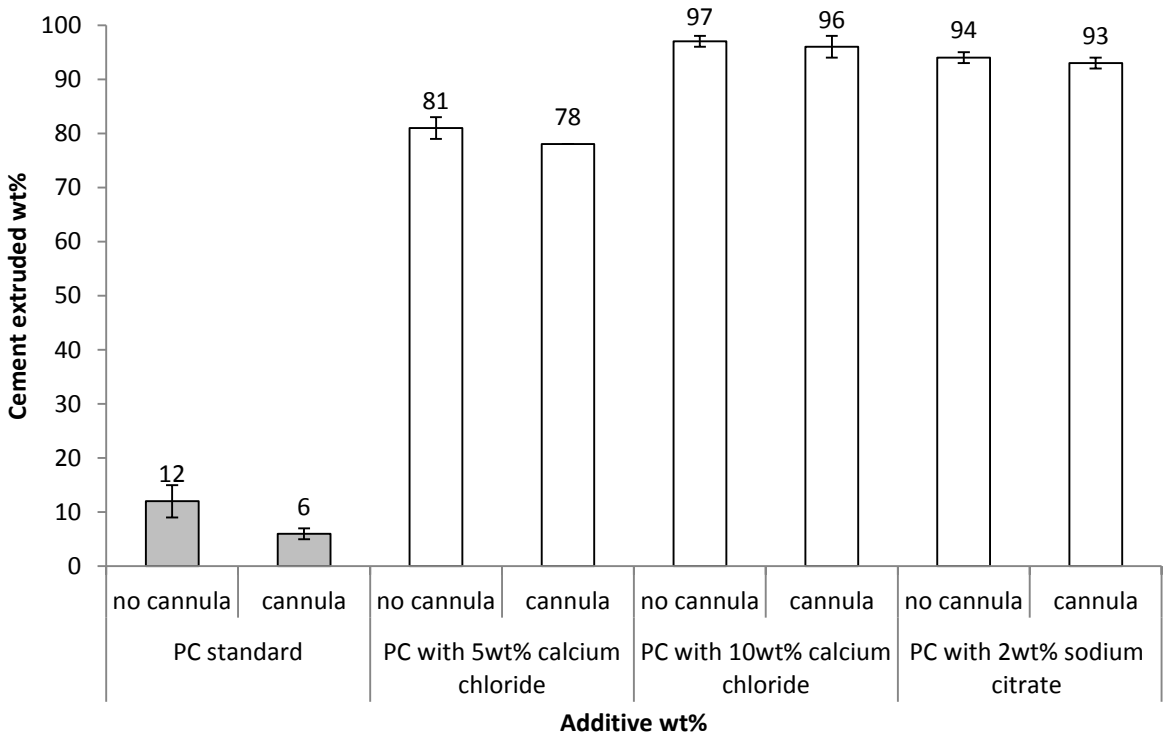

Figure 3.6.4 Graph demonstrating the effect of needle. There was a 50% decrease in cement injectability when injecting the PC standard through a needle. In contrast, the needle had only a minor impact on the injectability with PC containing an additive (sample number n=4).

There was a decrease in the displacement of the syringe plunger when needles were added to the end of the standard PC syringes (figure 3.6.5). This was reflected in the decrease in injectability of the standard cements.

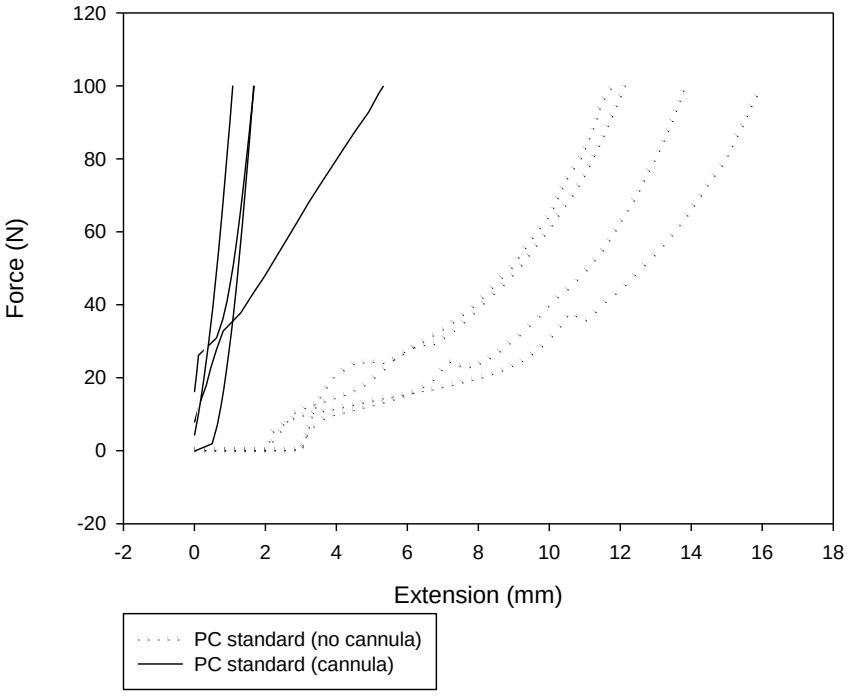

Figure 3.6.5 Force/displacement graph recorded during the injectability experiment of PC standard with and without cannula. The 50 % reduction in injectability of the PC standard can be visualised as the syringe plunger failed to extend with a cannula attached.

There was no noticeable effect of cannula addition on plunger displacement when either 2 wt% sodium citrate or 10 wt% calcium chloride was added to the cement powder (figure 3.6.6).

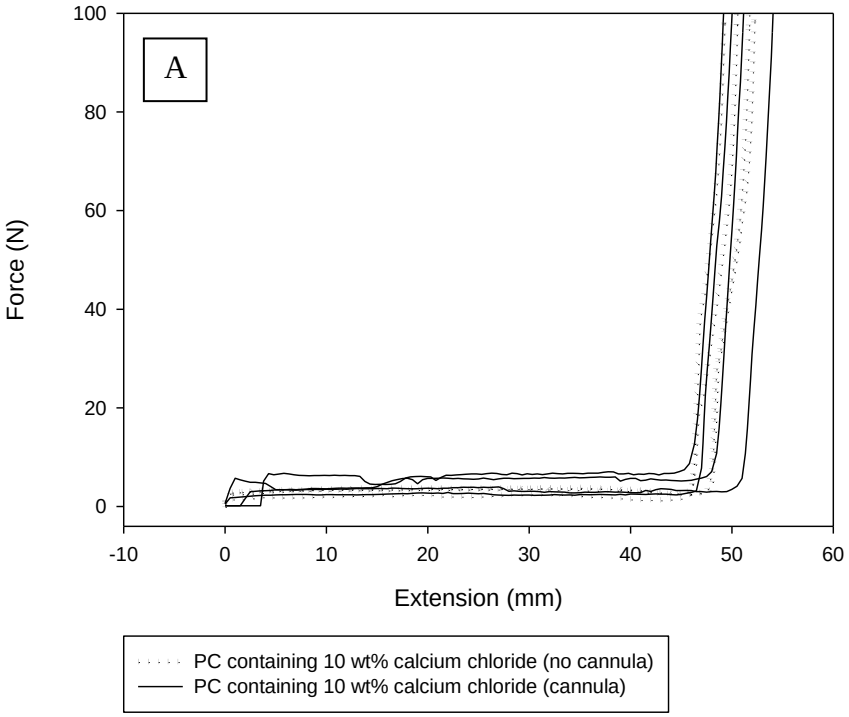

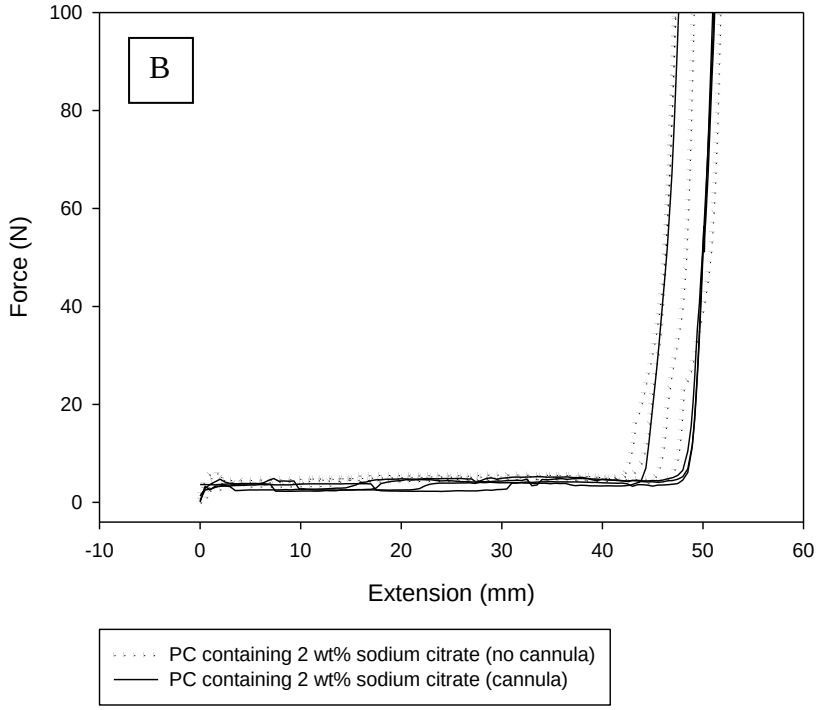

Figure 3.6.6 Force/displacement graphs recorded during the injectability experiment for cements containing (a) 2 wt% sodium citrate and (b) 10 wt% calcium chloride. There was no noticeable effect on plunger extension when a cannula was added to the syringes.

3.6.3 Monitoring the pressure drop of Portland cement with 2 wt% sodium citrate compared with PMMA

A modified universal testing machine was used to assess the pressure drop (N) of an injectable PC containing 2 wt% sodium citrate (figure 3.6.7). The cement required a mean of 20 N of force to be injected into porous Sawbone™ (200 µm pore diameter).

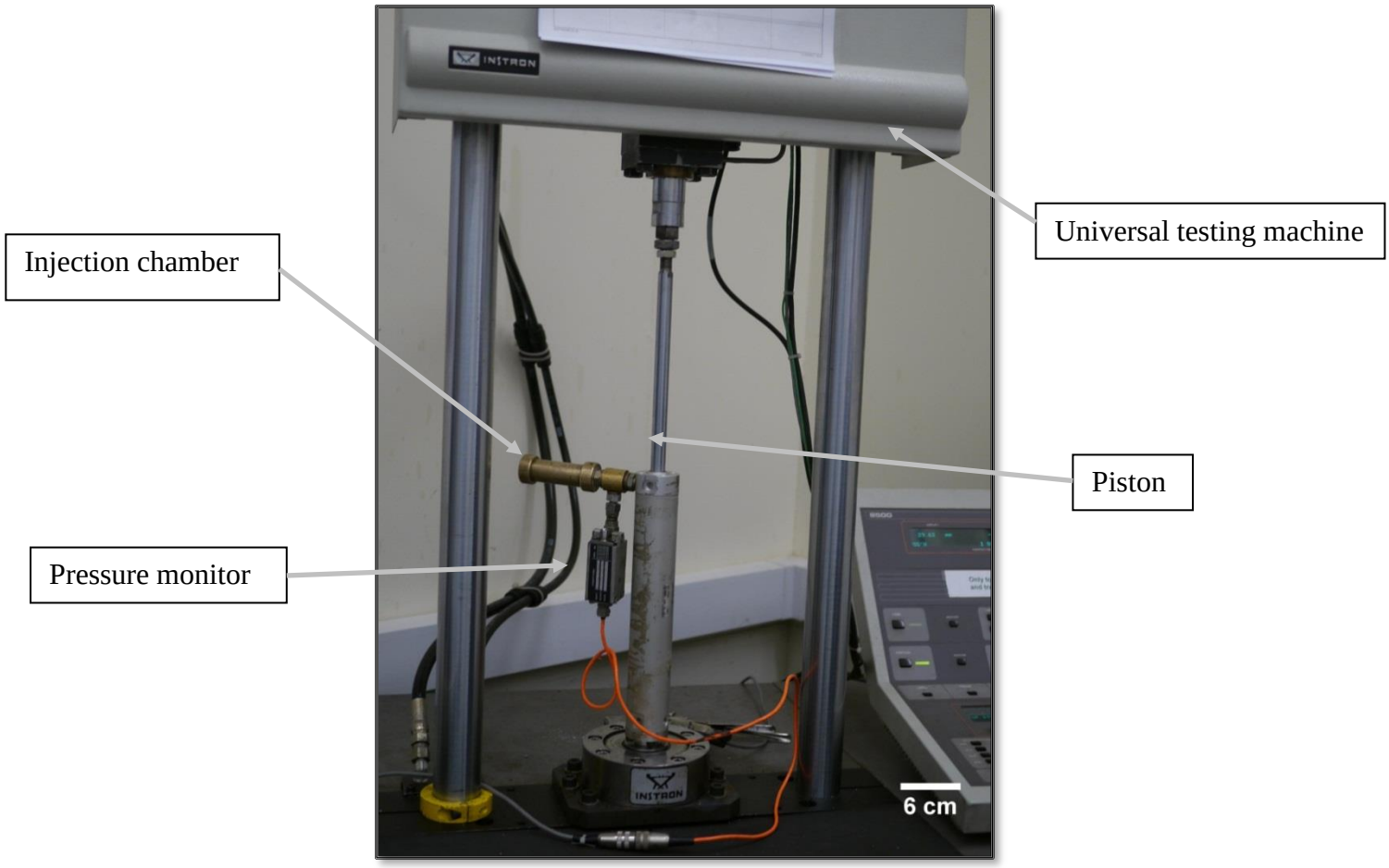

Figure 3.6.7 Injectability equipment measuring the pressure drop (N) when cements were injected into a Sawbone™ matrix with 200 µm pore size. Portland cement (PC) with a 2 wt% sodium citrate addition required less than 20 N to inject 100 ml of cement into the matrix (sample number n=3).

3.6.4 Investigate the use of Micro-CT (µ-CT) to assess cement phase separation during Portland cement injection

During the first part of the investigation a number of PC standard discs (6mm by 3mm) with ranging powder-to-liquid ratios (PLRs) were produced to assess if the µCT-grey value counts[5] varied between standards (figure 3.6.8). After producing the samples it was observed from static µ-CT images that a number of macro pores and macro cracks (>200 µm) became noticeably greater as the PLR of the cement was reduced from 5 to 2.5 g/ml. At a PLR of 2.5 macro cracks constituted approximately 10 % of the surface of the cement.

[5] Each pixel was assigned a grey scale value (from a total of 250). These values were then summed and the total percentage of each of the 250 grey values present within the image calculated.

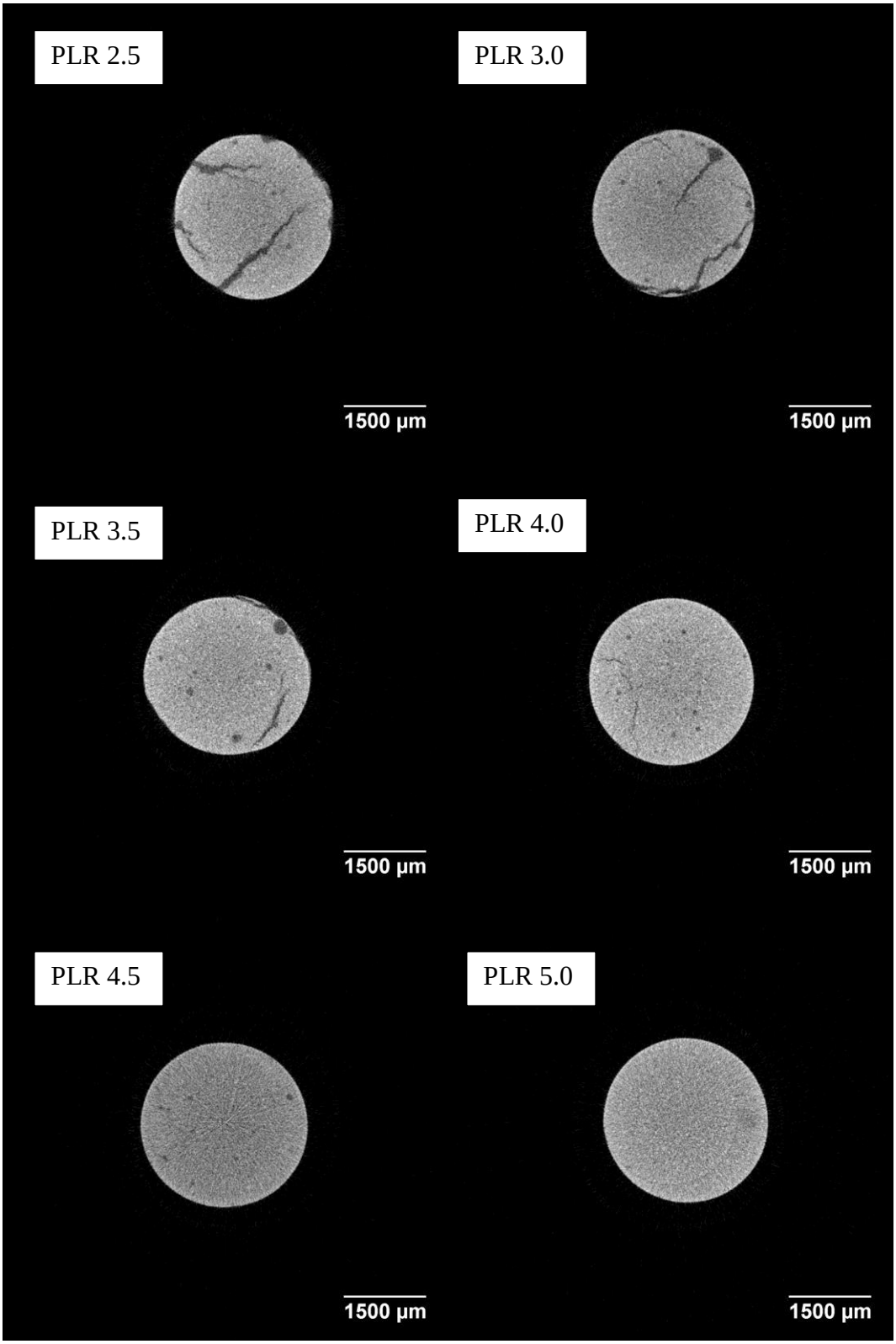

Figure 3.6.8 µ-CT images depicting the cross-section of a Portland cement standard disk with a 6 mm diameter ranging from a powder-to-liquid ratio of 2.5-5 g/ml.

The change is grey value counts were investigated using two different methods. Firstly, an 8-bit histogram was created around the circumference of the circular cement sample (figure 3.6.9a). In the second method a mask of the sample was created and the grey scale values threshold to remove the macro-pores and cracks (figure 3.6.9b).

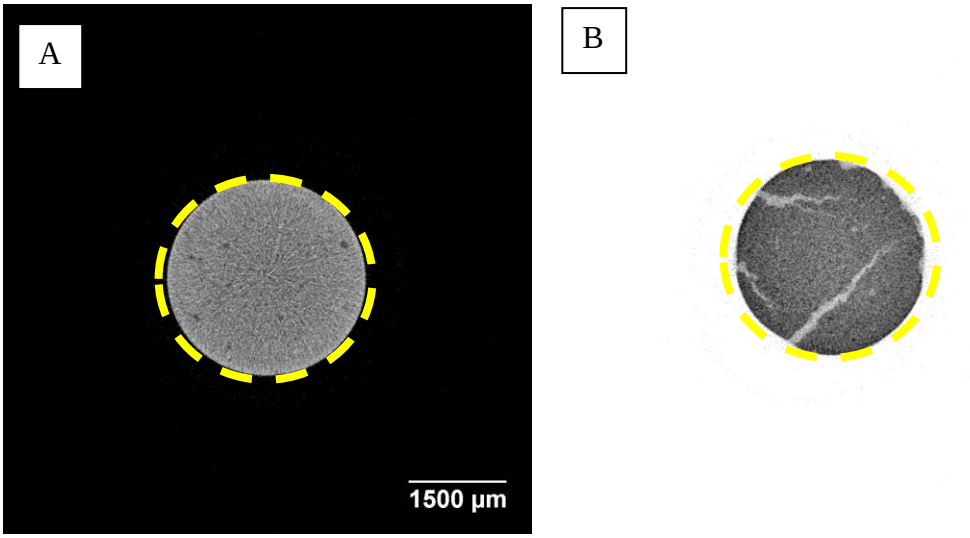

Figure 3.6.9 µ-CT images depicting the cross section of a Portland cement standard disk with a 6 mm diameter. Two different methods were used to calculate the change in grey values of the standard Portland cement. (a) In the first example the entire sample was selected and a grey-scale histogram created for the entire cement surface including macro pores and cracks. (b) In the second example a mask of the sample was created which excluded the macro pores and cracks from the grey-scale calculation.

When the grey value counts from figures 3.6.9a/b were plotted there was no noticeable difference in the counts (figure 3.6.10) indicating that even though the cracks were observable on the images this could not be quantified with an 8-bit image.

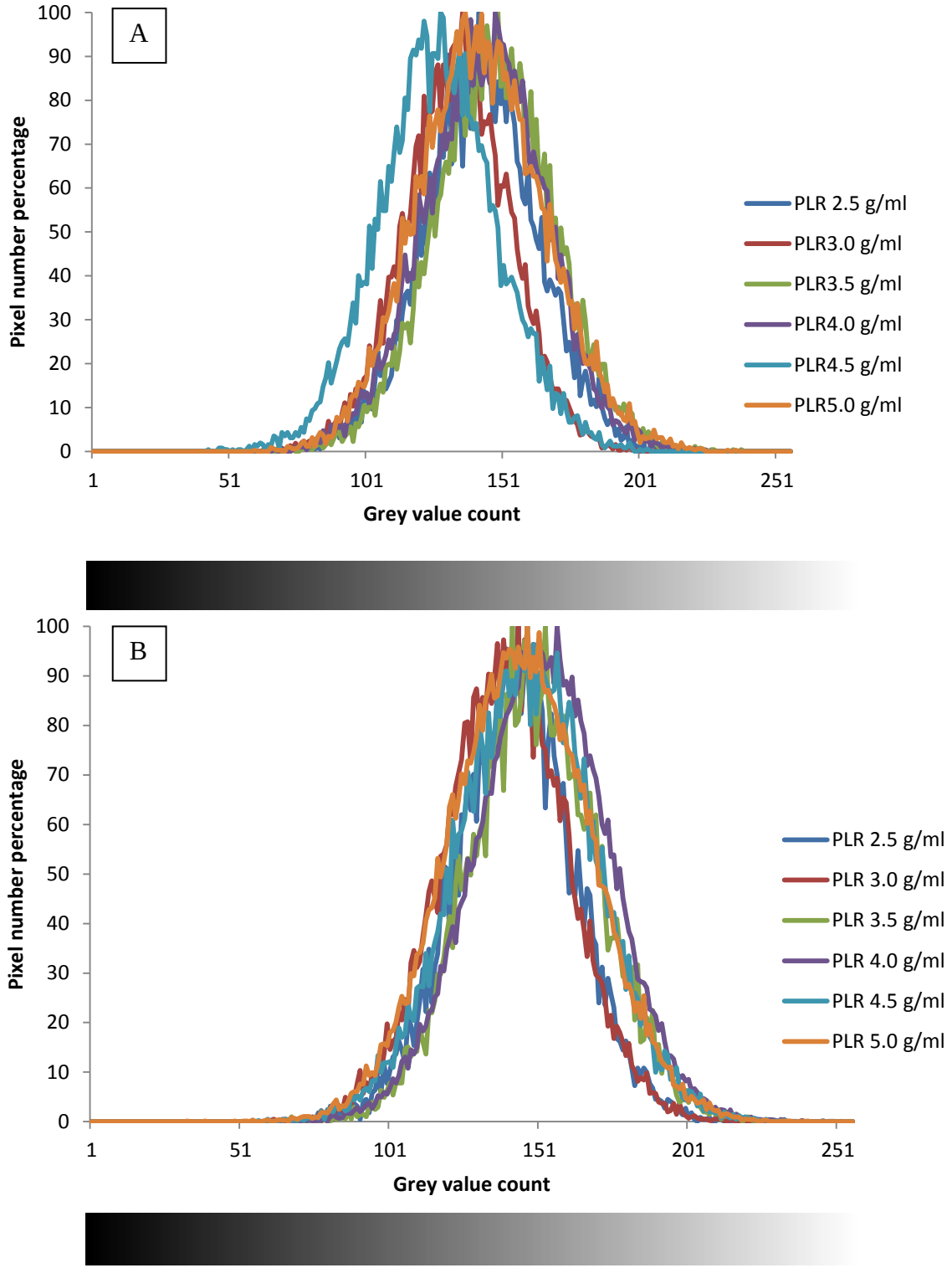

Figure 3.6.10 Grey value count of the Portland cement using (a) the entire sample including macro-pores and cracks from figure 3.6.9a (b) excluding the defects from figure 3.6.9b. There was no noticeable trend in grey values between varying PLRs (sample number n=3).

3.6.5 Micro-CT to assess localised cement diffusion within bone

The injection chamber in figure 3.6.11 contained Sawbone™ with a porosity of 200 µm replicating the porosity of cancellous bone. When PC was injected into the pores the cement spread out in a cloud formation. When the cement was injected into the porcine bone the cement did not appear to penetrate the pore system with an approximate diameter of 50 µm.

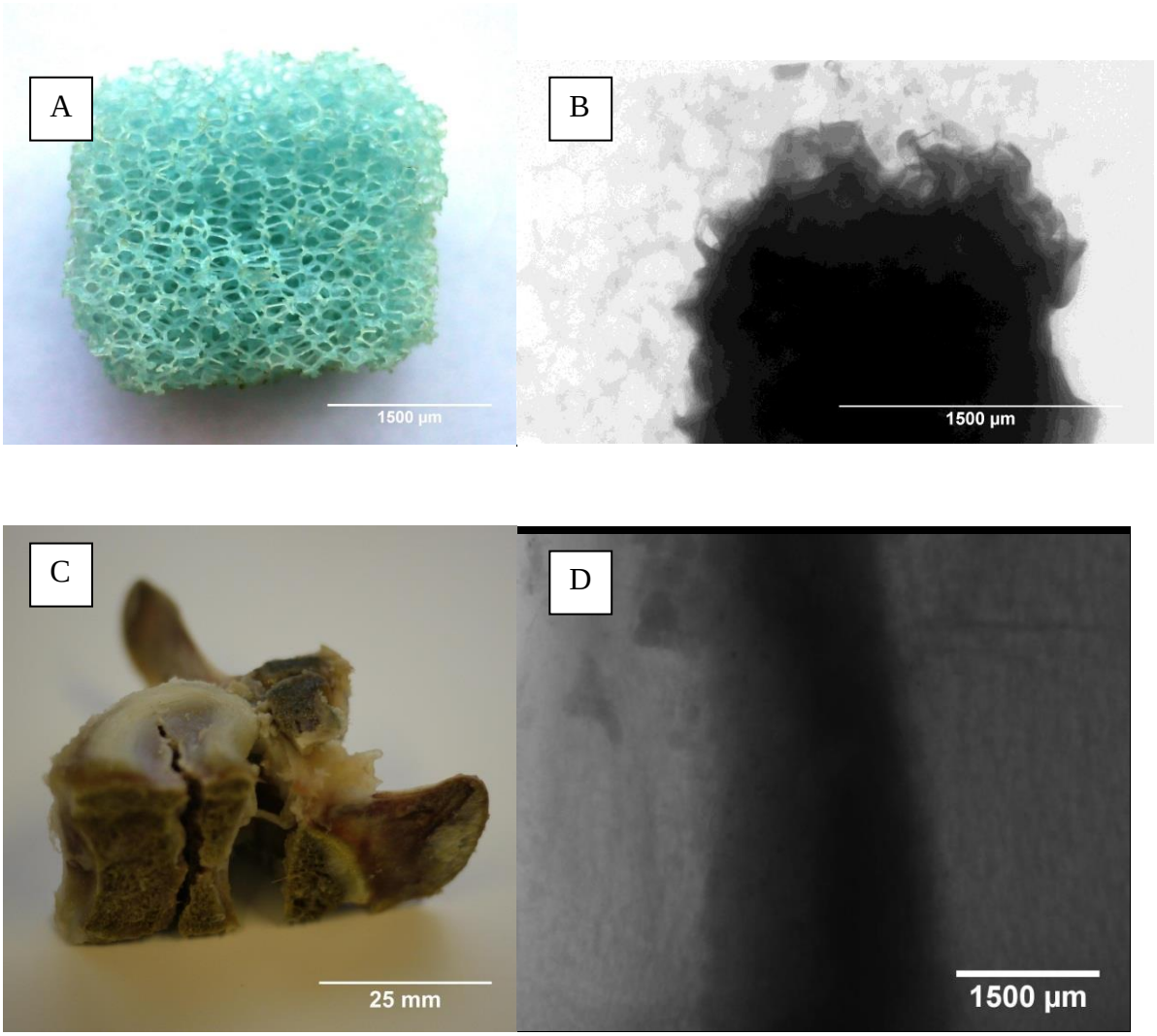

Figure 3.6.11 (a) sawbone polymer with a homogeneous pore diameter of approximately 200 µm. (b) Sawbone after injection with PC containing 2 wt% sodium citrate (see figure 3.57). The cement diffused in a spherical cloud shape (c) Porcine vertebrae bone with an artificial fracture created following loading using a universal testing machine. (d) µ-CT image of the porcine bone with PC bone cement injected.

3.7 Investigating the cytocompatibility of Portland cement

3.7.1 Growth curves for 3T3 fibroblasts incubated with Portland cement discs (6 mm by 3 mm)

3.7.1.1 Portland cement discs set for 24 h in split moulds removed and positioned in the centre of a 35 mm petri dish prior to seeding with 3T3 fibroblasts

After initially seeding 5000 cells the lag growth phase in all petri dishes continued for approximately the first 2 days of the experiment (figure 3.7.1). During the exponential growth phase at days 6 and 8 the number of cells in the control petri dishes, with no cement, were significantly ($p<0.05$) higher than the dishes containing PC discs. In contrast, at these same timepoints there was no significant ($p<0.05$) difference in cell numbers in petri dishes containing discs of standard PC and those containing PC discs with either calcium chloride or calcium nitrate. At the beginning of the stationary phase the control wells contained approximatly $35x10^4$ cells while cells incubated with the PC discs all contained under $31x10^4$ cells.

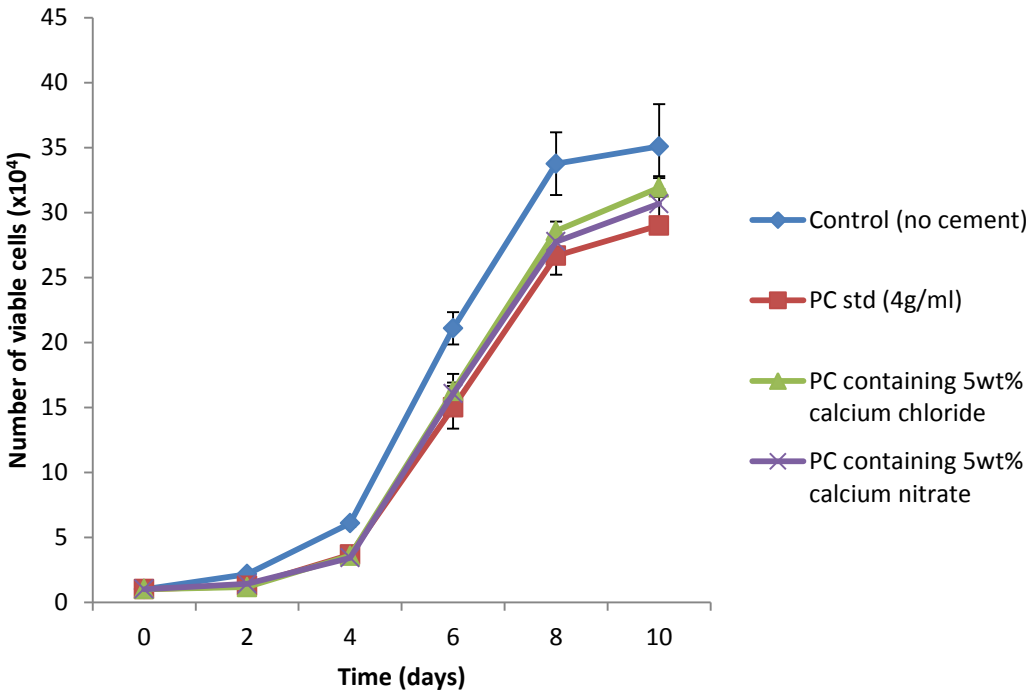

Figure 3.7.1Growth curves for 3T3 fibroblasts incubated with PC discs containing either 5 wt% of the setting accelerants calcium chloride or calcium nitrate (the cements were set for 24 h prior to incubation with the cells). At days 6 and 8 the cell count in the control dishes containing no cement were significantly ($p<0.05$) higher than dishes containing cement discs (sample number n=3).

3.7.1.2 Portland cement discs set for 6 h in split moulds removed and stored in distilled water for 18 h before being positioned in the centre of a 35 mm petri dish and seeded with 3T3 fibroblasts

The initial lag phase occurred for the first 3 days after seeding. At the end of this period there was no significant ($p<0.05$) difference in cell numbers between the control dishes and those containing any type of cement disc (figure 3.7.2). During the exponential growth phase between days 5 to 9 the cell numbers in the control petri dishes and those containing cement remained similar. At each time point at least one set of cement discs either PC standard or PC containing either calcium chloride or calcium nitrate demonstrated no significant ($p<0.05$) difference with the control. However, when all the time points over the 11-day experiment were grouped for

each set of discs the petri dishes which contained cement had overall significantly ($p<0.05$) lower cell numbers than the control.

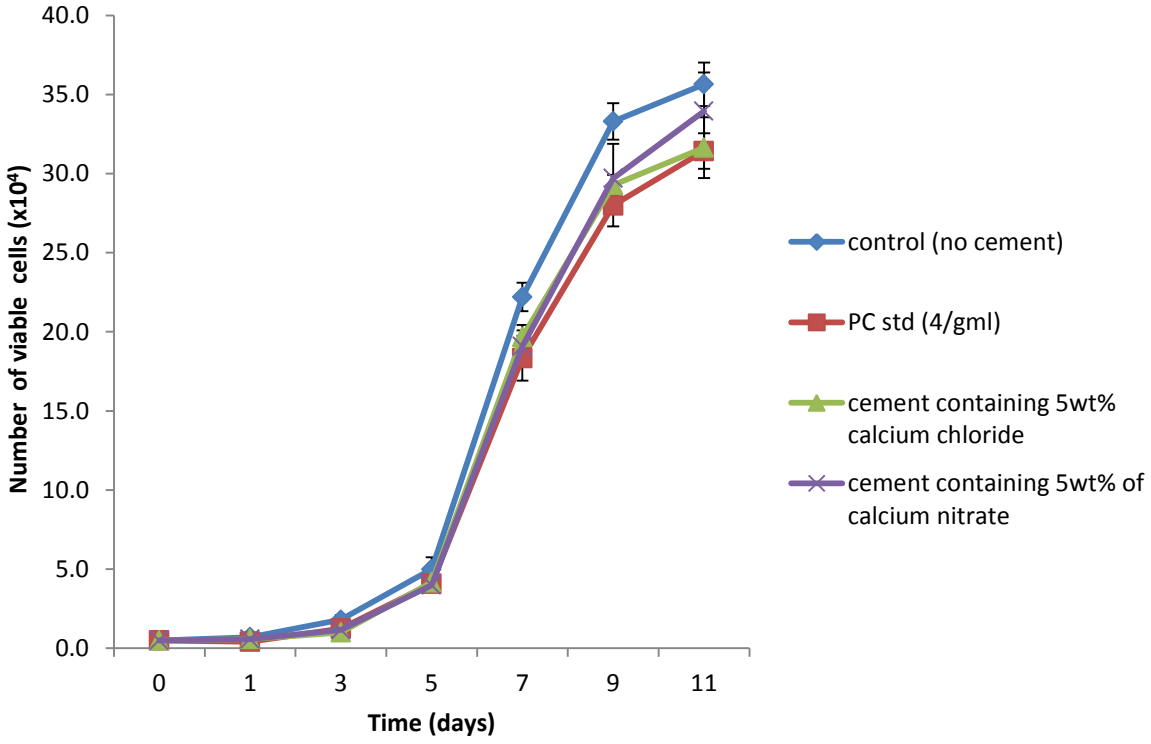

Figure 3.7.2 Growth curves for 3T3 fibroblasts incubated with PC or PC containing either 5 wt% of the setting accelerants calcium chloride or calcium nitrate (the cements were set for 6 h in split moulds and then for 18h in ddH_2O prior to incubation with the cells). Overall, during the 11 day experiment the cell counts in the control dishes containing no cement were significantly ($p<0.05$) higher than the dishes containing PC discs (sample number n=3).

3.7.1.3 Distribution of 3T3 fibroblast cells incubated with PC discs set for 24 h in a split mould

At 0, 3 and 7 days the cells incubated with the PC standard discs set for 24 h were imaged using phase contrast light microscopy (figure 3.7.3). The 3T3 fibroblasts appeared to initially cluster around the exterior of the cement discs when seeded (figure 3.7.3a). Cell density appeared evenly distributed around the material after 3-days of incubation with no distinct zone of growth inhibition (figure 3.7.3b). After 7-days cell density had increased with cells growing within approximately 50 μm of the surface of the cement (figure 3.7.3c).

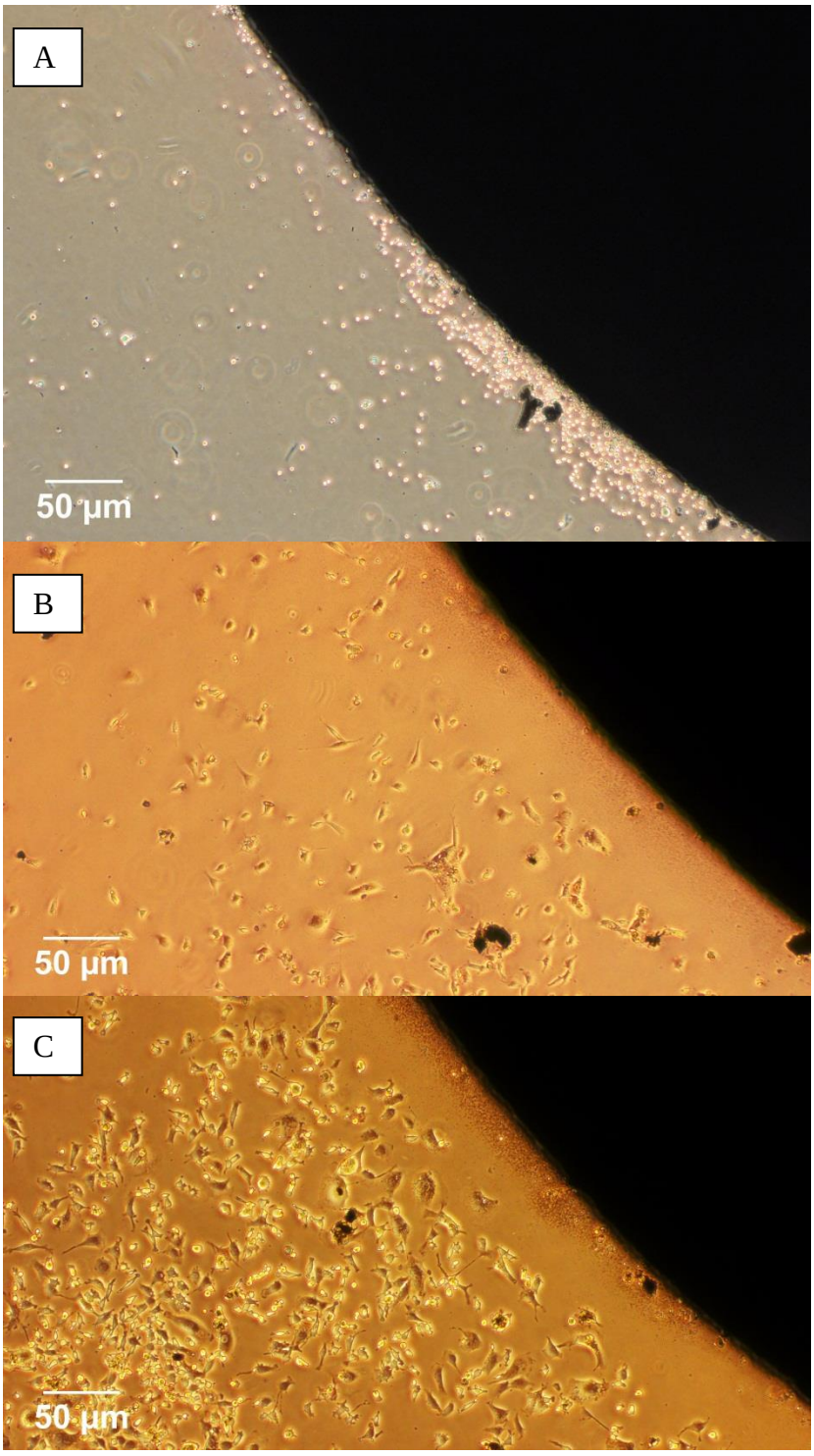

Figure 3.7.3 Phase contrast microscopy images of 3T3 fibroblasts incubated with 24 h set Portland cement for A) 0 B) 3 and C) 7 days. There was no distinct zone of inhibition and cells appeared to colonise up to the edge of the cement.

3.7.2 Growth curves of bone marrow stromal cells in the presence of PC

3.7.2.1 Portland cement discs set for 0.3 or 1 hour in split moulds removed and positioned in the centre of a 35 mm petri dish prior to seeding with bone marrow cells

Cements set for only 20 minutes prior to incubation with the bone marrow cells produced an acute cytotoxic effect leading to cell death (figure 3.7.4a). After 1 hour setting the PC standard discs remained cytotoxic to cells. However, the cells incubated with PC discs containing 2 wt% sodium citrate demonstrated moderate growth rates from 5 to 13 days but cell numbers remained significantly ($p<0.05$) lower than the control wells containing no cement (figure 3.7.4b).

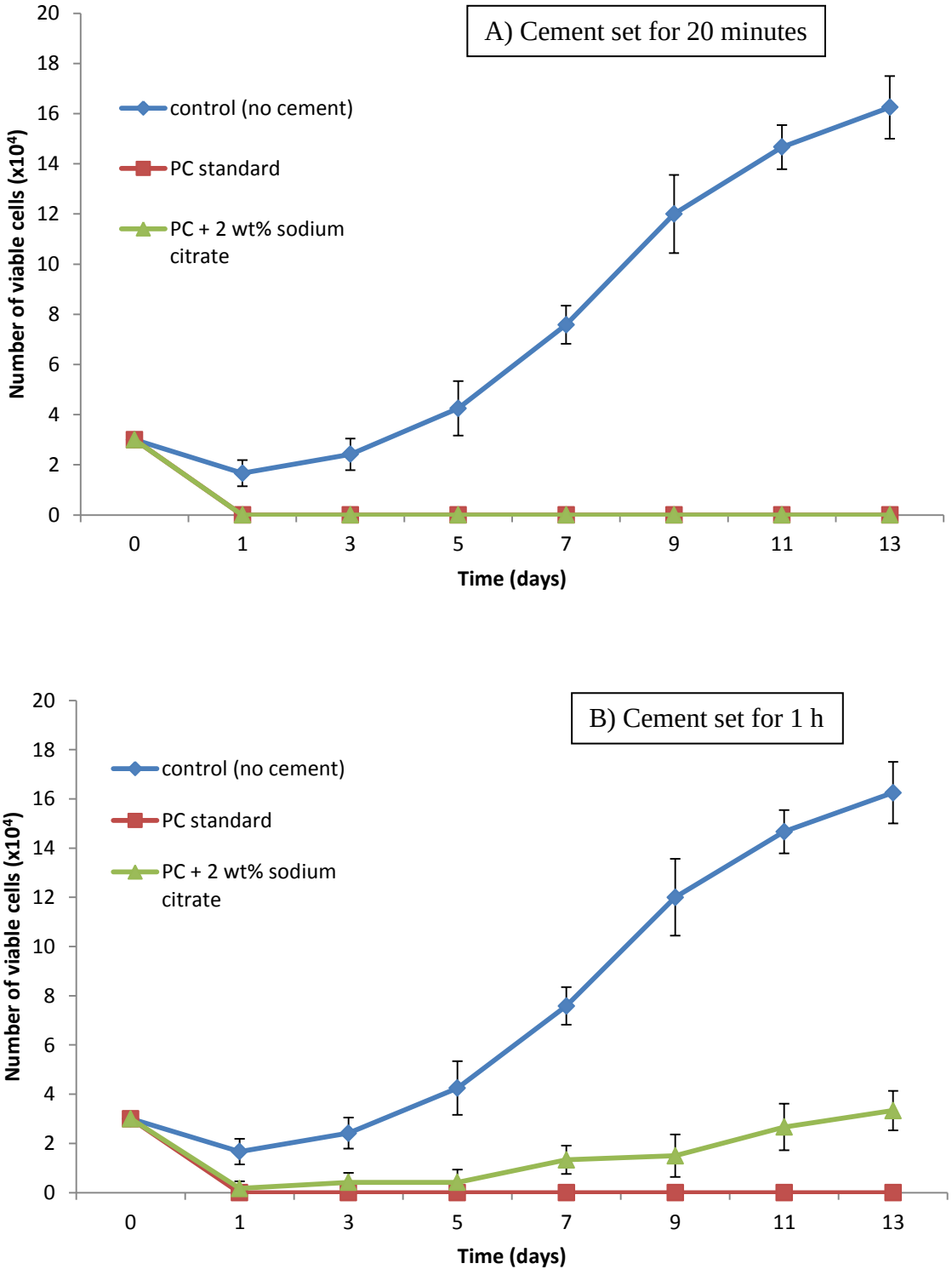

Figure 3.7.4 Growth curves of bone marrow cells incubated with Portland cement discs (6mm x 3mm) which had been set for either A) 20 minutes or B) 1 hour. Cements set for only 20 minutes prior to exposure to cells were cytotoxic causing cell death. After 1 h of cement setting there was moderate growth after 5 days in petri-dishes containing PC discs containing 2 wt% sodium citrate (sample number n=3).

3.7.2.2 Portland cement discs set for 3 or 12 hour in split moulds removed and positioned in the centre of a 35 mm petri dish prior to seeding with bone marrow cells

Cements set for 3 h containing the citrate additive had significantly ($p<0.05$) higher cell counts than the equivalent cement set for only 1 hour (figure 3.7.5a). At 3 h setting the cells incubated with the standard cement also demonstrated growth with 30,000 cells present after 13-days of incubation. When cells were incubated with cements that had been allowed to set for 12 hours (figure 3.7.5b) cell counts between the standard and cements with accelerant additives were not significantly ($p<0.05$) different yet both remained significantly ($P<0.05$) lower than the control wells.

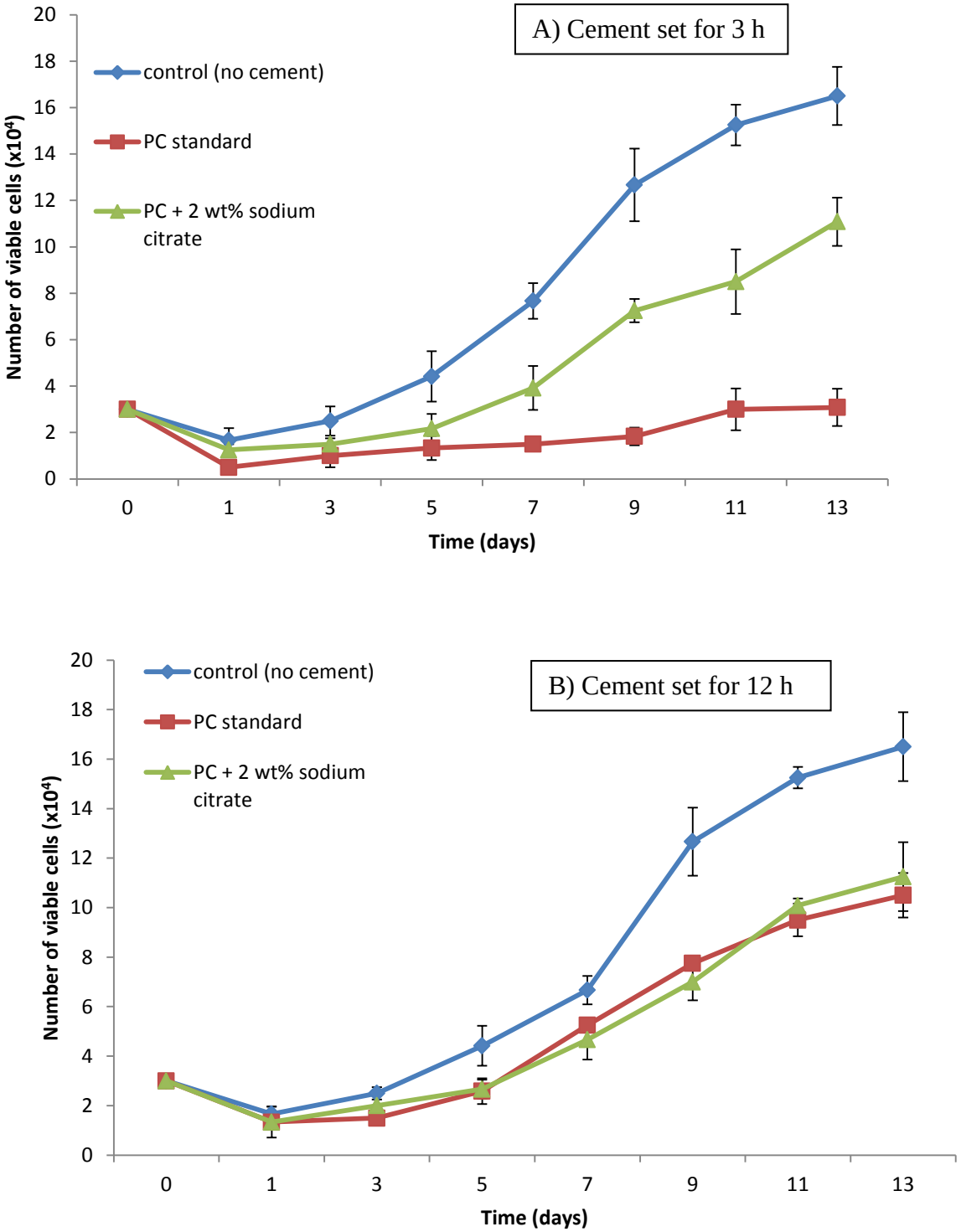

Figure 3.7.5 Growth curves of bone marrow cells incubated with Portland cement discs (6mm x 3mm) which had been set for A) 3 hours or B) 12 hours. The cement discs set for 3 h demonstrated significantly ($p<0.05$) higher cell counts after 13 days of incubation than when the cement was set for only 1 hour. At 12 hours of cement setting the cell counts in the dishes containing either standard discs or ones with the citrate additive were not significantly ($p<0.05$) different. However, the cell counts in the control dishes remained significantly ($p<0.05$) higher (sample number n=3).

3.7.2.3 Distribution and morphology of bone marrow cells incubated with PC discs

After exposing cells to cement discs set for 1 hour that contained 2 wt% sodium citrate there was initially a high cell death count in an approximate 1300 μm radius around the circumference of the material (figure 3.7.6a). Cellular morphology differentiated within this radius with cells within 1100 μm appearing ruptured and lysed (zone A). In zone B a transition occurred between cells with ruptured membranes to those of typical bone marrow morphology. Similar transition zones were observed when cells were incubated with cement discs containing 2 wt% sodium citrate set for 3 hours but the zones a, b and c were only a few 100 μm wide (figure 3.7.6b). Cells were able to colonise up to the edge of the cement discs containing sodium citrate which had set for 12 h.

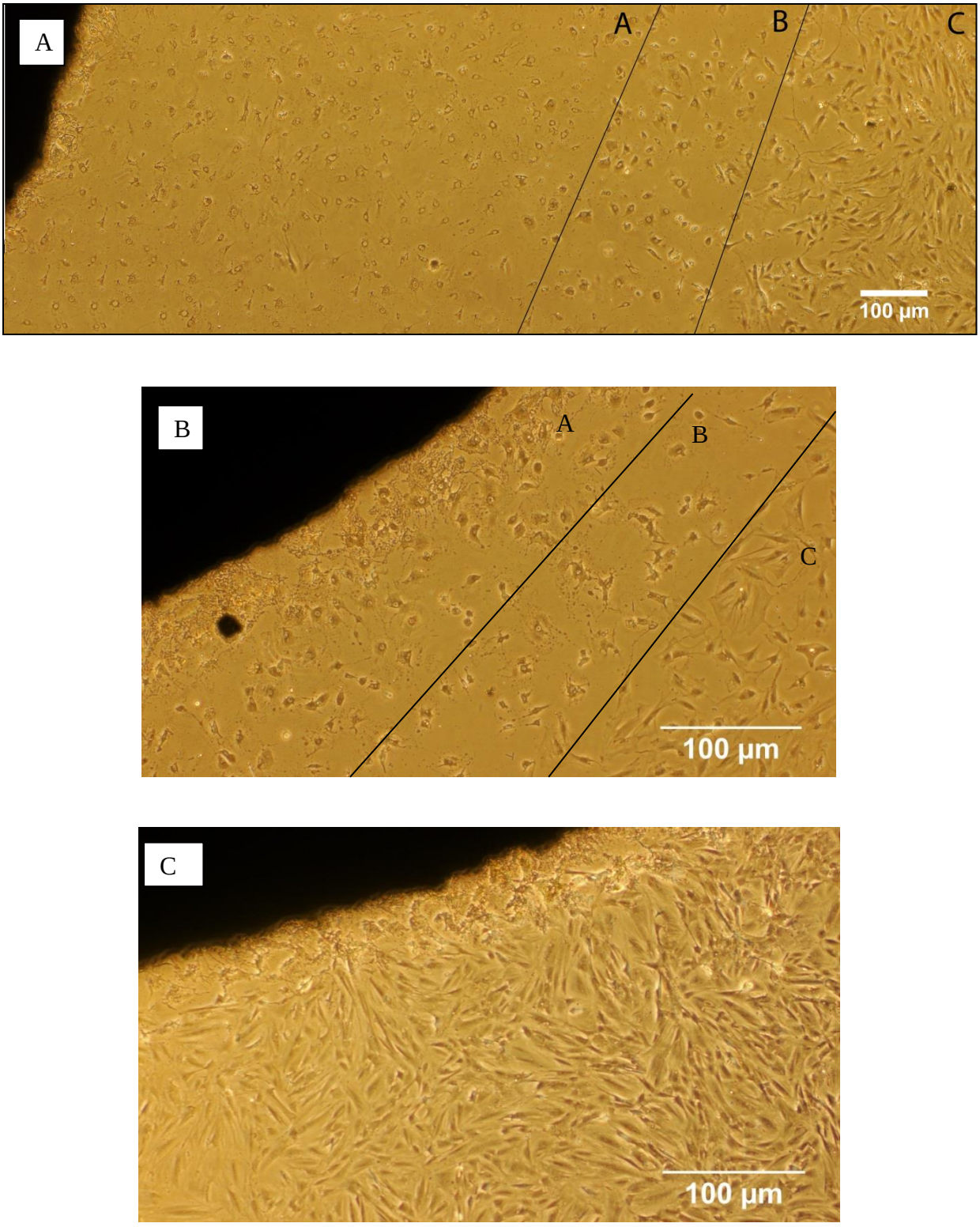

Figure 3.7.6 Distribution and morphology of mesenchymal bone marrow stem cells incubated with cement containing 2 wt% sodium citrate (A) citrate cements set for 1 h demonstrated a zone of cell growth inhibition of approximately 1300 µm surrounding the cement (B) after the same incubation period the cements set for 3h had a decreased zone of approximately 250 µm wide (C) cements set for 12 h produced no zone of cell growth inhibition.

3.7.3 Effect of cement induced pH changes on culture medium

Within 1-2 minutes of exposing freshly prepared cement (set for 20 minutes containing 2 wt% sodium citrate) to 3 ml of culture medium in a 35 mm Petri dish the phenol red indicator dye demonstrated a highly alkaline pH (figure 3.7.7). Measurements of pH revealed the media was in the region of pH 11.

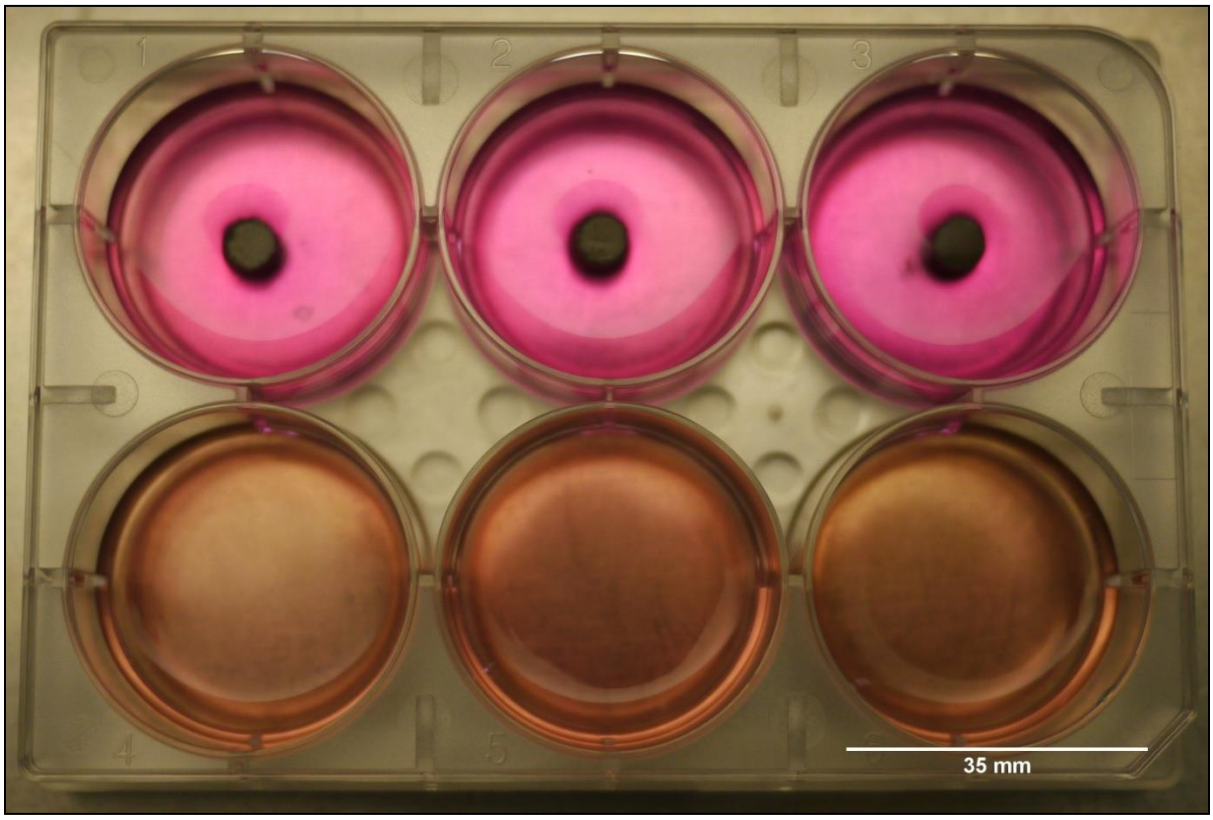

Figure 3.7.7 Photograph of 6-well plate containing PC samples (upper row) set for 20 minutes in culture medium. The phenol red dye is vivid pink indicating the high alkalinity of the media after exposure to the cement material.

3.7.4 Alizarin red staining to test for calcium mineralisation

After the PC discs containing 2 wt% sodium citrate set for 1 hour were removed from the petri dishes after 13 days incubation with bone marrow cells and stained with alizarin red dye a red halo emerged around the discs circumference (figure 3.7.8a). As alizarin red binds to calcium based material it would appear that a portion of the cements calcium species were eluted during the cellular incubation period. The high calcium content of the material made it difficult to assess calcification deposits that may have been produced by the bone marrow stromal cells (figure 3.7.8b).

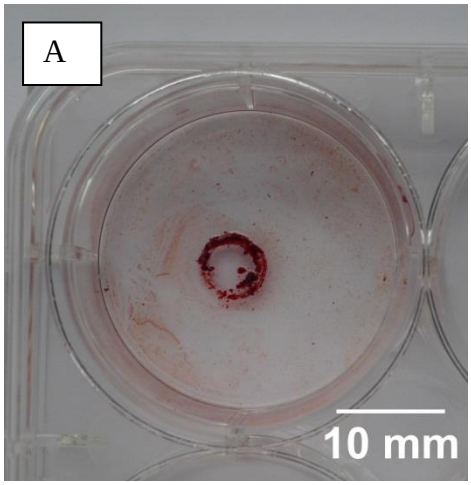

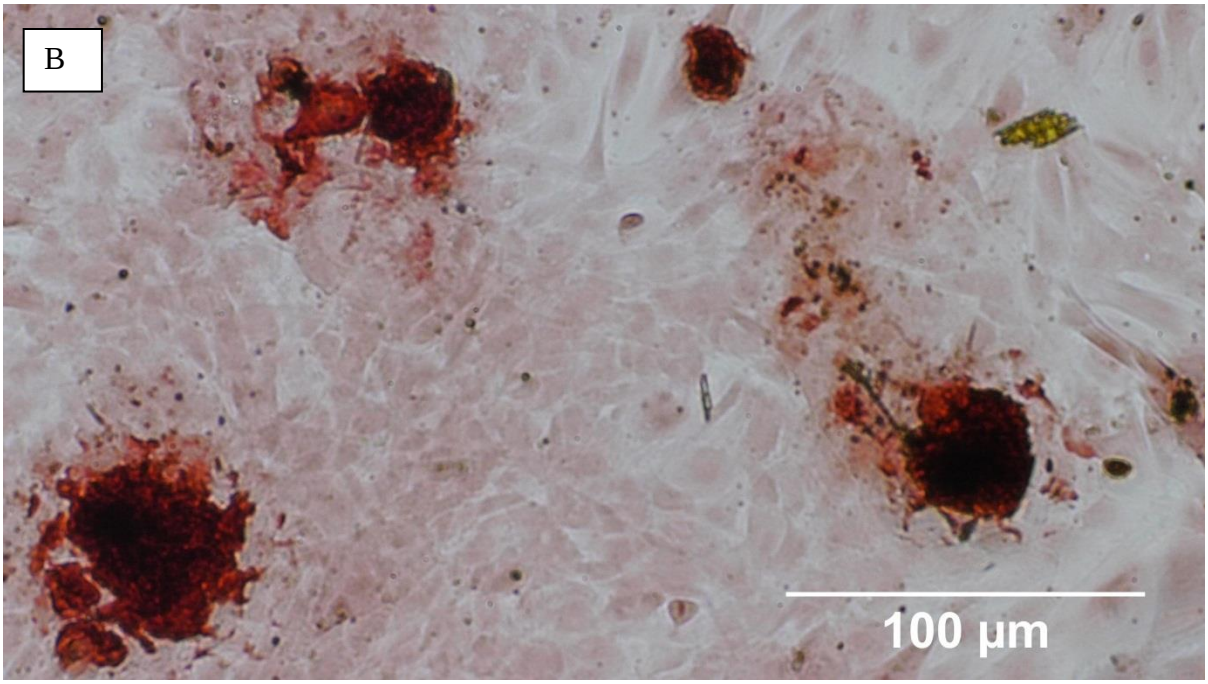

Figure 3.7.8 (A) A dark red halo was visible after alizarin red staining in the area where the cements set for 1 hour were originally aligned in the 35 mm petri dishes indicating calcium deposition surrounding the material. (B) Microscopy image of bone marrow cells after alizarin red staining. It was difficult to assess if calcification was caused by the bone marrow stromal cells or the mineral content of the material.

3.7.5 Reverse transcription polymerase chain reaction (RT-PCR)

The bone marrow stromal cells incubated with PC discs set for either 1 or 12 h demonstrated increased levels of gene transcription for several osteoblast phenotype genes compared with control wells containing no cement (figure 3.7.9). These included alkaline phosphatase (ALPase), bone sialoprotein (BSP), osteonectin (ON) and osteopontin (OPN). There was no observed difference in expression levels of osteoadherin and bone morphogenic protein compared with the control. Osteocalcin expression was absent in both the control and cements exposed to PC. There was no observable increase in the cell proliferation marker Ki-67 between the control wells and those containing PC.

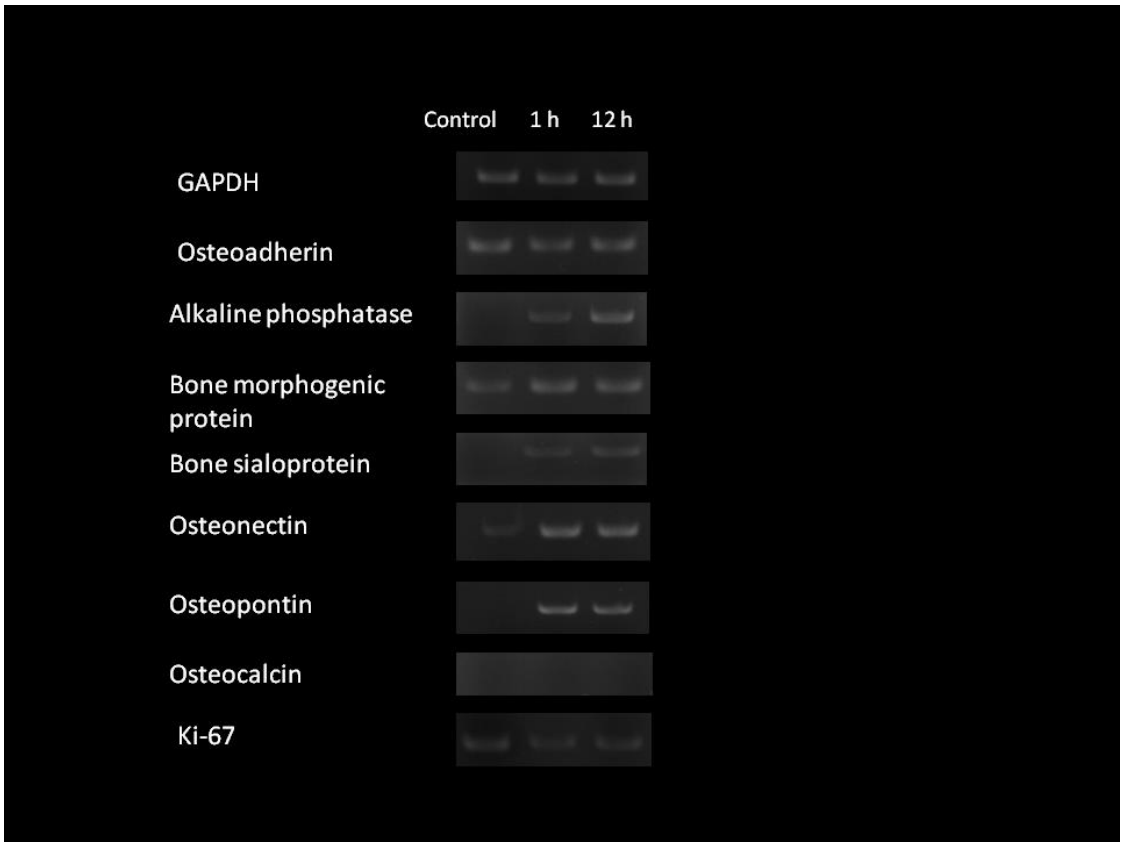

Figure 3.7.9 Cells were exposed to cement containing 2 wt% sodium citrate set for both 1 and 12 h and the gene expression of several osteoblast phenotype genes recorded by RT-PCR (visualised on agarose gel). In the presence of cement there was increased expression of alkaline phosphatase, Bone morphogenic protein, osteonectin and osteopontin.

3.7.6 Using buffers to reduce the alkalinity of the Portland cement setting reaction

An addition of 2 or 10 wt% sodium dihydrogen orthophosphate and 10 wt% additions of either potassium phosphate dibasic or Tris EDTA significantly ($p<0.05$) reduced the pH of the 20 minute set cement (figure 3.7.10). Cement containing 2 wt% sodium citrate was set for 12 h and pH measured as 8.92 ± 0.11 which was significantly ($p<0.05$) lower than the cement set for only 20 minutes. However, the reduction of pH remained above the physiological optimum for cell growth of pH 7.4 (183).

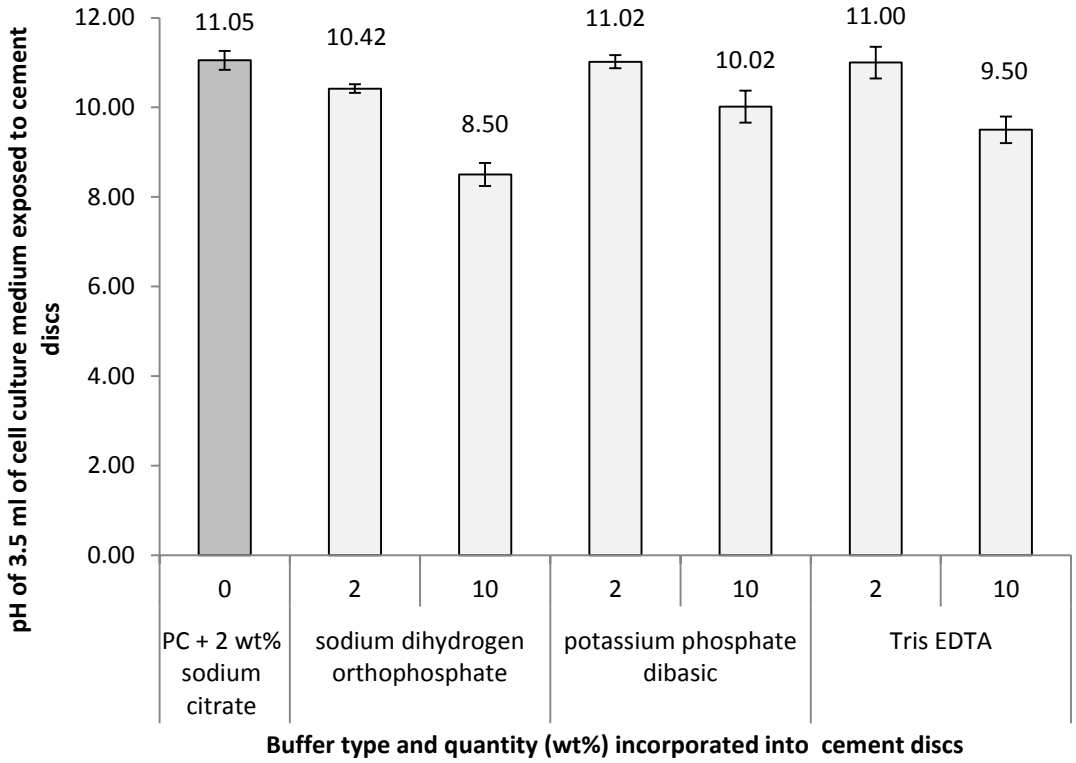

Figure 3.7.10 pH of 3.5 ml of cell culture medium incubated with a PC disc (6mm x 3mm) for 20 minutes. The standard contained 2 wt% sodium citrate the other discs contained 2 wt% sodium citrate in addition to 2 or 10 wt% of a chosen buffer. An addition of 2 or 10 wt% sodium dihydrogen orthophosphate and 10 wt% additions of either potassium phosphate dibasic or Tris EDTA significantly ($p<0.05$) reduced the pH of the setting cement (sample number n=3).

Additions of potassium phosphate dibasic, 10 wt% sodium dihydrogen orthophosphate and 10 wt% Tris EDTA prevented the cement from setting. Additions of both 2 wt% sodium dihydrogen orthophosphate and 2 wt% Tris EDTA significantly ($p<0.05$) increased the setting times compared with PC containing only 2 wt% sodium citrate (figure 3.7.11).

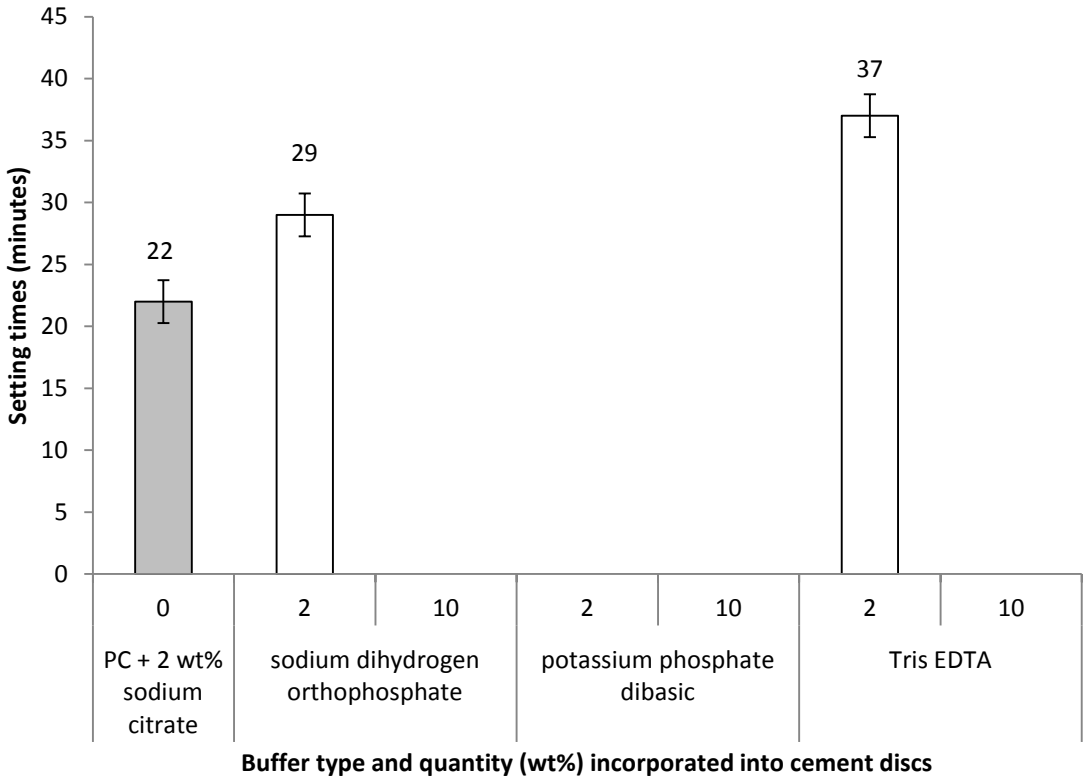

Figure 3.7.11 The effect on setting time of buffer additions to PC was tested with the Gilmore needles test. Additions of potassium phosphate dibasic, 10 wt% sodium dihydrogen orthophosphate and 10 wt% Tris EDTA prevented the cement from setting. Two wt% additions of sodium dihydrogen orthophosphate and 2 wt% Tris EDTA extended the material setting times (sample number n=3).

CHAPTER 4: DISCUSSION

4 DISCUSSION

4.1 CHAPTER: Investigating the parameters for an injectability model

4.1.1 The effect of powder-to-liquid ratio on cement injectability and setting times

The first stage of the injectability experiments assessed whether over 90 wt% cement extrusion, a prerequisite requirement of the industrial collaborator, would be feasible by simply increasing the water content of the standard cement. From figure 3.1.1, it became evident that even at a PLR of 2.2 g ml^{-1} which was considered low (184), it was not possible to achieve this goal without a liquefying additive. The rheology of the materials was not measured but it was observed that the dense cement particles were sedimenting at the bottom of the syringe. Phase separation of the cements powder and liquid phase is a known problem with ceramic materials and has been shown to be the leading cause of poor injectability in calcium phosphate cements (166, 185). Excess water in cements also leads to high cement porosity as the water is not consumed within the cement setting reaction which can result in poor compressive strengths (125). Setting times of PC without an additive were also in excess of the 15-20 minute window for the vertebroplasty operation (refer to figure 3.1.3) (186).

4.1.2 The effect of cross-head speed on injectability

Approximately 30 mm plunger depression was required to extrude fully the 5 g of cement from the syringe (figure 3.1.4). As the cross-head speeds under investigation ranged from 3-30 mm min^{-1} this equated to extrusion times between 1-10 minutes. A series of cross-head speeds from 10 mm min^{-1} (187) to over 120 mm min^{-1} (185) have previously been used in studies extruding calcium phosphate cements from similar size syringes (5 ml). It was observed, during the experiment, that when extruding the cement at 3 mm min^{-1} a set cement bolus formed at the

tip of the syringes when a setting accelerant was present and was momentarily preventing more cement from being extruded. Cement setting in the cement tip may have reduced the injectability of the slower extruded cements. Clinically acrylic bone cements are required to remain usable between 6.5-15 minutes (15). For instance, Osteopal ® (Heraeus, Germany) a PMMA based bone cement used extensively for PVP operations, has an injectability time of 7 minutes (188) whereas CMW1® (DePuy, UK) is just over 13 minutes (189). Personal communication with a radiographer routinely performing the operation also indicated that a working time of approximately 10 minutes was sufficient and preferable (167). When the formulations were further studied in chapter 3.6, time dependency of injectability was investigated in greater detail.

4.1.3 The effect of dispersing additives in the powder vs. liquid phase

During the initial stages of the project it was observed that many of the additives, including calcium acetate and sodium hexaphosphate, possessed dual functionality acting as both liquefying agents and setting accelerants. Both of the additives investigated were highly soluble and dissolved fully in the liquid phase (153, 190). The homogeneously mixed solutions may have provided the accelerating additives with greater access to the surface of the hydrating cement particles accounting for both the decreased setting times (figure 3.1.5) and conversely the reduced injectabilities when the additives were dissolved in the liquid phase. (166).

4.1.4 Batch variation and effect of cement aging and storage on the various phases of Portland cement

For a future commercial product, it is important that both the elemental and phase composition of the unhydrated cement powder remains consistent between batches. The EDX analysis indicated

that both batches of cement possessed similar levels of tricalcium silicate and that there were no major changes in the elemental composition of the material (table 3.1.1). However, the decreased XRD peak intensities of the 2005 compared with the 2011 batch of PC may indicate cement aggregate formation in the powder phase of the older batch of the material (figure 3.1.7). The XRD peak intensities for crystal structures associated with the unreacted/clinker phases had decreased in the older batch but equally there were no corresponding increases in peaks associated with hydrated cement phases. The older batch of cement may have become partially hydrated forming crystal unit structures distinct from the known fully hydrated phases of PC, but with no characteristic XRD absorption peaks (179).

4.1.5 Effect of cement powder filtering on the physical properties and phase composition of Portland cement

The increased XRD peak intensities (figure 3.1.8) as the filter aperture size was reduced from 500-63 µm may indicate the removal of non X-ray absorbing agglomerates at the lower diameter aperture size (179). The significantly ($p<0.05$) decreased setting times of the cement sieved through the 75 µm filter as opposed to the 63 µm filter, indicated that possibly an important cement phase was being removed within this range of filter apertures (figure 3.1.9). PC typically has 5 wt% calcium sulphate dihydrate (gypsum) added during production in order to coat the calcium aluminate phase, thus preventing early hydration (flash setting) which leads to a weak cement structure (113). However, the XRD determined phase composition did not alter after the sieving through a 63 µm aperture which may have provided an explanation for the reduced setting times. To examine whether there was any elemental differences between the cements

passed through different pore diameters, the cement would need to be examined via a technique such as EDX or X-ray fluorescence (XRF).

4.2 CHAPTER: Development of Portland cement for orthopaedic applications, establishing injectability and decreasing setting times using researched additives

4.2.1 Injectability studies in the presence of sodium chloride, sodium aluminate, sodium hexaphosphate and calcium acetate.

Sodium hexaphosphate has previously demonstrated to be a calcium phosphate cement liquefier (153). A 1-2 wt% addition modified cements from being un-injectable to enable extrusion of over 97 wt% from a syringe with a 2 mm aperture. A decrease in the surface charge of the calcium phosphate cements after mixing indicated the electrostatic adsorption of the charged hexaphosphate anion onto the cements positive surface. It has been suggested that binding of liquefiers, such as sodium hexaphosphate, results in repulsion between cement particles both electrostatically and sterically due to the large size of the anion (153). It has been inferred that these forces led to a dispersal of cement aggregates while also preventing further flocculation leading to the liquefying effect (23, 191, 192). Increasing the quantity of the liquefying additives in the present study from 5 to 10 wt% may have caused an increase in the electrostatic repulsion effect between the cement particles, leading to the improved liquefying abilities (figure 3.2.1). Future studies will examine the surface charge of the material using a zetasizer.

Similar to sodium hexaphosphate, sodium chloride and calcium acetate both fully ionise in water to form anionic species. The deprotonated carboxyl groups formed by these carboxylic acid salts form the basis of the binding groups for the commercially available PC liquefiers "polycarboxylate derivatives" (151). This group of liquefiers cause cement grain dispersion as a result of both electrostatic and steric repulsions generated by the extended anionic side chains (193). However, as acetate and chloride do not possess extended side chains the binding of ions onto the positive surface may simply neutralise positive charges such as Portlandite $[CaOH]^{+}$ and

forming Friedel salts $[Ca_2AlOH_6]^+$ forming on the cements surface (194). Zeta-potential measurements may be employed to investigate if charge neutralisation as opposed to electrostatic repulsion was occurring with the acetate and chloride additives. However, as the balancing cation calcium also interacts with the forming cement surface it may not be possible to accurately assess how the surface charge changes in the cement (195, 196).

Sodium aluminate may also act as a liquefier due to the large difference in electronegativity between aluminium (1.61) and oxygen (3.44) which provides oxygen with a disproportionate share of the π (pi) electrons in the aluminium oxygen bond (197). The transient negative dipole may attract the additive to the cements positive surface.

Gbureck *et al* (187) studied the injectability of calcium phosphate cements (CPC) and obtained similar extrusion graphs (figure 3.2.2) for cements containing liquefying additives with CPC cement. The low initial force required to extrude the majority of the cement paste containing a 10 wt% liquefier suggests a homogeneous cement paste with few agglomerates. There was a gradual increase in the force plateau level when the additive content was decreased to 5 wt%, perhaps indicating an increase in agglomerate levels. For the PC standard the continuous increase in force required to extrude the cement may be linked to the formation of high numbers of agglomerates.

4.2.2 Density and porosity studies

The specific density of the PC standard (≈ 2.5 g cm^{-3}) (table 3.2.1) was lower than the strut density of PC powder (≈3.1 g cm^{-3}) (198) as a result of the hydration reaction of water (≈1.0 g cm^{-3}) with the powder phase. The lower specific densities of PC containing 10 wt% sodium chloride (2.28 g cm^{-3}) and calcium acetate (2.20 g cm^{-3}) cements indicated a greater degree of conversion of reactants than the standard cement as water reacted with the cement powder. In contrast, the higher specific densities of the 10 wt% additions of the sodium aluminate and sodium hexaphosphate cements indicated a lower degree of hydration. Porosity within cement systems can stem from two sources. Firstly, from water added to form the cement paste, which was not consumed from the setting reaction, and secondly from entrapped air resulting from dry powder agglomerates (198). Thus, the relatively lower porosities of the sodium chloride and calcium acetate cements may reflect less unconsumed water within the cement system, whereas the higher porosities of the sodium aluminate and sodium hexaphosphate cements demonstrated the opposite.

4.2.3 Investigating cement phase composition with X-ray diffraction (XRD.)

The presence of the major hydration products of PC setting, calcium silicate hydrate (C-S-H) and ettringite, within the standard cements and cements containing sodium chloride and acetate indicated these cements formed the major hydration products of PC (figure 3.2.5) (113). The presence of crystalline calcium hydroxide, the major by-product of calcium silicate hydration provided further evidence that C-S-H formation was occurring within 24 h of these cements setting. In contrast, the absence of any of these phases in cements containing sodium aluminate or sodium hexaphosphate implied that typical cement setting was inhibited for at least the first

24 h. However, the presence of a C-S-H peak after 30-days indicated normal cement setting had resumed after the first 24 h. The production of C-S-H in the acetate cements appeared to have led to excessive calcium hydroxide by-product formation (figure 3.2.5). Excessive calcium hydroxide in cements has previously been linked to poor mechanical properties (199) which may partly explain the low compressive strengths of the acetate cements even though the major hydration products were present in the phase analysis. In previous investigations calcium acetate has been added up to 2.5 wt% and has demonstrated strength increasing effects on PC (165).

4.2.4 Investigating surface phase morphology using scanning electron microscopy (SEM) and elemental analysis using energy dispersive X-ray spectroscopy

The flat, hexagonal and needle shaped crystals present in the aluminate cement (figure 3.2.6e) were characteristic of calcium monosulphate which was confirmed by the elemental analysis. Typically, in PC when all the gypsum has been consumed by the formation of ettringite (equation 1.8.4) the remaining aluminate will begin to react with the formed ettringite to create calcium monosulphate which possesses a lower sulphate content (equation 1.8.5) (117).

$$3CaO.Al_2O_3 + 3CaSO_4.2H_2O + 26H_2O \longrightarrow 6CaO.Al_2O_3.3SO_3.32H_2O$$

(Tricalcium aluminate + gypsum + water $\longrightarrow$ ettringite)

(Equation 1.8.4)

$$2(3CaO.Al_2O_3) + 6CaO.Al_2O_3.3SO_3.32H_2O + 4\ H_2O \longrightarrow 3(4CaO.Al_2O_3.SO_3.12H_2O)$$

(calcium aluminate + ettringite + water ⟶ calcium monosulphate)

(Equation 1.8.5)

The monosulphate phase does not typically appear for at least 3-days after setting indicating its formation had been accelerated. Monosulphate possesses a weaker constitution than ettringite which may explain the comparatively low compressive strengths of the aluminate cements (200).

The PC standard (figure 3.2.6a) and cements containing chloride(figure 3.2.6b) both possessed a surface morphology which appeared to be composed of C-S-H which was also implicated by the elemental analysis (201). The surface structure of the calcium acetate cements appeared to be largely constituted of calcium hydroxide crystals which added more evidence that high calcium hydroxide levels were creating weak cements with the additive. The morphology of cements containing sodium hexaphosphate appeared to be radically different from known PC crystal structures and may have represented a novel complex formed between sodium hexaphosphate and PC.

4.2.5 Investigating sulphate species using FTIR.

Cements typically contain approximately 5 wt% calcium sulphate dihydrate (gypsum) to coat the calcium aluminate phase thus preventing early hydration and the formation of calcium aluminate hydrate, which forms a weak cement structure (equation 1.8.3) (113).

$$3CaO.Al_2O_3 + Ca(OH)_2 + 12H_2O \longrightarrow 4CaO.Al_2O_3.13H_2O$$

(Tricalcium aluminate + calcium hydroxide + water $\longrightarrow$ calcium aluminate hydrate)

(Equation 1.8.3)

The increased unbound gypsum absorbance which occurred during the first 60 minutes of setting, when sodium hexaphosphate and sodium aluminate (figure 3.2.4b) were present may have indicated these additives were removing gypsum bound to the surface of the aluminate phase resulting in flash setting. This hypothesis was tested by the addition of gypsum powder to the cements containing 5 wt% sodium hexaphosphate. The increased height of the absorbance peak when gypsum and sodium hexaphosphate (figure 3.2.4d) were combined in equal wt% indicated that at 5 wt% the hexaphosphate anions had the capacity to remove more gypsum from the aluminate phase than was contained in the cement. PC flash setting may have explained the early setting of cements containing sodium hexaphosphate but which ultimately lacked cement strength. The extended setting times of the combined gypsum/ sodium hexaphosphate cements indicated that even though sodium hexaphosphate was removing gypsum from the aluminate there was enough gypsum to prevent flash setting from occurring.

In summary, sodium aluminate has been used as an accelerant in several commercial formulations for the building industry (155, 202). With a 7 wt% addition of aluminate the setting time of PC had been accelerated to as low as 10 minutes (155). The accelerating effect of aluminate has been attributed to the early formation of both major strength producing phases of PC, C-S-H, as well as the secondary major hydration phase ettringite (157, 158). The present study indicated two setting reactions may have occurred simultaneously in the presence of sodium aluminate. Increasing the aluminate content within the cement led to a decrease in the

gypsum: aluminate ratio which may have caused premature aluminate hydration (flash setting). Possibly, the limited quantity of ettringite which was produced was immediately converted into calcium monosulphate due to the limited sulphate availability and excess concentrations of aluminate. This would result in calcium monosulphate crystals present in the SEM analysis but only a limited trace of crystalline ettringite and monosulphate because the quantities being converted were so small. Sodium hexaphosphate produced a novel cement structure which was highly porous and may have been a novel type of flash setting. Calcium acetate had both C-S-H and ettringite phases present within the crystal structure of the cement (figure 3.2.5) with low porosities and strut densities indicating hydrated cement. The additive may have produced cements with low compressive strengths due to high calcium hydroxide production which weakened the cement structure (110). The PC standard and cements modified with 5 wt% sodium chloride both possessed similar relative porosities, specific densities and developed C-S-H after the first 24 h of setting which indicated that the additive did not adversely affect the cement setting reaction. Setting of cements in the presence of sodium hexaphosphate appeared to be caused by flash setting, but the EDX did not confirm the presence of calcium aluminate hydrate, the product which forms during this type of setting. The complex formed between hexaphosphate and the hydrating cement powder appeared to be novel.

4.2.6 Conclusions

Seven Portland cement accelerants and one calcium phosphate liquefier were chosen from table 1.10.1 and 1.10.2 and tested for the ability to improve PC injectability. Sodium chloride, sodium aluminate, sodium hexaphosphate and calcium acetate all significantly ($p<0.05$) increased the injectability of the cement. In contrast, methyl cellulose, calcium sulphate dihydrate, calcium carbonate and oxalic acid significantly ($p<0.05$) decreased it. All of the additives which increased injectability also significantly ($p<0.05$) reduced the setting time of the cement. Sodium chloride and calcium acetate appeared to accelerate C-S-H production but an excess of the by-product of the setting reaction calcium hydroxide may have prevented acetate cements from achieving high compressive strengths. Sodium hexaphosphate appeared to form a novel complex which resembled flash setting. Based on the current set of additives modifying PC to become injectable and set in a time applicable for vertebroplasty operations is possible with cement strength in excess of a vertebra (1.4-9 MPa)(31-33).

4.3 CHAPTER: Establishing injectability and decreasing setting times using the additives calcium chloride and calcium nitrate

4.3.1 Injectability studies in the presence of calcium chloride and nitrate

Each hydrated phase of PC carries a different surface charge with Portlandite and Friedel salts being positive whereas ettringite and calcium monosulphate possess negative surface charges (194). The final cement surface charge is a combination of all of the various hydrating phases. However, the overall slight negative surface charge of PC can be explained by ionisation of the silanol groups of C-S-H, the major hydration product of PC (equation 4.3.1) (194-196, 203).

$$>SiOH \rightarrow SiO^- + H^+$$

(Equation 4.3.1)

The -12 mV value observed for the PC standard was close to the theoretical surface charge range for C-S-H (-9.2 to -12.7 mV) in a low calcium environment (196, 203). This may have been an indication that the surface charge of the hydrating PC was also determined by the calcium silicate phase (figure 3.3.4). Cement agglomerates which reduce cement flowability and possibly injectability of cement pastes are caused by attraction of oppositely charged surface particles (204). Typically, commercial liquefiers are large negatively charged polyvalent compounds which work by binding to the surface of PC creating an electrostatic repulsion force between the cement particles which disperses the aggregates, leading to the liquefying effect (191, 205, 206). In contrast, chloride in the presence of Ca^{2+}, appeared to neutralise the cement surface through a series of reactions. Firstly, neutralisation occurs through the adsorption of Ca^{2+} onto dissociated silanol groups (equation 4.3.2 and 4.3.3).

$$>SiOH + Ca^{2+} \rightarrow SiOCa^{+} + H^{+}$$

(Equation 4.3.2)

$$>SiOH + Ca^{2+} + Cl^{-} \rightarrow SiOCaCl + H^{+}$$

(Equation 4.3.3)

Secondly, chloride has also been shown to neutralise positively charged Portlandite (equation 4.3.4) (194).

$$[CaOH]^{+} + Cl^{-} \rightarrow CaOHCl$$

(Equation 4.3.4)

Lastly, both chloride and nitrate neutralise the forming Friedel salts of the hydrating aluminate phase (equation 4.3.5 and 4.3.6) (194, 207).

$$[Ca_2Al(OH)_6]^{+} + CaCl_2 + 2H_2O \rightarrow [Ca_2Al(OH)_6]Cl.2H_2O + Ca^{2+}$$

(Equation 4.3.5)

$$2[Ca_2Al(OH)_6]^{+} + 2Ca(NO_3)_2 + 6H_2O \rightarrow [Ca_2Al(OH)_6]\,(NO_3)_2.6H_2O + Ca^{2+}$$

(equation 4.3.6)

This leads to a neutralisation of the cement particles that may reduce agglomeration as there are less oppositely charged particles (194). Therefore, the liquefying effect of chloride and nitrate is likely to be based on charge neutralisation as opposed to other liquefiers which function through electrostatic or steric repulsion of cement particles (148).

4.3.2 Characterising the setting reaction in the presence of calcium chloride and nitrate.

Previous calorimetry studies have indicated that the accelerating effect of calcium chloride on PC setting may have been due to an increased early rate of heat evolution in the presence of the additive (208). The heat signature obtained during the present study indicated that the accelerating effect of chloride may be due to early energy generation that was not evident in the PC standard (figure 3.3.5). This initial exotherm appeared to be composed of three distinct sections which may have corresponded with three unique reactions, or, a single reaction with multiple exotherm stages. The early presence of the set cement phase ettringite within the first 2 h of cement setting indicated that at least a portion of this initial exotherm in cements with the chloride additive was due to early ettringite formation. It has been inferred from previous infra-red spectroscopy studies that calcium chloride modified PCs also demonstrated increased silicate polymerisation to produce a more structured C-S-H bond formation compared with standard PCs leading to the increased cement strength in the presence of the additive (160). The presence of a peak corresponding with C-S-H in the XRD phase analysis studies indicated that C-S-H was present within the first 24 h of setting (figure 3.3.7). However, as the peak was not present after the first 2 h of setting the primary mode of acceleration by calcium chloride appeared to be ettringite formation which is a known cause for early cement strength (113). The rate of the setting reaction for cements containing calcium nitrate has previously been linked to the belite (C_2S) content in the clinker phase (162). Belite dissolves slowly to form short C-S-H fibres

which provide long term strength for the cement and the short C-S-H bonds possibly contributed to the high cement strengths for the 5 wt% nitrate modified cements (161). The early presence of calcium hydroxide was observed in both the XRD and FTIR studies (figure 3.3.6) as a by-product of C-S-H formation, possibly indicating calcium silicate dissolution that led to early C-S-H development (110, 209). Even though the heat signatures of the PC standard and cements containing 5 wt% calcium nitrate were similar (figure 3.35b), the exotherms for nitrate containing cements were significantly higher ($p<0.05$). This may have indicated an increased rate of reaction of PC in the presence of 5 wt% calcium nitrate. After 24 h, both the PC standard and calcium nitrate possessed crystalline peaks corresponding with C-S-H (figure 3.3.7).

Decreased cement strength with increasing addition of supplements correlated with increased cement porosities (table 3.3.1). Increased porosity may have been an indication of a higher proportion of nitrate and chloride being washed out from the pores of the forming cements as additive addition increased (198). As water became adsorbed into the structure of cement the specific density of the material decreased (210). Therefore, the decreased strut densities of PC in the presence of chloride and nitrate compared with standard PC indicated the additives may have been accelerating the cement hydration reaction.

When combining additives a synergistic effect could be achieved with cements being more injectable and possessing higher compressive strengths (figure 3.3.1 and table 3.3.1 respectively). Increased injectability may be due to a degree of complementary surface binding of the two additives leading to a greater degree of surface charge neutralisation. The increased compressive strength may have been as a result of chloride stimulating ettringite formation, whereas nitrate enhances C-S-H production.

Polymethylmethacrylate (PMMA) is the bone cement used in the majority of vertebroplasty operations (72).However, the material possesses several major disadvantages, it cures at temperatures up to 90°C (15), the methylacrylate monomer is toxic and has been shown to damage osteocytes (76) and leakage of the monomer has also been linked to pulmonary embolism (19). Viable alternatives are actively being researched and several have been approved for clinical use e.g. "Cortoss™" by "Orhovita™" and "ChronOS Inject™" by "Synthes™" (48). For PC ceramic materials this is first study to fully address all the issues associated with using the material for vertebroplasty i.e. poor injectability and long setting time while characterising the material with zeta-potential measurements, XRD, FTIR and calorimetry. With addition of simple organic chemicals the material is now injectable, has setting times and compressive strengths equivalent with PMMA. The material also possesses good clinical equivalence as it is the major constituent of MTA a material used for dental applications (3). After clinical trials it may therefore be a viable alternative cement for use in the vertebroplasty procedure.

4.3.3 Conclusions.

Calcium chloride and calcium nitrate both acted as liquefying agents and setting accelerants producing cements which had compressive strengths equal to or greater than the PC standard. Calcium chloride appeared to accelerate the setting reaction through an early exotherm which was responsible for early ettringite formation. In contrast, calcium nitrate stimulated early C-S-H formation. Combining the additives had a synergistic effect increasing injectabilities whilst also improving compressive strengths.

4.4 CHAPTER: Modification of Portland cement with the citrate anion: underlying mechanisms

4.4.1 Injectability studies in the presence of sodium and potassium citrate.

The overall negative surface charge of PC has previously been attributed to the ionisation of the silanol groups of C-S-H (the major phase of PC) (equation 4.3.1) as a consequence of PC and C-S-H sharing similar zeta potentials (C-S-H ranges from -12.7 to -9.4 mV and hydrated PC has a value of approximately -10 mV) (194-196, 203).

$$>SiOH \rightarrow >SiO^- + H^+$$

(Equation 4.3.1)

The -11 mV surface charge of the hydrating PC obtained during the present study was also similar to the known range of C-S-H surface charge indicating that the hydrating surface of PC may also be dictated by the calcium silicate phase. The increase in the magnitude of surface charge of PC in the presence of sodium and potassium citrate and citric acid (-19, -18 and -14 mV respectively) indicated the adsorption of the citrate anion onto the surface of hydrating PC (figure 3.4.4). Once bound, the resulting electrostatic repulsion force between similarly negatively charged cement particles caused cement aggregate dispersion thus leading to improved injectability (191, 205, 206). The reduced charge magnitude of cements containing calcium citrate may have been due to binding of the calcium ion to PC which is known to decrease the overall surface charge of hydrated PC (equation 4.3.2).

$>SiOH + Ca^{2+} \rightarrow >SiOCa^{+} + H^{+}$

(Equation 4.3.2)

4.4.2 Early acceleration of the Portland cement setting reaction in the presence of sodium citrate.

At low concentrations sodium citrate has previously been described to be a cement retardant but acted as an accelerant when used at high concentrations, however, the underlying mechanism has never been satisfactorily explained (211). The cement surface morphology (SEM) (figure 3.4.8), surface structure composition (EDX) and phase analysis (XRD) (figure 3.4.6) studies of PC, all independently indicated that the early accelerating effect of citrate may be caused by the formation of ettringite, $[Ca_3Al(OH)_6]_2(SO_4)_3 \cdot 26H_2O$. Ettringite has previously been shown to be essential for generating the early strength of PC and was identified in the citrate modified cements after 2 h but not in standard cements, with both cements containing this phase after 24 h (figure 3.4.6) (110). The ettringite crystals in the presence of citrate did not develop the typical 'spherulite' structures produced by artificially seeding low densities of pure ettringite crystals (figure 3.4.8)(212). However, it has previously been demonstrated that the size and density of the needle shaped crystals of pure ettringite can be influenced by additives (212, 213). In particular, one previous study investigating the effect of sodium citrate on pure ettringite demonstrated that citrate produced "small, short needle", shaped ettringite crystals due to increased crystal nucleation (213). The central 'spherulite' core may simply have been masked by crystal density (refer to figure 3.3.8f). The initial lack of any exotherm generated during the first 15 minutes with any 2 wt% citrate additive indicated that citrate binding and consequent aggregate dispersion prevented early bond formation leading to a retardation effect (figure 3.4.5a).

In addition to ettringite formation the very short setting time of cement with a 5 wt% addition of citrate also indicated that the additive may have been causing the cement to flash set (figure 3.4.3). Cements typically contain approximately 5 wt% calcium sulphate dihydrate (gypsum) to coat the calcium aluminate phase thus preventing early hydration (flash setting) which leads to a weak cement structure (113). The increase in absorbance of the FTIR unbound gypsum peak at approximately 1100 cm^{-1} occurring during the first 60 minutes of cement setting when 5 wt% sodium citrate was added to PC indicated that citrate at this concentration was removing gypsum from the surface of the cement particles altering the quantity of bound/unbound gypsum (figure 3.4.7b) (209). Removing gypsum from the calcium aluminate phase then resulted in the formation of calcium aluminate hydrate (4 $CaO.Al_2O_3.13H_2O$), the cause of flash setting. This hypothesis was tested by the addition of gypsum to the cements containing 5 wt% sodium citrate where the rapid onset of cement setting was prevented by providing an additional source of gypsum to coat the aluminate phase. The increased height of the absorbance peak after 60 minutes when gypsum and sodium citrate were combined in equal wt% indicated that at 5 wt% the citrate anion had the capacity to remove more gypsum from the aluminate phase than was contained within the cement (figure 3.4.7b). The decreased height of the gypsum peak after 60 minutes of setting when only 2 instead of 5 wt% addition of sodium citrate was used indicated a decrease in the removal of gypsum from the aluminate phase (figure 3.4.7a). In small quantities citrate appeared to accelerate the reaction of tricalcium aluminate with gypsum to form ettringite but in excess all the gypsum was removed from the aluminate causing flash setting.

Sodium citrate additions at both 2 and 5wt% generated an initial exothermic peak which corresponded with the initial setting times of the respective cements (figures 3.4.5a and 3.4.3). It

has been reported that flash setting is an exothermic reaction and in both instances it is indicated that flash setting may have been responsible at least in part for early cement setting when sodium citrate was present (113). However, the formation of ettringite is also a known exothermic reaction and it is likely that ettringite formation may be responsible for the second characteristic exotherm in the DSC measurements at approximately 40 minutes (figure 3.4.5a) (110, 214).

The lack of a calcium hydroxide peak, the by-product of calcium silicate hydration, in the phase analysis of any cement containing citrate (figure 3.4.6) indicated that for at least the first 24 h of setting citrate was additionally blocking C-S-H production, thus preventing the consumption of water in this reaction which was subsequently available for increased ettringite generation.

4.4.3 Investigating long-term cement strength.

The lower porosities of the cements modified with 2 wt% citrate when compared with the PC standard indicated that water was consumed more rapidly in the hydration reaction when citrate was present thus causing lower porosity (as less excess water was present in the structure to cause porosity) (refer to table 3.4.1) (198). The low specific densities of the citrate modified cements indicated a higher degree of hydration when compared with the PC as the denser powder phase was hydrated into less dense material by chemically binding low density water.

A relationship between compressive strength and relative porosity has previously been established (equation 4.4.2) (215-217).

$$CS = \sqrt{\frac{Eo \cdot R}{\pi \cdot c}} \cdot e^{-cont\ RP}$$

(Equation 4.4.2)

Where CS is the compressive strength; Eo is the modulus of zero porosity material; R is the fracture surface energy; c is the critical flaw size; and RP is the relative porosity.

If the materials constants (under the square root) remain unchanged, Equation 4.4.3 simplifies to a linear relationship between the natural logarithm of compressive strength and relative porosity

$$ln\ (CS) = constant \cdot RP$$

(Equation 4.4.3)

The natural logarithms of the compressive strength values from table 1 were plotted as a function of relative porosity after 30-days setting. The strong linear relationship (R^2 =0.97) between ln (citrate CS) and porosity (figure 4.4.1) indicated that the material constants were not altered when the cements were modified with sodium or potassium citrate.

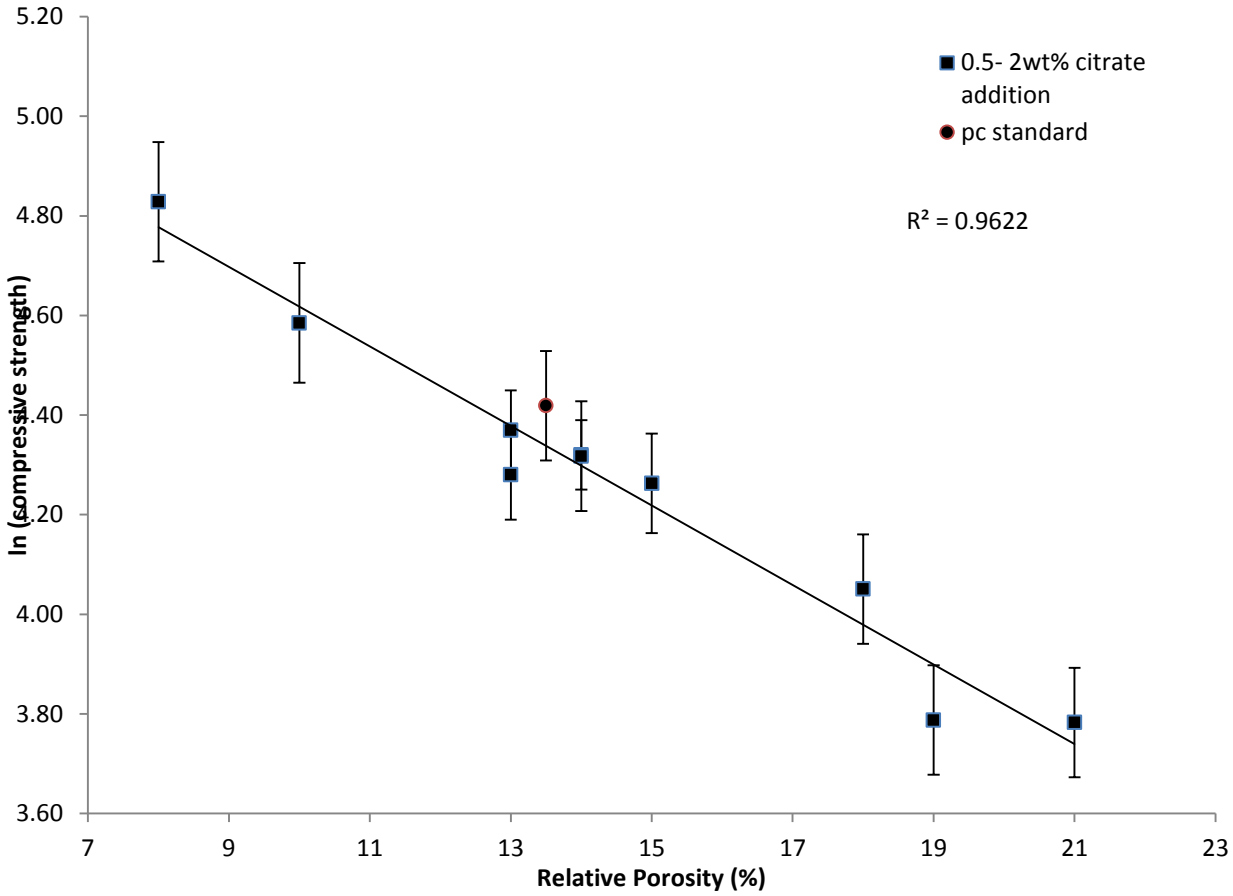

Figure 4.4.1Graph showing natural log of compressive strength vs. relative porosity after 30-days for 0.5- 2 wt% sodium and potassium citrate. The linear relationship between the samples indicated that the additives did not alter the cements material constants.

In summary the evidence suggested that a 2 wt% addition of sodium citrate blocked calcium silicate hydration. In turn, this left a limited amount of water in the high PLR cement, (cements are usually mixed at 3 g ml^{-1} whereas 5 g ml^{-1} was used in this study), to partake in an alternative reaction such as the hydration of the calcium aluminate phase. As sodium citrate has the ability to remove gypsum from the aluminate phase, a portion of the aluminate was simply hydrated causing flash setting. However, it appeared that the major proportion of the water was utilised to produce ettringite within the first two hours of cement setting. During the course of the

proceeding 30 days the phase analysis of the cements indicated that cements containing 2 wt% sodium or potassium citrate did develop a C-S-H phase later. A combination of accelerated early ettringite formation preceding C-S-H production provides a possible explanation for the low porosities of the citrate modified cements resulting in high compressive strengths (up to 50 % compared with standard Portland cement).

4.4.4 Accelerating the setting reaction of PC with other salts of citrate and citric acid.

The concentration of citrate anions contained within the liquid phase of the setting cement may determine the cements setting characteristics. Sodium citrate possesses a K_d value of 0.2 M and potassium citrate has a marginally higher value of 0.37 M (218). Both of these citrate salts had similar influences on setting characteristics including injectability, setting times and compressive strengths (refer to figures 3.4.1, 3.4.3 and table 3.4.1 respectively). In contrast, calcium citrate had a lower dissociation constant of 1 mM. The cement possessed extended setting times and reduced injectabilities compared with the sodium and potassium salts. The reduced exotherm of calcium citrate may be another indicator of a reduced citrate concentration (figure 3.4.5a). When the kinetics of the setting reaction were accelerated by increasing the setting temperature to 37 °C the exothermic trace had a similar profile to the ones of the sodium and potassium salts (refer to figure 3.4.5b). The phase analysis of the 2 wt% calcium citrate cements suggested that ettringite was present within the first 2 h of mixing but at a reduced quantity compared with sodium or potassium citrate (figure 3.4.6). Introducing hydrogen cations from citric acid into the liquid phase may have disrupted the alkaline setting conditions of PC (113). The cements were observed to set as a very dry powder which produced no exotherm and also possessed strut densities similar to unhydrated PC powder.

4.4.5 Conclusions

Sodium citrate additions established PC injectability and improved compressive strengths while reducing cement setting times compared with the standard cement, making PC a possible candidate for use as a bone cement. The present study suggests that the citrate anion reduced cement viscosity by binding to cement grain particles creating an electrostatic repulsion force within the cement paste. Citrate accelerated cement setting through a combination of early ettringite formation and calcium aluminate hydrate formation. This present study has demonstrated both the mechanism of citrates action with PC as well as the possibility to generate a durable high strength injectable PC based cement.

4.5 CHAPTER: Flexural strengths

4.5.1 Comparing compressive strength and biaxial flexural strength testing

Compressive strength testing constitutes an important role in acrylic bone cement testing and is present in implants for surgery ISO 5833:2002 (15). During axial compressive strength testing the compressive forces (σ_c) applied to the flat contact points at each end of the specimen (figure 4.5.1) resolve into both shear forces and tensile stresses (σ_t) (219). It is an unknown combination of the two forces which eventually leads to specimen failure.

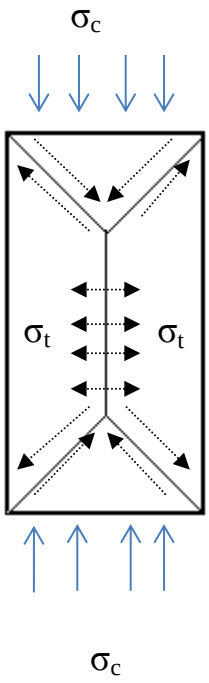

Figure 4.5.1. Diagram illustrating the forces created during compressive strength testing. Shear forces are experienced at the contact points forming shear cones which result in tensile stresses within the central portion of the cylinder.

In contrast, specimen failure for brittle samples with biaxial flexural strength testing occurs solely due to tensile forces on the lower face of the specimen (fig 4.5.2).

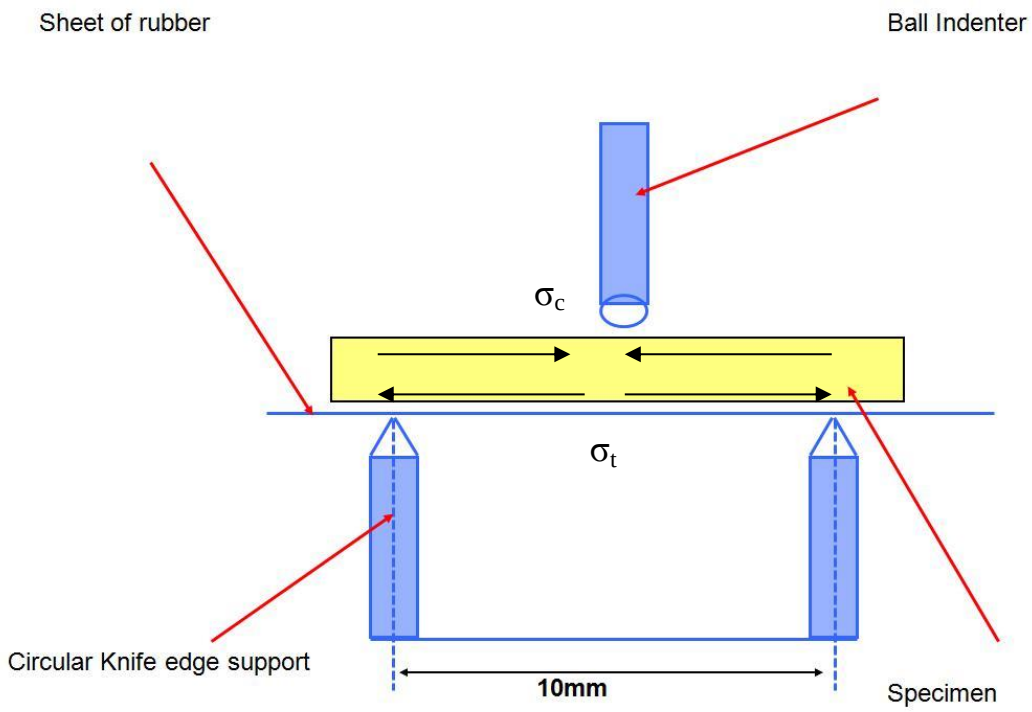

Figure 4.5.2 Diagram illustrating the forces being created during flexural strength testing. Specimen failure is a result of tensile forces on the underside of the sample.

As the maximum tensile stresses occur within the central loading area spurious edge failures are eliminated which is an advantage over the more commonly used three point flexure testing (220). Samples are also insensitive to specimen geometry and independent of flaw direction. According to ISO 5833: 2002 the minimum acceptable flexural strength for acrylic bone cements is 50 MPa which is approximately double the mean values for the PC based cements on test (15). Calcium phosphate ceramic cements possess bending strengths in the region of 4 MPa and

Hydroxyapatite materials failed before the test began (221). The bending strengths of ceramic materials may be viewed as a disadvantage compared with acrylic cements such as PMMA. However, as bone is also a ceramic material the bending strengths of PC may more closely match the native environment.

4.5.2 Weibull Modulus

The evaluation of mean strength data and associated standard deviations can be misleading, as the use of mean strength is based on the assumption that the materials possess a "normal" flaw size distribution. However, the defect population within all brittle materials, such as PC frequently lacks this level of homogeneity resulting in failure at lower strengths especially where a high defect distribution is present (222). The asymmetrical distribution of flexural strengths with cements containing 2.5 wt% calcium chloride and calcium nitrate (figure 3.5.1) may have indicated heterogeneity in the flaw size distribution of the "tail" samples which would not be evident from studying the mean strength values.

Statistical analysis, using alternative distribution functions such as the Weibull distribution can provide a more meaningful interpretation of the strength data, determining the reliability of the data and allowing prediction of the probability of failure of a brittle material (172, 222). Weibull modulus is the shape parameter of the defect distribution. A high Weibull modulus is indicative of narrow distributions of defects and increased reliability of the strength data of that particular material. The 95 % confidence intervals for the specimen groups under investigation all overlapped indicating that the additive additions did not significantly alter the flaw size distribution of the material.

The presence of a single defect population is indicated by an R^2 value of close to 1, which characterises a perfect distribution and a value less than 0.9 represents a multimodal distribution which distorts the strength data away from the straight line (223). The value of 0.89 for cements containing 2 wt% sodium citrate indicates that this specimen population may possess a multimodal defect distribution.

4.5.3 Conclusions

The Weibull moduli of specimen groups containing PC and a variety of additives indicated that the defect distribution was not altered by the addition of additives.

4.6 CHAPTER: Investigating the rheology and injectability of Portland cement

4.6.1 Injectability of Portland cement through needles with a 11 gauge diameter

Acrylic based bone cement materials such as PMMA are both rheopectic (i.e. the viscosity of the material alters during setting) and pseudoplastic (i.e. the viscosity varies with shear rate) (224) (225). During the present rheological study only the rheopectic property of the cements was investigated (figure 3.6.1). Portland cement (PC) sets via a chemical setting reaction and the high shear rate created by a plate rheometer could potentially disrupt bond formation decreasing cement viscosity potentially resulting in an inaccurate reflection of *in vivo* setting (113). The effect of a comparatively low shear force (0.3 s^{-1}) was observed in figure 3.6.3 as the 5 wt% sodium citrate cement failed to set on the rheometer. During the setting period the dynamic viscosity of the cement fluctuated possibly as a result of chemical bonds forming only to be broken by the shear forces created by the rheometer plates. Both calorimetry and FTIR studies (chapter 3.4) indicated that the initial cement setting of PC with 5 wt% sodium citrate arose from the early hydration of the tricalcium aluminate phase (flash setting) which created a weakly bonded cement structure that appeared to enhance early bond breakage under shear and other external forces.

Testing the rheopectic properties of the cement was also problematic due to the wide aspect ratio (15:1) of the plate rheometer (refer to figure 3.6.2). The large sample surface may have contributed to the observed acceleration of cement setting compared with the Gilmore needles test (2:1 aspect ratio) (figure 3.4.3). The marked increase in viscosity of the standard PC (figure 3.6.2), which previously was found to have an initial setting time of over 2 hours, was observed to begin setting within 4 minutes. Hence, the cements were only tested for 60 seconds periods on the rheometer before being discarded.

The initial viscosities of both acrylic and calcium phosphate cements have previously been investigated. After initial mixing the acrylic cements Vertebroplastic (DePuy Inc, England), DP-Pour (DenPlus Inc., Canada) and Simplex (Howmedical International Limited, England) had initial viscosities of 50, 70 and 300 Pa.s respectively (96). In contrast, the calcium phosphate based cements, Biopex (Taisho Pharmaceutical, Japan) and ChronOS (Palacos, US) both had lower initial viscosities of approximately 45 Pa.s. The initial viscosity of PC with a 2 wt% addition of sodium citrate was similar to commercial calcium phosphate cements (40 Pa.s) (figure 3.6.1a). However, without additives the initial viscosity of PC standard was considerably higher (25 times) at 1000 Pa.s. Decreased cement viscosity between the citrate modified and standard cements correlated with increased cement injectability from figure 3.4.1. Further rheological testing of other liquefying additives with PC would be required to verify the link between cement viscosity and injectability.

Identifying the ideal viscosity for cement injectability is difficult as the process is divided into; "cement delivery" which involves the flow of cement from the syringe into the needle and secondly the "infiltration" of the cement once it has entered the vertebrae (226-228). Clinical studies of vertebroplasty have demonstrated that the requirements for both external cement delivery and internal infiltration generate conflicting physical requirements and for successful injection a rheological compromise is required (96). The viscosity must be low enough so that when a surgeon applies pressure to the syringe the desired volume of cement is extruded through the needle without needle blockages. Needle blockages may render the syringe unusable requiring more cement to be mixed which is unfeasible in a time dependent operation such as vertebroplasty (229). However, in patients with low bone density the bone cement may penetrate into the macropore system of the cancellous bone forming "glove like" extensions (96,

225). If a surgeon identifies this type of cement distribution using fluoroscopy the operation will be stopped as these extensions are known to be weak and have been documented to cause post-operative complications such as cement leakage (226). During a successful vertebroplasty operation after an initial volume of approximately 2 ml the cement forms a “cloud” expansion pattern monitored using fluoroscopy as it uniformly expands within the vertebrae (226).

Baroud *et al* (96) investigated what clinicians constituted a successful injection by recording the pressure drop between the syringe and the needle. In a “successful injection” the pressure exerted to activate the syringe was between 0.5 -1.7 MPa, above 2 MPa the surgeons were unable to inject sufficient cement and below 0.5 MPa the “glove like” extensions of cement began to occur within the vertebrae. When determining the parameters for the injectability during the current project it was decided that the injection force which could be reasonably applied to a syringe plunger was approximately 100 N. Other studies have used forces in excess of 250 N with syringes using similar plunger mechanisms (187, 230). However, such high forces are only applicable for screw type plungers. The width of needle used also varies between studies Kreb *et al* (231) used an 8 gauge (3.6 mm) wide needle which was significantly wider than the 12 gauge (2.7 mm) commonly used within the vertebroplasty operation (167). The pressure drop across the syringe during the present investigation was a maximum of 0.65 MPa (figure 3.6.7) which was at the lower end of the scale and accordingly may result in “glove like” extensions of the bone cement within the vertebrae pore structure if the procedure was performed *in vivo* (45). However, the micro-CT scan of the sawbone model with a representative pore diameter of osteoporotic bone (200 µm) did not indicate that any “glove-like” extensions occurring (figure 3.6.11b) (232). Niewenhuijse *et al* (233) reported cement leakage of low and high viscosity cements and found

that there was no significant difference between the two types indicating that the link between low viscosity cements and leakage may not been conclusively determined.

Force balance equations have previously been applied to cement injectability in order to calculate which is greater the pressure required for “cement delivery” or “infiltration”. The two equations which were balanced were the Hagen-Poiseuille, which describes the delivery of a fluid through a cylindrical tube (i.e. needle) and Darcy’s law which describes the infiltration of a fluid through a porous media (230). The outcome of the calculation concluded that the infiltration pressure accounted for only 6 % of the total injection pressure and therefore the needle geometry was the limiting factor for cement delivery in vertebroplasty (96).

The ideal viscosity for injecting acrylic cement through an 8 gauge needle to obtain a “successful delivery” was determined to be in the region of 100 to 200 Pa.s (96). This viscosity range was higher than the ones recorded for four of the five commercial cements discussed earlier and is also higher than the 40 Pa.s for PC with a 2 wt% sodium citrate modification (refer to figure 3.6.1). All of the commercial cements have passed the extensive clinical trials set by the Medicines and Healthcare products Regulatory Agency (MHRA). Baroud *et al* (96) ideal viscosity for “successful delivery” outcomes were based on a statistically insignificant number of clinical cases and may require revising.

Modified Portland cement with a 2 wt% addition of sodium citrate maintained a viscosity of below 300 Pa s for the first 10 minutes of viscosity testing (refer to figure 3.6.1), which was approximately equal to the viscosity of the simplex bone cement. This may indicate that the bone cement remains injectable for this period of time, however, this would require testing using the “injectability testing” method as outlined in chapter one of the materials and methods.

4.6.2 Investigating phase separation with micro-CT.

The major limitation of ceramic cements such as calcium phosphate and PC is that under injection pressure the powder and liquid phases may separate. This effect known as "filter pressing" and decreases the powder-to-liquid ratio (PLR) of the extruded cement while conversely increasing the powder content of the cement remaining in the syringe (234). Understanding the process is of great interest as it is believed to be the primary cause of needle blockages (103). Filter pressing has been studied *ex-vivo* by recording the mass of cement extruded from the syringe compared with the mass of the cement remaining in the syringe using a defined plunger force. As the density of the cement is higher than the density of water 3.8 g ml^{-1} and 1 g ml^{-1} respectively, it is possible to calculate the extent of the phase separation of the material (125).

The current investigation extruded cements through 11 gauge needles and there was a maximum of 3 wt% decrease in injectability with any of the PC containing an additive when the needle was attached (refer to figure 3.6.4). The internal diameter of the syringe aperture of 2 mm may have been the limiting factor for cement injectability rather than the 50 mm needle with an internal diameter of 2.15 mm. Once an injectable PC has passed the syringe outlet the cement appeared unimpeded by the needle. The force/ displacement graphs illustrated the similarity in injectability profiles of cements with and without a needle when sodium citrate or calcium chloride was present (refer to figure 3.6.6).

During a vertebroplasty operation recording the mass of the syringe pre and post procedure would indirectly indicate if phase separation had occurred through the syringe outlet/needle during injection. However, during the "infiltration" process when the cement is percolating within the vertebrae filter pressing may also be occurring within the pores of the cement. It is

important to monitor this process as stated earlier the “glove like” extrusions which may occur are weak and may lead to cement extravasation.

Microtomography (µ-CT) is a commonly used procedure in a clinical environment and may be able to monitor phase separation *in vivo* as there should be a difference in density between cements with different PLR’s which may be detectable using µ-CT. The technique has previously been used on pathological vertebrae to assess the interface properties of bone and PMMA (235). Zhao *et al* (236) proposed the use of *in vivo* CT scans to model subject specific vertebral models to aid in assessment of orthopaedic interventions such as vertebroplasty. Lin *et al* (237) employed a similar technique for assessing bone formation prior to surgery in order to obtain a better clinical outcome.

The grey value count of the µ-CT images was measured for a range of different PLR cements measuring 6 mm width by 3 mm height (figure 3.6.8). There was no significant ($p<0.05$) difference in the grey scale value between samples when using a comparatively high µ-CT resolution of 13 µm even when the macropores, which appeared in dark black (figure 3.6.9b, PLR 2.5 g/ml), were excluded from the study. Therefore, it is unlikely that clinical µ-CT with far lower resolutions (500 µm) would be able to discern a grey scale count difference and hence a density and phase separation difference.

4.6.3 Injection of Portland cement into a porous vertebral model.

The µ-CT of the sawbone used in the vertebroplasty model (figure 3.6.11) indicated that even with a very small force (20 N) in a porous bone replica with an average pore size diameter of 200 µm the spread of the cement was observed to infiltrate in a “cloud” formation not “finger

like" extensions. The force to create the "cloud" formation was significantly less than the values for successful infiltration as characterised by Baroud *et al* (96, 225).

The present model did contain a number of assumptions which decreased its overall accuracy. There was no porosity gradient in the sawbone model which would have permitted the investigation of percolation of the cement in varying bone densities (238). The model was also made of a polymer which may inaccurately represent the binding of the bone cement *in vivo*. In addition, there was also lack of bone marrow substitute which if present may have decreased cement percolation.

4.6.4 Conclusions

The initial viscosity of PC with a 2 wt% addition of sodium citrate was consistent with the viscosity of injectable calcium phosphate bone cements used for vertebroplasty. The citrate modified cements remained injectable for approximately 10 minutes before beginning to set which was reflected by an increase in viscosity after 20 minutes. Needle addition had no significant effect on the injectability of PC containing liquefying additives. However, a needle reduced the injectability of PC standard by 50 wt%. Micro-CT was investigated as a possible method for detecting liquid from powder phase separation which may be occurring in the vertebrae and also as a method for cement extravasation. However, the technique was not sensitive enough to discern cement separation.

4.7 Investigating the cytocompatibility of Portland cement (PC)

Since the food and drug administration (FDA) approved the use of Portland cement (PC) based mineral trioxide aggregate for dental applications in the late 1990's there has been considerable interest in the cytocompatibility of PC (3, 139, 239-245). Many *in vitro* studies assessing the biological compatibility of the material have found it to be non-cytotoxic inferring PC possesses both osteoinductive and odontoinductive properties (138, 239, 246-249). However, unlike the material properties testing of bone cements there is no agreed standardised method when testing for cytocompatibility. Material volume to cell culture volumes vary with nearly every study, as does the length of material setting and whether the PC has been set in water prior to exposure to cells. Lack of a general testing consensus may have resulted in an inaccurate reflection of PCs cytocompatibility. For instance, Zhu *et al* (138) indicated "good adhesion and spreading (of osteoblasts) on the surface of MTA" based on SEM morphological studies. However, the media in which the material was set was "changed every day for 2 weeks". According to the author this allowed not only material setting but also "some cytotoxic material" to be eluted before exposure to primary osteoblasts. Min *et al* (247) used the MTT assay to determine the viability of cells in contact with PC and showed there was no statistical difference in viability between human pulp cells which were in contact with the material and those which were not. Again, the cement was not freshly prepared as it would be used *in vivo* and left to set for 24 h before exposure to the pulp cells. Balto *et al* (249) also used cement set for 24 h before exposure to PC and observed attachment of the material with SEM studies to the surface of PC. However, when the same experiment was repeated with freshly mixed material, cells were "round, less in density, exhibited surface defects and lacked attachment to MTA". During the vertebroplasty operation the cement will be injected directly into the vertebrae and immediately exposed to extracellular

fluid. Therefore, any *in vitro* study should include immediate exposure of mammalian cells to freshly prepared PC as shown in figure 3.7.4a. Exposure of cells to a highly alkaline environment produced by freshly mixed PC has previously been shown to induce cell lysis in mouse fibroblast and macrophage cell lines (250). The high alkalinity of PC (above pH 11 refer to figure 3.7.10) may account for the initial cytotoxic effect after the bone marrow cells were exposed to freshly mixed cement. However, the cytotoxicity of the newly formed material may also be caused by the dissolution of a calcium containing species from the material as demonstrated by the Alizarin red stain (refer to figure 3.7.8). Alizarin red binds to calcium containing species and demonstrated a positive reaction around the circumference of the cement. Interestingly, the cause of the high alkalinity, calcium hydroxide, is one of the reasons given for the favourable cell growth rates in the presence of the material due to increased calcium levels (136, 251, 252) .

The 3T3 fibroblast cultures were incubated with cement discs which had been set for either 24 h or for 6 h in a mould and then for 18 h in water (refer to figure 3.7.1). Even without setting accelerants the Gilmore needles test has previously indicated (chapters 3.3 and 3.4) that initial setting of all the cements including the PC standard (2 hours) should have occurred prior to exposure to the cell culture medium. As the cements were all set prior to incubation this may explain why cell growth was not significantly ($p<0.05$) different between cells incubated with standard or accelerated cement (refer to figures 3.7.1 and 3.7.2). The control wells consistently demonstrated higher cell numbers compared with the wells containing cement discs which may have indicated that even when set a constituent of the cement was hindering cell growth. The decrease in the cytotoxic effect of the material with bone marrow cells as material setting times were increased from 20 minutes to 12 h was directly linked to a decrease in the initial pH of the

culture medium when exposed to PC (refer to figures 3.7.4 and 3.7.5). However, the size and quantity of calcium deposited around the circumference of the material was not investigated and may also have demonstrated a correlation with material cytotoxicity. Calcium hydroxide is produced as both a by-product of calcium silicate hydration, the major phase of PC and as the mineral calcium oxide present within PC is hydrated (110, 113). Setting the cement in water should dissolve calcium hydroxide crystals that form so reducing concentrations within the material prior to cell exposure. This may explain the reduced cytotoxic effect of the material that was identified with the 3T3 cell line where the cements were essentially washed (refer to figures 3.7.1 and 3.7.2). As calcium hydroxide is produced as the cement sets, quantities should increase over time leading to higher levels in cements set for longer periods. Therefore, cement set for 12 hours as opposed to 20 minutes would have had greater concentrations of calcium hydroxide produced from the calcium silicate hydration. It may appear counter-intuitive then that the longer set cements were more cytotoxic if alkalinity was the major cause of cell death. However, there may be an explanation based on cement setting chemistry. Early PC setting is divided into two characteristically distinct phases, the first is the formation of a “gel like matrix” forming before the initial set of the material, whilst at completion of setting the material then possess a distinct pore structure (110, 253). A possible explanation for the decreased pH of the cement set for 12 hours as opposed to 20 minutes is that at the latter time point the material is in the “gel phase” and as a consequence all of the mineral calcium oxide has access and can dissolve into the culture medium. However, once set at 12 h only calcium oxide with direct contact with the pore solution can dissolve entrapping the remainder of the calcium oxide in the core of the cement thereby reducing the pH of the culture medium after exposure to the cement. Alternatively, the “calcium halo” eluted from the material could be reduced after setting allowing the cells to grow

in closer proximity to the material. However, the "calcium halo" was not measured during the present experiment but this could be accomplished in future experiments using light microscopy.

4.7.1 Investigating the use of buffers to reduce the pH of the material

During the vertebroplasty procedure the cement will be injected directly into the vertebrae being exposed to a hydraulic environment. The high alkalinity may pose a chronic risk to surrounding tissues as may any eluted materials. The material may also pose wider acute risk to the patient if the material or created alkalinity is dispersed by the posterior-intercostal blood supply (254). From the range of non-toxic[6] buffers chosen to reduce the alkalinity of the material none reduced the pH to a physiological range (pH 7.4) for cell survival while maintain the setting times of the cement (255). One alternative maybe to inject an FDA/MHRA approved fast waterproof resorbable dental sealant into the vertebral cavity first to protect the cement. This material would not be required to structurally support the vertebrae long-term.

4.8 The elution of calcium containing species from PC

The Alizarin red stain binds to calcium ions creating a chromophore species which can be viewed using calorimetry. During biomineralisation calcium ions accumulate at matrix nodules as a precursor material for hydroxyapatite (Ca_{10} (PO_4)6(OH_2)$_2$) formation (256) (257). The stain was used to assess if the bone marrow cells had initiated osteogenesis as indicated by the upregulation of many of the key osteoblast phenotype genes (refer to figure 3.7.9). However, it was unclear if the positive calcium stain was a result of biomineralisation or elution of a calcium

[6] Based on the Chemical Hazard and Risk Assessment (HAZDAT)

based material from the calcium silicate based PC, which was clearly evident in (alizarin red figure 3.7.8).

4.8.1 Investigating gene expression with RT-PCR

The genes osteoadherin (OSAD), alkaline phosphatase (ALPase), bone morphogenic protein (BMP), bone sialoprotein (BSP), osteonectin (ON), osteopontin (OPN) and osteocalcin (OCN) were all chosen for investigation due to their key role in the biomineralisation process. OSAD is a protein involved with hydroxyapatite formation, ALPase hydrolyses inorganic pyrophophates ($P_2O_7^{4-}$) which increases local orthophosphate ion (PO_4^{3-}) concentration for hydroxyapatite formation, BMP is a growth factor associated with osteogenesis, ON is a protein which binds calcium, BSP is a component of bone extracellular matrix, OPN is important in anchoring osteoclast cells and osteocalcin is involved in the metabolic regulation of osteoblast cells (122-124,138). The increased expression levels of ALPase, BSP, ON and OPN in the presence of PC may be an indication of the cells undergoing early osteogenic differentiation in the presence of the material (refer to figure 3.7.9). Increased transcription levels of the early osteogenic marker, alkaline phosphatase have been observed with RT-PCR in human pulp cells (122) (132), periodontal and gingival fibroblasts (131) and the MG-63 osteosarcoma cell line (240). In addition to an increase in gene expression levels of ALPase an increase in enzymatic activity has also been monitored directly using the Lowry *et al* (258) protocol utilising p-nitro phenyl phosphate assay. Human dental pulp (122) and rat osteosarcoma cells (259) have also demonstrated increases in ALPase activity when incubated with PC. Concentrations of the extracellular matrix protein, BSP, have been observed to increase in human orofacial bone mesenchymal stem cells (123), human dental pulp stem cells (139) (132) and MG63 Osteosarcoma cells lines (240) when in contact with calcium silicate based materials. The

extracellular matrix glycoprotein, osteonectin and the bone remodelling protein osteopontin have previously demonstrated increased expression in periodontal fibroblasts exposed to calcium silicate materials (131) whilst the OCN gene was not expressed in any cultures exposed to a cement or the control. However, the osteocalcin protein has demonstrated to be present in human dental pulp stem cells and MG63 in the presence of PC (122, 139, 240). The absence of OCN during the present investigation may be accounted for by either deterioration of the primers or inaccuracies in primer preparation.

This is the first study to investigate expression of the cellular proliferation marker, Ki-67 The protein is only present during the active phases of the cell cycle G1, S, G2 and mitosis but is absent in resting cells so its expression is used as an indicator that mitotic division is occurring (260). The lack of observable difference in gene expression of Ki-67 levels between the control cultures and those in the presence of cement indicate that cellular proliferation rates were similar at the 5-day time-point between all the cultures. The effects of PC on transcription markers for mitotic division have been investigated with the MAPKinase family of genes (ERK 1 and 2). Western blot studies measuring the concentration of the extracellular regulated kinases (ERKs)-1 and -2 demonstrated increased protein concentrations in the presence of PC in human osteosarcoma cells (U2OS) (261) The MAPKinases family are one of the central components of the phosphorylation signalling pathway which increases cellular proliferation through the mitogenic signalling pathway. The investigation suggested that a component of MTA maybe an external mitogen activator but further studies were required (261). In 2012 Zhao *et al* (139) used western blotting to study MAPK levels dental pulp cells when exposed to the PC derived material mineral trioxide aggregate (MTA). In addition to finding increased expression of

MAPK the study also found increased expression of a range of odontoblastic proteins including ALPase, dental sialoprotein, collagen 1, OCN and BSP. The study then prevented the translation of the MAPK protein by the addition of the inhibitor SP600125. Removing the MAPK protein lowered gene expression of many of the odontoblastic genes mentioned above. Based on this correlation the group suggested a link between MAPK and ododontogensis. As many of the genes between the odontogenesis and osteogenesis are shared a similar experiment investigating MAPK expression knockout in mesenchymal bone cells in the presence of PC may be a worthy future investigation.

Immuno-assay studies of the interleukin cytokine family have also yielded some interesting results. Osteosarcoma cells exposed to MTA have shown to increase quantities of interleukin-6 a potent bone resorbing factor produced by osteoblasts (262) and Interlukin 8 an important factor for angiogenesis. In contrast, the levels of the inflammatory cytokines Interlukin-1 did not increase in quantity, indicating that a PC vertebroplasty implant may not inflame surrounding tissue (263).

4.8.2 Conclusion

Freshly mixed Portland cement demonstrated a cytotoxic effect on bone marrow cells. This effect may be due to the alkalinity of the material or from degradation of the cement material leaking into cell cultures. The high alkalinity of the material may be caused by premature hydration of the calcium oxide mineral content of the cement. The cells which survive up-regulate several key genes for the biomineralisation process including alkaline phosphatase, bone

sialoprotein, osteonectin and osteopontin. Extending cement setting times appears to reduce the cytotoxicity of the material this may be as a result of hydroxide crystals in the core of the material not having access to the exterior cell culture media.

CHAPTER 5: FUTURE WORK

5 FUTURE WORK

During the current investigation the expression of 9 genes associated with the osteogenic phenotype were studied in bone marrow cells incubated with PC set for either 1 or 12 hours. Future studies should widen the selection of genes to include other osteogenic differentiation markers such as the transcription factor (Cbfa1), which activates osteocalcin production (264). Studying a marker such as Cbfa1 which is transcribed prior to another major osteogenic marker would permit the earliest possible identification of cells undergoing the differentiation process. In addition, studying transcription levels of bone marrow cells exposed to cement set in the interval between 1-12 hours may generate insights into gene transcription during the setting transition period. In the present study only one cellular proliferation marker was investigated, Ki-67, the MAPKinase family of genes (ERK 1 and 2) have also been studied as transcription markers for ceramic cements and may provide complementary insights into the state of cellular proliferation in the presence of PC (261). Performing a DNA micro-array on lysed bone marrow cells, which had been exposed to setting PC, would permit simultaneous identification of a large array of osteogenic genes expressed in the presence of the material.

The major issue observed from the biological studies was the occurrence of cellular necrosis in the presence of newly mixed cement. Buffer additions to the cements were investigated and appeared to interfere with the physical characteristics of the cement and only a select few significantly reduced the pH of the setting material. Another possible solution to address the initial high alkalinity of PC would be to inject a non-load bearing resorbable resin into the fracture cavity prior to the injection of the ceramic cement. The resin would resorb over time,

however, this generates new issues such as the integration of PC after resorption and the breakdown of the resin in the body.

Stability of PC was investigated using XRD characterisation to compare a new batch of PC with one was aged for 5 years and which demonstrated deterioration with time. A more comprehensive study comprising a number of aged batches is required to assess the deterioration of the material. A range of temperatures and humidity's could be employed to expedite the aging process. Only one type of grey Portland cement (Mastercrete, Lafarge, UK) was used during the current investigation as it had demonstrated high compressive strengths when used in previous model systems (184). However, the additives may need to be tested with other cements if the industrial sponsor requires a different source for the material.

During the project a range of techniques such as SEM, EDX, XRD and zeta potential have been employed to characterise the effect of additives on the hydration reactions of PC. However, as PC sets via several setting reactions often occurring simultaneously it is often difficult to determine the effect of an additive on a single hydration phase such as ettringite ($[Ca_3Al(OH)_6]_2(SO_4)_3.26H_2O$) (213) or calcium silicates (CaO_x. $SiO_2.H_2O_y$) (265). Carlson and Berman (266) developed a method to produce ettringite crystals from a saturated solution of calcium hydroxide (1.85 g l^{-1}) with aluminium sulphate solution ($Al_2(SO_4)_3.18H_2O$). The accelerants and liquefiers investigated in the present study could be added independently during the nucleation reaction of ettringite in order to assess the effects of an additive on a single cement phase.

The vertebroplasty model used a synthetic sawbone to inject the cement into instead of bone or hydroxyapatite. At the University of Bath presently a porous, synthetic calcium phosphate

structure modelled on cancellous vertebrae is being developed. Once the prototype is complete it would be possible to investigate the injectability and binding of the cement in with a composition the same as bone.

For a brittle ceramic material such as PC fatigue testing will be important in order to assess the cements durability. It will also be necessary to calculate the bending modulus using three point bending tests as they are a key component of bone cement ISO 5833 and compare the results with the biaxial flexural strength results (15). Biaxial flexural strength testing was used during the present study to limit spurious edge failures which may arise with 3-point bend tests (220).

CHAPTER 6: CLINICAL RELEVANCE AND CONCLUSIONS

6 CLINICAL RELEVANCE AND CONCLUSIONS

There are presently a number of commercially available PMMA based bone cements specifically designed for vertebroplasty; Osteopal® manufactured by Heraeus, Germany, CMW1® by Depuy, UK and KyphX HVR® by Medtronic Spinal, USA. All of the PMMA based cements present similar clinical complications including an exothermic setting reaction, toxic monomer and lack of osseointegration. Cortoss® by Orthovita, USA has emerged as the only real commercially viable alternative to PMMA and possesses lower curing temperatures, appropriate setting times for the vertebroplasty procedure and sufficient injectability through an orthopaedic needle. In the future calcium phosphate based cements with excellent osseointegration may become a commercial success as vertebroplasty cements, however, they are currently only applicable for non-load bearing operations such as cranioplasty due to the lack of mechanical strength.

In its native form PC is not a viable material for use in vertebroplasty as it is non-injectable and sets in hours not the 15-20 minutes required for the stabilising procedure (167). The material does however possess several advantages including compressive strengths equivalent to PMMA and high durability. Encapsulation of drugs or biologically active compounds is also possible with porous cement systems such as PC and calcium phosphates.

The current research has demonstrated that with simple inorganic chemicals, of known structure and with no known previously documented harmful biological effects, it is possible to inject over 97 wt% PC paste from a syringe with a 2 mm aperture. The attachment of an 11 g needle (chapter 3.6) to the syringe reduced extrusion by only 1-3 %. The limited rheology testing also demonstrated that cement with added liquefier (i.e. 2 wt% sodium citrate) possessed significantly

($p<0.05$) lower viscosities than the standard cement. Adding the liquefier in the liquid as opposed to the powder phase of the cement reduced injectability and cement setting times. Many of the additives demonstrated dual functionality possessing both liquefying and setting accelerant capabilities. Dissolving additives in the liquid phase may have accelerated the setting process which reduced injectability. During the initial stages of the project sieving cements was demonstrated to significantly ($p<0.05$) reduce the setting time of the standard cement and XRD analysis indicated that filtering removed reacted cement aggregate. Hygroscopic PC appeared to absorb water from the air as the cement aged creating aggregate. This may have indicated that the cement requires airtight sealing at the end of the manufacturing process.

A wide range of cement characterisation techniques were employed during the present study which provided an insight into the effect of liquefiers and accelerants on PCs complex setting reaction. On several occasions the data from multiple techniques indicated that a particular accelerant e.g. calcium chloride or sodium citrate was accelerating the formation of a particular cement phase e.g. ettringite.

PC when freshly mixed was acutely cytotoxic to bone marrow cells incubated with the material. The cytotoxicity may have been as a result of the alkalinity of the material (pH 11) or the elution of cement material into the growth media. For the vertebroplasty procedure the material would be injected directly into a fractured vertebra in contact with bodily fluids with the potential of entering the blood supply of the patient potentially causing acute cytotoxic effects. Buffer addition to reduce the setting pH interfered with the physical characteristics of the setting cement and may not be a feasible solution for reducing cement alkalinity. One possible solution for reducing the alkalinity of the material is the injection of a resorbable resin into the fracture cavity prior to the injection of the cement. However, this generates a new set of issues including

integration of PC after material resorption and the breakdown of the resin inside the body. Once PC has set the material up-regulates several genes associated with the osteogenic phenotype including osteoadherin, alkaline phosphatase, bone sialoprotein, osteonectin and osteopontin.

There are presently a host of biomaterials being studied which are also addressing the disadvantages with PMMA (89, 267). Some of the most interesting involve hybrid materials which incorporate resins for structural integrity with calcium phosphate for osseointegration (104).

Portland cement is one of a number of materials being researched to address the issues presented by PMMA. With the addition of liquefiers and setting accelerants the cement is injectable, sets in a time appropriate for the vertebroplasty procedure and possesses compressive strengths similar with PMMA. However, the acute cytotoxicity of the newly mixed material will have to be resolved before the cements use in vertebroplasty can be realised.

CHAPTER 7: APPENDICES

7 APPENDICES

7.1 EDX analysis

Atomic element	Atomic mass
Calcium	40
Silicon	28
Sulphur	32
Aluminium	27
Oxygen	16
Hydrogen	1
Iron	56

Major elements present within Portland cement

Cement clinker phase	***Chemical formula***	***atom***	***Molecular mass***	***% of total mass***
Tricalcium silicate	$3CaO.SiO_2$	Ca	120	53
		O	80	35
		Si	28	12
		Total =	**228**	**100**
Dicalcium silicate	$2CaO.SiO_2$	Ca	2	80
		O	4	64
		Si	1	28
		Total =	**172**	**100**
Tricalcium aluminate	$3CaO.Al_2O_3$	Ca	120	44
		O	96	36
		Al	54	20
		Total =	**270**	**100**
Tetracalcium aluminoferrite	$4CaO.Al_2O_3.Fe_2O_3$	Ca	160	33
		O	160	33
		Al	54	11
		Fe	112	23
		Total =	**486**	**100**
Calcium sulphate dihydrate	$CaSO_4.2H_2O$	Ca	40	23
		S	32	19
		O	96	56
		H	4	2
		Total =	**172**	**100**
Calcium sulphate hemihydrate	$CaSO_4.H_2O$	Ca	40	26
		S	32	21
		O	80	52

		H	2	1
			154	100
		Total =	**154**	**100**
Calcium sulphate anhydrous	$CaSO_4$	Ca	40	30
		S	28	21
		O	64	48
		Total =	**132**	**100**
Hydration Phases	***Chemical formula***	***atom***	***Molecular mass***	***% of total mass***
Ettringite (Aft phase)	6 $CaO.Al_2O_3.3SO_3.32H_2O$	Ca	240	19
		O	800	64
		Al	54	4
		S	96	8
		H	64	5
		Total =	**1254**	**100**
Calcium monosulphate (afm phase)	$4CaO.Al_2O_3.SO_3.12H_2O$	Ca	160	26
		O	352	57
		Al	54	9
		S	32	5
		H	24	4
		Total =	**622**	**100**
Calcium silicate hydrate (C-S-H)	3 $CaO.2SiO_2.8H_2O$	Ca	120	30
		O	240	59
		Si	28	7

		H	16	4
		Total =	**376**	**100**
Calcium aluminate hydrate	$4CaO.Al_2O_3.13H_2O$	Ca	160	29
		O	320	57
		Al	54	10
		H	26	5
		Total =	**560**	**100**

7.1.1 Theoretical optimum ratios for Portland cement clinker and hydration products

Compounds prior to hydration	Ca/O	Ca/Si	O/Si	Ca/Al	O/Al	Ca/Fe	O/Fe	Al/Fe	Ca/S	O/S	S/Al
tricalcium silicates	1.50	4.29	2.86								
dicalcium silicates	1.25	2.86	2.29								
tricalcium aluminates	1.25			2.22	1.78						
tetracalcium aluminoferrite	1.00			2.96	2.96	1.43	1.43	0.48			
calcium sulphate di-hydrate	0.42								1.25	3.00	
calcium sulphate hemihydrate	1.25								1.25	2.50	
calcium sulphate anhydrous	0.63								1.43	2.29	
Compounds after hydration											
Ettringite	0.30			4.44	14.81	4.44			2.50	8.33	1.78
calcium monosulphate	0.45			2.96	6.52				5.00	11.00	0.59
calcium silicate hydrate (C-S-H)	0.50	4.29	8.57								
tricalcium aluminate hydrate	0.5			2.962963	5.925926						

Element	Weight%	Atomic%
O	52.35	71.40
Na	0.50	0.47
Mg	0.73	0.65
Al	2.10	1.70
Si	6.83	5.31
S	2.07	1.41
K	1.15	0.64
Ca	32.66	17.78
Fe	1.61	0.63
Totals	100.00	

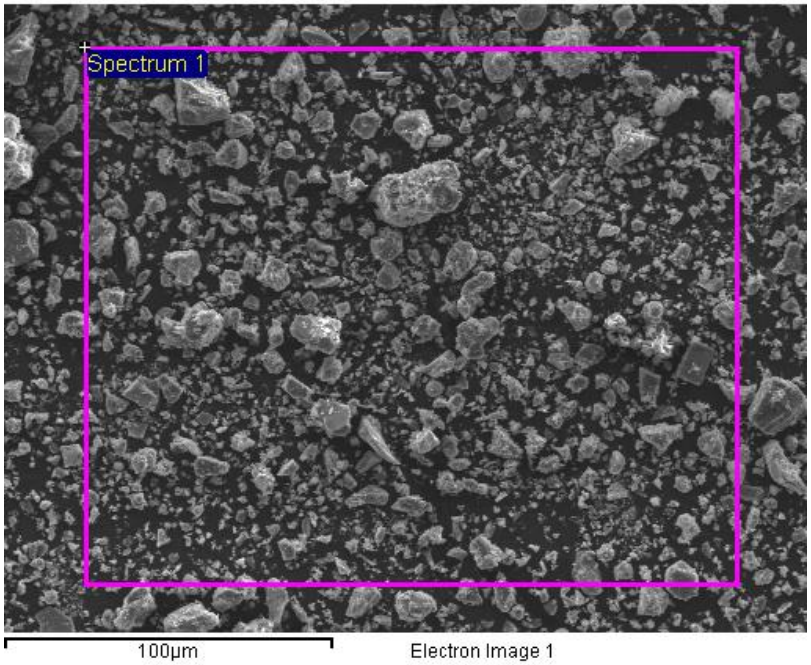

	Ca/O	Ca/Si	O/Si	Ca/Al	O/Al	Ca/Fe	O/Fe	Al/Fe	Ca/S	O/S	S/Al
Observed ratios	0.62	4.78	7.66	15.55	24.93	20.29	32.52	1.30	15.78	25.29	0.99
	Percentage difference in observed vs. theoretical ratios										
Compounds prior to hydration	Ca/O*	Ca/Si*	O/Si*	Ca/Al*	O/Al*	Ca/Fe*	O/Fe*	Al/Fe*	Ca/S*	O/S*	
tricalcium silicates	58.41	-11.46	-168.00								
dicalcium silicates	50.09	-67.20	-234.70								
tricalcium aluminates	50.09			-600.56	-1300.48						
tetracalcium aluminoferrite	37.61			-425.42	-742.18	-1318.58	-2173.81	-171.74			
calcium sulphate di-hydrate	-48.54								-1162.22	-743.00	
calcium sulphate hemihydrate	-24.78								-1162.22	-911.59	
calcium sulphate anhydrous	0.97								-1003.34	-532.25	
Compounds after hydration											
Ettringite	-107.96			-250.28	-68.32				-531.11	-51.71	50.71
calcium monosulphate	-38.64			-425.42	-282.34				-215.56	-129.91	-79.22
calcium silicate hydrate (C-S-H)	-7.57	-123.45	-106.60								
calcium aluminoferrite hydrate (C-AF-H)	0.97			-250.28	-250.61	-847.93	-847.97	-171.74			

$$* \ 1 - \left(\frac{Observed\ ratio}{theoretical\ ratio} \right) * 100$$

EDX New batch of Portland cement (results section 3.1.5)

S

Element	Weight%	Atomic%
O	53.16	72.20
Na	0.47	0.44
Mg	0.69	0.62
Al	1.76	1.41
Si	6.31	4.88
S	2.05	1.39
K	0.87	0.49
Ca	33.14	17.97
Fe	1.55	0.60
Totals	100.00	

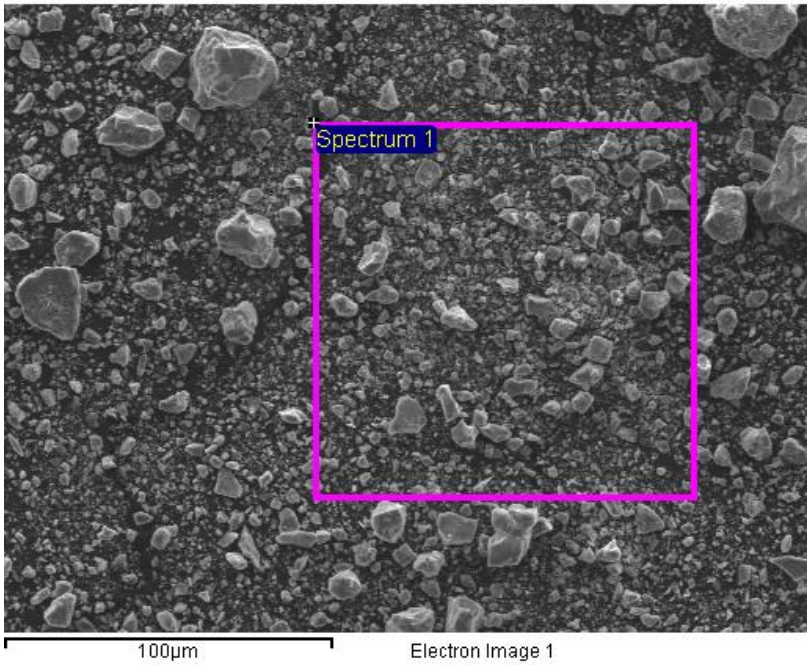

	Ca/O	Ca/Si	O/Si	Ca/Al	O/Al	Ca/Fe	O/Fe	Al/Fe	Ca/S	O/S	S/Al
Observed ratios	0.62	5.25	8.42	18.83	30.20	21.38	34.30	1.14	16.17	25.93	1.16
	Percentage difference in observed vs. theoretical ratios										
Compounds prior to hydration	Ca/O	Ca/Si	O/Si	Ca/Al	O/Al	Ca/Fe	O/Fe	Al/Fe	Ca/S	O/S	
tricalcium silicates	58.44	-22.42	-194.57								
dicalcium silicates	50.13	-83.64	-267.89								
tricalcium aluminates	50.13			-748.18	-1596.88						
tetracalcium aluminoferrite	37.66			-536.13	-920.42	-1395.15	-2298.38	-136.56			
calcium sulphate di-hydrate	-48.43								-1193.27	-764.39	
calcium sulphate hemihydrate	-24.68								-1193.27	-937.27	
calcium sulphate anhydrous	1.05								-1030.48	-548.29	
Compounds after hydration											
Ettringite	-107.80			-324.09	-103.95				-546.63	-55.56	41.76
calcium monosulphate	-38.53			-536.13	-363.26				-223.32	-135.74	-111.78
calcium silicate hydrate (C-S-H)	-7.48	-145.42	-127.08								
calcium aluminoferrite hydrate (C-AF-H)	1.05			-324.09	-324.82	-899.10	-899.91	-136.56			

Element	Weight%	Atomic%
O	54.42	74.92
Si	0.13	0.11
Ca	45.45	24.98
Totals	100.00	

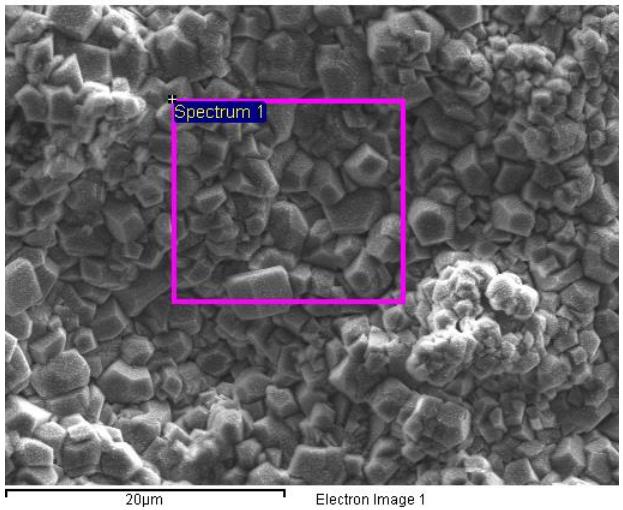

	Ca/O	Ca/Si	O/Si	Ca/Al	O/Al	Ca/Fe	O/Fe	Al/Fe	Ca/S	O/S	S/Al
Observed ratios	1	349	419								
Percentage difference in observed vs. theoretical ratios											
Compounds prior to hydration	Ca/O	Ca/Si	O/Si	Ca/Al	O/Al	Ca/Fe	O/Fe	Al/Fe	Ca/S	O/S	
tricalcium silicates	44	-8044	-14537								
dicalcium silicates	33	-12116	-18180								
tricalcium aluminates	33										
tetracalcium aluminoferrite	17										
calcium sulphate di-hydrate	-99										
calcium sulphate hemihydrate	-67										
calcium sulphate anhydrous	-32										
Compounds after hydration											
Ettringite	-178										100
calcium monosulphate	-85										100
calcium silicate hydrate (C-S-H)	-44	-16226	-11183								
calcium aluminoferrite hydrate (C-AF-H)	-32										

Element	Weight%	Atomic%
O	57.62	74.94
Na	0.58	0.52
Al	8.31	6.41
Si	2.13	1.58
P	0.45	0.30
S	1.53	0.99
Ca	29.38	15.25
Totals	100.00	

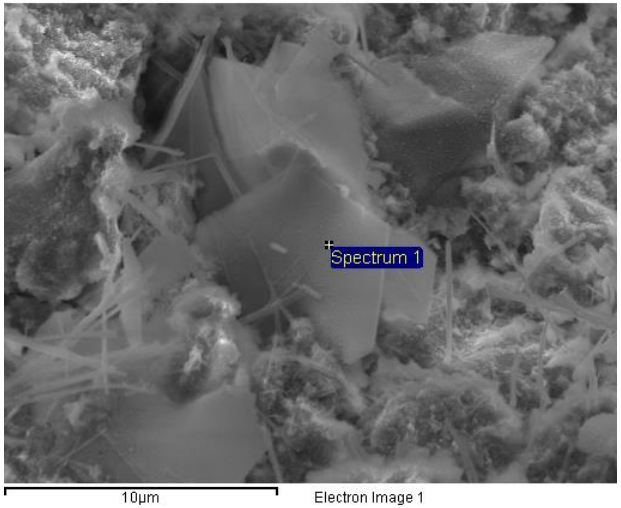

	Ca/O	Ca/Si	O/Si	Ca/Al	O/Al	Ca/Fe	O/Fe	Al/Fe	Ca/S	O/S	S/Al
Observed ratios	1	14	27	4	7				19	38	0
Percentage difference in observed vs. theoretical ratios											
Compounds prior to hydration	Ca/O	Ca/Si	O/Si	Ca/Al	O/Al	Ca/Fe	O/Fe	Al/Fe	Ca/S	O/S	
tricalcium silicates	66	-222	-846								
dicalcium silicates	59	-382	-1081								
tricalcium aluminates	59			-59	-290						
tetracalcium aluminoferrite	49			-19	-134						
calcium sulphate di-hydrate	-21								-1436	-1155	
calcium sulphate hemihydrate	-2								-1436	-1406	
calcium sulphate anhydrous	19								-1243	-842	
Compounds after hydration											
Ettringite	-70			20	53				-668	-126	91
calcium monosulphate	-13			-19	-6				-284	-242	67
calcium silicate hydrate (C-S-H)	12	-545	-629								
calcium aluminoferrite hydrate (C-AF-H)	19			20	2						

Element	Weight%	Atomic%
O	33.17	52.84
Na	0.41	0.46
Mg	0.33	0.34
Al	2.32	2.19
Si	13.60	12.34
S	2.26	1.79
K	1.20	0.78
Ca	44.23	28.12
Fe	2.48	1.13
Totals	100.00	

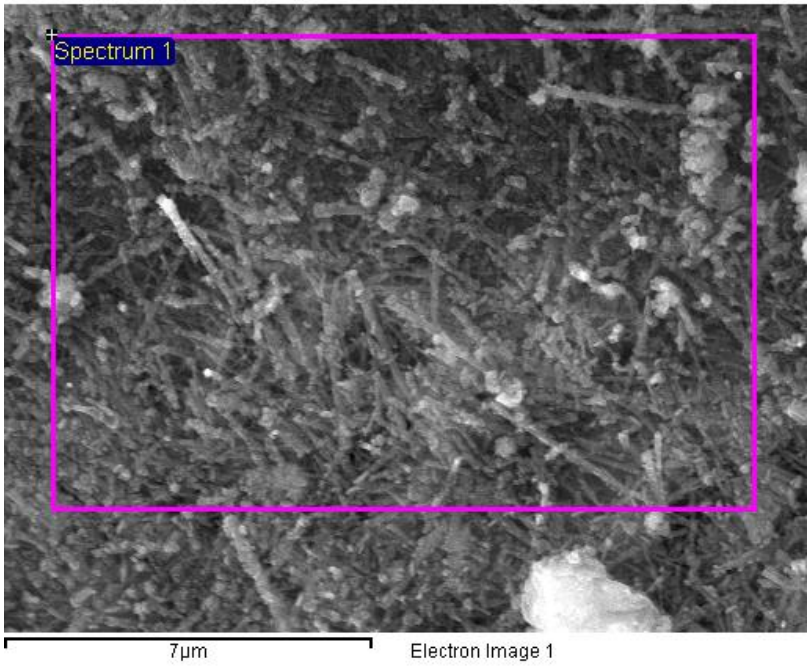

Ratios											
	Ca/O	Ca/Si	O/Si	Ca/Al	O/Al	Ca/Fe	O/Fe	Al/Fe	Ca/S	O/S	S/Al
	1	3	2	19	14	18	13	1	20	15	1
Compounds prior to hydration	Ca/O	Ca/Si	O/Si	Ca/Al	O/Al	Ca/Fe	O/Fe	Al/Fe	Ca/S	O/S	
tricalcium silicates	11	24	15								
dicalcium silicates	-7	-14	-7								
tricalcium aluminates	-7			-759	-703						
tetracalcium aluminoferrite	-33			-544	-383	-1147	-835	-95			
calcium sulphate di-hydrate	-217								-1466	-389	
calcium sulphate hemihydrate	-167								-1466	-487	
calcium sulphate anhydrous	-112								-1269	-267	
Compounds after hydration											
Ettringite	-344			-329	3				-683	12	51
calcium monosulphate	-196			-544	-119				-291	-33	-77
calcium silicate hydrate (C-S-H)	-130	-52	34								
calcium aluminoferrite hydrate (C-AF-H)	-112			-329	-101	-733	-290	-95			

Journal Paper:

Wynn-Jones G, Shelton RM, Hofmann MP. 2012. Development of Portland cement for orthopedic applications, establishing injectability and decreasing setting times. J Biomed Mater Res Part B 2012:100B:2213–2221.

CHAPTER 8: REFERENCES

8 REFERENCES

1. Leung C. Concrete as a building material, encyclopaedia of materials. 4th edition. Oxford, UK: Elsevier; 2001. p.1471-1449
2. Lee SJ, Monsef M, Torabinejad M. Sealing ability of mineral trioxide aggregate for repair of lateral root perforations. J Endod 1993; 19(11): 541-544
3. Torabinejad M, Hong CU, McDonald F, Ford P. Physical and chemical properties of a new root-end filling material. J Endod 1995; 21(7): 349-353
4. Maroto M, Barberia E, Vera V, Godoy F. Mineral trioxide aggregate as pulp dressing agent in pulpotomy treatment of primary molars: 42- month clinical study. Am J Dent 2007; 20(5): 283-286
5. Colak A. A new model for the estimation of compressive strength of Portland cement concrete. Cement Concrete Res 2006; 36(7): 1409-1413
6. Glasser FP, Marchand J and Samson E. Durability of concrete, degradation phenomena involving detrimental chemical reactions. Cement Concrete Res 2008; 38(2): 226-246
7. Darvell BW. Materials Science for Dentistry. 9th edition. Cambridge, UK: Woodhead Publishing in Materials; 2009. p. 1-59
8. Torabinejad M, Hong C, Ford P. Tissue reaction of implanted Super-EBA and mineral trioxide aggregate in the mandible of guinea pigs: a preliminary report. J Endod 1995; 21: 569-571
9. Yu HF, Sun W, Zhang YS, Guo LP, Li M. Durability of concrete subjected to the combined actions of flexural strength, freeze-thaw cycles and bittern solutions. J Wuhan Univ Technol-Mat Sci 2008; 23(6): 893-900

10. Coleman NJ, Nicholson JW, Awosanya K. A preliminary investigation of the in vitro bioactivity of Portland cement. Cement Concrete Res 2007; 37(11): 1518-1523
11. Guduguntla M, Subamaniam R. Vertebroplasty- a new treatment for vertebral compression fractures. Aust Fam Physician 2006; 35(5): 304-307
12. Kim DH, Vaccaro AR. Osteoporotic compression fractures of the spine; current options and considerations for treatment. Spine J 2006; 6(5): 479-487
13. Peh W, Munk PL, Rashid F, Gilula LA. Percutaneous vertebral augmentation: vertebroplasty, kyphoplasty and skyphoplasty. Radiol Clin N Am 2008; 46(3): 611-617
14. Peutzfeldt A. Resin composites in dentistry: the monomer systems. Eur J Oral Sci 1997; 105(2): 97-116
15. British standard for implants for surgery: acrylic resin cements. BS ISO 5833: 2002
16. Hee HT. Percutaneous vertebroplasty: current concepts and local experience. Neurol India 2005; 53(4): 475-482
17. Belkoff SM, Molly S. Temperature measurement during polymerisation of polymethylmethacrylate cement used for vertebroplasty. Spine 2003; 28: 1555-1559
18. Ylmen R, Wadso L, Panas I. Insights into early hydration of Portland limestone cement from infrared spectroscopy and isothermal calorimetry. Cement Concrete Res 2003; 40(10): 1541-1546
19. Laredo JD, Hamze B. Complications of percutaneous vertebroplasty and their prevention. Skeletal Radiol 2004; 33(9): 493-505
20. Ber BS, Hatton JF, Steward GP. Chemical modifications of ProRoot MTA to improve handling characteristics and decrease setting time. J Endod 2007; 33(10): 1231-1234

21. Singh NB, Savahi R, Singh NP. Effect of superplasticisers on the hydration of cement. Cement concrete Res 1992; 22(5): 725-735

22. Papo A, Piani L. Effect of various superplasticisers on the rheological properties of Portland cement paste. Cement Concrete Res 2004; 34(11): 2097-2101

23. Kong HJ, Bike SG, Li VC. Effects of a strong polyelectrolyte on the rheological properties of concentrated cementitious suspensions. Cement Concrete Res 2006; 36(5): 851-857

24. Chandra S, Bjonstrom J. Influence of cement and superplasticisers type and dosage on the fluidity of cement mortars- Part I. Cement Concrete Res 2006; 32 (10): 1605-1611

25. Ramachandran VS, Malhotra VM. Concrete admixtures handbook. 2nd edition. New Jersey, USA: William Andrew Publishing; 1996. p. 410-517

26. Middleditch A, Oliver J. Functional anatomy of the spine. 1st edition. Oxford, UK: Butterworth-Heinemann Publishing; 2005.p. 28-39

27. Teoh SH, Chui CK. Bone material properties and fracture analysis: Needle insertion for spinal surgery. J Mech Behav Biomed Mater 2008; 1(2): 115-139

28. Moor L, Dalley F. Clinically oriented anatomy. 6th edition. Philadelphia, USA: Lippincott Williams and Wilkins: 2009. p. 108-187

29. Bogduk N. Clinical anatomy of the lumbar spine and sacrum. 3rd edition. Edinburgh, UK: Churchill Livingstone: 1997. p. 18-28

30. Trammell A. Normal spine anatomy. 2nd edition. Philadelphia, USA: Elsevier: 2009. p. 9-22

31. Buckley JM, Kuo CC, Cheng LC, Loo K, Motherway J, Slyfield C. Relative strength in thoracic vertebrae in axial compression versus flexion. Spine J 2009; 9(6): 478-485

32. Perilli E, Briggs AM, Kantor S, Codrington J, Wark JD, Parkinson IH. Failure strength of human vertebrae: Prediction using bone mineral density measured by DXA and bone volume by micro-CT. Bone 2012; 50(6): 1416-1425

33. Tencer F, Johnson K. Biomechanics in orthopaedic trauma. 1st edition. London, UK: Dunitz publishing: 1994.p. 102-116

34. Kanis JA. Osteoporosis. 1st edition. Oxford, UK: Blackwell Science: 1994. p. 18-24

35. Anagnostis P, Karagiannis A, Kakafika AI, Tzomalos K, Athyros VG, Mikhailidis KP. Atherosclerosis and osteoporosis: age-dependent degenerative process or related entities. Osteoporosis Int 2009; 20(2): 197-207

36. Akesson K, Adami S. The year in osteoporosis. 2nd edition. Oxford, UK: Clinical Publishing: 2006. p. 5-35

37. Kanis J. Who scientific group on the assessment of osteoporosis at primary healthcare level. Brussels, Belgium: 2004

38. Johnell O. Economic implication of osteoporotic spine disease: cost to society. Eur Spine J 2003; 12: 168-169

39. McLaughlin D, Stamford J, White DA. Instant notes in human physiology. 1st edition. London, UK: Hames, Hooper and Houghton: 2006. p. 92-98

40. Melton L. Epidemiology of vertebral fractures in women. Am J Epidemiol 1989; 129: 1000-1011

41. Silverman S. The clinical consequences of vertebral compression fractures. Bone 1992; 13: 27-31

42. Roy DK, O'Neil DW. Determinants of incident vertebral fracture in men and women: results from the European Prospective Osteoporosis Study (EPOS). Osteoporos Int 2003; 14: 19-26

43. Rigg B, Melton LJ. The worldwide problem of osteoporosis: insights afforded by epidemiology. Bone 1995; 17: 505-511

44. Provenzano MJ, Murphy K, Riley LH. Bone cements: review of their physiochemical and biochemical properties in percutaneous vertebroplasty. Am J Neuroradiol 2004; 25(7): 1286-1290

45. Jensen ME, Evans AJ, Mathis JM, Kallmes DF, Cloft HJ, Dion JE. Percutaneous polymethylmethacrylate vertebroplasty in the treatment of osteoporotic vertebral body compression fractures: technical aspects. Am J Neuroradiol 1997; 18: 1897-904

46. Cortet B, Cotton A, Boutry N. Percutaneous vertebroplasty in patients with osteolytic metastases or multiple myeloma. Revue du rhumatisme (English edition) 1997: 2; 177-183

47. Taylor RS, Taylor RJ, Fritzell P. Balloon kyphoplasty and vertebroplasty for vertebral compression fractures- a comparative systematic review of efficacy and safety. Spine 2006; 31(23): 2747-2755

48. Lewis G. Injectable bone cements for use in vertebroplasty and kyphoplasty: State-of-the-art review. J Biomed Mater Res Part B 2006; 76(2): 456-468

49. Heini PF, Orler R. Kyphoplasty for treatment of osteoporotic vertebral fractures. Eur Spine J 2004; 13(3): 184-192

50. Taylor RS, Fritzell P, Taylor RJ. Balloon kyphoplasty in the management of vertebral compression fractures: an updated systematic review and meta-analysis. Eur Spine J 2007; 16(8): 1085-2000

51. Verlann JJ, Oner FC, Dhert W. Anterior spinal column augmentation with injectable bone cements. Biomater 2006; 27 (3): 290-301

52. Tong SC, Eskey CJ, Pomerantz SR, Hirsh JA. "Skyphoplasty": a single institution's initial experience. J Vasc Interv Radiol 2006; 17(6): 1025-1030

53. Galibert P, Deramond H, Rosat P, Le gars K. Preliminary note on the treatment of vertebral angioma by percutaneous acrylic vertebroplasty. Neurochirurgie 1987; 33: 166-168

54. What is fluoroscopy [internet]. 2009 [cited 2012 Nov 15]. Available from URL: http://rad.usuhs.mil/rad/home/flouro.html

55. Use of Kirscher Wire [internet]. 2009 [cited 2012 Nov 14]. Available from URL: http://orthopedics.about.com

56. Francis RM, Aspray TJ, Hide G, Sutcliffe AM, Wilkinson P. Back pain in osteoporotic vertebral fractures. Osteoporosis Int 2008; 19(7): 895-903

57. Kozic N, Weber S, Ballester MAG, Abdo G, Refenacht DA. Ferguson SJ. Automated cement segmentation in vertebroplasty. Comput Aided Surg 2010; 15: 49-55

58. Widmer RP, Ferguson SJ. A mixed boundary representation to simulate the displacement of a biofluid by a biomaterial in porous media. J Biomech Eng 2011; 133(5): 1000-1007

59. Rohlmann A, Bostani HN, Bergmann G, Zander T.A. Probabilistic finite element analysis of the stresses in the augmented vertebral body after vertebroplasty. Eur Spine J 2010; 19(9): 1585-95

60. Kinzl M, Boger A, Zysset PK, Pahr DH. The effects of bone and pore volume fraction on the mechanical properties of PMMA/bone biopsies extracted from augmented vertebrae. J Biomech 2011; 44(15): 2732-2736

61. Unnikrishnan GU, Morgan EF. A new material mapping procedure for quantitative computed tomography-based, continuum finite element analyses of the vertebrae. J Biomech Eng 2011: 133(7): 710

62. Rodrigues DC, Ordway NR, Ma C, Fayyazi AH, Hasenwinkel JM. An ex vivo exothermal and mechanical evaluation of two-solution bone cements in vertebroplasty. Spine J 2011; 11(5): 432-439

63. Golz T, Graham CR, Busch LC, Wulf J, Winder RJ. Temperature elevation during stimulated polymethylmethacrylate (PMMA) cranioplasty in a cadaver model. J Clin Neurosci 2010; 17(5): 617-22

64. Hoell T, Huschak G, Beier A, Holzhausen HJ, Meisel HJ, Emmrich F. Vertebral osteoporosis perfused animal cadaver model for testing new vertebroplastic agents. Spine 2010; 35(25): 1449-1455

65. Romenz R. Data management and clinical trials. 1st edition. Oxford, UK: Elsevier; 1989. p. 5-17

66. Galovich LA, Perez-Higueras A, Altonaga JR, Orden JM, Barba ML. Biomechanical, histological and histomorphometric analyses of calcium phosphate cement compared

with PMMA for vertebral augmentation in a validated animal model. Eur Spine J 2011; 20: 376-382.

67. Krebs J, Ferguson SJ, Goss B, Stauffer E, Ettinger L, Aebli N. Effect of vertebral cement augmentation with polymethymethacrylate on intervertebral disc and bone tissue. J Biomed Mater Res Part B 2012; 100(3): 660-667
68. Lu J, Deng JL, Zhao HT. Safety and feasibility of percutaneous vertebroplasty with radioactive Sm-153 PMMA in an animal model. Eur J Radiol 2011; 78(2): 296-301
69. Axelsen M, Thomassen LD, Bunder C, Bendtsen M, Zou XN, Flo C. Estimating risk of pulmonary neoplastic embolism during vertebroplasty. Spine J 2012; 37(7): 551-556
70. Charnley J. Anchorage of the femoral head prosthesis to the shaft of the femur journal of bone & joint surgery. Brit Vol 1960; 42: 28-30
71. Lewis G, Towler MR, Boyd D, German MJ, Wren AW, Clarkin OM. Evaluation of two novel aluminium-free, zinc-based glass cements as alternatives to PMMA. J Mater Sci-Mater Med 2010; 21(1): 59-66
72. Burton AW, Rhines LD, Mendel E. Vertebroplasty and kyphoplasty: a compreshensive review. Neurosurg Focus 2005; 18(3): 1-9
73. Darre E, Holmich P, Jensen JS. The use of handling of acrylic bone cement in Danish orthopaedic departments. Pharmacol Toxicol 1993; 72: 332-335
74. Gopalakrishnanchettiyar S, Mohanty M, Kumary TV, Valappil MP, Varma HK. Surface-phosphorylated copolymer promotes direct bone bonding. Tissue Eng Part A 2009; 15(10): 3061-3069

75. Robinson Y, Heyde CE, Forsth P, Olerud C. Kyphoplasty in osteoporotic vertebral compression fractures-guidelines and technical considerations. J Orthop Surg Res 2011; 19: 6-15

76. Dahl OE, Garvik LJ, Lyberg T. Toxic effects of methylmethacrylate monomer on leukocytes and endothelial cells in vitro. Acta Orthopaedica Scandinavica 1994; 65: 147-153

77. Mishra A, Malhotra AV, Graft copolymers of xyloglucan and methyl methacrylate. Carbo Poly 2012; 87(3): 1899-904

78. Tan HL, Peng ZX, Li QT, Xu XF, Tang TT. The use of quaternised chitosan-loaded PMMA to inhibit biofilm formation and downregulate the virulence-associated gene expression of antibiotic-resistant staphylococcus. Biomater 2012; 33(2): 365-377

79. Yang K, Gu M, Jin Y, Mu G, Pan X. Influence of surface treated multi-walled carbon nanotubes on cure behaviour of epoxy nanocomposites. Comp Part A 2008; 39(10) 1670-1678

80. Ormsby R, McNally T, Mitchell C, Halley P, Martin D, Nicholson T. Effect of MWCNT addition on the thermal and rheological properties of polymethylmethacrylate bone cement. J Mater 2011; 49(9): 2893-2904

81. Goto K, Kawanabe K, Kowalski R, Baker D, Nakamura T. Bonding ability evaluation of bone cement on the cortical surface of rabbit's tibia. J Mater Sci-Mater Med 2010; 21(1): 139-146

82. Arabmotlagh M, Sommer U, Dingeldein E, Rauschmann M, Schnetteller R. Nanocrystalline hydroxyapatite facilitates bone apposition to polymethylmethacrylate: Histological investigation using a sheep model. J Orthop Res 2012; 30(8): 1290-1295

83. Smith, M. Biological evaluation of medical devices Part 6 tests for local effects after implantation. J Mater Sci 2007; 06: 1215-1220

84. Roberts F, Hota B, Schabowski S. Hospital and societal costs of antimicrobial-resistant infections in a Chicago teaching hospital: implications of antibiotic stewardship 2009; 09: 1537-6591

85. Hawkey PM. The growing burden of antimicrobial resistance. J Antimicrob Chemother 2008; 62: 1-9

86. Kaplan L, Kurdziel M, Baker KC, Verner J. Characterisation of Daptomycin-loaded antibiotic cement. Orthop 2012; 35(4): 503-509

87. Virto MR, Frutos P, Torrado S, Frutos G. Gentamicin release from modified acrylic bone cements with lactose and hydroxypropylmethylcellulose. Biomater 2003; 24(1): 79-87

88. Giaveresi G, Minelli EB, Satori M, Benini S. Microbiological and pharmacological tests on new antibiotic-loaded PMMA-based composites for the treatment of osteomyelitis. J Orthop Res 2012; 30(3): 348-355

89. Wei WB, Abdullayev E, Hollister A, Mills D, Lvov YM. Clay nanotube/ polymethymethacrylate bone cement composites with sustained antibiotic release. Macromol Mater Eng 2012; 297 (7): 645-653

90. Srivastav AK, Nadkarni B, Agarwal S. Prophylactic use of antibiotic-loaded bone cement in primary total knee arthroplasty: Justified or not. Indian J Orthop 2009; 43(3): 259-263

91. Kay MI, Young R, Posner A. Crystal structure of hydroxyapatite. Nature 1964; 204: 1050-1052

92. Curry N, Jones DW. Crystal structure of brushite, calcium hydrogen orthophosphate dihydrate: a neutron diffraction investigation. Chem Soc 1971: 1; 3725-3729

93. Oda M, Takeuchi A, Lin X, Matsuya S, Ishikawa K. Effects of liquid phase on basic properties of alpha-tricalcium phosphate-based apatite cement. Dent Mater J 2008; 27(5): 672-677

94. Musha Y, Umeda T, Mizutani K. Effects of blood bone cement made of calcium phosphates: problems and advantages. J Biomed Mater Res Part B 2010; 92(1): 95-101

95. Lim TH, Breback GT, Renner SM. Biomechanical evaluation of an injectable calcium phosphate cement for vertebroplasty. Spine J 2002; 27: 1297-1302

96. Baroud G, Bohner M, Heini P, Steffen T. Injection of biomechanics of bone cements used in vertebroplasty. Biomed Mater Eng 2004; 14(4): 487-504

97. Barralet JE, Grover LM, Gbureck U. Ionic modification of calcium phosphate cements viscosity. Part II: hypodermic injection and strength improvement of brushite cement. Biomater 2004; 25(11): 2197-2203

98. O'Hara RM, Dunne NJ, Orr JF, Barton DC. Optimisation of the mechanical handling properties of an injectable calcium phosphate cement. J Mater Sci-Mater Med 2010; 21(8): 2299-2305

99. Hofmann MP, Mohammed AR, Perrie Y, Gbureck U, Barralet JE. High-strength resorbable brushite bone cement with controlled drug-releasing capabilities. Acta Biomater 2009; 5(1): 43-49

100. Nath S, Dubey AK, Basu B. Mechanical properties of novel calcium phosphate-mullite biocomposites. J Biomater Appl 2012; 27(1): 67-78

101. Bohner M, Brunner TJ, Stark WJ. Controlling the reactivity of calcium phosphate cements. J Mater Chem 2008; 18(46): 5669-5675

102. Bohner M, Merkle HP, Landuyt PV, Trophardy G, Lemaitre J. Effect of several additives and their admixtures on the physic-chemical properties of a calcium phosphate cement. J Mater Sci-Mater Med 1999; 11(2): 111-116

103. Bohner M, Gbureck U, Barralet JE. Technological issues for the development of more efficient calcium phosphate bone cements: A critical assessment. Biomat 2005; 26(33): 6423-6429

104. Barounian M, Hesaraki S, Kazemzadeh A. Development of strong and bioactive calcium phosphate cement as a light-cure organic-inorganic hybrid. J Mater Sci 2012; 23(7): 1569-1581

105. Nakano M, Hirano N, Zukawa M, Suzuki K, Kimura T. Vertebroplasty using calcium phosphate cement for osteoporotic vertebral compression fractures: study of outcomes at a minimum follow-up of two years. Spine J 2012; 6(1): 34-42

106. Ryu KS, Shim JH, Heo HY, Park CK. Therapeutic efficacy of injectable calcium phosphate cement in osteoporotic vertebral compression fractures: prospective non-randomised controlled study at 6 month follow-up. World Neurosurg 2010; 73(4): 408-411

107. Boyd D, Towler MR, Wren A, Clarkin OM. Comparison of an experimental bone cement with Surgical Simplex P, Spineplex and Cortoss. J Mater Sci Mater Med 2008; 19(4): 1745-1752

108. Bae H, Shen M, Maurer P, Peppelman W, Beutler W, Linovitz R. Clinical experience using Cortoss for treating vertebral compression fractures with vertebroplasty and kyphoplasty. Spine J 2010; 35(20): 1030-1036

109. Palussiere J, Berge J, Gangi A, Cotton A, Pasco A, Bertagnoli R. Clinical results of an open prospective study of a bis-GMA composite in percutaneous vertebral augmentation. Eur Spine J 2005; 14(10): 982-991

110. Taylor H. Cement chemistry. 2nd edition. Slough, UK: Thomas Telford, 2004.p. 1-125

111. Kosmatka S, Kerfhoff B, Panarese C. Design and control of concrete mixtures. 14th edition. Oxford, UK: Portland cement association, 2003.p. 10-25

112. Chen JJ, Thomas P, Taylor H, Jennings H. Solubility and structure of calcium silicate hydrate. Cement Concrete Res 2004; 34(9): 1499-1519

113. Lea FM. The chemistry of cement and concrete. 2nd edition. Oxford, UK: Butterworth-Heinemann, 2003 p. 7-89

114. Brown PW. Hydration behaviour of calcium phosphates is analogous to hydration behaviour of calcium silicates. Cement Concrete Res 1999; 29(8): 1167-1171

115. Moore AE, Taylor H. Crystal structure of ettringite. Acta Crystallographica 1970; 26(4): 386-393

116. Griffin L, Davey R. Design and synthesis of macrocyclic ligands for specific interaction with crystalline ettringite and demonstration of a viable mechanism for the setting of cement. J Chem Soc 1999: 10; 1973-1981

117. Lea FM. The chemistry of cement and concrete. 1st edition. Oxford, UK: Butterworth-Heinemann, 1975 p. 8-92

118. Darvell BW. "MTA"-An hydraulic silicate cement: review update and setting reaction. Dent Mater 2011; 27(5): 407-422

119. Torabinejad M, Watson TF, Ford P. Sealing ability of a mineral trioxide aggregate when used as a root end filling material. J Endod 1993; 19(12): 591-595

120. Yaltirik M, Ozbas H, Bilgic B, Issever H. Reactions of connective tissue to mineral trioxide aggregate and amalgam. J Endod 2004; 30(2): 95-99

121. Estrela C, Bammann L, Silva R. Antimicrobial and chemical study of MTA, Portland cement, calcium hydroxide paste, Sealapex and Dycal. Braz Dent J 2000; 11: 3-9

122. Peng W, Liu W Zhai W, Chang J. Effect of tricalcium silicate on the proliferation and odontogenic differentiation of human dental pulp cells. J Endod 2011; 37(9): 1240-1246

123. Gandolfi MG, Shah SN, Feng RX. Biomimetic calcium silicate cements support differentiation of human orofacial mesenchymal stem cells. J Endod 2011; 37(8): 1102-1108

124. Coomarswamy KS, Lumley PJ, Shelton RM, Hofmann MP. Evaluation of different radiopacifiers for an MTA-like dental material. International symposium on ceramics in medicine 2007; nantes, France: Trans tech publications ltd.

125. Coomaraswamy KS, Lumley PJ, Hofmann MP. Effect of bismuth oxide radiopacifier content on the material properties of an endodontic Portland cement-based (MTA-like) system. J Endod 2007; 33(3): 295-298

126. Ber BS, Hatton JF, Stewart GP. Chemical modification of ProRoot MTA to improve handling characteristics and decrease setting time. J Endod 2007; 33(10): 1231-1234

127. Camilleri J. The biocompatibility of modified experimental Portland cements with potential for use in dentistry. Int Endod J 2008; 41(12): 1101-1114

128. Camilleri J. Characterisation and chemical activity of Portland cement and two experimental cements with potential for use in dentistry. Int Endod J 2008; 41(9): 791-9

129. Gandolfi MG, Ciapetti G, Perut F, Rossi PL. Biomimetic calcium silicate cements aged in simulated body solutions. Osteoblast response and analyses of apatite coating. J Appl Biomater Biomech 2009; 7(3): 160-170

130. Koh ET, Torabinejad M, Ford P. Mineral trioxide aggregate stimulates a biological response in human osteoblasts. J Biomed Mater Res 1997; 37(3): 432-439

131. Bonson S, Jeansonne BG, Lallier TE. Root-end filling materials alter fibroblast differentiation. J Dent Res 2004; 83(5): 408-413

132. Chen CC, Shie MY, Ding SJ. Human dental pulp cell responses to new calcium silicate based endodontic materials. Int Endod J 2011; 44(9): 836-842

133. Washington JT, Schneiderman E, Opperman LA. Biocompatibility and osteogenic potential of new generation endodontic materials established by using primary osteoblasts. J Endod 2011; 37(8): 1166-1170

134. Salles LP, Bao SN. Mineral trioxide aggregate based endodontic sealer stimulates hydroxyapatite nucleation in human osteoblast like cell culture. J Endod 2012; 38(7): 971-976.

135. Sarkar NK, Caicedo R, Ritwik P, Kawashima I. Physiochemical basis of the biologic properties of mineral trioxide aggregate. J Endod 2005; 31(2): 97-100

136. Camilleri J, Montesin FE, Brady K. The constituents of mineral trioxide aggregate. Dent Biomat 2005; 21: 297-303

137. Mansur P, Mansur H. Preparation, characterisation and cytocompatibility of bioactive coatings on porous calcium silicate hydrate scaffolds. Mater Sci Eng 2010; 30(2): 288-294

138. Zhu Q, Haglund R, Safavi KE, Spangberg L. Adhesion of human osteoblasts on root-end filling materials. J Endod 2000; 26(7): 404-406

139. Zhao X, Ni LX. Mineral trioxide aggregate promotes odontoblastic differentiation via mitogen-activated protein kinase pathway in human dental pulp stem cells. Mol Biol Rep 2012; 39(1): 215-220

140. Kim B, Bae K. Gene Expression profiling concerning mineralisation in human dental pulp cells treated with mineral trioxide aggregate. J Endod 2010; 36(11): 1831-1838

141. Salako N, Joseph B, Ritwik P, Salonen J, John P, Junaid TA. Comparison of bioactive glass, mineral trioxide, ferric sulphate, and formocresol as pulpotomy agents in rat molar. Dent Traumatol 2003; 19(6): 314-320

142. Andelin WE, Shababhang S, Torabinejad M. Identification of hard tissue after experimental pulp capping using dentin Sialoprotein (DSP) as a marker. J Endod 2003; 29(10); 646-650

143. Kao CT, Tsai CH, Huang TH. Tissue and cell reactions to implanted root-end filling materials. J Mater Sci-Mater Med 2006; 17(9): 841-847

144. Portland cement chemical admixture additions [internet]. 2010 [cited 2012 Oct 17]. Available from URL: http://www.cement.org

145. Aiad I. Influence of time addition of superplasticiser on the rheological properties of fresh cement pastes. Cement Concrete Res 2003; 33(8): 1229-1234

146. Chandra S, Bjornstrom J. Influence of superplasticisers type and dosage on the slump loss of Portland cement mortars-Part II. Cement Concrete Res 2003; 32(10): 1613-1619

147. Pan LS, Qiu XQ, Pang YX, Yang DJ. Effect of water-reducing chemical admixtures on early hydration of cement. Adv Cem Res 2008; 20(3): 93-100

148. Erdogdu S. Compatibility of superplasticisers with cements different in composition. Cement Concrete Res 2000; 30(5): 767-773

149. Agarwal SK, Masood I, Malhotra SK. Compatibility of superplasticisers with different cements. Constr Build Mater 200; 14(5): 253-259

150. Yoshioka K, Tazawa E, Kawai K, Enohata T. Adsorption characteristics of superplasticisers on cement component minerals. Cement Concrete Res 2002; 32(10): 1507-1513

151. Alonso MM, Palados M, Puertas F, Aranda G. Effect of polycarboxylate admixture structure on cement paste rheology. Materialses De Construction 2007; 57(286): 65-81

152. Sahmaran M, Christianto HA, Yaman I. The effect of chemical admixtures and mineral additives on the properties of self-compacting mortars. Cem Con Comp 2006; 28(5): 432-440

153. Hesaraki S, Zamanian A, Moztaradeh F. Effect of adding sodium hexametaphosphate liquefier on basic properties of calcium phosphate cements. J Biomed Mater Res 2009; 88(2): 314-321

154. Safety data for formaldehyde, 37% solution [internet]. 2009 [cited 2012 Nov 20]. Available from URL: http://msds.chem.ox.ac.uk

155. Maltese C, Pistolesi C, Bravo A, Cella F, Cerulli T, Salvioni D. A case history: Effect of moisture on the setting behaviour of a Portland cement reacting with an alkali-free accelerator. Cement Concrete Res 2007; 37(6): 856-865

156. Prudencio LR, Armelin HS, Helene P. Interaction between accelerating admixtures and Portland cement shotcrete: The influence of the admixture's chemical base and the correlation between paste tests and shotcrete performance. J Mater 1996; 93(6): 619-28

157. Andersen MD, Jakobsen HJ, Skibsted J. Characterisation of white Portland cement hydration and the C-S-H structure presence of sodium aluminate by Al-27 and Si-29 MAS NMR spectroscopy. Cement Concrete Res 2004; 34(5): 857-868

158. Bravo A, Cerulli T, Maltese C, Pistolesi C, Salvioni A. Effect of increasing dosages of an alkali-free accelerator on the physical and chemical properties of a hydrating cement paste. Am Concre Int 2003; 217: 211-226

159. Wiltbank KB, Schwartz SA, Schindler WG. Effect of selected accelerants on the physical properties of mineral trioxide aggregate and Portland cement. J Endod 2007; 33 (10): 1235-1238

160. Singh NB, Singh VD, Rai S, Chaturvedi S. Effect of lignosulfonate, calcium chloride and their mixture on the hydration of RHA-blended Portland cement. Cement Concrete Res 2002; 32(3): 387-392

161. Chikh NB, Cheikh-Zouaoui M, Chikh N, Duval R. Effect of calcium nitrate and triisopropanolamine on the setting and strength evolution of Portland cement pastes. Mater Struct 2008; 41(1): 31-36

162. Aggoun S, Cheikh-Zouaoui M, Chikh N, Duval R. Effect of some admixtures on the setting time and strength evolution of cement pastes at early stages. Constr Build Mater 2008; 22(2): 106-110

163. Singh NK, Mishra PC, Singh VK, Narang KK. Effects of hydroxyethyl cellulose and oxalic acid on the properties of cement. Cement Concrete Res 2003; 33(9): 1319-1329

164. Huang TH, Shie MY, Kao CT, Ding SJ. The effect of setting accelerator on properties of mineral trioxide aggregate. J Endod 2008; 34(5): 590-593

165. El-Didamony H, Amer A, Heikal M, Shoaib M. Effect of calcium acetate as accelerator and water reducer on the properties of silica fume blended cement. Ceramics Silkaty 1999; 43(1): 29-33

166. Habib M, Baroud G, Gitzhofer F, Bohner M. Mechanisms underlying the limited injectability of hydraulic calcium phosphate paste. Acta Biomater 2008; 4(5): 1465-1471

167. Wilson D. Essential details of the vertebroplasty procedure [personal communication]. Received in 2009

168. ASTM-Standard C266-99: Standard test method for time of setting hydraulic cement paste by Gilmore needles. ASTM international 2002.

169. Timoshenko S. Symmetrical bending of circular plates. 2nd edition. New York, USA: McGraw-Hill; 1959.p. 22-28

170. Swamy N. Poisson's ratio of Portland cement paste, mortar and concrete. Cement Concrete Res 1971; 1: 559-583

171. Hill K. Zeta potential theory. 1st edition. Oxford, UK: Heines; 2006.p. 35

172. Weibull W. A statistical distribution function of wide applicability. J Appl Mech 1951; 18(3): 293-297

173. Trustrum K, Jayatilaka AD. On estimating the Weibull modulus for a brittle material. J Mater Sci 1979; 14(5): 1080-1084

174. Barnes HA, Measuring the viscosity of large-particle (and flocculated) suspensions- a note on the necessary gap size of rotational viscometers. J Non-Newtonian Fluid Mech 2000: 94(2): 213-217

175. Bentz DP, Garboczi EJ, Haecker CJ. Effects of cement particle size distribution on performance properties of Portland cement basted materials. Cement Concrete Res 1999; 29(10): 1663-1671

176. Todaro GJ, Green SM. Quantitative studies of the growth of mouse embryo cells in culture and their development into established cell lines. J Cell Biol 1962; 17: 299-313

177. Maniatopoulos C, Sodek J, Melcher AH. Bone-Formation in-vitro by stromal cells obtained from bone marrow of young adult rats. Cell Tissue Res 1988; 254(2): 317-330

178. Mastercrete Lafarge product data sheet [internet] 2008 [cited 2012 Nov 15]. Available from URL: http://www.lafarge.co.uk

179. Garnier E. Powder Diffraction. Theory and Practice. Acta Crystallogr Sect A 2009; 65(1): 51

180. Mollah M, Yu W, Schennach R, Cocke DL. A Fourier transform infrared spectroscopic investigation of the early hydration of Portland cement and the influence of sodium lignosulfonate. Cement Concrete Res 2000; 30(2): 267-273

181. Hughes TL, Methven CM, Jones T, Hall C. Determining cement composition by Fourier transform infrared spectroscopy. Adv Cem Based Mater 1995; 2(3): 91-104

182. Ghosh SN, Handoo SK. Infrared and Raman spectral studies in cement and concrete. Cement Concrete Res 1980; 10(6): 771-782

183. Weatherby ND. Blood chemistry and CBC analysis. 2nd edition. Oregon, USA; Bear Mountain; 2004.p. 21-38

184. O'Beirne J. Characterisation and generation of a model system for MTA for root fillings [MSc] 2006; College of Medical and Dental Sciences, University of Birmingham

185. Habib M, Baroud G, Gitzhofer F, Bohner M. Mechanisms underlying the limited injectability of hydraulic calcium phosphate paste. Part II: Particle separation study. Acta Biomater 2010; 6(1): 250-256

186. Wilson D. Requirements for vertebroplasty [personal communication]. Received in 2009

187. Gbureck U, Barralet JE, Thull R. Ionic modification of calcium phosphate cement viscosity. Part I: hypodermic injection and strength improvement of apatite cement. Biomater 2004; 25(11): 2187-2195

188. Heraeus. Osteopal radiopaque bone cement for filling and stabilising vertebral bodies [instruction leaflet]. Published in 2012.

189. Depuy U. Depuy orthopaedic gentamicin bone cements [instruction leaflet]. Published in 2012.

190. Saury C, Boistelle R, Dalemat F, Bruggeman J. Solubilities of calcium acetates in the temperature range 0-100 degrees C. J Chem Eng Data 1993; 38(1): 56-59

191. Palacios M, Puertas F, Bowen P, Houst YF. Effect of PCs superplasticisers on the rheological properties and hydration process of slag-blended cement pastes. J Mater Sci 2009; 44(10): 2714-2723

192. Plank J, Winter C. Competitive adsorption between superplasticiser and retarder molecules on mineral binder surface. Cement Concrete Res 2008; 38(5): 599-605

193. Yamada K, Takahashi T, Matsuhisa M. Effect of the chemical structure on the properties of polycarboxylate-type superplasticiser. Cement Concrete Res 2000; 30(2): 197-207

194. Elakneswaran Y, Nawa T, Kurumisawa K. Electrokinetic potential of hydrated cement in relation to adsorption of chlorides. Cement Concrete Res 2009; 39(4): 340-344

195. Elakneswaran Y, Nawa T, Kurumisawa K. Zeta potential study of paste blends with slag. Cem Conc Comp 2009; 31(1): 72-76

196. Viallis-Terrisse H, Petit C. Zeta-Potential study of calcium silicate hydrates interacting with alkaline cations. J Colloid Interface Sci 2001; 244(1): 58-65

197. Clayden J, Greeves N, Warren S, Wothers P. Organic Chemistry: 3rd edition. Oxford, UK: Oxford University Press, 2007. p. 122-143

198. Coomarswamy KS, Shelton RM, Hofmann MP. Effect of bismuth oxide radiopacifer content on the material properties of an endodontic Portland cement-based (MTA-like) system. Key Eng Mat 2007; 7: 361-363

199. GrattanBellew PE. Microstructural investigation of deteriorated Portland cement concretes. Constr Build Mater 1996; 10(1): 3-16

200. Newman B, Choo B. Advanced concrete technology: constituent material. 2nd edition. Oxford, UK; Elsevier, 2003.p. 10-78

201. Baur I, Johnson CA. Dissolution-precipitation behaviour of ettringite, monosulfate and calcium silicate hydrate. Cement Concrete Res 2004; 34(2): 341-348

202. Anderson MD, Jakobsen HK, Skibsted J. Characterisation of white Portland cement hydration and the C-S-H structure in the presence of sodium aluminate by 27Al and 29Si MAS NMR spectroscopy. Cement Concrete Res 2004; 34(5): 857-868

203. Pointeau I, Reiller P, Mace N, Landesman C, Coreau N. Measurement and modelling of the surface potential evolution of hydrated cement pastes as a function of degradation. J Colloid Inter Sci 2006; 300(1): 33-44

204. Wongkornchaowalit N, Lertchirakarn V. Setting time and flowability of accelerated Portland mixed with polycarboxylate superplasticiser. J Endod 2011; 37(3): 387-389

205. Kong HJ, Bike SG, Li V. Electrosteric stabilisation of concentrated cement suspensions imparted by a strong anionic polyelectrolyte and a non-ionic polymer. Cement Concrete Res 2006; 36(5): 842-850

206. Plank J, Winter C. Competitive adsorption between superplasticisers and retarder molecules on mineral binder surface. Cement and Concrete Res 2008; 38(5): 599-605

207. Balonis M, Glasser FP. Calcium nitrate corrosion inhibitor in Portland cement. J Am Ceram Soc 2011; 94(7): 2230-2241

208. Cheeseman CR, Asavapisit S. Effect of calcium chloride on the hydration and leaching of lead-retarded cement. Cement Concrete Res 1999; 29(6): 885-892

209. Ylemen R, Jaglid U, Panas I. Early hydration and setting of Portland cement monitored by IR, SEM and Vicat techniques. Cement Concrete Res 2009; 39(5): 433-439

210. Murphy JC, Hofmann MP, Shelton RM. Monitoring the accelerated setting of Portland cement based dental materials. Key Eng Mater 2008: 1-9

211. Pacanovsky J. Hydration control of cementitious systems. Cement Concrete Res 1997: 5(2): 328-337

212. Komatsu R, Makida K, Tsukamoto K. In-situ observation of ettringite crystals. J Crystal Growth 2009; 311(3): 1005-1008

213. Cody AM, Lee H, Spry PG. The effects of chemical environment on the nucleation, growth, and stability of ettringite. Cement Concrete Res 2004; 34(5): 869-881

214. Pratt PL, Ghose A, Hewlett PC. Electron microscope studies of Portland cement microstructures during setting and hardening. Math Phys Sci 1983: 310(1511): 93-103

215. Takahashi T, Yamomoto M, Loku K, Goto S. Relationship between compressive strength and pore structure of hardened cement pastes. Adv Cem Res 1997; 9: 25-30

216. Barralet J, Hofmann MP, Grover L. Gbureck U. Effect of porosity reduction by compaction on compressive strength and microstructure of calcium phosphate cement. J Biomed Mater Res Part B: App Biomater 2002; 63: 1-9

217. Barralet J, Hofmann MP, Grover L, Gbureck U. High-strength apatitic cement by modification with alpha-hydroxy acid salts. Adv Mater 2003; 15; 2091-2094

218. Mackenzie W. Ion association vs dissociation constants for complexes of citrate with sodium, potassium calcium and magnesium ions. Am Chem J 1969: 65: 159-161

219. Berenbaum R, Brodie I. Measurement of the tensile strength of brittle materials. Brit JApp Phys 1959; 10(6): 281-287

220. Palin WM, Fleming G, Randall RC. The reliability in flexural strength testing of a novel dental composite. J Dent 2003; 31(8): 549-557

221. Drosos GI, Verettas DA. Mechanical characterisation of bone graft substitute ceramic cements. Injury 2012: 43(3): 266-271

222. McCabe JF, Carrick TE. A statistical approach to the mechanical testing of dental materials. Dent Mater 1986; 2(4): 139-142

223. Bhamra G, Palin WM, Fleming G. The effect of surface roughness on the flexure strength of an alumina reinforced all ceramic crown material. J Dent 2002; 30(4): 153-60

224. Krause WR, Miller J. The viscosity of acrylic bone cements. J Biomed Mater Res Part A 1982: 16(3): 219-243

225. Baroud G, Yahia FB. A finite element rheological model for polymethylmethacrylate flow: analysis of the cement delivery in vertebroplasty. Proc Inst Mech Eng H 2004; 218(5): 331-338

226. Heini PF, Walchli B, Berlemann U. Percutaneous transpedicular vertebroplasty with PMMA: operative technique and early results. A prospective study for the treatment of osteoporotic compression fractures. Eur Spine J 2000; 9(5): 445-450

227. Jensen ME, Evans AJ, Mathis JM, Kallmes DF, Dion JE. Percutaneous polymethylmethacrylate vertebroplasty in the treatment of osteoporotic vertebral body compression fractures: technical aspects. Am J Neuroradiol 1997; 18(10): 1897-1904

228. Mathis JM, Barr JD, Belkoff SM, Barr MS, Jensen ME, Deramond H. Percutaneous vertebroplasty: a developing standard of care for vertebral compression fractures. Am J Neuroradiol 2001; 22(2): 373-381

229. Hargunani R, Marchinkow L, Mudri MJ. An overview of vertebroplasty: current status. Controversies and future directions. Radiol J 2012; 63: 11-17

230. Bohner M, Gasser B, Baroud G, Heini P. Theoretical and experimental model to describe the injection of polymethylmethacrylate cement into a porous structure. Biomater 2003: 24(16): 2721-2730

231. Krebs J, Ferguson SJ, Bohner M, Baroud G, Steffen T, Heini PF. Clinical measurements of cement injection pressure during vertebroplasty. Spine 2005; 30(5): 118-122

232. Solid rigid polyurethane foam [internet]. 2010 [cited 2012 Oct]. Available from URL: http://www.sawbones.com

233. Nieuwenhuijse MJ, Dijkstra SP. A clinical comparative study on low versus medium viscosity polymethylmethacrylate bone cement in percutaneous vertebroplasty: viscosity associated with cement leakage. Spine 2010; 35(20): 1037-1044

234. Khairoun I, Planell JA. Some factors controlling the injectability of calcium phosphate bone cements. J Mater Sci Mater Med 1998; 9(8): 425-428

235. Kinzl M, Boger A, Pahr DH. The mechanical behaviour of PMMA/bone specimens extracted from augmented vertebrae: A numerical study of interface properties, PMMA shrinkage and trabecular bone damage. J Biomech 2012; 45(8): 1478-1484

236. Zhao Y, Jin ZM Wilcox RK. Modelling cement augmentation: a comparative experimental and finite element study at the continuum level. Proc Inst Mech Eng H 2010; 224(7): 903-911

237. Lin WC, Wu RW, Cheng YF. Dynamic contrast enhanced magnetic resonance imaging for evaluating intraosseous cleft formation in patients with osteoporotic vertebral compression fractions before vertebroplasty. Spine 2011; 36(15): 1244-1250

238. Hsu YH, Turner IG, Miles AW. Fabrication of porous bioceramics with porosity gradients similar to the bimodal structure of cortical and cancellous bone. J Mater Sci 2007; 36(15): 2251-2256

239. Camilleri J, Ford T. Biocompatibility of two commercial forms of mineral trioxide aggregate. Int J Endod 2004; 37(10): 699-704

240. Chen CL, Kao CT. Comparison of calcium and silicate cement and mineral trioxide aggregate biologic effect and bone markers expression in MG63 Cells. J Endod 2009; 35(5): 682-685

241. Huang TH, Chou M. Inflammatory cytokines reaction elicited by root-end filling materials. J Biomed Mater Res Part B 2005; 73(1): 123-128

242. Koh ET, Torabinejad M, Pitt F. Mineral trioxide aggregate stimulates a biological response in human osteoblasts. J Biomed Mater Res 1997; 37(3): 432-439

243. Peng W, Chang J. Effect of tricalcium silicate proliferation and odontogenic differentiation of human dental pulp cells. J Endod 2011; 37(9): 1240-1246

244. Thomson TS, Berry JE, Kirkwood KL. Cementoblasts maintain expression of osteocalcin in the presence of mineral trioxide aggregate. J Endod 2003; 29(6): 407-412

245. Zeferino EG, Bueno C, Oyama LM, Ribeiro DA. Ex vivo assessment of genotoxicity and cytotoxicity in murine fibroblasts exposed to white MTA or white Portland cement with 15% bismuth oxide. J Int Endod 2010; 43(10): 843-848

246. Reyes-Carmona JP, Felippe WT. Biomineralisation ability and interaction of mineral trioxide aggregate and white Portland cement with dentin in a phosphate containing fluid. J Endod 2009; 35(5): 731-736

247. Min KS, Kim HI, Park HJ, Pi SH, Kim EC. Human pulp cells response to Portland cement in vitro. J Endod 2007; 33(2): 163-6

248. Fayad MI, Hawkinson R, Daniel J, Hao J. The effect of carbon dioxide laser irradiation on PDL cell attachment to resected root surfaces. J Endod 2004; 97(4): 518-523

249. Balto HA. Attachment and morphological behaviour of human periodontal ligament fibroblasts to mineral trioxide aggregate: scanning electron microscope study. J Endod 2004; 30 (1): 25-29

250. Haglund R, Zhu Q. Effects of root-end filling materials on fibroblasts and macrophages in vitro. J Endod 2003; 95(3): 345-347

251. Duarte H, Demarchi O, Yamashita JC, Kuga MC, Fraga C. pH and calcium ion release of 2 root end filling materials. J Radiol 2003: 95(6): 345-347

252. Marcela F, Rafael R. Mineral Trioxide Aggregate (MTA) solubility and porosity with different water-to-powder ratios. J Endod 2003; 29(12): 814-817

253. Chen JJ, Jennings HM. Solubility and structure of calcium silicate hydrate. Cement Concrete Res 2004: 34(9): 1499-1519

254. Hall J. Guyton and Hall Textbook of medical physiology. 2nd edition. Oxford, UK: Elsevier, 2001. p. 471-459

255. ISO 5833:2002. Implants for surgery-acrylic resin cements [ISO]. Published 2002

256. Gregory CA, Grady Gunn W, Prockop D. An alizarin red-based assay of mineralisation by adherent cells in culture: comparison with cetylpyridinium chloride extraction. Anal Biochem 2004; 329(1): 77-84

257. Anderson HC. Vesicles associated with calcification in the matrix of epiphyseal cartilage. Nature 1969: 2: 50-63

258. Lowry OH, Roberts NR, Crawford EJ. The quantitative histochemistry of brain. J Biol Chem 1954: 207(1): 19-38

259. Ogata H, Hayashi M, Sugawara A. Effects of a calcium phosphate cement on mineralised nodule formation compared with endodontic cements. Dent Mater J 2012; 31(1): 92-97

260. Scholzen T, Gerdes J. The Ki-67 protein: from the known to the unknown. J Cell Physiol 2000; 182(3): 311-322

261. Huang TH, Ding SJ, Hsu TC, Kao CT. Effects of mineral trioxide aggregate (MTA) extracts on mitogen-activated protein kinase activity in human osteosarcoma cell line (U2OS). Biomater 2003; 24(22): 3909-3913

262. Meghji S. Bone remodelling. J Brit Dent 1992; 172: 235-242

263. Mitchell P, Pitt F, Torabinejad M, McDonald F. Osteoblast biocompatibility of mineral trioxide aggregate. Biomater 1999; 20(2): 167-173

264. Qi HL, Aguiar DJ, Williams SM, Verfaillie CM. Identification of genes responsible for osteoblast differentiation from human mesodermal progenitor cells. PNAS 2003; 100(6); 3305-3310

265. Chen JJ, Thomas JJ, Taylor W, Jennings HM. Solubility and structure of calcium silicate hydrate. Cement Concrete Res. 2004; 34(9): 1499-1519

266. Carlson ET, Berman HA. Some observations of the calcium aluminate carbonate hydrates. J Res Phys Chem 1960; 64(4): 333-341

267. Tan HL, Guo SR, Yang SB, Xu XF, Tang TT. Physical characterisation and osteogenic activity of the quarternised chitosan-loaded PMMA bone cement. Acta Biomater 2012; 8(6): 2166-2174